University of Hamburg

Faculty of Mathematics, Informatics and Natural Sciences

Stella Zora Buchwald

The response of molecular fossils in shallow marine ecosystems to the Permian–Triassic environmental crisis

Universität Hamburg
DER FORSCHUNG | DER LEHRE | DER BILDUNG

2025

The response of molecular fossils in shallow marine ecosystems to the Permian–Triassic environmental crisis

Dissertation

with the aim of achieving the doctoral degree

at the Faculty of Mathematics, Informatics and Natural Sciences

Department of Earth System Sciences

At the University of Hamburg

submitted by

Stella Zora Buchwald

Hamburg, 2025

Cover picture: Aerial picture of the Selmaneset section on the northwest coast of Svalbard with the Permian–Triassic mass extinction horizon exposed on top of the silicified mudstones forming the mountain ridge, and softer Triassic sedimentary rocks towards the Esmarkbreen glacier at the right side of the photo (photo credit: Tereza Mosočiová).

Department of Earth System Sciences

Chair of the Subject Doctoral Committee Earth System Sciences:	Prof. Dr. Dirk Notz
Dean of Faculty MIN:	Prof. Dr.-Ing. Norbert Ritter
Reviewers:	Prof. Dr. William Foster
	Dr. Anja Frank
	Dr. Sylvain Richoz
Defense date:	10/12/2025

Eidesstattliche Versicherung | Declaration on Oath

Hiermit erkläre ich an Eides statt, dass ich die vorliegende Dissertationsschrift selbst verfasst und keine anderen als die angegebenen Quellen und Hilfsmittel benutzt habe.
Sofern im Zuge der Erstellung der vorliegenden Dissertationsschrift generative Künstliche Intelligenz (gKI) basierte elektronische Hilfsmittel verwendet wurden, versichere ich, dass meine eigene Leistung im Vordergrund stand und dass eine vollständige Dokumentation aller verwendeten Hilfsmittel gemäß der Guten wissenschaftlichen Praxis vorliegt. Ich trage die Verantwortung für eventuell durch die gKI generierte fehlerhafte oder verzerrte Inhalte, fehlerhafte Referenzen, Verstöße gegen das Datenschutz- und Urheberrecht oder Plagiate.

I hereby declare and affirm that this doctoral dissertation is my own work and that I have not used any aids and sources other than those indicated.
If electronic resources based on generative artificial intelligence (gAI) were used in the course of writing this dissertation, I confirm that my own work was the main and value-adding contribution and that complete documentation of all resources used is available in accordance with good scientific practice. I am responsible for any erroneous or distorted content, incorrect references, violations of data protection and copyright law or plagiarism that may have been generated by the gAI.

29|09|2025
Hamburg, Date | date


Unterschrift | Signature

Table of Content

Acknowledgements

I would like to express my greatest gratitude to my supervisor, William Foster – thank you for taking me on this journey. Thank you for your unwavering support, for giving me the opportunity to discover my love for fieldwork during months in the field across the globe, for always encouraging me to go further, your scientific guidance, our discussions about research and everything else, and your dedication to improving my manuscripts. I really cannot thank you enough!

I am deeply grateful to Daniel Birgel for his patience when I first delved into biomarker research, his insightful feedback, and our long conversations about science and beyond! Thank you, Anja Frank, for introducing me to the world of redox proxies, and for always being so supportive.

To the entire research group and everyone in the office – thank you for your support (in the lab and morally!) Thank you, Francesca Galasso, Pierre-Antoine Tranchet, M. Alejandra Gómez Correa, Adam Shatwell, Luyi Miao, Rieke Steinkrauss, Annie Couey, Lily Matts, Caro Suchau, Christoph Bonow, Julia Läufer, Florian Purwin, and Hinrich Schmid-Beurmann. The coffee machine Anja donated to the office in my third year may have not made us faster in brewing coffee, but our coffee breaks were invaluable moments of fun and exchange for me!

A special thanks to Sabine Beckmann. Your incredible knowledge of solvents, the mass spectrometer, and computers was matched only by your kindness, patience, and willingness to share it all with me. Your support and our conversations brightened many challenging days!

During the work for my PhD, I have spent almost seven months abroad, mostly in the field collecting samples and learning so much. This was an incredible time, and I own immense gratitude to those who made it possible. Even if I name some of them, I am sure there are many more to thank. In Turkey, thank you to Erdal Koşun for sharing your knowledge of the Permian/Triassic boundary sections and always welcoming us with tea in Antalya. Thank you to Baran Karapunar for making sure we survive without being able to communicate properly, and for the friendship beyond fieldwork. In Italy, our fieldwork would not have been possible without

Evelyn Kustatscher and Herwig Prinoth. Your expertise and generosity with your knowledge of the region and its fossils were indispensable!

I was so excited that I got the opportunity to do fieldwork in China, where Xia Wang was the best host one can ever imagine! Together with Xuanni Xu, Zhen Yuhan and so many others this trip was made unforgettable, both scientifically and culturally. Finally, I would have never thought that I would ever travel to the Arctic (not to mention even three times). However, during my PhD I learned it is by far the most stunning place I will probably ever visit. Svalbard gave me the most breathtaking memories of nature and my favorite samples! I am incredibly grateful to Kim Senger and UNIS for enabling our expeditions, and for the life-changing idea of chartering a boat instead of camping. Special thanks to everyone who joined in the field: Tereza Mosočiová, Muriel Bühlhoff, Brian Beaty, Val Zuchuat, Hannah Brooks, Lydia Tarhan, Noah Planavsky, Davey Woods and Eagle, Terry Isson, Sophia Rauzi, Sverre Planke, Shouzhong Shen, Haipeng Xu, Dongxun Yuan, Hua Zhang and Yaofeng Cai. I also thank the Czech Arctic Research station and the crew of *Clione*, David Vostárek and Jiří Štojdl jr, as well as the crew of *Meridian*, Pål Remen and Jens Johnson, and the crew of *Ulla Rinman*, Mana Walther, Jan Walther and Karlis. You all truly gave us a home during Svalbard's eternal days!

I will not end without thanking my biggest mentor and supporter, Dieter Korn. You made me fall in love with rocks, otherwise I am sure I would have become something completely different, maybe a modern botanist (isn't this what biology students become?). Through you I discovered the world of paleontology, geology, and really research in general. Since already eight years you keep pushing me in the right direction, and I wouldn't be where I am today without you and your advice – not even close!

Finally, of course, I would like to thank my family and friends, without whom all of this would not have been possible. Thank you all for your support and enduring my endless babbling about geochemistry and science gossip. Finally, my deepest thanks to Chris, who just continues to support my journey. No matter where we moved, I know you had my back, and I cannot be grateful enough for that. Thank you for becoming my husband, making this not only an exciting time scientifically, but also a time of growth for the both of us.

Summary

The Permian–Triassic environmental crisis, which occurred approximately 252 million years ago, triggered the most severe mass extinction event of the Phanerozoic. A range of environmental stressors are suggested to collectively have caused the extinction event. Despite the Permian–Triassic transition has been studied for decades, the individual and combined effects on of these stressors on biodiversity as well as the timing of the extinction event are still debated. The understanding of the response of the marine microbial and photoautotrophic community in particular is equivocal, with contradictory results obtained on primary productivity reconstructions in the aftermath of the Permian–Triassic mass extinction.

Biogeochemical and ecological changes, that accompanied the extinction event and the subsequent recovery, can be traced by the analysis of molecular fossils. Molecular fossils are mostly derived from cell membrane lipids and photosynthetic pigments, that can be preserved over geological timescales. They can provide insights into the various types of organisms that synthesized the precursor molecules of the molecular fossils, as well as into the prevailing environmental conditions during their deposition.

As organic material in the environment is constantly exposed to degradation processes, only a few shallow marine sections reveal a sufficient preservation of lipid biomarkers, with only short time intervals across the Permian/Triassic boundary thus far explored. To investigate changes in the molecular fossil inventory that reflect changes in the marine microbial community structure and environmental dynamics across the Permian–Triassic environmental crisis, novel molecular fossil datasets were produced from shallow marine settings across paleolatitudes: the tropical Neotethys (Taurus Mountains, Turkey), and both the western (Dolomites, Italy) and the eastern Palaeotethys (Guizhou, China), and the Boreal Realm (Svalbard, Norway). The obtained molecular fossil records thereby extent and complement existing datasets both spatially and temporally.

A comparison of the distribution of the two molecular fossils C_{33}-*n*-alkylcyclohexane and phytanyl toluene across paleolatitudes revealed that both record peak abundances following the extinction

event, especially in higher-latitude settings away from the paleotropical Tethys Ocean, such as in the Boreal Realm in Svalbard. Both extinction markers correlate with the content of chlorophyll-derived biomarkers. Furthermore, paleoredox conditions return relatively rapidly from anoxic conditions shortly below the extinction horizon to oxic conditions following the mass extinction event. Hence, the two molecules could be assigned to oxygenic photoautotrophs thriving in the extinction aftermath, that formed regional phytoplankton blooms in higher paleolatitude ecosystems.

The multi-proxy analysis from Svalbard applying complementary redox-sensitive trace metal enrichment patterns and lipid biomarker proxies, that unveiled these post-extinction paleoredox patterns, additionally showed that the late Permian was characterized by intervals of deoxygenation pre-dating the extinction. Hence, the community was adapted to fluctuating redox-conditions prior to the extinction, which questions anoxia, that is often hypothesized as one of the main drivers of the Permian–Triassic mass extinction, at least as the sole driver of the extinction at this site.

This highlights the importance of establishing pre-extinction baseline conditions, which is also shown by the molecular fossil record from the Dolomites (northern Italy). At a more proximal site, late Permian sea level changes unrelated to the mass extinction event are the main control on the origin of organic matter, paleoredox conditions, and the composition of the photoautotrophic community. During regressive intervals, marine conditions became more restricted than in a more distal site with a deeper paleo-water depth and a more stable molecular fossil inventory. It is therefore important to consider the regional environmental context, to gain a deeper understanding of the response of life to severe environmental stress, ecosystem resilience and the adaptability of ecological communities during global environmental crises.

Zusammenfassung

Die Umweltkrise am Ende des Perms vor etwa 252 Millionen Jahren führte zum gravierendsten Massenaussterben des Phanerozoikums. Als potenzielle Auslöser werden unterschiedliche Umweltfaktoren in Betracht gezogen. Deren Einzel- und Wechselwirkungen auf die Biodiversität sowie der zeitliche Verlauf des Aussterbegeschehens bleiben jedoch Gegenstand von Kontroversen. Insbesondere die Reaktion mariner mikrobieller und photoautotropher Lebensgemeinschaften ist bislang nicht eindeutig geklärt, wie divergierende Rekonstruktionen der Primärproduktion nach dem Massenaussterben aufzeigen.

Biogeochemische und ökologische Veränderungen im Zusammenhang mit dem Massenaussterben und der anschließenden Erholung lassen sich durch die Analyse von Lipid-Biomarkern rekonstruieren. Lipid-Biomarker sind molekulare Fossilien aus dem Abbau von Zellmembranen und photosynthetischen Pigmenten, die über geologische Zeiträume hinweg erhalten bleiben. Sie liefern Informationen sowohl über die Produzenten der Vorläufermoleküle als auch über die Umweltbedingungen zum Zeitpunkt der Ablagerung.

Geologische Aufschlüsse mit flachmarinen Ablagerungen, die trotz kontinuierlichen Abbaus organischen Materials einen hinreichenden Erhaltungsgrad von Lipid-Biomarkern aufweisen, sind selten. Zudem beschränken sich bisherige Untersuchungen meist auf kurze Zeitintervalle über die Perm-Trias-Grenze hinweg. Vor diesem Hintergrund wurden neue Lipid-Biomarker-Datensätze aus flachmarinen Sedimentabfolgen unterschiedlicher paläogeographischer Breiten erhoben, um Veränderungen im Lipid-Biomarker-Inventar zu erfassen, die Rückschlüsse auf die Zusammensetzung mariner mikrobieller Gemeinschaften sowie auf die Dynamik der Umweltbedingungen während der Krise ermöglichen. Die hier vorgestellten Daten stammen aus der Neotethys (Taurusgebirge, Türkei), der westlichen Paläotethys (Dolomiten, Italien), der östlichen Paläotethys (Guizhou, China) sowie aus dem Borealen Ozean (Svalbard, Norwegen). Damit werden bestehende Datensätze sowohl in räumlicher als auch in zeitlicher Hinsicht erweitert.

Die Verteilung von C_{33}-*n*-Alkylcyclohexan und Phytanyltoluol zeigt insbesondere in höheren Paläobreiten außerhalb der Tethys, wie in Spitzbergen, deutlich erhöhte Konzentrationen nach

dem Aussterbeereignis. Beide Lipid-Biomarker korrelieren mit dem Gehalt von Derivaten aus dem Abbau von Chlorophyll. Nach einer Phase der Sauerstoffarmut kurz vor und während des Massenaussterbens wurde in Svalbard zudem eine für geologische Maßstäbe rasche Rückkehr zu sauerstoffreichen Bedingungen in der Wassersäule dokumentiert. C_{33}-*n*-Alkylcyclohexan und Phytanyltoluol werden daher Phytoplanktontaxa zugeordnet, die in höheren Breiten regionale Blüten nach dem Massenaussterben ausbildeten.

Darüber hinaus weisen multiproxy-basierte Untersuchungen, die die Anreicherung von redox-sensitive Spurenelementen und Lipid-Biomarker zur Rekonstruktion der Paläo-Redoxbedingungen in Spitzbergen kombinieren, auf Intervalle wiederholter Sauerstoffarmut im Ozean bereits vor dem Massenaussterben im späten Perm hin. Dies legt nahe, dass die dortige ökologische Gemeinschaft bereits vor dem Ereignis an schwankende Redoxbedingungen angepasst war. Eine Abnahme des Sauerstoffgehalts und Ozean-Anoxie, häufig als Hauptursache für das Massenaussterben angenommen, erscheint daher als alleinige Erklärung für das Aussterben in Svalbard nicht ausreichend.

Diese Ergebnisse unterstreichen die Relevanz der Rekonstruktion der Ausgangsbedingungen im späten Perm vor dem Massenaussterben, wie auch die Lipid-Biomarker-Analyse aus den Dolomiten (Norditalien) belegt. An einem Standort mit vergleichsweise geringer Paläowassertiefe erwiesen sich natürliche Meeresspiegelschwankungen im späten Perm, die unabhängig vom Massenaussterben auftraten, als dominanter Faktor für die Herkunft des organischen Materials (terrestrisch vs. marin), die Paläoredox-Bedingungen sowie die Zusammensetzung der marinen photoautotrophen Gemeinschaft. Regressive Intervalle hatten dort einen stärkeren Einfluss auf die ökologische Gemeinschaft und die Umweltbedingungen als an einem Standort mit größerer Paläowassertiefe. Die Berücksichtigung des regionalen Umweltkontextes ist daher entscheidend, um die Reaktion der Biosphäre auf massive Umweltveränderungen sowie die Resilienz von Ökosystemen und die Anpassungsfähigkeit ökologischer Gemeinschaften während globaler Krisen adäquat zu erfassen.

I List of manuscripts

I.I Main manuscripts

In this thesis, I present three manuscripts, that are accepted for publication in a peer-reviewed journal (Manuscript I), or submitted to peer-reviewed journals (Manuscript II and III). For all three manuscripts, I was involved in designing the study, organizing fieldwork and sample collection, sample preparation and data analysis, writing the original draft of the manuscript, figure preparation, and editing. For Manuscript I, I led the review process, which I will also do for Manuscript II and III. For Manuscript I and II, I was involved in acquiring funding for the fieldwork. I acknowledge that all co-authors contributed constructively to data collection and discussions to improve the manuscripts.

Manuscript I: Buchwald SZ, Birgel D, Senger K, Mosociova T, Pei Y, Zuchuat V, Tarhan LG, Frank AB, Galasso F, Gómez Correa MA, Koşun E, Karapunar B, Wang X, Kustatscher E, Prinoth H, Lahajnar N, Steinkrauss R, Peckmann J, Foster WJ. Phytoplankton blooms on the Barents Shelf, Svalbard, associated with the Permian–Triassic mass extinction. *Accepted in AGU Advances.*

Manuscript II: Buchwald SZ, Frank AB, Birgel D, Senger K, Mosociova T, Pei Y, Beaty B, Tarhan LG, Galasso F, Gómez Correa MA, Grasby SE, Struck U, Steinkrauss R, Gliwa J, Lahajnar N, Peckmannn J, Foster WJ. Reconstructing environmental and microbial ecosystem changes across the Permian–Triassic mass extinction at Lusitaniadalen, Svalbard. *Submitted to Paleoceanography and Paleoclimatology.*

Manuscript III: Buchwald SZ, Birgel D, Kustatscher E, Prinoth H, Galasso F, Karapunar B, Frank AB, Gómez Correa MA, Lahajnar N, Peckmann J, Foster WJ. Molecular fossils record marine and terrestrial ecosystem changes prior to and across the Permian–Triassic mass extinction in the Dolomites (Italy). *Submitted to Biogeosciences.*

I.II Data and code

All data and code related to the manuscripts are openly accessible online in the Zenodo repository.

Manuscript I (data): Buchwald SZ, Birgel D, Senger K, Mosociova T, Pei Y, Zuchuat V, Tarhan LG, Frank AB, Galasso F, Gómez Correa MA, Koşun E, Karapunar B, Wang X, Kustatscher E, Prinoth H, Lahajnar N, Steinkrauss R, Peckmann J, Foster WJ (2025). Phytoplankton blooms on the Barents Shelf, Svalbard, associated with the Permian–Triassic mass extinction. StellaZBuchwald/Permian-Triassic_Extinction_Markers, published Apr 14, 2025 [Dataset, Computational Notebook], Zenodo, https://www.doi.org/10.5281/zenodo.16032548

Manuscript II (data): Buchwald SZ, Frank AB, Birgel D, Senger K, Mosociova T, Pei Y, Beaty B, Tarhan LG, Galasso F, Gómez Correa MA, Grasby SE, Struck U, Steinkrauss R, Gliwa J, Lahajnar N, Peckmann J, Foster WJ (2025). Reconstructing environmental and microbial ecosystem changes across the Permian–Triassic mass extinction at Lusitaniadalen, Svalbard. StellaZBuchwald/Permian-Triassic_Lusitaniadalen, published Aug 28, 2025 [Dataset, Computational Notebook], Zenodo, https://doi.org/10.5281/zenodo.16983603

Manuscript II (Digital 3D Outcrop Model Lusitaniadalen): Buchwald, SZ, Mosociova T, Gómez Correa MA, Foster WJ, Senger K (2025). Digital outcrop model Lusitaniadalen, published Sep 26, 2025 [Computational Notebook], Zenodo, https://doi.org/10.5281/zenodo.15981864

Manuscript III (data): Buchwald SZ, Birgel D, Kustatscher E, Prinoth H, Galasso F, Karapunar B, Frank AB, Gómez Correa MA, Lahajnar N, Peckmann J, Foster WJ (2025). Molecular fossils record shallow marine ecosystem changes prior to and across the Permian–Triassic mass extinction in the Dolomites (Italy). StellaZBuchwald/Permian-Triassic_Dolomites_Biomarker, published Sep17, 2025 [Dataset, Computational Notebook], Zenodo, https://doi.org/10.5281/zenodo.17139993

I.III Contribution to other articles

Over the course of my PhD, I contributed as a co-author to additional publications (published and in review), that are not part of this thesis.

Foster WJ, Asatryan G, Rauzi S, Botting J, Buchwald SZ, Lazarus D, Isson T, Renaudie J, Kiessling W (2023). Response of siliceous marine organisms to the Permian-Triassic climate crisis based on new findings from central Spitzbergen, Svalbard. *Paleoceanography and Paleoclimatology, 23*(12), e2023PA004766, https://doi.org/10.1029/2023PA004766

Beaty B, Foster WJ, Zuchuat V, Moller SR, Buchwald SZ, Brooks H, Rauzi S, Isson T, Planke S, Rodríguez-Tovar FJ, Senger K, Planavsky N, Tarhan L (2025). Bioturbation shapes marine biogeochemical cycling following the end-Permian mass extinction in northern Pangea. *Geobiology, 23*(5), e70032, https://doi.org/10.1111/gbi.70032

Karapunar B, Wang X, Frank AB, Gürsoy M, Buchwald SZ, Gómez Correa MA, Liu Z, Xu X, Meng L, Demir D, Koşun E, Foster WJ. Environmental and ecological changes across the Permian–Triassic transition in Türkiye: Integrating virtual outcrop models and new fieldwork data. *In review at The Depositional Record. Preprint available at: https://doi.org/10.31223/X5KQ9B*

Frank AB, Karapunar B, Grasby SE, Koşun E, Lahajnar N, Gómez Correa MA, Buchwald SZ, Metzke M, Foster WJ. Assessing the role of anoxia as a potential extinction driver in the shallow marine Neotethys during the Permian–Triassic mass extinction. *In review at Chemical Geology.*

Karapunar B, Wolniewicz A, Romano C, Ozsvárt P, Rochín-Bañaga H, Kustatscher E, Buchwald SZ, Galasso F, Donald D, López-Arbarello A, Prinoth H, Bernardi M, Foster W. New insights into the extinction and recovery of marine vertebrates across the Permian–Triassic mass extinction event in the Dolomites, Southern Alps, Italy. *In review at the Journal of Vertebrate Paleontology. Preprint available at: https://doi.org/10.1101/2025.08.23.671916*

Ozsvart P, Foster WJ, Asatryan G, Buchwald SZ, Gómez Correa MA, Mosociova T, Zajzon N. Exceptional preservation and unexpected diversity of radiolarians in the aftermath of the end-Permian mass extinction. *Submitted to Palaeontology.*

II Presentations and conference participations

I attended five international scientific conferences, where I presented the status of my research in short talks.

Buchwald SZ, Birgel D, Pei Y, Steinkrauss R, Senger K, Peckmann J, Foster WJ. Insights and perspectives from lipid biomarkers from the Permian/Triassic boundary in Svalbard. *Across the End Permian "Great Extinction": From Field Studies to Scientific Results*, Lausanne, Switzerland (talk). 2023.

Buchwald SZ, Birgel D, Pei Y, Steinkrauss R, Senger K, Peckmann J, Foster WJ. The microbial lipid biomarker record from the Permian/Triassic boundary in Svalbard. *The 6th International Conference of Palaeogeography*, Nanjing, China (talk). 2024.

Buchwald SZ, Birgel D, Pei Y, Frank AB, Gómez Correa MA, Mosociova T, Senger K, Peckmann J, Foster WJ. Molecular fossils from the Barents Shelf across the Permian/Triassic boundary in Svalbard. *Annual Meeting of the Palaeontological Associaton*, Erlangen, Germany (talk). 2024.

Buchwald SZ, Birgel D, Pei Y, Frank AB, Gómez Correa MA, Mosociova T, Senger K, Peckmann J, Foster WJ. The lipid biomarker record across the Permian/Triassic boundary in Svalbard. *The 10th International Conference on Arctic Margins*, Bremen, Germany (talk). 2025.

Buchwald SZ, Birgel D, Kustatscher E, Prinoth H, Galasso F, Karapunar B, Frank AB, Gómez Correa MA, Peckmann J, Foster WJ. Lipid biomarkers record marine and terrestrial ecosystem responses across the Permian–Triassic mass extinction in the Dolomites (Italy). *International workshop on Mesozoic-Palaeogene hyperthermal events & fifth IGCP739 workshop*, Nanjing, China (talk). 2025.

1. Introduction

1.1. The Permian–Triassic mass extinction

1.1.1 Biotic response

The Permian–Triassic mass extinction, which occurred approximately 252 million years ago, was the most severe of the 'big five' mass extinction events of the Phanerozoic. The estimated duration of the extinction event is very short within only 61 kyr ± 48 ka as reconstructed from the sedimentary record in South China (Burgess et al., 2014; Y. Wang et al., 2014), but affected both marine and terrestrial ecosystems. In the marine realm, 81% of the species are estimated to have gone extinct (Stanley, 2016). Due to a more incomplete record, the consequences of the mass extinction event in terrestrial ecosystems are more challenging to infer. However, estimates suggest that 89% of terrestrial tetrapod genera have gone extinct (Benton & Newell, 2014), and also the terrestrial flora has experienced a major compositional restructuring from gymnosperm forests and *Glossopteris*-dominated assemblages to mainly herbaceous plants and lycophytes (e.g., Hermann et al., 2011; Hochuli et al., 2010). However, the severity of the impact of the extinction event on terrestrial plants remains disputed (Nowak et al., 2019).

The Permian–Triassic mass extinction was selective, with substantial taxonomic turnover in surviving groups such as ostracods and bivalves (e.g., Foster et al., 2024; Gliwa et al., 2021; Prinoth & Posenato, 2023). Furthermore, extinction selectivity occurred not only on the taxonomic-level, but on certain ecological or physiological traits. For example, benthic, non-mobile taxa, that were unable to buffer against changes in ocean chemistry, suffered greater losses in species richness than other groups (Clapham & Payne, 2011; Foster et al., 2023; Knoll et al., 2007a).

While such extinction patterns can be investigated when micro- and macrofossil assemblages are well-preserved, the effect of deteriorating environmental conditions on the microbial community during the Permian–Triassic environmental crisis can be challenging to observe directly. Microbes are important members of marine ecosystems by providing diverse ecosystem services, with photoautotrophic microbes at the base of the food web supplying energy and nutrients to higher

trophic levels, or by mediating several major elemental cycles such as the carbon, phosphorous or nitrogen cycles (e.g., Arrigo, 2005; Karl, 2014; Pajares & Ramos, 2019). Hence, understanding the effect of the Permian–Triassic environmental crisis on the aquatic microbial community is crucial for our understanding of the consequences of major environmental perturbations.

An obvious change in the rock record, indicative of an effect of the Permian–Triassic environmental crisis on the marine microbial community, is the widespread appearance of thick microbialites following the mass extinction event. Microbialites occurring on paleotropical carbonate platforms in the Tethys Ocean (Kershaw et al., 2012) may have been able to proliferate due to reduced metazoan grazing pressure in the extinction aftermath (Foster et al., 2020; Kershaw et al., 1999). When formed by oxygenic cyanobacteria, these microbial mats are hypothesized to have also directly affected extinction dynamics by providing oxygenated refugia for heterotrophic benthic organisms, such as ostracods, to survive on an otherwise potentially anoxic sea floor (Forel et al., 2013). However, subsequent studies showed that the observed co-occurrence of microbial mats and ostracods was possibly a taphonomic signal (Wan et al., 2021).

Due to persisting unfavorable environmental conditions in the Early Triassic, ecosystem recovery after the mass extinction took exceptionally long, and biodiversity did not reach pre-extinction species richness until the Middle or Late Triassic in most regions (Benton & Twitchett, 2003; Chen & Benton, 2012; Foster & Sebe, 2017; Song et al., 2018). Compositionally, however, the fauna never recovered towards the pre-extinction community structure, but rather transitioned from the Paleozoic into the Mesozoic evolutionary fauna (Sepkoski, 1981), which led to the interpretation that ecosystems did not recover at all, but rather record a taxonomic and functional restructuring following the mass extinction event (Jablonski & Edie, 2025).

1.1.2 Causes and drivers of the extinction event

The Permian–Triassic mass extinction coincided with the emplacement of the Siberian Traps Large Igneous Province (e.g., Burgess et al., 2017; Burgess & Bowring, 2015; Reichow et al., 2009). Igneous deposits from the Siberian Traps cover an area of 2.5 million km^2 in Siberia today (Fedorenko et al., 1996), while reconstructions suggest that they extended over 5 million km^2 prior

to erosion during the initial deposition (e.g., Augland et al., 2019; Reichow et al., 2009). Several phases of volcanic activity were recognized with the majority of deposits being emplaced within a period of approximately one million years (Burgess et al., 2014, 2017). During this period, up to 36,000 gigatons of carbon (Gt C) (Cui et al., 2021) or > 100,000 Gt CO_2 (Svensen et al., 2009) and other greenhouse gases were ejected into the atmosphere, causing a several-fold increase in atmospheric pCO_2 (Joachimski et al., 2022; Wu et al., 2021). In addition, toxic substances like heavy metals (Bond & Grasby, 2017) were released, that dispersed as fly ash over thousands of kilometers, potentially globally (Grasby et al., 2011).

Due to the temporal correlation of the eruption of the Siberian Traps, and especially the initial emplacement of sills intruding into organic-rich sedimentary rocks and evaporites, and the mass extinction (Burgess et al., 2017), a causal relationship between mega-scale volcanism and the mass extinction has been hypothesized (e.g., Grasby & Bond, 2023). Most commonly, the ejection of vast amounts of CO_2 is thought to have induced the 'deadly trio of carbon dioxide' in marine ecosystems, encompassing (1) thermal stress causing high absolute temperatures and a sea surface temperature increase of 8-10°C (Gliwa et al., 2022; Joachimski et al., 2012; Sun et al., 2012) at a high rate of up to 1°C/kyr (Song et al., 2021); (2) sea floor deoxygenation combined with the expansion of oceanic oxygen minimum zones (Brennecka et al., 2011; Lau et al., 2016; Takahashi et al., 2021); (3) and ocean acidification (Clarkson et al., 2015; Hinojosa et al., 2012; Payne et al., 2010). However, several other environmental perturbations are frequently hypothesized to have contributed to the severity of the mass extinction event, including increased heavy metal loading in the environment (Grasby et al., 2013, 2017; Shen et al., 2023), which, if present in a bioavailable form, would have had toxic effects on organisms (Galasso et al., 2025), or changes in nutrient availability (Foster et al., 2024; Müller et al., 2022; Schobben et al., 2020). Furthermore, the terrestrial ecosystem may have been additionally affected by a depletion of ozone (Benca et al., 2018) as well as enhanced soil erosion (Sephton et al., 2005), wildfires (Jiao et al., 2024; Nabbefeld et al., 2010a; Song et al., 2022), and acidic rain (Sephton et al., 2015). Which of these drivers or which combination of drivers acted to which extent on local or regional

ecological communities is thus far not well constrained, and there are only few studies that directly link the impact of extinction drivers on ecological communities (Foster et al., 2024).

Additionally, there is an ongoing debate about the timing of the environmental deterioration, with some studies suggesting that the onset of several of the environmental conditions often linked to the mass extinction pre-date the extinction event by several thousand up to hundreds of thousands of years, as for example rising global temperatures (Gliwa et al., 2022; Sun et al., 2018). Others have argued contrarily for rapid warming post-dating the extinction (Chen et al., 2016), highlighting the need for constraining both the timing and causes of the extinction more precisely.

1.2. Lipid biomarkers

1.2.1 Lipid biomarker preservation and alteration

Organic macromolecules enabling the investigation of microbial communities are so-called biomarkers. They can be preserved over geological time scales in sediments, rocks, fossils and oils after the degradation or fossilization of most biological material (Luo et al., 2019; Peters et al., 2005; Summons et al., 2022) with varying preservation potential of different groups of organic macromolecules. Nucleic acids such as RNA and DNA are usually degraded very quickly in the environment, but under preferential conditions, DNA can be preserved over several thousand up to hundreds of thousands of years (e.g., Armbrecht, 2020; Capo et al., 2022). Proteins can be preserved over longer timescales up to a few million years (Demarchi et al., 2022; Stolarski et al., 2023), with the oldest protein sequence extracted to date being 21-24 million years old (Paterson et al., 2025). In contrast, the hydrocarbon skeletons of lipids, mainly derived from cell membranes and photosynthetic pigments, are among the most resistant macromolecules withstanding degradation. This property makes them suitable as molecular fossils over even longer geological timescales. Among the oldest molecular fossils are lipid biomarkers derived from green and purple sulfur bacteria extracted from rocks as old as 1.6 billion years (Brocks et al., 2005).

Lipid biomarkers preserve information about the original molecule and the organisms that synthesized them with various degrees of specificity. Lipid biomarkers usually provide a relatively low taxonomic resolution and are often rather indicative of certain metabolic activities, such as anoxygenic photosynthesis or methane oxidation (e.g., Brocks & Grice, 2011; Luo et al., 2019). They can thereby complement the micro- and macrofossil record by recording the metabolic activity of their microbial producers. In addition, lipid biomarkers can be used to infer about the paleoenvironmental conditions, for instance, the depositional environment and ocean redox state, by tracing both the biogeochemical processes mediated by their producers and the composition of the microbial paleo-community itself (e.g., Luo et al., 2019; Peters et al., 2005; Summons et al., 2022).

The preservation of lipid biomarkers is highly selective. If the biomass of the source organism is high and the environmental conditions are favorable, the preservation of a signal is more likely. In an oxic environment, most organic matter is recycled rapidly, whereas anoxic or euxinic environments may provide more suitable conditions for organic matter preservation (Canfield, 1994). Molecules originated from communities that inhabited passive continental margins, marine and continental evaporitic environments, deltas and estuarine systems are best represented in the lipid biomarker record as these depositional environments are less exposed to erosion, uplift, subduction or other forms of destruction (Knoll et al., 2012). Also, in sulfur-rich environments, sulfide can replace functional groups with C-S-cross-linkages, thereby enhancing organic matter preservation in recalcitrant macromolecules, that can be cleaved to release the sulfur-bound compounds (e.g., Sabino et al., 2021; Sinninghe Damsté et al., 1999, 2007; Wang et al., 2024).

Although lipids are more stable than other organic molecules, they are exposed to biodegradation. Among the various lipid compounds, some are preferentially degraded, while others are more resistant, resulting in a semi-sequential succession of biodegradation (Wenger et al., 2002). For example, normal alkanes (*n*-alkanes) are more susceptible to microbial degradation and shorter *n*-alkanes are degraded faster, while other compounds such as hopanoids or steroids degrade only under more intense microbial activity (Soman et al., 2024; Wenger et al., 2002). With proceeding biodegradation, a “baseline hump”, the so-called “unresolved complex mixture”

(UCM), is becoming increasingly prominent in chromatograms, which consists of bio-resistant compounds (Peters et al., 2005).

Since lipids become defunctionalized during early diagenesis (Brocks & Grice, 2011), usually only the hydrocarbon fraction is preserved in organic matter from the Permian–Triassic transition. With hydrocarbons, the source rock depositional environment, biodegradation and maturation can be analyzed (Peters et al., 2005). For example, thermal maturation of organic matter will result in predictable stereochemical or structural modifications of lipid biomarkers. While often a specific stereoisomer is biologically produced during biosynthesis, samples from the geological past often contain a mixture of stereoisomers of the same precursor molecule. The analysis of such isomers can be deduced by calculating empirically derived proxies, such as the homohopane index or the methylphenanthrene index (Cassani et al., 1988; Mackenzie et al., 1984; Peters et al., 1996; Radke et al., 1982). Such proxies allow for the reconstruction of the thermal history of a sample, which is an important measure to determine to which degree the preservation of organic matter and the primary lipid inventory is affected in their interpretative value.

1.2.2 Reconstruction of paleo-communities and environmental conditions

Apart from recording post-depositional processes, certain lipid biomarkers are source specific, and hence inform about the composition of the ecological community, even in deep-time. For example, steroids are membrane lipids that are, with only very few exceptions, produced by eukaryotes for regulating the fluidity of their cell membrane (e.g., Dufourc, 2008). The alkylation pattern of the side-chain is thereby principally characteristic for animal, plant or fungal membrane physiology (Knoll et al., 2007b; Volkman, 2003). In contrast, hopanoids ($C_{30–35}$ pentacyclic triterpenoids) are hypothesized to have a similar physiological function as steroids, but they are only synthesized by bacteria (Sinninghe Damsté et al., 2017; Welander et al., 2010). Moreover, unlike steroids that are required by all eukaryotes for correct membrane functioning, hopanoids are not universally required by bacteria (Pearson et al., 2007). Their absence must, therefore, be interpreted with caution. However, the ratio of the defunctionalized and saturated degradation products of steroids and hopanoids, the sterane/hopane ratio, has been applied in studies across

the Permian–Triassic transition to infer about the relative abundance of eukaryotes and bacteria in paleo-communities (Cao et al., 2009).

Other lipid biomarkers are less common than steroids and hopanoids, but are more specific. Examples are lipid biomarkers of cyanobacteria, that have been shown to produce high quantities of *n*-heptadecane compared to other *n*-alkanes, as well as accompanying mono-, di- and tri-methylated short-chain alkanes (Coates et al., 2014; Gelpi et al., 1970; Heindel et al., 2018; Plet et al., 2020). These compounds, extracted from Early Triassic microbialites in Turkey and Iran (Heindel et al., 2018), enabled the identification of a cyanobacterial contribution to the build-up of post-extinction microbial mats in association with other microbes such as anoxygenic phototrophic bacteria, sulfate-reducing bacteria, and halophilic archaea. Other characteristic compounds extracted from sedimentary rocks are aryl-isoprenoids or derivatives of aromatic carotenoid pigments such as isorenieratane and chlorobactane (e.g., Koopmans et al., 1996; Summons & Powell, 1987). Their precursor molecules are synthesized by green sulfur bacteria, that inhabit anoxic and sulfidic (euxinic) environments (e.g., Imhoff, 2014; Sousa Júnior et al., 2013). These compounds are, therefore, important for demonstrating the presence of green sulfur bacteria and their required environmental conditions, i.e., photic zone euxinia. Photic zone euxinia has been identified as common environmental stressor in shallow marine ecosystems across the Permian–Triassic transition based on the presence of these biomarkers in Western Australia (Grice et al., 2005a), Svalbard (Nabbefeld et al., 2010b), Turkey (Heindel et al., 2018) or South China (Cao et al., 2009).

Water column redox conditions can also be reconstructed based on the ratio of the two regular isoprenoids pristane (C_{19}-isoprenoid) and phytane (C_{20}-isoprenoid). Both isoprenoids can derive from the degradation of the side-chain of chlorophyll, and are markers for the photoautotrophic community (Didyk et al., 1978). Moreover, early diagenetic processes on chlorophyll are redox-sensitive. Pristane results from the oxidation of the ester bond linking the phytol side chain of chlorophyll and the porphyrin ring, whereas phytane is the product formed under reducing conditions (Luo et al., 2019). Consequently, a ratio of pristane to phytane (Pr/Ph) > 1 indicates deposition in an oxic environment, and Pr/Ph < 1 suggests an anoxic setting (Didyk et al., 1978).

However, pristane and phytane can also originate from other sources, such as the degradation of archaeal membrane di- and tetraether lipids (Rontani & Bonin, 2011; Rowland, 1990; Vandier et al., 2021). Thus, while utilizing pristane and phytane as indicators of photoautotrophs and reconstructing paleo-redox conditions can be informative, a thorough exclusion of significant contribution from Archean sources to the pristane and phytane pool should be conducted.

1.2.3 Limitations of lipid biomarkers

As for all groups of molecular fossils, the lipid biomarker inventory of a sample must be evaluated with caution, especially in the deep-time record, to avoid misinterpretation caused by diagenetic or thermal alteration. Generally, the likelihood of functional groups and unsaturated carbon bonds being preserved decreases with increasing age of the material, although it is rather a function of thermal maturation than age (Brocks & Grice, 2011). From Permian and Triassic sedimentary rocks, only saturated aliphatic hydrocarbons and apolar aromatic compounds are preserved, which prevents the analysis of compounds containing functional groups, such as fatty acids or ketones. This loss of information is often challenging, especially for the phylogenetic assignment of the extracted lipid biomarkers. The necessity of a manual identification and curation of peaks in chromatograms, that can also be co-eluted or have only very low intensities due to low quantities of lipid biomarkers in organic-lean or old material, further contributes to some uncertainty and exacerbates reproducibility.

Furthermore, some groups of lipid biomarkers are not preserved at all over long geological timescales, which limits the possibilities of compositional or environmental interpretations solely based on lipid biomarkers. An example are the commonly reported glycerol dialkyl glycerol tetraethers (GDGTs) in modern environments, a group of archaeal membrane lipids, that show a temperature-dependent cyclisation pattern of their isoprenoid side-chains, which can be used for paleo-temperature reconstructions in marine settings when calculating the TEX_{86} proxy (Schouten et al., 2002). Additionally, the abundance of branched GDGTs relative to crenarchaeol can be used to reconstruct the terrestrial organic matter input into aquatic ecosystems by calculating the Branched and Isoprenoid Tetraethers (BIT) index (Hopmans et al., 2004), and terrestrially derived

branched GDGT were used as proxies for soil pH (Peterse et al., 2012). However, GDGTs are usually not preserved in material older than the Early Jurassic (Robinson et al., 2017), and even their degradation products, biphytanes, are only poorly preserved in Paleozoic and Mesozoic samples (Bentley et al., 2022). Another example is IP_{25} (Ice Proxy with 25 carbon atoms), that is utilizing a highly branched isoprenoid alkene synthesized by sea ice associated diatoms to reconstruct past sea ice distribution (Belt et al., 2007), but its preservation is restricted to the Quaternary (Stein & Fahl, 2013), caused by the loss of the specific double bonds over time.

Additional challenges in the application of lipid biomarker studies are the knowledge gaps with respect to the assignment of lipid biomarkers extracted from ancient organic matter to specific biological sources. The attribution of a lipid biomarker to a taxonomic group or a metabolic pathway depends on information about the association of the respective biomarker to this group or pathway in modern organisms. Yet, only a fraction of organisms, especially microorganisms, are investigated for their lipid inventory, and studies often rely on laboratory isolation and culturing of the organisms (Brocks & Grice, 2011). However, the vast majority of microorganisms is, thus far, uncultured or unculturable (e.g., Lloyd et al., 2018; Staley & Konopka, 1985), hence only sparse information exists on their physiology and lipid inventory.

Some of these limitations may be overcome in the future, for example, if more detailed knowledge about precursor molecules and the lipid inventory in extant organisms will be gained through culture-independent techniques like metagenomic or metabolomic analyses (e.g., Kamble et al., 2020; Segers et al., 2019), and the estimation of evolutionary rates in biosynthetic pathways enable an assignment to an ancient biological source (e.g., Ho & Duchêne, 2014). Other challenges, such as the diagenetic defunctionalization of organic molecules or low quantities of lipids in millions of years old material, will remain. Hence, lipid biomarker analysis is a practical tool to investigate the microbial community composition and track their metabolic activity in deep-time; however, it is especially meaningful when complemented by independent signals such as the fossil and sedimentary record or other geochemical proxies.

2. Thesis objectives

Despite decades of work, the timing of the Permian–Triassic mass extinction and the significance of the numerous proposed causes for the event remain debated. Especially the role of microorganisms, particularly the photoautotrophic community, in shallow marine ecosystems is not well constrained.

This thesis aims to investigate the response of shallow marine ecosystems to severe and complex environmental perturbations across the Permian–Triassic transition, and how the microbial community structure was affected, emphasizing the community of primary producers. By analyzing newly derived lipid biomarker datasets from Permian–Triassic sedimentary successions across paleolatitudes (Appendix A1), this research will address the following research questions:

1. Do lipid biomarker signatures associated with the Permian–Triassic environmental crisis vary with paleolatitude, and what do these patterns reveal about the variability in the phytoplankton community composition and primary productivity?

2. What are the baseline redox conditions prior to the Permian–Triassic environmental crisis, and is anoxia the main extinction driver across paleolatitudes?

3. Did the microbial community respond to late Permian environmental stress culminating in the mass extinction event, and is a recovery of the microbial ecosystem recorded by molecular fossils?

Together, the three studies herein provide new insights into environmental baselines and stressors, as well as microbial responses, that shaped shallow marine ecosystems before, during and after the Permian–Triassic mass extinction event.

3. Overview of the manuscripts

This thesis contains three manuscripts. Manuscript I is accepted for publication in *AGU Advances*. Manuscripts II and III are submitted to *Paleoceanography and Paleoclimatology* and *Biogeosciences*, respectively. For this thesis, the formatting of the accepted or submitted articles was modified for consistency within this thesis. The following provides an overview of the content and implications of the three studies, the manuscripts and related Supplementary Material.

Manuscript I: Phytoplankton blooms on the Barents Shelf, Svalbard, associated with the Permian–Triassic mass extinction

---

Accepted in AGU Advances

This manuscript focuses on two lipid biomarkers, C_{33}-*n*-alkylcyclohexane (C_{33}-*n*-ACH) and its pseudohomologs, and phytanyl toluene, that are recognized to be enriched in the post-extinction interval at several Permian/Triassic boundary sections in Svalbard. This record decouples the lithological changes at the extinction horizon in Svalbard from biotic responses to environmental stress across the Permian–Triassic environmental crisis by extending the sampling interval of previous studies, thereby covering pre- and post-extinction strata recording a similar depositional environment. Additionally, late Permian and Early Triassic samples from the Dolomites (Italy), South China and the Taurus Mountains (Turkey) were analyzed, which combined provide a perspective on the global distribution of these biomarkers.

The analysis revealed that the content of C_{33}-*n*-ACH and phytanyl toluene was increased in higher paleolatitude ecosystem (Svalbard) following the extinction event, whereas it was low in lower paleolatitude settings, demonstrating heterogeneous ecosystem responses during the environmental crisis. Furthermore, this study challenges previous hypotheses regarding the sources of C_{33}-*n*-ACH and phytanyl toluene, and proposes an alternative link to oxygenic phytoplankton, with implications for marine ecosystem dynamics, including primary productivity, during a major climate crisis. For the first time, also the diagenetic degradation products of C_{33}-*n*-ACH were quantified, expanding its use as an extinction marker in settings where only these degradation products are preserved.

These findings enhance the understanding of ecosystem responses during the Permian–Triassic environmental crisis across paleolatitudes, contributing to three key areas:

(1) The global distribution of molecular fossils that mark the Permian–Triassic mass extinction event in the geological record;

(2) Regional differences in marine microbial community responses to severe environmental changes;

(3) A potential explanation for the altered latitudinal biodiversity gradient following the mass extinction, as enhanced primary productivity may have stabilized higher latitude marine food webs at higher latitudes.

The finding of regional post-extinction phytoplankton blooms is also relevant for understanding how marine ecosystems respond to extreme environmental stress. This study thereby contributes to ongoing discussions on the spatial variability in extinction survival and recovery dynamics, such as the hypothesis of higher-latitude settings providing refugia for some taxa during and after severe global environmental perturbations, and emphasizes the role of environmental conditions in shaping ecosystem resilience following global environmental crises.

Manuscript II: Reconstructing environmental and microbial ecosystem changes across the Permian–Triassic mass extinction at Lusitaniadalen, Svalbard

---

Submitted to *Paleoceanography and Paleoclimatology*

In this study, a multi-proxy approach was applied to reconstruct both the environmental conditions and their effect on the microbial, primarily photosynthetic community, in a shallow marine ecosystem across the Permian–Triassic mass extinction in Svalbard. It is the first study from a higher paleolatitude region that also includes an extended pre- and post-extinction interval, which allowed for the establishment of a baseline for paleoenvironmental conditions, and enables a reassessment of environmental changes across the extinction event. This approach offers a new perspective on the widely hypothesized role of expanding anoxia and photic zone euxinia as the primary drivers of the Permian–Triassic mass extinction.

Using both enrichment patterns of redox-sensitive trace metals and lipid biomarkers, the record reveals an intense, but relatively short-lived anoxic interval across the extinction horizon.

However, episodes of fluctuating redox-conditions prior to the extinction event are also recorded, yet without major ecosystem collapse or a distinct response of the phototrophic community, suggesting anoxia not to be the sole driver of extinction. Furthermore, a pronounced post-extinction increase in the content of chlorophyll-derived biomarkers indicates a restructuring of the photoautotrophic community associated with the extinction event, and point towards regionally enhanced primary productivity.

The new data advances the understanding of ecosystem changes and responses during the Permian–Triassic environmental crisis by highlighting:

(1) the importance of establishing ecosystem baseline conditions to assess the impact of environmental change on paleocommunities;

(2) the spatial heterogeneity of oxygen availability and the necessity of evaluating the regional environmental context before inferring extinction drivers;

(3) a restructuring of the microbial community following the Permian–Triassic mass extinction, with an increase in primary productivity that may reflect regional phytoplankton blooms due to altered nutrient cycling in the wake of terrestrial and marine ecological collapse.

These findings underscore the complex interplay of environmental variables during episodes of rapid environmental change, especially with respect to the heterogeneous response of paleoproductivity and paleoredox evolution during major biotic crises.

Manuscript III: Molecular fossils record marine and terrestrial ecosystem changes prior to and across the Permian–Triassic mass extinction in the Dolomites (Italy)

Submitted to *Biogeosciences*

This study analyzes the lipid biomarker inventory from two sites on a late Permian shallow marine carbonate ramp in northern Italy, thereby providing a nuanced perspective on microbial ecosystem dynamics and the environmental conditions along a water depth gradient. To investigate whether the microbial community, with an emphasis on the community of photoautotrophs, responded to environmental conditions that were previously hypothesized to deteriorate preceding the Permian–Triassic mass extinction event by several hundred thousand years, the hydrocarbon inventory from the late Permian sedimentary record was analyzed. It therefore expands on the sparse Permian–Triassic lipid biomarker record from this region, and provides new insights into the dynamics of environmental stress.

A change in the lipid biomarker inventory associated with the environmental conditions that contributed to the mass extinction event was identified, such as peak abundances of polycyclic aromatic hydrocarbons (PAHs) derived from the combustion of organic material coinciding with the extinction event. This increase was identified at both the shallower and the deeper site due to the aerial transport of PAHs into the marine environment.

In contrast, the abundance of other redox-sensitive and source-specific biomarkers rather responds to previously identified third-order transgressive-regressive cycles in the late Permian, which affected the shallower site, that potentially became episodically very restricted or even subaerially exposed, more strongly than the deeper site. However, these sea level changes as the main driver of variability in the lipid biomarker inventory at the shallower site compared to more stable conditions at the deeper site indicate a naturally more stressed shallower environment, which is not related to environmental stress associated to the Permian–Triassic environmental crisis.

These results highlight the need of a careful evaluation when inferring extinction dynamics and the identification of extinction drivers, as regional or even local baseline conditions can differ notably between sites, with ecological communities adapted to these conditions being differently affected by different environmental stressors of the Permian–Triassic environmental crisis.

Manuscript I

Buchwald SZ, Birgel D, Senger K, Mosociova T, Pei Y, Zuchuat V, Tarhan LG, Frank AB, Galasso F, Gómez Correa MA, Koşun E, Karapunar B, Wang X, Kustatscher E, Prinoth H, Lahajnar N, Steinkrauss R, Peckmann J, Foster WJ. Phytoplankton blooms on the Barents Shelf, Svalbard, associated with the Permian–Triassic mass extinction. *Accepted in AGU Advances.* Preprint: https://www.doi.org/10.22541/essoar.174558961.14311943/v1

SZB conceptualized the study; SZB curated the data and performed the formal analysis; SZB, WJF and WX acquired funding; SZB, KS, TM, YP, VZ, LGT, FG, MAGC, EK, BK, XW, EK, HP, ABF and WJF were involved in planning and conducting fieldwork; KS, JP, DB and WJF provided institutional resources; SZB and RS conducted the lipid biomarker lab work; NL provided TOC data; SZB wrote the original draft; all co-authors were involved in reviewing and editing; SZB led the review process.

Phytoplankton blooms on the Barents Shelf, Svalbard, associated with the Permian–Triassic mass extinction

S. Z. Buchwald[1], D. Birgel[1], K. Senger[2], T. Mosociova[3], Y. Pei[4], V. Zuchuat[5], L. G. Tarhan[6], A. B. Frank[1], F. Galasso[1], M. A. Gómez Correa[1], E. Koşun[7], B. Karapunar[8], X. Wang[9], E. Kustatscher[10], H. Prinoth[11], N. Lahajnar[1], R. Steinkrauss[1], J. Peckmann[1], and W. J. Foster[1]

[1]Department of Earth System Sciences, University of Hamburg, Hamburg, Germany

[2]Department of Arctic Geology, University Centre in Svalbard, Longyearbyen, Norway

[3]Department of Geosciences, University of Oslo, Oslo, Norway

[4]State Key Laboratory of Geomicrobiology and Environmental Changes, China University of Geosciences, Wuhan, China

[5]CSIRO Mineral Resources, Kensington, WA, Australia

[6]Department of Earth and Planetary Sciences, Yale University, New Haven, USA

[7]Department of Geological Engineering, Akdeniz University, Antalya, Türkiye

[8]School of Earth and Environment, University of Leeds, Leeds, United Kingdom

[9]Institute of Sedimentary Geology, Chengdu University of Technology, Chengdu, China

[10]Department of Natural History, Tirolean State Museums, Hall in Tirol, Austria

[11]Museum Ladin Ciastel de Tor, San Martino in Badia, Italy

Corresponding author: Stella Zora Buchwald (stella.buchwald@uni-hamburg.de)

Key Points:

- On the Barents Shelf, uppermost Permian and Lower Triassic sedimentary rocks record peak C_{33}-*n*-alkylcyclohexane and phytanyl toluene content
- C_{33}-*n*-alkylcyclohexane from phytoplankton indicates blooms of certain primary producers during the Permian–Triassic environmental crisis
- Phytanyl toluene and C_{33}-*n*-alkylcyclohexane may be derived from organisms occupying a similar ecological niche

Abstract

Mid- to higher-latitude shallow marine environments are suggested to serve as refugia for organisms during intervals of rapid environmental change associated with hyperthermals. To understand the role of these environments during hyperthermals, we herein investigate the Permian–Triassic environmental crisis, which led to the most severe mass extinction event in the Phanerozoic. Our analysis of siliciclastic deposits from the Boreal Ocean from Lusitaniadalen, Svalbard, reveals a distinct increase of the lipid biomarkers C_{33}-*n*-alkylcyclohexane (C_{33}-*n*-ACH) and phytanyl toluene following the extinction event. This increase does not appear to reflect facies change. Rather, it coincides with the extinction horizon, and persists into the lowermost Triassic (Griesbachian). Our findings suggest that neither C_{33}-*n*-ACH nor phytanyl toluene are linked to short periods of photic zone euxinia recorded at Lusitaniadalen, but rather are derived from a specific group of phytoplankton. This indicates that higher-latitude ecosystems may have supported regional blooms of unknown primary producers after the Permian–Triassic mass extinction, thus explaining the selective survival of some marine organisms. We also identify (albeit in lower abundance) C_{33}-*n*-ACH and its pseudohomologs in northern Italy, which is the first report of *n*-ACHs in the tropical Tethys region across the Permian–Triassic transition outside of South China, highlighting the wide paleogeographic distribution of this biomarker. Phytanyl toluene, however, is found exclusively in deposits recording higher-latitude ecosystems, and is likely linked to organisms occupying a similar ecological niche as the source organism of C_{33}-*n*-ACH in these settings.

Plain Language Summary

Environmental changes can have detrimental effects on marine ecosystems. Studying Earth's history can help us to understand how ecosystems respond to environmental changes. The Permian–Triassic mass extinction, the biggest mass extinction in Earth's history, is linked to rapid environmental changes. Here, we analyze two molecular fossils (lipid biomarkers), C_{33}-*n*-alkylcyclohexane (C_{33}-*n*-ACH) and phytanyl toluene, that are associated with this mass extinction, from samples from different paleolatitudes and paleo-oceans. These biomarkers increase

several-fold in the aftermath of the extinction in higher-latitude settings, such as Svalbard, while we detect only traces of C_{33}-*n*-ACH in tropical settings, if any. Although the organisms producing these biomarkers are unknown, they were likely synthesized by organisms able to survive the harsh environmental conditions during this interval of Earth's history. This is particularly true for higher-latitude ecosystems, which may have experienced less severe environmental stress, such as less extreme (though potentially greater changes in) temperatures, compared to tropical ecosystems. C_{33}-*n*-ACH mirrors patterns of other biomarkers indicative of increased primary productivity during the same time interval, suggesting that it could be another molecule produced by a specific group of phytoplankton. Phytanyl toluene was probably produced by different phytoplankton found in the Boreal Ocean but not the tropical locations.

1 Introduction

Rapid environmental changes can lead to biodiversity crises and mass extinctions. To understand the response of organisms to these changes, plasticity, adaptation or range shifts of modern species or populations can be studied (e.g., Donelson et al., 2019). However, ecosystem responses are highly complex and depend on multiple factors that are challenging to fully capture through laboratory experiments. To better understand the long-term effects of rapid environmental changes on communities, past hyperthermal events can be studied, such as the Paleocene–Eocene Thermal Maximum (PETM) (e.g., McInerney & Wing, 2011) and the Permian–Triassic environmental crisis; the latter triggered the most severe mass extinction in the Phanerozoic, often referred to as the Permian–Triassic mass extinction or end-Permian mass extinction (e.g., Dal Corso et al., 2022; Payne & Clapham, 2012).

During the Permian–Triassic mass extinction, ca. 252 million years ago, approximately 81% of marine species went extinct globally (Stanley, 2016), but extinction patterns and functional diversity were geographically variable (Foster & Twitchett, 2014). The mass extinction event in marine ecosystems is constrained to 60 ± 48 ka in well-dated sections in China (Burgess et al., 2014), and was accompanied by a sharp negative carbon isotope ($\delta^{13}C$) excursion, observed globally (Korte & Kozur, 2010). This $\delta^{13}C$ excursion reflects a perturbation to the carbon cycle,

which remained volatile for the following ca. 500 ka before $\delta^{13}C$ values returned to pre-extinction levels (Burgess et al., 2014). Hence, although the extinction event (i.e., elevation in extinction rates) occurred in a geologically relatively short time interval, the environmental crisis culminating in the mass extinction probably lasted much longer. A variety of environmental factors are hypothesized to have acted as extinction drivers in marine ecosystems, such as global warming (e.g., Gliwa et al., 2022; Joachimski et al., 2012; Schobben et al., 2014) and changes in temperature gradients (Sun et al., 2024), the expansion of oxygen minimum zones (e.g., Cao et al., 2009; Penn et al., 2018; Xiang et al., 2020; Zhang et al., 2020), and changes in nutrient cycling (Grasby et al., 2020; Sun 2024; Sun et al., 2019). Several marine ecosystems are thought to have acted as refugia for marine life during the environmental crisis, such as deep-water thermal refugia (Foster et al., 2023; Godbold et al., 2017). Similarly, modern mid- to high-latitude ecosystems may provide opportunities for equatorial taxa to escape (sub-)tropical thermal stress (Poloczanska et al., 2016). Cool-water ecosystems can, therefore, exhibit characteristic community compositions during past crises. These are reflected in the geological record, e.g., in the aftermath of the Permian–Triassic mass extinction, when the northwestern shelf of Pangea was characterized by a diverse ichnofauna (Beatty et al., 2008) and contained taxa that either migrated to the Boreal Ocean or whose geographic ranges contracted to this ecosystem (Foster et al., 2023; Nakrem & Mørk, 1991), thereby flattening latitudinal diversity gradients in the extinction aftermath (e.g., Beatty et al., 2008; Foster & Twitchett, 2014; Song et al., 2020; Twitchett & Barras, 2004).

While previous studies have focused particularly on biomineralizing micro- and macrofossil communities, this study exclusively investigates molecular fossils (lipid biomarkers), aiming to enhance our understanding of ecosystem responses, particularly among primary producers, to the Permian–Triassic environmental crisis. By assessing the appearance and prevalence of the molecular fossils C_{33}-*n*-alkylcyclohexane (C_{33}-*n*-ACH) and phytanyl toluene, we aim to document differences across paleolatitudes, and determine their environmental significance in different paleo-ocean basins. Our findings therefore offer new insights into the mechanisms underlying ecosystem resilience and recovery after severe environmental perturbations.

2 Materials and Methods

2.1 Geological Setting and Sample Acquisition

The molecular fossil inventories from different Permian–Triassic successions were investigated across paleolatitudes including sites around the Tethys, with a focus on Boreal sites recorded by the sedimentary succession of Svalbard (Fig. 1.1). These deposits are of special interest, because Svalbard has been migrating north from the equator since the Devonian, currently occupying a

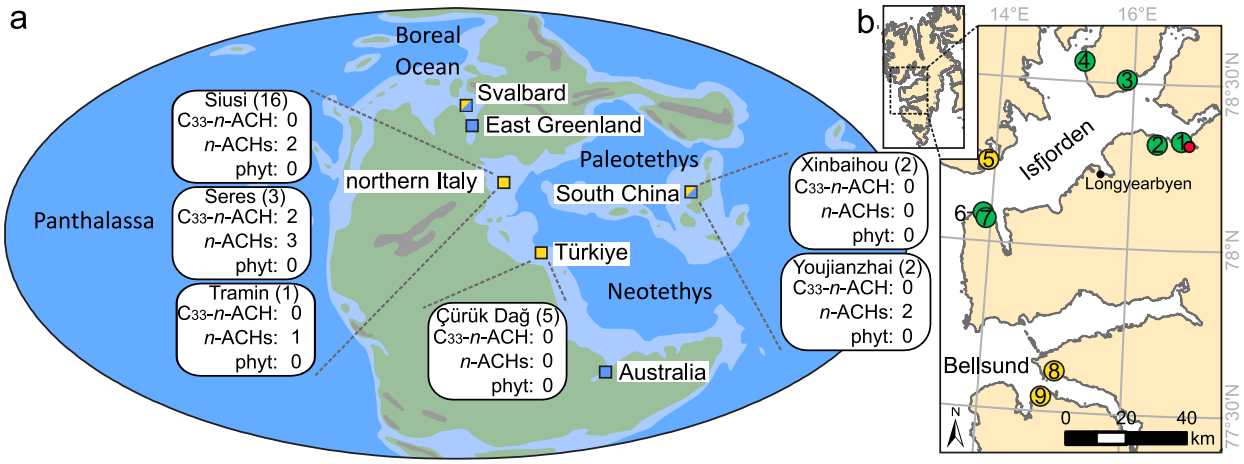

Figure 1.1: *Sample locations. a — Paleogeographic reconstruction of continental configuration at the Permian/Triassic boundary (map modified from Blakey, 2012). Yellow: sections studied here and summary of the findings (number of samples in parentheses after the section's name, and number of samples in which a compound was found is given); n-ACH — n-alkylcyclohexane; phyt — phytanyl toluene; blue: C_{33}-n-ACH findings from other studies (Svalbard: Grotheer et al., 2017; Nabbefeld et al., 2010; East Greenland and Australia: Grice et al., 2005; Hays et al., 2012; South China: Saito et al., 2022; Xie et al., 2017. b — Sampling locations on Spitsbergen, Svalbard (Base map projection: WGS 84/Arctic Polar Sterogeographic); 1: Lusitaniadalen; 2: Ledalen; 3: Høgskulefjellet; 4: Kongressfjellet; 5: Selmaneset; 6: Festningen (Vardebukta); 7: Starostinaksla; 8: Bravaisberget; 9: Reinodden. Green: C_{33}-n-ACH and pseudohomologs detected; yellow: only pseudohomologs of C_{33}-n-ACH detected; Red point next to (1): Deltadalen.*

high-latitude position (74–81°N), whereas it was situated at a paleolatitude of approximately 45°N during the Permian–Triassic transition (Elvevold et al., 2007, Smyrak-Sikora et al., 2025). Due to its location on the Barents Shelf in the Boreal Ocean at the northern margin of Pangea, it was isolated from the warm, equatorial water of the Tethys Ocean, thus representing a relatively cold-water shallow-marine ecosystem (e.g., Beauchamp & Baud, 2002; Worsley, 2008) contrasting with Permian–Triassic sections recording tropical settings in the Paleo- and Neotethys (Fig. 1.1a). On the main island of Svalbard's archipelago, Spitsbergen, the strata are tilted, folded and thrusted in the West Spitsbergen Fold and Thrust Belt (Dallmann et al., 1993), which represents a more proximal part of the shelf at that time (Mørk et al., 1982). In contrast, the Permian–Triassic sedimentary successions in the more distal part of the shelf in central Spitsbergen are horizontally bedded and have undergone only small to moderate thermal alteration (Olaussen et al., 2023).

A key section for studying the Permian–Triassic transition from multiple perspectives is Lusitaniadalen (Fig. 1.1b). The Kapp Starostin Formation and the lowermost overlying Vikinghøgda Formation record the Changhsingian, whereas most of the Vikinghøgda Formation represents the Early Triassic (Mørk et al., 1999; Zuchuat et al., 2020). We place the Kapp Starostin/Vikinghøgda formation boundary according to the definition by Nagy et al. (2025) on top of the last glauconitic sandstone bed. Due to the scarcity of macro- and microfossils in uppermost Kapp Starostin Formation, the extinction horizon at Lusitaniadalen was previously determined based on the absence of complex bioturbation in strata overlying the last glauconitic sandstone bed (Foster et al., 2023; Nabbefeld et al., 2010; Uchman et al., 2016). The transition from the last glauconitic sandstone to the very fine-grained sandstones of the Vikinghøgda Formation also records an abrupt negative organic carbon isotope excursion at Lusitaniadalen (Nabbefeld et al., 2010), that has been observed globally to coincide with the extinction event (e.g., Cao et al., 2009; Sephton et al., 2005; Xie et al., 2007). The Permian/Triassic boundary, however, is not well-constrained in Lusitaniadalen, but in Deltadalen, the adjacent valley to the east (Fig. 1.1b), it is placed approximately 2.40 m above the last glauconitic sandstone bed based on a tephra layer dated to 252.13 ± 0.62 Ma, deposited just above the local First Appearance Datum of the conodont *Hindeodus parvus* (Zuchuat et al., 2020).

Thirty-two samples were collected at Lusitaniadalen, Svalbard, from the succession of alternating bioturbated mudstones and silica-rich fine-grained sandstones (-41.51 m to -30.58 m below the formation boundary) and from the uppermost glauconitic sandstone beds (-0.86 m to -0.23 m) of the Kapp Starostin Formation prior to the extinction, as well as from the overlying laminated siltstones and very fine-grained sandstones from the post-extinction interval of the Vikinghøgda Formation (0.51 m to 29.70 m), in which abundant concretionary horizons can be found. Samples were collected from unweathered outcrop exposures and wrapped in aluminum foil to avoid contamination. In particular, we focused on intervals of the Kapp Starostin Formation below the glauconitic sandstones, as the bioturbated mudstones deposited here represent conditions prior to the Permian–Triassic environmental crisis, but are lithologically comparable to the lowermost Vikinghøgda Formation. This enabled us to better account for a potential bias in the biomarker inventory introduced by the lithological change at the extinction horizon. In addition to Lusitaniadalen, eight other sections in western and central Spitsbergen were sampled to identify regional patterns in biomarker signals (Fig. 1.1b). Lastly, we compared data from Spitsbergen with results from Tethyan sections, including data from northern Italy (western Paleotethys), the Great Bank of Guizhou in South China (eastern Paleotethys), and the Taurus Mountains in Türkiye (western Neotethys) (Fig. 1.1a). These tropical sections are predominantly carbonate successions with thick microbialites formed in the post-extinction interval in Türkiye and South China. A more detailed description of the geological setting in northern Italy (Broglio Loriga et al., 1990; Farabegoli et al., 2007; Groves et al., 2007; Horacek et al., 2010; Massari et al., 1994; Noé, 1987; Posenato, 2010; Prinoth & Posenato, 2023), South China (Foster et al., 2018, 2019; Lehrmann et al., 1998, 2001, 2003, 2005, 2007; Payne et al., 2006), and Turkiye (Angiolini et al., 2007; Altıner & Zaninetti, 1980; Baud et al., 2005, 2007; Crasquin-Soleau et al., 2002, 2004; Lys & Marcoux, 1978; Marcoux & Baud, 1988; Özgül 1984, 1997; Richoz, 2006; Şahin & Altıner, 2019; Stampfli et al., 1991) can be found in the Supporting Information.

2.2 Sample Preparation and Data Processing

We analyzed molecular fossils from both carbonate (23 samples) and siliciclastic (66 samples) settings. To extract molecular fossils from carbonates (the majority of the samples from the

Tethys), the surfaces were cut off and samples were cleaned three times with acetone to remove any contaminants from the surfaces prior to being dissolved by slowly pouring 10% hydrochloric acid onto approximately 1 cm^3-sized pieces following the procedure by Birgel et al. (2006). The siliciclastic samples were cleaned with acetone and then manually powdered in an agate mortar. The total lipid extract was retrieved by extracting the samples four times with dichloromethane:methanol (3:1, v:v) for 15 min in an ultrasonic bath, and separate them into maltenes (*n*-hexane soluble fraction) and asphaltene (*n*-hexane insoluble fraction). The maltene fraction was further separated by polarity (fractions F1–F4) using solid-phase column chromatography with a NH_2-modified silica gel column (Birgel & Peckmann, 2008). The hydrocarbons (F1) were predominantly composed of *n*-alkanes. For a better identification and quantification of the two compounds of interest (C_{33}-*n*-ACH and phytanyl toluene), the *n*-alkanes were removed from the hydrocarbons with a molecular sieve (pore size of 5 Å), following the procedure described by Sabino et al. (2021). The compounds of interest were identified using coupled gas chromatography-mass spectrometry (GC-MS; Thermo Scientific Trace Ultra GC and Thermo Scientific DSQ II MS), searching for *m/z* = 83 and *m/z* = 106 for identification of C_{33}-*n*-ACH and phytanyl toluene, respectively (Fig. 1.2), and comparison with published spectra (McIldowie & Alexander, 2005). The aromatic hydrocarbon fraction (F2) was also scanned for phytanyl toluene, but it was not detected. For quantification, hydrocarbons were measured on a gas chromatograph coupled to a flame ionization detector (GC-FID; Thermo Scientific Trace 1310 GC). Quantification was achieved using Chromeleon 7 (version 7.2.10; Thermo Fisher Dionex) by calculating compound quantity in relation to 5α(H)-cholestane, the co-injection standard, and normalizing it to the sample's TOC content. For TOC determination (Supplementary Fig. S1), samples were de-carbonated with 100 µL 1M HCl and analyzed with a Euro EA 3000 (Euro Vector) elemental analyzer with a precision of ±0.05% and standard deviations <0.08. C_{33}-*n*-ACH and phytanyl toluene could only be quantified in samples from Lusitaniadalen. In other sections both targeted compounds either co-elute with other compounds or their content was too low to be

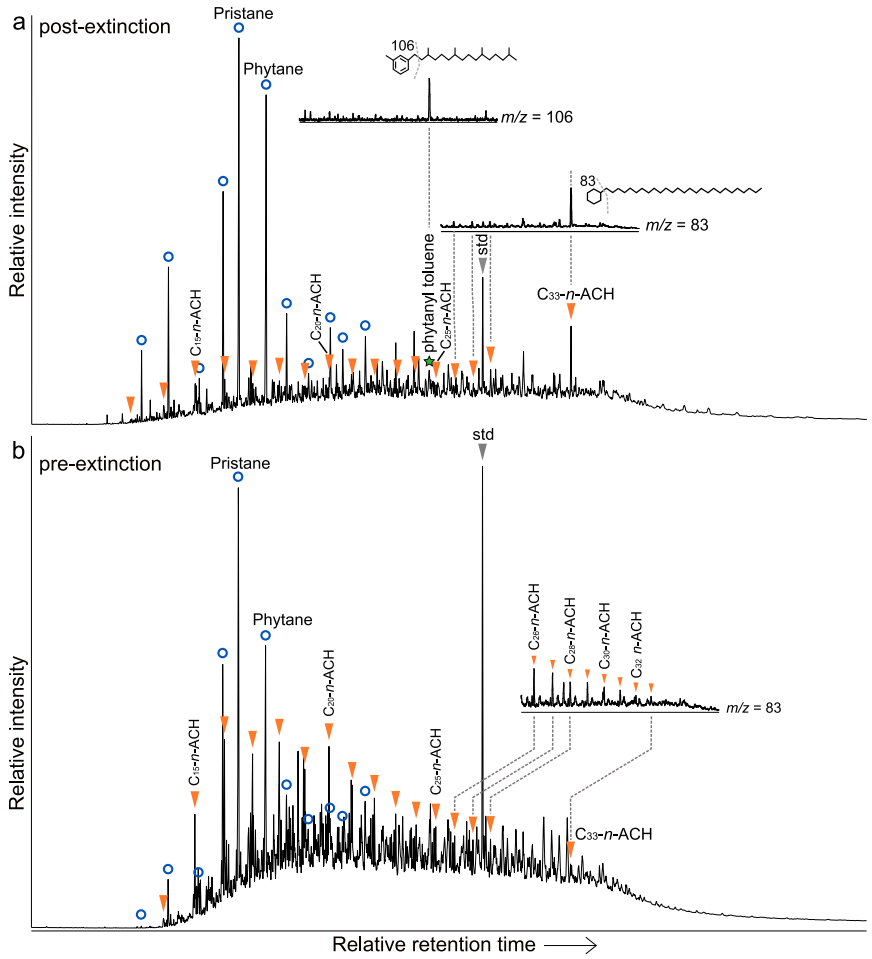

Figure 1.2: *Total ion chromatograms of molecular sieve-treated hydrocarbon samples from Lusitaniadalen, Svalbard. a — post-extinction: 0.51 m above the extinction horizon; b — pre-extinction: -36.87 m below the extinction horizon; orange triangles: C_{33}-n-alkylcyclohexane (C_{33}-n-ACH) and its pseudohomologs; green star: phytanyl toluene; blue circles: pseudohomologous series of head-to-tail linked $C_{15–25}$-isoprenoids; grey triangle: 5α(H)-cholestane standard (std). The mass ranges of m/z = 83 to scan for C_{33}-n-ACH and its pseudohomologs and m/z = 106 to scan for phytanyl toluene are shown.*

quantified. Where only trace amounts were identified, only the presence or absence is reported. Correlations between the content of biomarkers were determined with the software R (version 4.3.2). The maturity of the samples was estimated with the methylphenanthrene index (MPI) after Cassani et al. (1988) by using the peak areas of 1-, 2-, 3- and 9-methylphenanthrene (MP) from

m/z = 192, and phenanthrene (P) from *m/z* = 178 in the mass chromatogram of the F2 fraction, following MPI = 1.89(2-MP + 3-MP)/[P + 1.26(1-MP + 9-MP)]. Due to incomplete chromatographic separation, a proportion of phenanthrene and the methylphenanthrenes often co-eluted in the F1 fraction. However, a recalculation of the MPI from the F1 fraction revealed that methylphenanthrene and phenanthrene co-eluted proportionally, and the general pattern per region (central Svalbard, western Svalbard, northern Italy, South China, Türkiye) is preserved (Supplementary Fig. S2).

3 Results and Discussion

3.1 Occurrence and paleogeographic distribution of C_{33}-n-alkylcyclohexane and phytanyl toluene

The content of C_{33}-*n*-ACH in samples from Lusitaniadalen, Svalbard, shows a more than ten-fold increase from 8.1–43.3 µg/g TOC in the pre-extinction samples to values up to 513.5 µg/g TOC right above the extinction horizon (Fig. 1.3a). Although the pre-extinction samples may have experienced stronger microbial degradation than post-extinction samples as indicated by the larger hump of the unresolved complex mixture (UCM; Fig. 1.2), the signal of increased post-extinction abundance of C_{33}-*n*-ACH is also preserved in the ratio of C_{33}-*n*-ACH and *n*-C_{34} (Supplementary Fig. S1). Since *n*-ACHs are more resistant to biodegradation than *n*-alkanes (Koma et al., 2003; Perry & Gibson, 1977), the higher post-extinction ratios cannot be attributed to differential degradation, but instead point to a genuine increase in C_{33}-*n*-ACH. The content of C_{33}-*n*-ACH within the first 30 m above the extinction horizon remains elevated, which indicates persistent favorable environmental conditions for the producers of C_{33}-*n*-ACH or its unknown precursor molecule during the Permian–Triassic environmental crisis. Furthermore, *n*-ACHs with shorter (< C_{33}) alkyl-chains are detected, and show a similar sharp increase in abundance from 156.0–710.7 µg/g TOC (sum of $C_{14–28}$-*n*-ACH) before the environmental crisis to up to 4948 µg/g TOC above the extinction horizon (Fig. 1.3b). Similar to the early diagenetic shortening of the alkyl-chains of acyclic isoprenoids (Moldowan & Seifert, 1979) and hopanoids (Rohmer 1980), microbial activity and early diagenetic fragmentation may result in a series of pseudohomologous *n*-ACHs (Luo et al., 2013; Saito et al., 2022) that derived from the same precursor. We find a

strong correlation between C_{33}-*n*-ACH and shorter-chain $C_{14–28}$-*n*-ACH above the extinction horizon (correlation coefficient r = 0.73–0.97, Supplementary Fig. S3). However, correlations are generally weaker between C_{33}-*n*-ACH and $C_{18–28}$-*n*-ACH (correlation coefficient r = 0.60–0.83), and insignificant for $C_{14–17}$-*n*-ACH below the extinction horizon (Supplementary Fig. S3). The strong correlation above the extinction horizon suggests that $C_{14–28}$-*n*-ACH are degradation

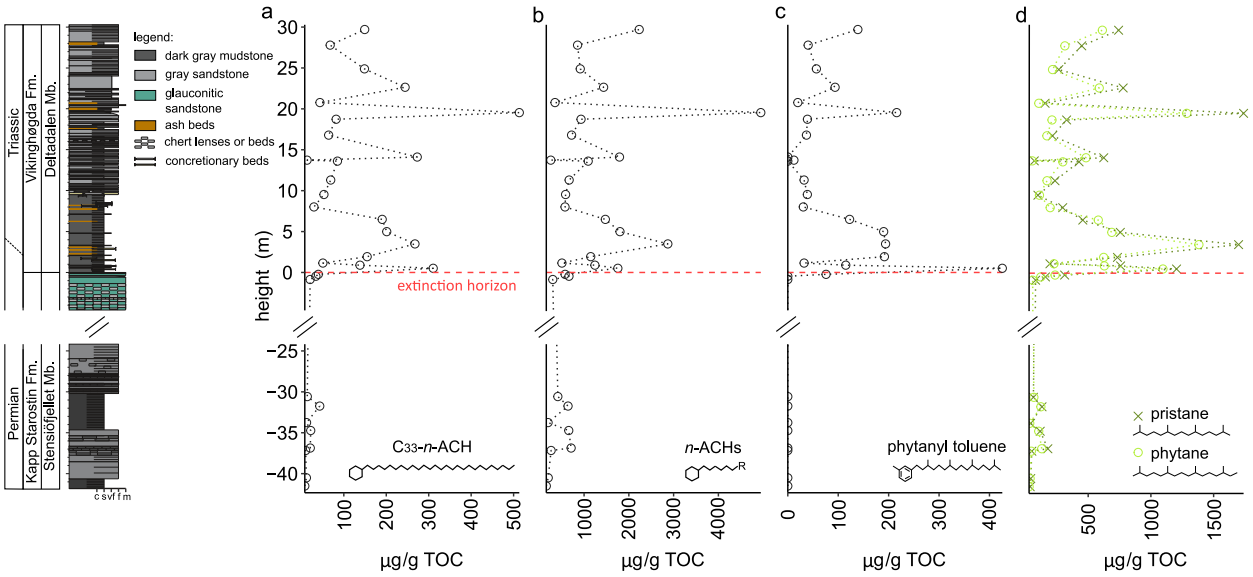

Figure 1.3: *Biomarker profiles across the siliciclastic Permian–Triassic succession at Lusitaniadalen, Svalbard. a — content of C_{33}-n-alkylcyclohexane (C_{33}-n-ACH); b — sum of the content of shorter-chain pseudohomologs of C_{33}-n-ACH ($C_{14–28}$-n-ACH quantified; $C_{29–32}$-n-ACH are present in the samples but co-elute with other compounds, and cannot be quantified); c — content of phytanyl toluene; d — content of pristane (head-to-tail linked C_{19}-isoprenoid) and phytane (head-to-tail linked C_{20}-isoprenoid). The red dashed line marks the extinction horizon (Foster et al., 2023; Nabbefeld et al., 2010; Uchman et al., 2016). Note that the y-axis is broken (as indicated by parallel diagonal line segments) to focus on sampling intervals; similar pre- and post-extinction lithologies were targeted to control for potential lithofacies bias on the biomarker data. c – claystone; s – siltstone; vf – very fine-grained sandstone; f – fine-grained sandstone; m – medium-grained sandstone.*

products and pseudohomologs of C_{33}-*n*-ACH. The weaker correlations below the extinction horizon suggest that an additional source of *n*-ACHs potentially contributed to the *n*-ACH pool, such as degraded fatty acids (e.g., Rubenstein & Strausz, 1979; Shimoyama & Johns, 1972). Also, post-depositional carbon chain elongation may have contributed minor amounts of *n*-ACHs originating from shorter-chain fatty acids, although shortening of the carbon chain is the dominant reaction during diagenesis and thermal maturation, and carbon chain elongation has never been observed for alkyl-chains longer than C_{28} (Shimoyama & Johns, 1972). However, even in pre-crisis samples where both C_{33}-*n*-ACH and shorter-chain *n*-ACHs are detected, a proportion of these shorter-chain *n*-ACHs are likely pseudohomologs of C_{33}-*n*-ACH. This implies that the absence of C_{33}-*n*-ACH does not necessarily indicate that the source organism(s) were absent, but may suggest enhanced degradation of the precursor molecule for instances in which shorter *n*-ACHs are present.

Phytanyl toluene is absent in the samples taken from horizons preceding the onset of the Permian–Triassic environmental crisis, except for the last sample below the extinction horizon at -0.23 m with 75.9 µg/g TOC (Fig. 1.3c). Above the extinction horizon at Lusitaniadalen, phytanyl toluene occurs with a maximum content of 425.4 µg/g TOC in the lowest post-extinction sample at 0.51 m. Its content varies but, except for the sample at 13.73 m, remains elevated throughout the section between 12.2 and 216.0 µg/g TOC, thereby resembling the Lower Triassic C_{33}-*n*-ACH content (correlation coefficient r = 0.75, Supplementary Fig. S3).

The occurrence of C_{33}-*n*-ACH and its pseudohomologs at Lusitaniadalen is not restricted to samples above the extinction horizon; it also occurs in uppermost Permian pre-crisis samples. Compared to previous studies on lipid biomarkers at Lusitaniadalen (Grotheer et al., 2017; Nabbefeld et al., 2010), this study provides a temporally extended record of the Lusitaniadalen profile. This extended record into the Lower Triassic possibly accounts for the differences in the absolute content of post-extinction C_{33}-*n*-ACH compared to that reported by Nabbefeld et al. (2010; Supplementary Fig. S4), who may have captured only the onset of the increase in the content of this biomarker. Additionally, the extended sampling range of our study allows for the establishment of a pre-extinction biomarker base line, and a decoupling of biotic from abiotic (e.g.,

facies-related) effects on the biomarker inventory, such as a lithological control on biomarker preservation (Peters 1986; Peters et al., 2005), and the actual biotic change by comparing the C_{33}-*n*-ACH and phytanyl toluene content below and above the extinction horizon from similar lithologies and depositional environments. Previously reported content changes of C_{33}-*n*-ACH and phytanyl toluene across the extinction horizon at Lusitaniadalen were limited to the glauconitic sandstones for the pre-crisis signal (Grotheer et al., 2017; Nabbefeld et al., 2010), raising the possibility that the reported changes may have resulted from lithological rather than environmental change. Our new data clearly support that lithology was not the main control on the C_{33}-*n*-ACH and phytanyl toluene content. Instead, the source organism(s) of C_{33}-*n*-ACH showed resilience to the significant environmental perturbations across the Permian/Triassic boundary, and the source organisms of both C_{33}-*n*-ACH and phytanyl toluene thrived in the post-extinction ecosystem.

C_{33}-*n*-ACH and its pseudohomologs were not only detected in Lusitaniadalen, but also in other Permian–Triassic sites from central Spitsbergen, including Kongressfjellet and Høgskulefjellet, and in the Olenekian at Ledalen (Fig. 1.1b). From western Spitsbergen, at Starostinaksla and Festningen (Fig. 1.1b), C_{33}-*n*-ACH is only detected above the extinction horizon, but pseudohomologs are nonetheless abundant in underlying strata prior to the environmental crisis. Three other western Spitsbergen sections (Reinodden, Bravaisberget, Selmaneset) contain only trace amounts of pseudohomologs that are commonly co-eluted with other compounds in the molecular sieve-treated samples. The apparently enhanced preservation of C_{33}-*n*-ACH in central Spitsbergen compared to western Spitsbergen is likely caused by the lower maturity of the material in central Spitsbergen. In the western Spitsbergen sections, enhanced tectonic activity during the formation of the West Spitsbergen Fold and Thrust Belt in the Eocene (Braathen et al., 1999; Leever et al., 2011; Saalmann & Thiedig, 2001) led to higher temperature and pressure, which in turn increased maturity and the degradation of sedimentary organic molecules (cf. Peters et al., 2005). As the methylphenantrene index (MPI) exhibits a non-linear relationship with thermal maturity with a maximum MPI at a vitrinite reflectance (R_o) of 1.35 % (Boreham et al., 1988; Radke & Welte, 1983), we infer that the lower MPI in samples from central Spitsbergen, compared to the higher MPI in western Spitsbergen sites reflects thermally less mature material (Fig. 1.4). Except

for an outlier at 13.73 m, the MPI at Lusitaniadalen is within a relatively narrow range (MPI = 0.69–0.98; Supplementary Fig. S1), indicating a similar thermal history across the section. However, as the shorter-chain *n*-ACHs are likely derived from the degradation of C_{33}-*n*-ACH (especially above the extinction horizon), the source organism(s) appear to have thrived across a range of depositional environments from the more distal area in central Spitsbergen to the more proximal

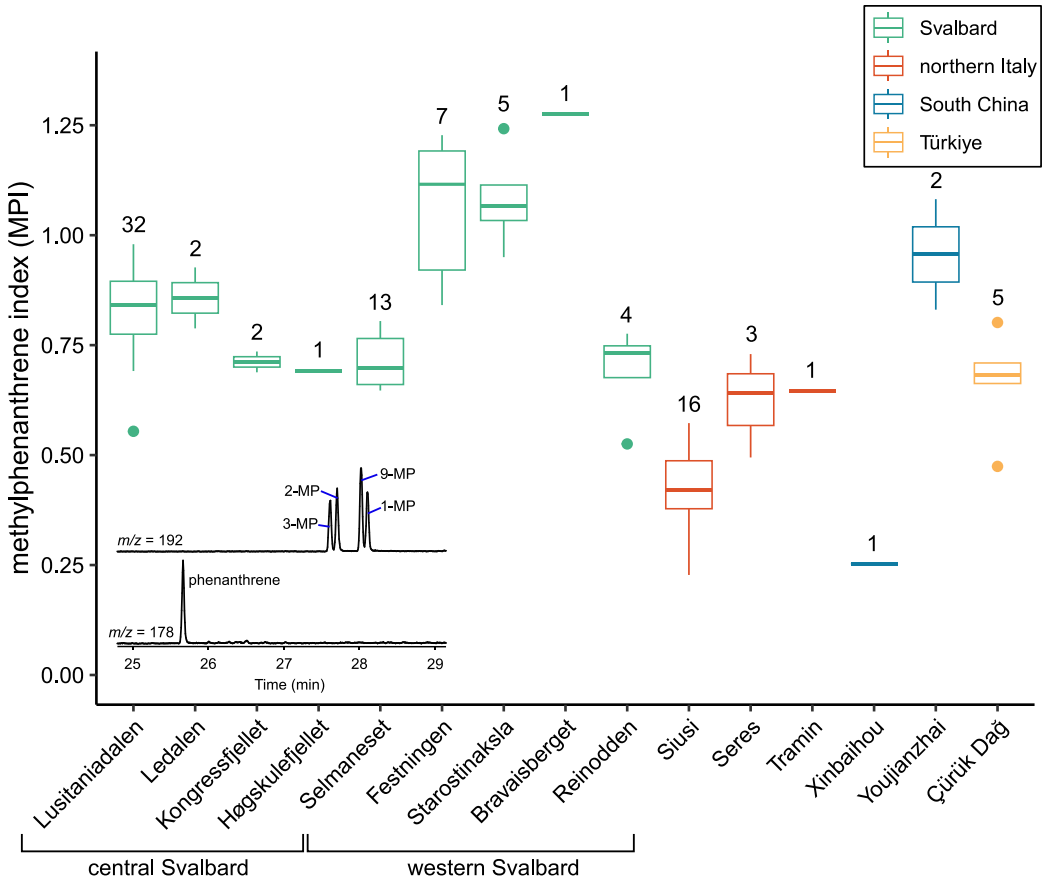

Figure 1.4: *Methylphenanthrene index (MPI) for an estimation of thermal maturity across all investigated sections. The numbers on the boxes denote the total number of analyzed samples per section that contained all compounds required to calculate the MPI. MPI = 1.89(2-MP + 3-MP)/[P + 1.26(1-MP + 9-MP)]; MP = peak area of methylphenanthrene from m/z = 192 mass chromatogram; P = peak area of phenanthrene from m/z = 178 mass chromatogram (see inserted example of mass chromatograms).*

area in western Spitsbergen (Mørk et al., 1982). Phytanyl toluene, however, was detected in samples from all sites in central Spitsbergen (Lusitaniadalen, Kongressfjellet, Høgskulefjellet, Ledalen; Fig. 1.1b), but could not be detected in western Spitsbergen samples. This absence may suggest greater susceptibility to degradation during maturation of the host lithologies, or the exclusion of the source organism(s) from the more proximal part of the basin.

The increased content of C_{33}-*n*-ACH above the extinction horizon agrees with previous findings, primarily from temperate settings like Western Australia and East Greenland (Grice et al., 2005; Hays et al., 2012) and earlier work from Svalbard (Grotheer et al., 2017; Nabbefeld et al., 2010). In contrast, phytanyl toluene was less frequently recognized across the Permian/Triassic boundary than C_{33}-*n*-ACH. It has thus far been detected in sections cropping out in Svalbard, Western Australia and East Greenland, whereas it is absent in sites recording lower-paleolatitude ecosystems like the Meishan section in South China (Cao et al., 2009; Grotheer et al., 2017) and other tropical settings in the Tethys Ocean investigated in this study. Both compounds, therefore, represent valuable geochemical markers of the Permian–Triassic environmental crisis and the Early Triassic in higher-latitude ecosystems. However, the distinctly high abundance of the C_{33}-*n*-ACH homolog seems to be restricted to Permian–Triassic successions, whereas phytanyl toluene is less temporally restricted and has also been recognized from deposits formed during other geological intervals (e.g., Jurassic: Plet et al., 2020; Cretaceous: Moura et al., 2019; Neogene: Sinninghe Damsté et al., 1993).

Existing reports of C_{33}-*n*-ACH in paleo-(sub)tropical ecosystems are restricted to South China (Shangsi section: Xie et al., 2017; Chaohu section: Saito et al., 2022). In this study, pseudohomologs of C_{33}-*n*-ACH in South China were only found in samples from Youjianzhai (Fig. 1.1a). However, the thermal maturity of the organic matter at Youjianzhai is rather high (mean MPI = 0.96), and methylphenanthrenes were only present in one of the samples from Xinbaihou, the second section in South China (Fig. 1.4). These samples may record a post-mature signal, also reflected in the very low MPI of 0.25 of the sample from Xinbaihou. While neither C_{33}-*n*-ACH nor *n*-ACHs were recorded across the Permian/Triassic boundary in the Taurus Mountains in Türkiye, we detected pseudohomologs of C_{33}-*n*-ACH and minor traces of C_{33}-*n*-ACH in pre-

extinction samples from northern Italy, which is the first report of late Permian *n*-ACHs in the Tethys region outside South China. However, contents were too low for quantification and the pseudohomologs commonly co-elute with other compounds. C_{33}-*n*-ACH has only been quantified in the Tethys region at Shangsi, with an increase from 0 µg/g TOC prior to the Permian–Triassic environmental crisis to up to 35.08 µg/g TOC above the extinction event (Xie et al., 2017). This post-extinction content at Shangsi is within the same order of magnitude as the pre-crisis content at Lusitaniadalen. Although no pseudohomologs are reported from Shangsi accounting for degraded C_{33}-*n*-ACH, the low C_{33}-*n*-ACH content suggests less favorable conditions for the source organism(s) to proliferate at this equatorial site.

While the studied sections from the Boreal Ocean are exclusively siliciclastic successions, the Tethys sections analyzed for C_{33}-*n*-ACH and phytanyl toluene are carbonate-dominated deposits. Carbonate and clastic systems vary in their pore water chemistry, cementation or sedimentation rate and adsorption of organic matter to minerals, which might affect the preservation of organic compounds (e.g., Hemingway et al., 2019; Peters et al., 2005). Hence, a depositional control on the preservation of biomolecules cannot be excluded. To fully understand factors controlling the geographic variability in both C_{33}-*n*-ACH and phytanyl toluene content, their abundance needs to be further constrained in tropical siliciclastic deposits such as the Bódvaszilas Sandstone Formation in Hungary (Hips, 1996) or the Yinkeng Formation in Meishan, South China (Yin et al., 2001).

3.2 Potential sources of the extinction markers

Although the absolute content of C_{33}-*n*-ACH and its pseudohomologs is several-fold smaller in the tropical Tethys region compared to the Boreal Ocean and higher-latitude regions, an increase of this biomarker after the onset of the Permian–Triassic environmental crisis can be globally observed, but its source organism(s) remain enigmatic. Dong et al. (1993) suggested that *n*-ACHs were formed by cyclisation of long-chain (> C_{25}) fatty acids during diagenesis. Long-chain fatty acids and *n*-alkanes are important components of leaf waxes of land plants (Buschhaus & Jetter, 2011), and would therefore imply terrestrial plant material as the source of long-chain *n*-ACHs. In

such a case, the *n*-ACHs would originate from the same precursor molecules as *n*-alkanes with the same carbon number, which would be reflected in a similar carbon number distribution of *n*-ACHs and *n*-alkanes. However, unlike C_{33}-*n*-ACH, the *n*-C_{33} alkane does not record peak abundances compared to other *n*-alkanes above the extinction horizon (Supplementary Figs. S1, S5). A terrestrial plant source is therefore unlikely.

Others have suggested a phytoplankton source of C_{33}-*n*-ACH, as its content shows a similar stratigraphic trend to that of the chlorophyll-derived biomarkers pristane and phytane, although the absolute contents differ (Nabbefeld et al., 2010), as well as increased abundance of the spinose acritarch genera *Michrystridium* and *Veryhachium* at the onset of the C_{33}-*n*-ACH increase (Grice et al., 2005). In addition, C_{33}-*n*-ACH exhibits a similar $\delta^{13}C$ composition as phytane with -33.4‰ and -32.7‰, respectively (Grice et al., 2005). At Lusitaniadalen, strong correlations between the content of pristane and C_{33}-*n*-ACH (correlation coefficient r = 0.91; Supplementary Fig. S3) and between phytane and C_{33}-*n*-ACH (correlation coefficient r = 0.90; Supplementary Fig. S3) are recorded. Both pristane and phytane contents increase several fold from 28.8 to 312.3 µg/g TOC prior to the environmental crisis to 1204 µg/g TOC and 1096 µg/g TOC, respectively, immediately above the extinction horizon (Fig. 1.3d). Notably, the highest pre-crisis content of pristane and phytane at Lusitaniadalen is recorded in the penultimate glauconitic sandstone bed at -0.23 m below the extinction horizon. This aligns with the lowermost detection of phytanyl toluene in the same bed, indicating a gradual increase in the presence of the source organism(s) of phytanyl toluene, rather than an abrupt onset. In addition to chlorophyll and algal tocopherols, pristane and phytane can also derive from the degradation of archaeal isoprenoid compounds (Rontani & Bonin, 2011; Rowland, 1990). Indeed, head-to-tail linked isoprenoid pseudohomologs from C_{21} up to C_{25} were detected in the samples (Fig. 1.2), potentially representing degradation products of extended archaeol (Vandier et al., 2021). However, the abundance of pristane and phytane strongly exceeds the usual ratios of phytanyl to sesterterpanyl-chains in archaea producing extended archaeol in seawater (cf. Vandier et al., 2021) (Fig. 1.2). This suggests that the majority of pristane and phytane in our samples can be interpreted as derived from phototrophic source organisms rather than from the degradation of

membrane lipids of archaea, which might only partially contribute to the total pristane and phytane pools.

Additionally, the source organism(s) of C_{33}-*n*-ACH have been previously assumed to be associated with euxinic conditions, based on increased content of green sulfur bacteria-derived biomarkers, aryl isoprenoids, which indicate photic zone euxinia within two meters across the extinction horizon at Lusitaniadalen (Nabbefeld et al., 2010). Instead of anoxygenic green sulfur bacteria, we suggest phytoplankton as the source of C_{33}-*n*-ACH, particularly in the post-extinction interval at Lusitaniadalen. This interpretation is supported by the diverse pelagic and benthic fauna, i.e., radiolarians, sponges, bivalves, gastropods, brachiopods and ammonoids preserved in the basal Vikinghøgda Formation (Foster et al., 2017, 2023). The presence of these aerobic, heterotrophic organisms excludes persistently anoxic or euxinic conditions in either the water column or bottom waters at Lusitaniadalen. Furthermore, redox conditions reconstructed from independent geochemical proxies indicate that the persistence of anoxic and euxinic conditions in Svalbard was comparatively short-lived; these signals disappear approximately 10 m above the extinction horizon (Grasby et al., 2015; Zuchuat et al., 2020). In contrast, both C_{33}-*n*-ACH and phytanyl toluene contents generally remain elevated throughout the investigated interval up to 30 m above the extinction horizon, indicating the source organism(s) were able to grow in oxygenated water. Nonetheless, waxing and waning of photic zone euxinia could have been an important control during the environmental crisis, and the aryl isoprenoids detected by Nabbefeld et al. (2010) as well as variability in extents and styles of burrowing (Rodríguez-Tovar et al., 2021) could indicate intermittent pulses of oxygen stress. Even during episodes of expanding euxinia, oxygenic phototrophs could have persisted and bloomed in an oxygenated surface water layer (e.g., Kasprak et al., 2015; Słowakiewicz et al., 2015). Enhanced remobilization of phosphorus from the seafloor during euxinic or anoxic periods during the Permian–Triassic environmental crisis in Svalbard (Schobben et al., 2020) could have provided otherwise limited nutrients that fertilized phytoplankton blooms. With specific (albeit of unknown affinity) photoautotrophic primary producers able to cope with and even thrive under Early Triassic environmental conditions, blooms of these organisms may have helped sustain planktic food webs and the comparatively

less depauperate benthic communities recorded in the Svalbard fossil record (Foster et al., 2017, 2023) through sufficient organic carbon export to the seafloor. Yet, the small size of benthic species and large number of premature and larval shells also suggest that the environmental crisis persisted into the Griesbachian, preventing full ecological recovery.

A change in the composition of primary producers and an increased flux of marine algal material to the sediment, potentially indicating increased primary productivity, was also recognized across the extinction event in the Canadian Sverdrup basin (Algeo et al., 2012). In contrast, in South China, in sections recording a tropical setting and in which we found C_{33}-*n*-ACH and phytanyl toluene to be less abundant or absent, an abrupt decline in primary productivity was observed right before the onset of the extinction (Zhang et al., 2018). A follow-up meta-analysis has identified this decline as a potential factor explaining the severe loss of biodiversity during the Permian–Triassic environmental crisis (Foster et al., 2024). Hence, primary productivity was likely geographically variable across a range of paleolatitudinal settings (Algeo et al., 2013). Productivity and the community composition of primary producers are influenced by diverse factors, such as nutrient availability, growth temperature, depth of the photic zone, or oxidant availability, as shown by studies of modern primary productivity (e.g., Arrigo, 2005; Domingues & Barbosa, 2023; Grimaud et al., 2017; Pajares & Ramos, 2019; Wong et al., 2023). An interplay of these factors likely also affected the phototrophic community across the Permian–Triassic transition (e.g., Algeo et al., 2012; Grasby 2016, 2019; Schobben et al., 2020; Shen et al., 2015). Factors such as global warming likely played a role in shaping the phototrophic community composition and gross primary productivity during the Permian–Triassic environmental crisis (e.g., Gliwa et al., 2022; Joachimski et al., 2012), but regional factors must also be considered. For example, terrestrial erosion has been proposed to have increased during the Permian–Triassic environmental crisis in the Paleotethys (Sephton et al., 2005; Wu et al., 2023) and a large delta plain developed on the Early Triassic Barents Shelf, discharging massive amounts of terrestrial material to the shelf (Eide et al., 2018; Gilmullina et al., 2022). Although these terrestrial inputs could provide an important nutrient source and may fertilize phytoplankton (e.g., Putland et al., 2014), increased turbidity may have alternatively impeded increased productivity or led to

changes in the primary producer community composition (e.g., Domingues & Barbosa, 2023). Hence, changes in past productivity remain challenging to reconstruct, due to a paucity of direct proxy records and dependence on the complex interplay of many factors. Thus, although a phytoplankton bloom is indicated in the Boreal Realm at Svalbard, we cannot directly infer a local change in primary productivity. However, the post-extinction increases of the chlorophyll-derived biomarkers pristane and phytane as well as relatively diverse higher trophic levels suggest that regional primary productivity was maintained, if not even promoted.

While the tropical Tethys Ocean may have experienced a decrease in primary productivity (Algeo et al., 2013; Zhang et al., 2018), tropical carbonate successions are often characterized by the formation of microbialites (e.g., Foster et al., 2020; Kershaw et al., 2012). These have been attributed to a cyanobacterial origin, e.g., in Türkiye, Iran (Heindel et al., 2018) and South China (Xie et al., 2010), which suggests benthic microbial mats contributed to primary production. Neither C_{33}-*n*-ACH nor phytanyl toluene have been previously reported from these Lower Triassic microbialites in Türkyie, Iran, and South China, but shorter-chain *n*-ACHs have been detected at Cili, South China, by Luo et al. (2013), who found distinctly elevated relative abundances of C_{21}-*n*-ACH compared to C_{20}-*n*-ACH. Furthermore, an increase of characteristic cyanobacterial biomarkers such as *n*-C_{17} compared to other *n*-alkanes, or mono-, di- and trimethylated alkanes (e.g., Coates et al., 2014; Gelpi et al., 1970; Heindel et al., 2018; Plet et al., 2020) was not found in samples with increased contents of C_{33}-*n*-ACH or phytanyl toluene (this study). Consequently, a cyanobacterial source of C_{33}-*n*-ACH and phytanyl toluene is unlikely.

The source organism(s) of phytanyl toluene remains enigmatic. Phytanyl benzenes were previously hypothesized to originate from diagenetically altered carotenoids (Gallegos, 1981; Grotheer et al., 2017; Summons & Powell, 1987) or isoprenoid quinones (Sinninghe Damsté et al., 1988). In the case of phytanyl toluene, this would suggest a defunctionalized and demethylated benzoquinone (an isoprenoid quinone with a single benzene ring) as a potential precursor molecule. However, quinones are ubiquitous across the domains of life, especially in archaea and bacteria (Collins & Jones, 1981), but also in metazoans and plants (Nowicka & Kruk, 2010). The strong correlation of phytanyl toluene and C_{33}-*n*-ACH observed at Lusitaniadalen

supports that both compounds derived from organisms with similar ecological requirements. However, phytanyl toluene is absent throughout most of the investigated interval prior to the environmental crisis whereas C_{33}-*n*-ACH was detected in pre-extinction strata at selected sites, which suggests that although the source organisms of phytanyl toluene and C_{33}-*n*-ACH were likely different, they may have occupied a similar ecological niche during the Permian–Triassic environmental crisis. Both compounds were most likely derived from phototrophic algae.

5 Conclusions

The biomarker data for C_{33}-*n*-ACH and phytanyl toluene presented here extend their record in Svalbard temporally and spatially, enabling the decoupling of lithological change at the extinction horizon from changes in the biomarker inventory. The increased content of both biomarkers above the extinction horizon is interpreted as a response to the Permian–Triassic environmental crisis rather than being driven by changes in the depositional environment. However, their preservation is likely substantially influenced by enhanced degradation at thermally more altered sites, underscoring the importance for careful evaluation when biomarkers are absent. Our findings challenge the previous hypothesis that the source organism(s) of C_{33}-*n*-ACH are associated with photic zone euxinia as we found no evidence of extended euxinic conditions during the whole interval of increased C_{33}-*n*-ACH content. Instead, C_{33}-*n*-ACH was likely produced during blooms of specific planktonic oxygenic phototrophs in the Boreal Ocean and at higher paleolatitudes in the Early Triassic, potentially forming the base of a resilient ecological community, reflected in the diverse Early Triassic fossil assemblage in Svalbard. Phytanyl toluene, exclusively observed in higher paleolatitude siliciclastic successions and absent in tropical carbonate deposits, appears to have a different source than C_{33}-*n*-ACH. The spatial disparity in their paleogeographic distribution may reflect differences in environmental requirements, depositional settings, or the distribution of their source organism(s).

Acknowledgments

We acknowledge the logistical support from the Czech Arctic Research Station including RV *Clione* and its crew David Vostárek and Jiří Štojdl jr, the crew of *Ulla Rinman* Mana Walther and

Jan Walther, as well as UNIS, and the Governor of Svalbard for granting us sampling permission (permit No. 23/00910-2 and 24/00386-4). Also, we would like to thank everyone who helped us in planning and conducting fieldwork in Svalbard, northern Italy, South China and Türkiye for their support and guidance, and Sabine Beckmann for her support in the lab. We are grateful for the thoughtful and constructive comments of three reviewers. This research was funded by two Arctic Field Grants from the Research Council of Norway (Project No. 342069 and 250229) and the Deutsche Forschungsgemeinschaft (Project No. FO1297/1-1). Fieldwork in South China was funded by the National Natural Science Foundation of China (Project No. 42293291, 42102143). We also acknowledge financial support from the Open Access Publication Fund of the University of Hamburg.

Conflict of Interest

The authors declare no conflict of interest.

Open Research

The biomarker data, metadata and R code used in the study are available at Zenodo (Buchwald et al., 2025: https://www.doi.org/10.5281/zenodo.16032548).

References

Algeo, T., Henderson, C. M., Ellwood, B., Rowe, H., Elswick, E., Bates, S., et al. (2012). Evidence for a diachronous late Permian marine crisis from the Canadian Arctic region. *GSA Bulletin, 124*(9-10), 1424–1448. https://doi.org/10.1130/B30505.1

Algeo, T. J., Henderson, C. M., Tong, J., Feng, Q., Yin, H., & Tyson, R. V. (2013). Plankton and productivity during the Permian–Triassic boundary crisis: An analysis of organic carbon fluxes. *Global and Planetary Change, 105*, 52-67. https://doi.org/10.1016/j.gloplacha.2012.02.008

Altıner, D., & Zaninetti, L. (1980). Le Trias dans la région de Pinarbasi, Taurus oriental, Turquie: Unités lithologiques, micropaléontologie, milieux de dépôt. *Rivista Italiana di Paleontologia e Stratigrafia, 86*(4), 705–760.

Angiolini, L., Carabelli, L., Nicora, A., Crasquin-Soleau, S., Marcoux, J., & Rettori, R. (2007). Brachiopods and other fossils from the Permo–Triassic boundary beds of the Antalya Nappes (SW Taurus, Turkey). *Geobios, 40*(6), 715–729. https://doi.org/10.1016/j.geobios.2007.01.007

Arrigo, K. R. (2005). Marine microorganisms and global nutrient cycles. *Nature, 437*(7057), 349–355. https://doi.org/10.1038/nature04159

Baud, A., Richoz, S., & Marcoux, J. (2005). Calcimicrobial cap rocks from the basal Triassic units: Western Taurus occurrences (SW Turkey). *Comptes Rendus Palevol, 4*(6–7), 569–582. https://doi.org/10.1016/j.crpv.2005.03.001

Baud, A., Richoz, S., & Pruss, S. (2007). The lower Triassic anachronistic carbonate facies in space and time. *Global and Planetary Change, 55*(1–3), 81–89. https://doi.org/10.1016/j.gloplacha.2006.06.008

Beatty, T. W., Zonneveld, J. P., & Henderson, C. M. (2008). Anomalously diverse Early Triassic ichnofossil assemblages in northwest Pangea: A case for a shallow-marine habitable zone. *Geology*, *36*(10), 771–774. https://doi.org/10.1130/G24952A.1

Beauchamp, B., & Baud, A. (2002). Growth and demise of Permian biogenic chert along northwest Pangea: Evidence for end-Permian collapse of thermohaline circulation. *Palaeogeography, Palaeoclimatology, Palaeoecology*, *184*(1–2), 37–63. https://doi.org/10.1016/S0031-0182(02)00245-6

Birgel, D., & Peckmann, J. (2008). Aerobic methanotrophy at ancient marine methane seeps: A synthesis. *Organic Geochemistry*, *39*(12), 1659–1667. https://doi.org/10.1016/j.orggeochem.2008.01.023

Birgel, D., Thiel, V., Hinrichs, K. U., Elvert, M., Campbell, K. A., Reitner, J., et al. (2006). Lipid biomarker patterns of methane-seep microbialites from the Mesozoic convergent margin of California. *Organic Geochemistry*, *37*(10), 1289–1302. https://doi.org/10.1016/j.orggeochem.2006.02.004

Blakey, R. (2012). Global paleogeography. Retrieved from http://www2.nau.edu/rcb7/globaltext2.html [accessed July 2014]

Boreham, C. J., Crick, I. H., & Powell, T. G. (1988). Alternative calibration of the Methylphenanthrene Index against vitrinite reflectance: Application to maturity measurements on oils and sediments. *Organic Geochemistry, 12*(3), 289–294. https://doi.org/10.1016/0146-6380(88)90266-5

Braathen, A., Bergh, S. G., & Maher Jr., H. D. (1999). Application of a critical wedge taper model to the Tertiary transpressional fold-thrust belt on Spitsbergen, Svalbard. *GSA Bulletin*, *111*(10), 1468–1485. https://doi.org/10.1130/0016-7606(1999)111<1468:AOACWT>2.3.CO;2

Broglio Loriga, C., Góczán, F., Haas, J., Lenner, K., Neri, C., Oravecz Scheffer, A., et al. (1990). The Lower Triassic sequences of the Dolomites (Italy) and Transdanubian Mid-Mountains (Hungary) and their correlation. *Memorie Di Scienze Geologiche, 11*(2), 41–103.

Buchwald, S. Z., Birgel, D., Senger, K., Mosociova, T., Pei, Y., Zuchuat, V., et al. (2025). Phytoplankton blooms on the Barents Shelf, Svalbard, associated with the Permian–Triassic mass extinction. StellaZBuchwald/Permian-Triassic_Extinction_Markers, published Apr 14, 2025 [Dataset, Computational Notebook], Zenodo, https://www.doi.org/10.5281/zenodo.16032548

Burgess, S. D., Bowring, S., & Shen, S. Z. (2014). High-precision timeline for Earth's most severe extinction. *Proceedings of the National Academy of Sciences, 111*(9), 3316–3321. https://doi.org/10.1073/pnas.1317692111

Buschhaus, C., & Jetter, R. (2011). Composition differences between epicuticular and intracuticular wax substructures: How do plants seal their epidermal surfaces? In *Journal of Experimental Botany*, *62*(3), 841–853. https://doi.org/10.1093/jxb/erq366

Cao, C., Love, G. D., Hays, L. E., Wang, W., Shen, S., & Summons, R. E. (2009). Biogeochemical evidence for euxinic oceans and ecological disturbance presaging the end-Permian mass extinction event. *Earth and Planetary Science Letters*, *281*(3–4), 188–201. https://doi.org/10.1016/j.epsl.2009.02.012

Cassani, F., Gallango, O., Talukdar, S., Vallejos, C., & Ehrmann, U. (1988). Methylphenanthrene maturity index of marine source rock extracts and crude oils from the Maracaibo Basin. *Organic Geochemistry*, *13*(3), 73–80. https://doi.org/10.1016/B978-0-08-037236-5.50013-0

Chappe, B., Michaelis, W. and Albrecht, P. (1980). Molecular fossils of archaebacteria as selective degradation products of kerogen. In G. Douglas, A. G, & Maxwell, J. R. (Eds.), *Advances in Organic Geochemistry*, Pergamon Press, Oxford (pp. 265–74).

Coates, R. C., Podell, S., Korobeynikov, A., Lapidus, A., Pevzner, P., Sherman, D. H., et al. (2014). Characterization of cyanobacterial hydrocarbon composition and distribution of biosynthetic pathways. *PLoS ONE*, *9*(1), e85140. https://doi.org/10.1371/journal.pone.0085140

Collins, M. D., & Jones, D. (1981). Distribution of isoprenoid quinone structural types in bacteria and their taxonomic implications. *Microbiological Reviews*, *45*(2), 316–354.

Crasquin-Soleau, S., Marcoux, J., Angiolini, L., Richoz, S., Nicora, A., Baud, A., & Bertho, Y. (2004). A new ostracode fauna from the Permian-Triassic boundary in Turkey (Taurus, Antalya Nappes). *Micropaleontology, 50*(3), 281–295. https://doi.org/10.2113/50.3.281

Crasquin-Soleau, S., Richoz, S., Marcoux, J., Angiolini, L., Nicora, A., & Baud, A. (2002). Les événements de la limite Permien–Trias: Derniers survivants et/ou premiers re-colonisateurs parmi les ostracodes du Taurus (Sud-Ouest de la Turquie). *Comptes rendus. Géoscience, 334*(7), 489–495. https://doi.org/10.1016/S1631-0713(02)01782-0

Dal Corso, J., Song, H., Callegaro, S., Chu, D., Sun, Y., Hilton, J., et al. (2022). Environmental crises at the Permian–Triassic mass extinction. *Nature Reviews Earth and Environment*, *3*(3), 197–214. https://doi.org/10.1038/s43017-021-00259-4

Dallmann, W. K., Andresen, A., Bergh, S., Maher, Jr., H. D., & Ohta, Y. (1993). Tertiary fold-and-thrust belt of Spitsbergen, Svalbard. *Norsk Polarinstitutt Meddelelser*, 128.

Domingues, R. B., & Barbosa, A. B. (2023). Evaluating underwater light availability for phytoplankton: Mean light intensity in the mixed layer versus attenuation coefficient. *Water, 15*(16), 2966. https://doi.org/10.3390/w15162966

Donelson, J. M., Sunday, J. M., Figueira, W. F., Gaitán-Espitia, J. D., Hobday, A. J., Johnson, C. R., et al. (2019). Understanding interactions between plasticity, adaptation and range shifts in response to marine environmental change. *Philosophical Transactions of the Royal Society B, 374*(1768), 20180186. https://doi.org/10.1098/rstb.2018.0186

Dong, J.-Z., Vorkink, W. P., & Lee, M. L. (1993). Origin of long-chain alkylcyclohexanes and alkylbenzenes in a coal-bed wax. *Geochmica et Cosmmhimica Acta, 57*(4), 837–849. https://doi.org/10.1016/0016-7037(93)90172-S

Eide, C. H., Klausen, T. G., Katkov, D., Suslova, A. A., & Helland-Hansen, W. (2018). Linking an Early Triassic delta to antecedent topography: Source-to-sink study of the southwestern Barents Sea margin. *GSA Bulletin, 130*(1–2), 263–283. https://doi.org/10.1130/B31639.1

Elvevold, S., Dallmann, W., & Blomeier, D. (2007). Geology of Svalbard. *Norwegian Polar Institute.*

Farabegoli, E., Perri, M. C., & Posenato, R. (2007). Environmental and biotic changes across the Permian-Triassic boundary in western Tethys: The Bulla parastratotype, Italy. *Global and Planetary Change, 55*(1–3), 109–135. https://doi.org/10.1016/j.gloplacha.2006.06.009

Foster, W. J., & Twitchett, R. J. (2014). Functional diversity of marine ecosystems after the late Permian mass extinction event. *Nature Geoscience, 7*(3), 233–238. https://doi.org/10.1038/ngeo2079

Foster, W. J., Asatryan, G., Rauzi, S., Botting, J. P., Buchwald, S. Z., Lazarus, D. B., et al. (2023). Response of siliceous marine organisms to the Permian-Triassic climate crisis based on new

findings from central Spitsbergen, Svalbard. *Paleoceanography and Paleoclimatology*, *38*(12), e2023PA004766. https://doi.org/10.1029/2023PA004766

Foster, W. J., Danise, S., & Twitchett, R. J. (2017). A silicified Early Triassic marine assemblage from Svalbard. *Journal of Systematic Palaeontology*, *15*(10), 851–877. https://doi.org/10.1080/14772019.2016.1245680

Foster, W. J., Frank, A. B., Li, Q., Danise, S., Wang, X., & Peckmann, J. (2024). Thermal and nutrient stress drove Permian–Triassic shallow marine extinctions. *Cambridge Prisms: Extinction*, *2*, e9. https://doi.org/10.1017/ext.2024.9

Foster, W. J., Heindel, K., Richoz, S., Gliwa, J., Lehrmann, D. J., Baud, A., et al. (2020). Suppressed competitive exclusion enabled the proliferation of Permian/Triassic boundary microbialites. *Depositional Record*, *6*(1), 62–74. https://doi.org/10.1002/dep2.97

Foster, W. J., Lehrmann, D. J., Hirtz, J. A., White, M., Yu, M., Li, J., & Martindale, R. C. (2019). Early Triassic benthic invertebrates from the Great Bank of Guizhou, South China: Systematic palaeontology and palaeobiology. *Papers in Palaeontology, 5*(4), 613–656. https://doi.org/10.1002/spp2.1252

Foster, W. J., Lehrmann, D. J., Yu, M., Ji, L., & Martindale, R. C. (2018). Persistent environmental stress delayed the recovery of marine communities in the aftermath of the latest Permian mass extinction. *Paleoceanography and Paleoclimatology, 33*(4), 338–353. https://doi.org/10.1002/2018PA003328

Gelpi, E., Schneider, H, Mann, J., & Oró, J. (1970). Hydrocarbons of geochemical significance in microscopic algae. *Phytochemistry, 9*(3), 603–612. https://doi.org/10.1016/S0031-9422(00)85700-3

Gilmullina, A., Klausen, T. G., Doré, A. G., Rossi, V. M., Suslova, A., & Eide, C. H. (2022). Linking sediment supply variations and tectonic evolution in deep time, source-to-sink systems—The Triassic Greater Barents Sea Basin. *Bulletin of the Geological Society of America, 134*(7–8), 1760–1780. https://doi.org/10.1130/B36090.1

Gliwa, J., Wiedenbeck, M., Schobben, M., Ullmann, C. V., Kiessling, W., Ghaderi, A., et al. (2022). Gradual warming prior to the end-Permian mass extinction. *Palaeontology, 65*(5), e12621. https://doi.org/10.1111/pala.12621

Godbold, A., Schoepfer, S., Shen, S., & Henderson, C. M. (2017). Precarious ephemeral refugia during the earliest Triassic. *Geology*, *45*(7), 607–610. https://doi.org/10.1130/G38793.1

Grasby, S. E., Beauchamp, B., Bond, D. P. G., Wignall, P., Talavera, C., Galloway, J. M., et al. (2015). Progressive environmental deterioration in northwestern Pangea leading to the latest Permian

extinction. *Bulletin of the Geological Society of America*, *127*(9–10), 1331–1347. https://doi.org/10.1130/B31197.1

Grasby, S. E., Beauchamp, B., & Knies, J. (2016). Early Triassic productivity crises delayed recovery from world's worst mass extinction. *Geology, 44*(9), 779–782. https://doi.org/10.1130/G38141.1

Grasby, S. E., Knies, J., Beauchamp, B., Bond, D. P., Wignall, P., & Sun, Y. (2020). Global warming leads to Early Triassic nutrient stress across northern Pangea. *GSA Bulletin, 132*(5–6), 943–954. https://doi.org/10.1130/B32036.1

Grasby, S. E., Them II, T. R., Chen, Z., Yin, R., & Ardakani, O. H. (2019). Mercury as a proxy for volcanic emissions in the geologic record. *Earth Science Reviews*, *196*, 102880. https://doi.org/10.1016/j.earscirev.2019.102880

Grice, K., Twitchett, R. J., Alexander, R., Foster, C. B., & Looy, C. (2005). A potential biomarker for the Permian–Triassic ecological crisis. *Earth and Planetary Science Letters*, *236*(1–2), 315–321. https://doi.org/10.1016/j.epsl.2005.05.008

Grimaud, G. M., Mairet, F., Sciandra, A., & Bernard, O. (2017). Modeling the temperature effect on the specific growth rate of phytoplankton: A review. *Reviews in Environmental Science and Bio/Technology, 16*(4), 625–645. https://doi.org/10.1007/s11157-017-9443-0

Grotheer, H., Le Métayer, P., Piggott, M. J., Lindeboom, E. J., Holman, A. I., Twitchett, R. J., & Grice, K. (2017). Occurrence and significance of phytanyl arenes across the Permian-Triassic boundary interval. *Organic Geochemistry*, *104*, 42–52. https://doi.org/10.1016/j.orggeochem.2016.12.002

Groves, J. R., Rettori, R., Payne, J. L., Boyce, M. D., Demi, D., & Altıner, D. (2007). End-Permian mass extinction of lagenide foraminifers in the Southern Alps (northern Italy). *Journal of Paleontology, 81*(3), 415–434. https://doi.org/10.1666/05123.1

Hays, L. E., Grice, K., Foster, C. B., & Summons, R. E. (2012). Biomarker and isotopic trends in a Permian–Triassic sedimentary section at Kap Stosch, Greenland. *Organic Geochemistry*, *43*, 67–82. https://doi.org/10.1016/j.orggeochem.2011.10.010

Heindel, K., Foster, W. J., Richoz, S., Birgel, D., Roden, V. J., Baud, A., et al. (2018). The formation of microbial-metazoan bioherms and biostromes following the latest Permian mass extinction. *Gondwana Research*, *61*, 187–202. https://doi.org/10.1016/j.gr.2018.05.007

Hemingway, J. D., Rothman, D. H., Grant, K. E., Rosengard, S. Z., Eglinton, T. I., Derry, L. A., & Galy, V. V. (2019). Mineral protection regulates long-term global preservation of natural organic carbon. *Nature*, *570*(7760), 228–231. https://doi.org/10.1038/s41586-019-1280-6

Hips, K. (1996). Stratigraphic and facies evaluation of the Lower Triassic formations in the Aggtelek-Rudabánya Mountains, NE Hungary. *Acta Geologica Hungarica, 39*(4), 369–411.

Horacek, M., Povoden, E., Richoz, S., & Brandner, R. (2010). High-resolution carbon isotope changes, litho- and magnetostratigraphy across Permian-Triassic boundary sections in the Dolomites, N-Italy. New constraints for global correlation. *Palaeogeography, Palaeoclimatology, Palaeoecology, 290*(1–4), 58–64. https://doi.org/10.1016/j.palaeo.2010.01.007

Joachimski, M. M., Lai, X., Shen, S., Jiang, H., Luo, G., Chen, B., et al. (2012). Climate warming in the latest Permian and the Permian-Triassic mass extinction. *Geology, 40*(3), 195–198. https://doi.org/10.1130/G32707.1

Kasprak, A. H., Sepúlveda, J., Price-Waldman, R., Williford, K. H., Schoepfer, S. D., Haggart, J. W., et al. (2015). Episodic photic zone euxinia in the northeastern Panthalassic Ocean during the end-Triassic extinction. *Geology*, *43*(4), 307–310. https://doi.org/10.1130/G36371.1

Kershaw, S., Crasquin, S., Li, Y., Collin, P. Y., Forel, M. B., Mu, X., et al. (2012). Microbialites and global environmental change across the Permian–Triassic boundary: A synthesis. *Geobiology*, *10*(1), 25–47. https://doi.org/10.1111/j.1472-4669.2011.00302.x

Koma, D., Hasumi, F., Chung, S. Y., & Kubo, M. (2003). Biodegradation of *n*-alkylcyclohexanes by co-oxidation via multiple pathways in *Acinetobacter* sp. ODDK71. *Journal of Bioscience and Bioengineering, 95*(6), 641–644. https://doi.org/10.1016/S1389-1723(03)80178-0

Korte, C., & Kozur, H. W. (2010). Carbon-isotope stratigraphy across the Permian–Triassic boundary: A review. *Journal of Asian Earth Sciences, 39*(4), 215–235. https://doi.org/10.1016/j.jseaes.2010.01.005

Leever, K. A., Gabrielsen, R. H., Faleide, J. I., & Braathen, A. (2011). A transpressional origin for the West Spitsbergen fold-and-thrust belt: Insight from analog modeling. *Tectonics*, *30*(2). https://doi.org/10.1029/2010TC002753

Lehrmann, D. J., Enos, P., Payne, J. L., Montgomery, P., Wei, J., Yu, Y., et al. (2005). Permian and Triassic depositional history of the Yangtze platform and Great Bank of Guizhou in the Nanpanjiang basin of Guizhou and Guangxi, south China. Albertiana, 33(1), 149–168.

Lehrmann, D. J., Jiayong, W., & Enos, P. (1998). Controls on facies architecture of a large Triassic carbonate platform; the Great Bank of Guizhou, Nanpanjiang Basin, South China. *Journal of Sedimentary Research, 68*(2), 311–326. https://doi.org/10.2110/jsr.68.311

Lehrmann, D. J., Payne, J. L., Felix, S. V., Dillett, P. M., Wang, H., Yu, Y., & Wei, J. (2003). Permian–Triassic boundary sections from shallow-marine carbonate platforms of the Nanpanjiang Basin, South China: Implications for oceanic conditions associated with the end-Permian extinction and its aftermath. *Palaios, 18*(2), 138–152. https://doi.org/10.1669/0883-1351(2003)18<138:PBSFSC>2.0.CO;2

Lehrmann, D. J., Payne, J. L., Pei, D., Enos, P., Druke, D., Steffen, K., et al. (2007). Record of the end-Permian extinction and Triassic biotic recovery in the Chongzuo-Pingguo platform, southern Nanpanjiang basin, Guangxi, South China. *Palaeogeography, Palaeoclimatology, Palaeoecology, 252*(1–2), 200–217. https://doi.org/10.1016/j.palaeo.2006.11.044

Lehrmann, D. J., Wan, Y., Wei, J., Yu, Y., & Xiao, J. (2001). Lower Triassic peritidal cyclic limestone: An example of anachronistic carbonate facies from the Great Bank of Guizhou, Nanpanjiang Basin, Guizhou province, South China. *Palaeogeography, Palaeoclimatology, Palaeoecology, 173*(3–4), 103–123. https://doi.org/10.1016/S0031-0182(01)00302-9

Luo, G., Wang, Y., Grice, K., Kershaw, S., Algeo, T. J., Ruan, X., et al. (2013). Microbial–algal community changes during the latest Permian ecological crisis: Evidence from lipid biomarkers at Cili, South China. *Global and Planetary Change, 105,* 36–51. https://doi.org/10.1016/j.gloplacha.2012.11.015

Lys, M., Marcoux, J., 1978. Les niveaux du Permien supérieurdes Nappes d'Antalya (Taurides occidentales, Turquie). *Comptes Rendus de l'Académie des Sciences 286*, 1417–1420.

Marcoux, J., & Baud, A. (1988). The Permo-Triassic boundary in the Antalya Nappes (Western Taurides-Turkey). *Memoir Società Geologica Italiana, 34*, 243–252.

Massari, F., Neri, C., Pittau, P., Fontana, D., & Stefani, C. (1994). Sedimentology, palynostratigraphy and sequence stratigraphy of a continental to shallow-marine rift-related succession: Upper Permian of the eastern Southern Alps (Italy). *Memorie Di Scienze Geologiche, 46*, 119–243.

McIldowie, M., & Alexander, R. (2005). Identification of a novel C_{33} *n*-alkylcyclohexane biomarker in Permian–Triassic sediments. *Organic Geochemistry*, *36*(10), 1454–1458. https://doi.org/10.1016/j.orggeochem.2005.06.009

McInerney, F. A., & Wing, S. L. (2011). The Paleocene-Eocene thermal maximum: A perturbation of carbon cycle, climate, and biosphere with implications for the future. *Annual Review of Earth and Planetary Sciences*, *39*, 489–516. https://doi.org/10.1146/annurev-earth-040610-133431

Moldowan, J. M., & Seifert, W. K. (1979). Head-to-head linked isoprenoid hydrocarbons in petroleum. *Science, 204*(4389), 169–171. https://doi.org/ 10.1126/science.204.4389.169

Mørk, A., Elvebakk, G., Forsberg, A. W., Hounslow, M. W., Nakrem, H. A., Vigran, J. O., & Weitschat, W. (1999). The type section of the Vikinghøgda formation: A new Lower Triassic unit in central and eastern Svalbard. *Polar Research, 18*(1), 51–82. https://doi.org/10.1111/j.1751-8369.1999.tb00277.x

Mørk, A., Knarud, R., & Worsley, D. (1982). Depositional and diagenetic environments of the Triassic and lower Jurassic successions of Svalbard In Embry, A. F., & Balkwill, H. R. (Eds.), *Arctic Geology and Geophysics, Canadian Society of Petroleum Geologists*, 371–298.

Moura, A. K., Ribeiro, D. O., do Carmo, I. S., Araújo, B. Q., Pereira, V. B., Azevedo, D. A., & Citó, A. M. (2019). An assay on alkyl aromatic hydrocarbons: Unexpected group-type separation of diaromatic hydrocarbons in Cretaceous crude oils from Brazilian Marginal Basin. *Energy & Fuels, 33*(2), 691–69. https://doi.org/10.1021/acs.energyfuels.8b03268

Nabbefeld, B., Grice, K., Twitchett, R. J., Summons, R. E., Hays, L., Böttcher, M. E., & Asif, M. (2010). An integrated biomarker, isotopic and palaeoenvironmental study through the late Permian event at Lusitaniadalen, Spitsbergen. *Earth and Planetary Science Letters*, *291*(1–4), 84–96. https://doi.org/10.1016/j.epsl.2009.12.053

Nagy, J., Svensen, H. H., & Planke, S. (2025). Severe oxygen and carbonate depletion during the end-Permian mass extinction and its aftermath in Boreal waters reflected by foraminifera from Spitsbergen. *Preprint at SSRN*, 4460346.

Nakrem, H. A., & Mørk, A. (1991). New Early Triassic Bryozoa (Trepostomata) from Spitsbergen, with some remarks on the stratigraphy of the investigated horizons. *Geological Magazin*, *128*(2), 129–140. https://doi.org/10.1017/S001675680001832X

Noé, S. (1987). Facies and paleogeography of the marine upper Permian and of the Permian-Triassic boundary in the Southern Alps (Bellerophon Formation, Tesero Horizon). *Facies, 16*, 89–142. https://doi.org/10.1007/BF02536749

Nowicka, B., & Kruk, J. (2010). Occurrence, biosynthesis and function of isoprenoid quinones. *Biochimica et Biophysica Acta – Bioenergetics*, *1797*(9), 1587–1605. https://doi.org/10.1016/j.bbabio.2010.06.007

Olaussen, S., Grundvåg, S.-A., Senger, K., Anell, I., Betlem, P., Birchall, T., et al. (2023). Svalbard composite tectono-sedimentary element, Barents Sea. *Geological Society, London, Memoirs*, *57*(1), M57-2021. https://doi.org/10.1144/m57-2021-36

Özgül, N. (1984). Stratigraphy and tectonic evolution of the Central Taurides. Geology of the Taurus belt. *International symposium*, 77–90.

Özgül, N. (1997). Bozkır-Hadım-Taşkent (orta toroslar'in kuzey kesimi) dolayinda yer alan tektono-stratigrafik birliklerin stratigrafisi. *Maden Tektik ve Arama Dergisi, 119*, 113–174.

Pajares, S., & Ramos, R. (2019). Processes and microorganisms involved in the marine nitrogen cycle: Knowledge and gaps. *Frontiers in Marine Science, 6*, 739. https://doi.org/10.3389/fmars.2019.00739

Payne, J., & Clapham, M. (2012). End-permian mass extinction in the oceans: An ancient analog for the twenty-first century? *Annual Review of Earth and Planetary Sciences*, *40*, 89–111. https://doi.org/10.1146/annurev-earth-042711-105329

Payne, J. L., Lehrmann, D. J., Wei, J., & Knoll, A. H. (2006). The pattern and timing of biotic recovery from the end-Permian extinction on the Great Bank of Guizhou, Guizhou Province, China. *Palaios, 21*(1), 63–85. https://doi.org/10.2110/palo.2005.p05-12p

Penn, J. L., Deutsch, C., Payne, J. L., & Sperling, E. A. (2018). Temperature-dependent hypoxia explains biogeography and severity of end-Permian marine mass extinction. *Science*, *362*(6419), eaat1327. https://doi.org/10.1126/science.aat1327

Perry, J. J., & Gibson, D. T. (1977). Microbial metabolism of cyclic hydrocarbons and related compounds. *CRC Critical Reviews in Microbiology, 5*(4), 387–412. https://doi.org/10.3109/10408417709102811

Peters, K. E. (1986). Guidelines for evaluating petroleum source rock using programmed pyrolysis. *AAPG bulletin, 70*(3), 318–329. https://doi.org/10.1306/94885688-1704-11D7-8645000102C1865D

Peters, K. E., Walters, C. C., & Moldowan, J. M. (2005). *The Biomarker Guide: Volume 1*, Biomarkers and isotopes in the environment and human history, 2nd ed., Vol. 1. Cambridge University Press.

Plet, C., Grice, K., Scarlett, A. G., Ruebsam, W., Holman, A. I., & Schwark, L. (2020). Aromatic hydrocarbons provide new insight into carbonate concretion formation and the impact of eogenesis on organic matter. *Organic Geochemistry*, *143*, 103961 . https://doi.org/10.1016/j.orggeochem.2019.103961

Poloczanska, E. S., Burrows, M. T., Brown, C. J., Molinos, J. G., Halpern, B. S., Hoegh-Guldberg, O., et al. (2016). Responses of marine organisms to climate change across oceans. *Frontiers in Marine Science*, *3*, 62. https://doi.org/10.3389/fmars.2016.00062

Posenato, R. (2010). Marine biotic events in the Lopingian succession and latest Permian extinction in the Southern Alps (Italy). *Geological Journal, 45*(2–3), 195–215. https://doi.org/10.1002/gj.1212

Prinoth, H., & Posenato, R. (2023). Bivalves from the Changhsingian (upper Permian) Bellerophon Formation of the Dolomites (Italy): Ancestors of Lower Triassic post-extinction benthic communities. *Papers in Palaeontology, 9*(2), e1486. https://doi.org/10.1002/spp2.1486

Putland, J. N., Mortazavi, B., Iverson, R. L., & Wise, S. W. (2014). Phytoplankton biomass and composition in a river-dominated estuary during two summers of contrasting river discharge. *Estuaries and Coasts, 37*, 664–679. https://doi.org/10.1007/s12237-013-9712-2

R Core Team (2023). R: A Language and Environment for Statistical Computing. *R Foundation for Statistical Computing, Vienna, Austria.* https://www.R-project.org/

Radke, M, & Welte D. H. (1983). The Methylphenanthrene Index (MPI): A maturity parameter based on aromatic hydrocarbons, In Bjoroy, M. (Ed.), *Advances in Organic Geochemistry*, Wiley, Chichester (pp. 504–512).

Richoz, S. (2006). Stratigraphie isotopique du Permien superieur et Trias inferieur de quelques localites de la Neotethys. *Memoire de Geologie (Lausanne), 46*, 283.

Rodríguez-Tovar, F. J., Dorador, J., Zuchuat, V., Planke, S., & Hammer, Ø. (2021). Response of macrobenthic trace maker community to the end-Permian mass extinction in central Spitsbergen, Svalbard. *Palaeogeography, Palaeoclimatology, Palaeoecology, 581*, 110637. https://doi.org/10.1016/j.palaeo.2021.110637

Rohmer, M., Dastillung, M., & Ourisson, G. (1980). Hopanoids from C_{30} to C_{35} in recent muds: Chemical markers for bacterial activity. *Naturwissenschaften, 67*, 456–458. https://doi.org/10.1007/BF00405643

Rontani, J. F., & Bonin, P. (2011). Production of pristane and phytane in the marine environment: Role of prokaryotes. *Research in Microbiology*, *162*(9), 923–933. https://doi.org/10.1016/j.resmic.2011.01.012

Rowland, S. J. (1990). Production of acyclic isoprenoid hydrocarbons by laboratory maturation of methanogenic bacteria. *Organic Geochemistry*, *15*(15), 9–16. https://doi.org/10.1016/0146-6380(90)90181-X

Saalmann, K., & Thiedig, F. (2001). Tertiary West Spitsbergen fold and thrust belt on Brøggerhalvøya, Svalbard: Structural evolution and kinematics. *Tectonics*, *20*(6), 976–998. https://doi.org/10.1029/2001TC900016

Sabino, M., Dela Pierre, F., Natalicchio, M., Birgel, D., Gier, S., & Peckmann, J. (2021). The response of water column and sedimentary environments to the advent of the Messinian salinity crisis: Insights

from an onshore deep-water section (Govone, NW Italy). *Geological Magazine*, *158*(5), 825–841. https://doi.org/10.1017/S0016756820000874

Şahin, N., & Altıner, D. (2019). Testing of Permian–Lower Triassic stratigraphic data in a half-graben/tilt-block system: Evidence for the initial rifting phase in Antalya Nappes. *Canadian Journal of Earth Sciences, 56*(11), 1262–1283. https://doi.org/10.1139/cjes-2018-0169

Saito, R., Tian, L., Kaiho, K., & Takahashi, S. (2022). Biomarker evidence for the prolongation of multiple phytoplankton blooms in the aftermath of the end-Permian mass extinction. *Palaeogeography, Palaeoclimatology, Palaeoecology*, *600*, 111077. https://doi.org/10.1016/j.palaeo.2022.111077

Schobben, M., Foster, W. J., Sleveland, A. R. N., Zuchuat, V., Svensen, H. H., Planke, S., et al. (2020). A nutrient control on marine anoxia during the end-Permian mass extinction. *Nature Geoscience*, *13*(9), 640–646. https://doi.org/10.1038/s41561-020-0622-1

Schobben, M., Joachimski, M. M., Korn, D., Leda, L., & Korte, C. (2014). Palaeotethys seawater temperature rise and an intensified hydrological cycle following the end-Permian mass extinction. *Gondwana Research*, *26*(2), 675–683. https://doi.org/10.1016/j.gr.2013.07.019

Sephton, M. A., Looy, C. V., Brinkhuis, H., Wignall, P. B., de Leeuw, J. W., & Visscher, H. (2005). Catastrophic soil erosion during the end-Permian biotic crisis. *Geology, 33*(12), 941–944. https://doi.org/10.1130/G21784.1

Shen, J., Schoepfer, S. D., Feng, Q., Zhou, L., Yu, J., Song, H., et al. (2015). Marine productivity changes during the end-Permian crisis and Early Triassic recovery. *Earth-Science Reviews, 149*, 136–162. https://doi.org/10.1016/j.earscirev.2014.11.002

Sinninghe Damsté, J. S. S., Keely, B. J., Betts, S. E., Baas, M., Maxwell, J. R., & de Leeuw, J. W. (1993). Variations in abundances and distributions of isoprenoid chromans and long-chain alkylbenzenes in sediments of the Mulhouse Basin: A molecular sedimentary record of palaeosalinity. *Organic Geochemistry, 20*(8), 1201–1215. https://doi.org/10.1016/0146-6380(93)90009-Z

Sinninghe Damsté, J. S., Kock-van Dalen, A. C., & De Leeuw, J. W. (1988). Identification of long-chain isoprenoid alkylbenzenes in sediments and crude oils. *Geochimica et Cosmochimica Acta, 52*(11), 2671–2677. https://doi.org/10.1016/0016-7037(88)90035-X

Słowakiewicz, M., Tucker, M. E., Perri, E., & Pancost, R. D. (2015). Nearshore euxinia in the photic zone of an ancient sea. *Palaeogeography, Palaeoclimatology, Palaeoecology*, *426*, 242–259. https://doi.org/10.1016/j.palaeo.2015.03.022

Smyrak-Sikora, A., Betlem, P., Engelschiøn, V. S., Foster, W. J., Grundvåg, S.-A., Jelby, M. E., et al. (2025). Phanerozoic paleoenvironmental and paleoclimatic evolution in Svalbard. *Preprint at EGUsphere*, 2024-3912. https://doi.org/10.5194/egusphere-2024-3912

Song, H., Huang, S., Jia, E., Dai, X., Wignall, P. B., & Dunhill, A. M. (2020). Flat latitudinal diversity gradient caused by the Permian–Triassic mass extinction. *Proceedings of the National Academy of Sciences, 117*(30), 17578–17583. https://doi.org/10.1073/pnas.1918953117

Stanley, S. M. (2016). Estimates of the magnitudes of major marine mass extinctions in earth history. *Proceedings of the National Academy of Sciences*, *113*(42), E6325–E6334. https://doi.org/10.1073/pnas.1613094113

Stampfli, G., Marcoux, J., & Baud, A. (1991). Tethyan margins in space and time. *Palaeogeography, Palaeoclimatology, Palaeoecology, 87*(1-4), 373–409. https://doi.org/10.1016/0031-0182(91)90142-E

Sun, Y. (2024). Dynamics of nutrient cycles in the Permian–Triassic oceans. *Earth-Science Reviews, 258*, 104914. https://doi.org/10.1016/j.earscirev.2024.104914

Sun, Y., Farnsworth, A., Joachimski, M. M., Wignall, P. B., Krystyn, L., Bond, et al. (2024). Mega El Niño instigated the end-Permian mass extinction. *Science, 385*(6714), 1189–1195. https://doi.org/10.1126/science.ado2030

Sun, Y. D., Zulla, M. J., Joachimski, M. M., Bond, D. P. G., Wignall, P. B., Zhang, Z. T., & Zhang, M. H. (2019). Ammonium ocean following the end-Permian mass extinction. *Earth and Planetary Science Letters, 518*, 211–222. https://doi.org/10.1016/j.epsl.2019.04.036

Twitchett, R. J., & Barras, C. G. (2004). Trace fossils in the aftermath of mass extinction events. In McIlroy, D. (Ed.), *The Application of Ichnology to Palaeoenvironmental and Stratigraphic Analysis, Geological Society, London, Special Publications*, 228 (pp. 397–418). https://doi.org/10.1144/GSL.SP.2004.228.01.18

Uchman, A., Hanken, N. M., Nielsen, J. K., Grundvåg, S.-A., & Piasecki, S. (2016). Depositional environment, ichnological features and oxygenation of Permian to earliest Triassic marine sediments in central Spitsbergen, Svalbard. *Polar Research, 35*(1), 24782. https://doi.org/10.3402/polar.v35.24782

Vandier, F., Tourte, M., Doumbe-Kingue, C., Plancq, J., Schaeffer, P., Oger, P., & Grossi, V. (2021). Reappraisal of archaeal C_{20}-C_{25} diether lipid (extended archaeol) origin and use as a biomarker of

hypersalinity. *Organic Geochemistry*, *159*, 104276. https://doi.org/10.1016/j.orggeochem.2021.104276

Wong, J. C., Raven, J. A., Aldunate, M., Silva, S., Gaitán-Espitia, J. D., Vargas, C. A., et al. (2023). Do phytoplankton require oxygen to survive? A hypothesis and model synthesis from oxygen minimum zones. *Limnology and Oceanography, 68*(7), 1417–1437. https://doi.org/10.1002/lno.12367

Worsley, D. (2008). The post-Caledonian development of Svalbard and the western Barents Sea. *Polar research*, *27*(3), 298–317. https://doi.org/10.1111/j.1751-8369.2008.00085.x

Wu, J., Chu, D., Luo, G., Wignall, P. B., Algeo, T. J., & Xie, S. (2023). Stepwise deforestation during the Permian-Triassic boundary crisis linked to rising temperatures. *Earth and Planetary Science Letters, 620*, 118350. https://doi.org/10.1016/j.epsl.2023.118350

Xiang, L., Zhang, H., Schoepfer, S. D., Cao, C., Zheng, Q., Yuan, D., et al. (2020). Oceanic redox evolution around the end-Permian mass extinction at Meishan, South China. *Palaeogeography, Palaeoclimatology, Palaeoecology*, *544*, 109626. https://doi.org/10.1016/j.palaeo.2020.109626

Xie, S., Algeo, T. J., Zhou, W., Ruan, X., Luo, G., Huang, J., & Yan, J. (2017). Contrasting microbial community changes during mass extinctions at the middle/late Permian and Permian/Triassic boundaries. *Earth and Planetary Science Letters*, *460*, 180–191. https://doi.org/10.1016/j.epsl.2016.12.015

Xie, S., Pancost, R. D., Wang, Y., Yang, H., Wignall, P. B., Luo, G., et al. (2010). Cyanobacterial blooms tied to volcanism during the 5 m.y. Permo-Triassic biotic crisis. *Geology*, *38*(5), 447–450. https://doi.org/10.1130/G30769.1

Yin, H., Zhang, K., Tong, J., Yang, Z., & Wu, S. (2001). The Global Stratotype Section and Point (GSSP) of the Permian-Triassic Boundary. *Episodes Journal of International Geoscience, 24*(2), 102–114.

Zhang, Y., Wen, H., Zhu, C., Fan, H., & Cloquet, C. (2018). Cadmium isotopic evidence for the evolution of marine primary productivity and the biological extinction event during the Permian-Triassic crisis from the Meishan section, South China. *Chemical Geology*, *481*, 110–118. https://doi.org/10.1016/j.chemgeo.2018.02.005

Zhang, F., Shen, S., Cui, Y., Lenton, T. M., Dahl, T. W., Zhang, H., et al. (2020). Two distinct episodes of marine anoxia during the Permian-Triassic crisis evidenced by uranium isotopes in marine dolostones. *Geochimica et Cosmochimica Acta*, *287*, 165–179. https://doi.org/10.1016/j.gca.2020.01.032

Zuchuat, V., Sleveland, A. R. N., Twitchett, R. J., Svensen, H. H., Turner, H., Augland, L. E., et al. (2020). A new high-resolution stratigraphic and palaeoenvironmental record spanning the end-Permian mass extinction and its aftermath in central Spitsbergen, Svalbard. *Palaeogeography, Palaeoclimatology, Palaeoecology*, *554*, 109732. https://doi.org/10.1016/j.palaeo.2020.109732

AGU Advances

Supporting Information for

Phytoplankton blooms on the Barents Shelf, Svalbard, associated with the Permian–Triassic mass extinction

S. Z. Buchwald[1], D. Birgel[1], K. Senger[2], T. Mosociova[3], Y. Pei[4], V. Zuchuat[5], L. G. Tarhan[6], A. B. Frank[1], F. Galasso[1], M. A. Gómez Correa[1], E. Koşun[7], B. Karapunar[8], X. Wang[9], E. Kustatscher[10], H. Prinoth[11], N. Lahajnar[1], R. Steinkrauss[1], J. Peckmann[1], and W. J. Foster[1]

[1]Department of Earth System Sciences, University of Hamburg, Hamburg, Germany

[2]Department of Arctic Geology, University Centre in Svalbard, Longyearbyen, Norway

[3]Department of Geosciences, University of Oslo, Oslo, Norway

[4]State Key Laboratory of Geomicrobiology and Environmental Changes, China University of Geosciences, Wuhan, China

[5]CSIRO Mineral Resources, Kensington, WA, Australia

[6]Department of Earth and Planetary Sciences, Yale University, New Haven, USA

[7]Department of Geological Engineering, Akdeniz University, Antalya, Türkiye

[8]School of Earth and Environment, University of Leeds, Leeds, United Kingdom

[9]Institute of Sedimentary Geology, Chengdu University of Technology, Chengdu, China

[10]Department of Natural History, Tirolean State Museums, Hall in Tirol, Austria

[11]Museum Ladin Ciastel de Tor, San Martino in Badia, Italy

Contents of this file

Text S1. Geological setting of the paleotropical sections

1. Dolomites (northern Italy)

During the Permian–Triassic transition, the Dolomites in northern Italy were located in a shallow marine environment in the tropical western Paleotethys. The three sites Tramin (46.34307°N; 11.23453°E), Siusi (46.53280°N; 11.56213°E) and Seres (46.63990°N; 11.67433°E) record deposition on a homoclinal carbonate ramp with a water depth gradient from the southwest toward northeast (Noé, 1987), i.e., the Tramin section was deposited in the shallowest environment, followed by Siusi (medium water depth on the carbonate ramp) and Seres (deepest section of the three investigated sites). The Permian Bellerophon Formation is characterized by fossiliferous limestones and dolostone, which are interbedded with marly mud- and siltstones (e.g., Massari et al., 1994; Posenato, 2010; Prinoth & Posenato, 2023), and records transgressive-regressive cycles with episodes of extremely shallow conditions with potentially subaerial exposure at locations on the inner shelf (e.g., Massari et al., 1994; Prinoth & Posenato, 2023). The Bellerophon Formation is overlain by the mixed carbonate/siliciclastic Werfen Formation (e.g., Broglio Loriga et al., 1990). The main phase of the Permian–Triassic mass extinction event is recorded in the lowermost Werfen Formation within the oolitic bed of the Tesero Member (Farabegoli et al., 2007; Groves et al., 2007; Posenato, 2010). It predates the Permian/Triassic boundary as defined by the First Appearance Datum (FAD) of the conodont *Hindeodus parvus* at the Global Stratotype Section and Point (GSSP) at Meishan, China (Yin et al., 2001), which is located 1.45 m above the base of the Werfen Formation at Siusi (Horacek et al., 2010). The Werfen Formation records the whole Early Triassic. In this study, however, we sampled only up to the Mazzin Member at Siusi, and the upper Bellerophon Formation at Tramin and Seres.

2. Taurus Mountains (Türkiye)

Çürük Dağ (36.70100°N; 30.45118°E) is a section in the Taurus Mountains in Türkiye southwest of Antalya, which is part of the Antalya Nappes (Özgül 1984, 1997, Şahin & Altıner, 2019). During the Permian–Triassic transition, it was located in the tropical Neotethys and constituted an open marine environment on a shallow shelf (e.g., Marcoux & Baud, 1988; Stampfli et al., 1991). The

middle and late Permian is represented by fossiliferous packstones of the Pamucak Formation (e.g., Angiolini et al., 2007; Crasquin-Soleau et al., 2004; Lys & Marcoux, 1978). They are overlain by a thin oolitic layer that records the negative carbon isotope excursion coinciding with the Permian–Triassic mass extinction (Richoz, 2006). Above, the Korkarkoyu Formation is expressed in thick stromatolitic and thrombolitic beds (Altıner & Zaninetti, 1980; Baud et al., 2005, 2007), which also contain the index fossil *H. parvus*, thus placing the Permian/Triassic boundary within the lowermost microbialites (Crasquin-Soleau et al., 2002; Richoz, 2006). The samples investigated here all derive from the uppermost Permian in the Pamucak Formation.

3. Great Bank of Guizhou (South China)

The Great Bank of Guizhou is the northernmost of several isolated carbonate platforms in the Nanpanjiang Basin in South China, which was located in the tropical eastern Paleotethys during the Permian–Triassic transition (Lehrmann et al., 2005, 2007). It evolved on the margin of the former Yangtze platform during a late Permian regional transgression, and prevailed until the Late Triassic (Lehrmann et al., 2005). Both upper Permian and Lower Triassic deposits record open shallow-marine conditions (Lehrmann et al., 1998). The two sections Xinbaihou (25.58265°N; 106.74832°E) and Youjiangzhai (25.74803°N; 106.97622°E) host strata deposited on the inner platform and closer to the platform margin, respectively (Foster et al., 2019; Lehrmann et al., 2001). Upper Permian packstone deposits contain an abundant and diverse fossil assemblage including foraminifera, calcareous sponges, calcareous algae, corals, and echinoderms (Payne et al., 2006), and chert nodules (Lehrmann et al., 2003). They are overlain by thick stromatolitic and thrombolitic beds (Foster et al., 2019, 2018; Lehrmann et al., 1998), intercalated with wacke-, pack- and grainstones (Foster et al., 2018; Payne et al., 2006), that were deposited following the extinction. The Xinbaihou section is represented by two post-extinction microbialite samples, and Youjianzhai by one pre-extinction packstone sample and one post-extinction microbialite sample.

Figures S1 to S5.

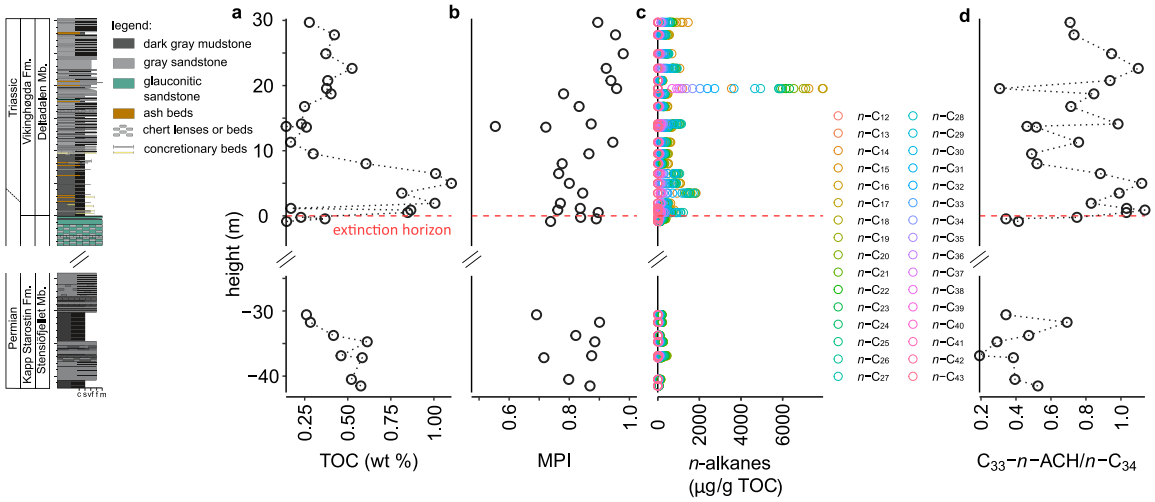

Figure S1. *Lusitaniadalen profile with stratigraphic changes of (a) total organic carbon (TOC), (b) methylphenanthrene index (MPI) after Cassani et al. (1988) with MPI = 1.89(2-MP + 3-MP)/[P + 1.26(1-MP + 9-MP)]; MP = peak area of methylphenanthrene from m/z = 192 mass chromatogram; P = peak area of phenanthrene from m/z = 178 mass chromatogram, (c) n-$C_{12–43}$-alkanes, and (d) ratio of C_{33}-n-ACH and n-C_{34}. The red dashed line marks the extinction horizon (Foster et al., 2023; Nabbefeld et al., 2010; Uchman et al., 2016). Note that the y-axis is broken (as indicated by parallel diagonal line segments) to focus on sampling intervals; similar pre- and post-extinction lithologies were targeted to control for potential lithofacies bias on the biomarker data. c – claystone; s – siltstone; vf – very fine-grained sandstone; f – fine-grained sandstone; m – medium-grained sandstone.*

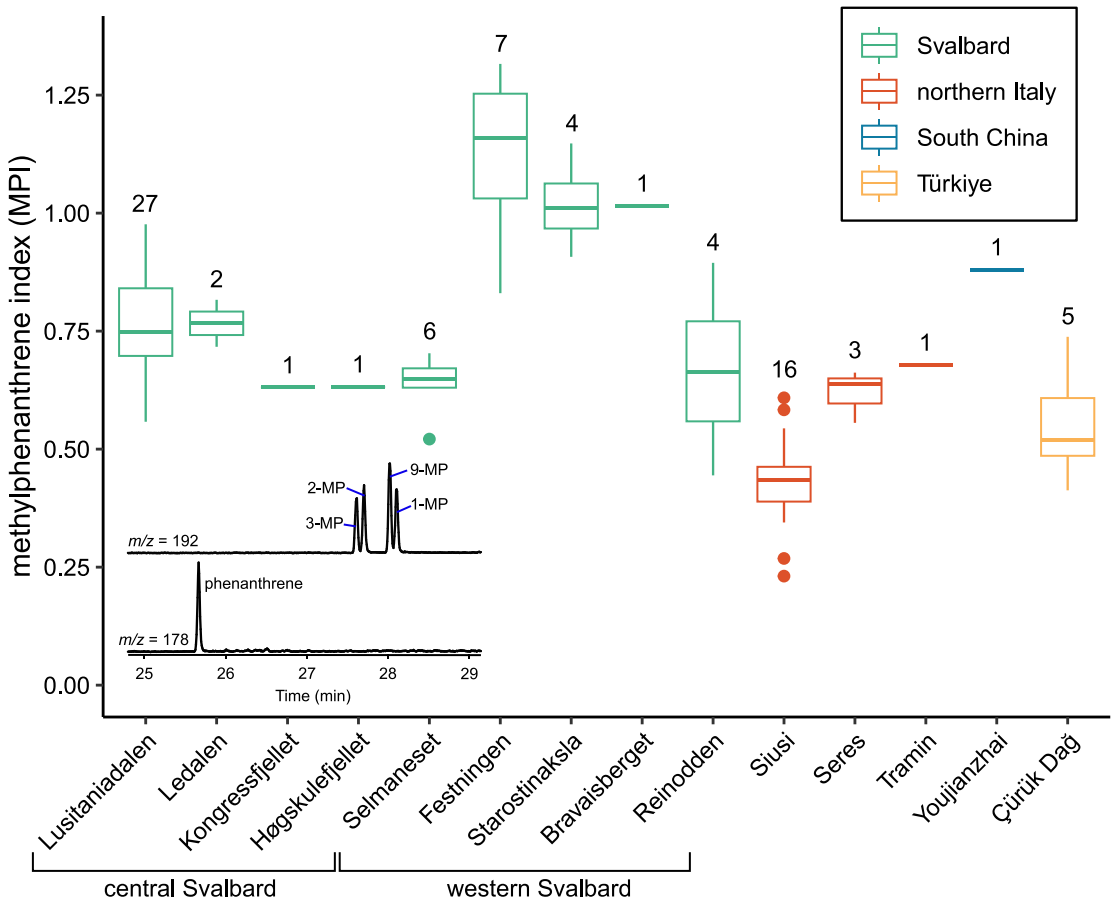

Figure S2. *Methylphenanthrene index (MPI) from all investigated sections calculated from the F1 fraction with MPI = 1.89(2 MP + 3 MP)/[P + 1.26(1 MP + 9 MP)]; MP = peak area of methylphenanthrene from m/z = 192 mass chromatogram; P = peak area of phenanthrene from m/z = 178 mass chromatogram (see inserted example of mass chromatograms). The numbers on the boxes denote the total number of analyzed samples per section that contained all required compounds to calculate the MPI. Note that methylphenanthrenes and phenanthrene were absent at Xinbaihou.*

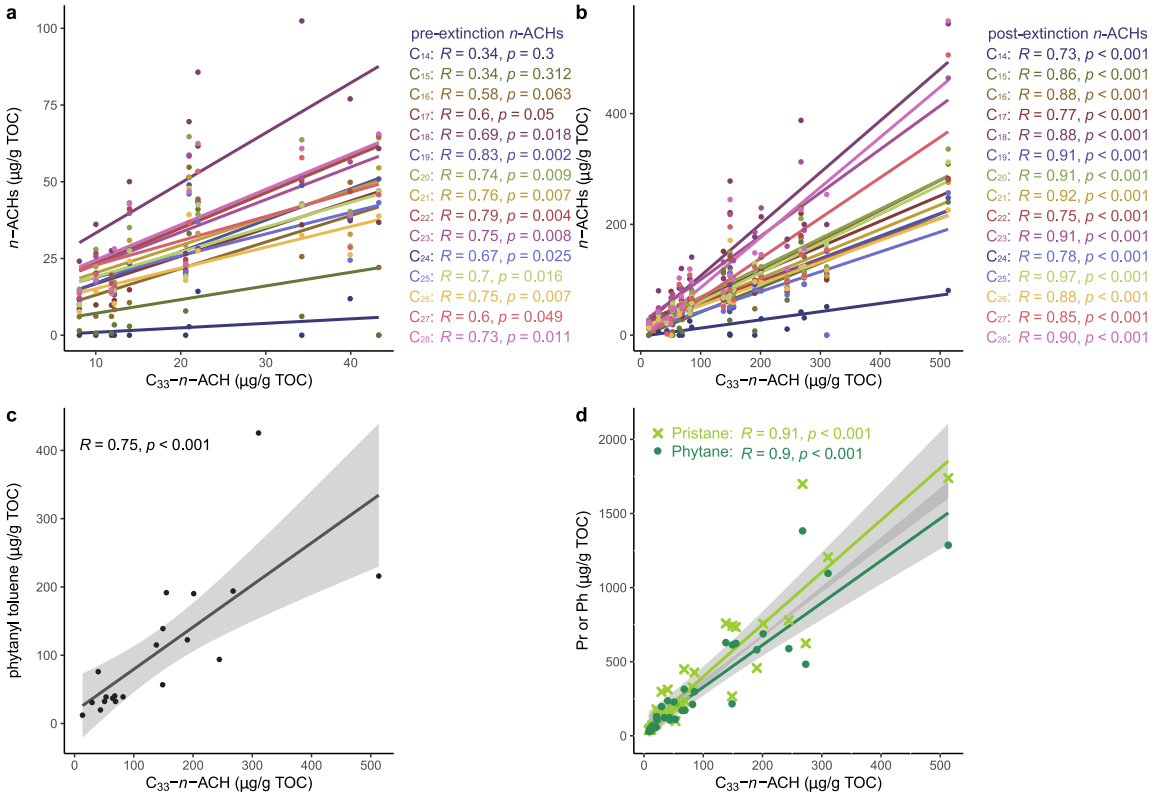

Figure S3. *Scatterplots of C_{33}-n-alkylcyclohexane (C_{33}-n-ACH) and various biomarkers including (a) pre-extinction short-chain n-ACHs, (b) post-extinction short-chain n-ACHs, (c) phytanyl toluene, and (d) pristane (Pr) and phytane (Ph). Grey shaded areas mark confidence intervals. Correlation coefficients (R) are indicated, and significance is assumed for $p < 0.05$.*

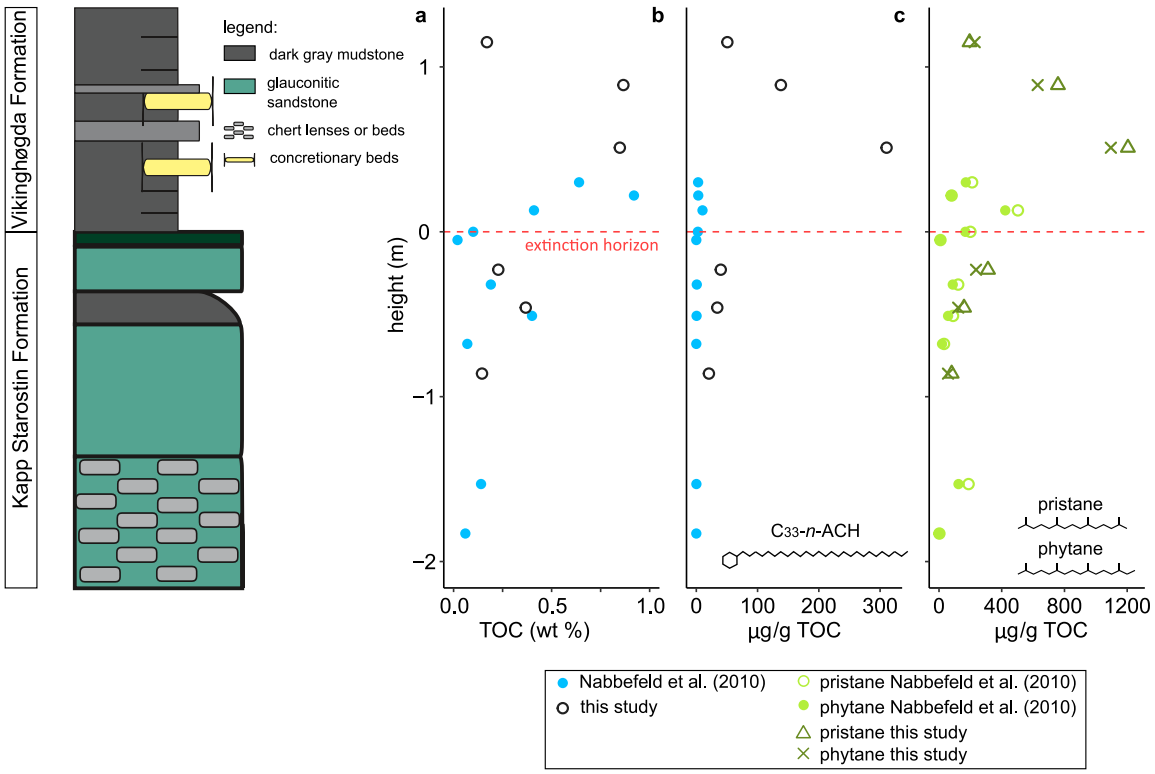

Figure S4. *Comparison to (a) total organic carbon (TOC), (b) C_{33}-n-alkylcyclohexane (C_{33}-n-ACH), and (c) pristane and phytane content from Nabbefeld et al. (2010), who investigated a shorter interval across the extinction horizon. The red dashed line marks the extinction horizon (Foster et al., 2023; Nabbefeld et al., 2010; Uchman et al., 2016).*

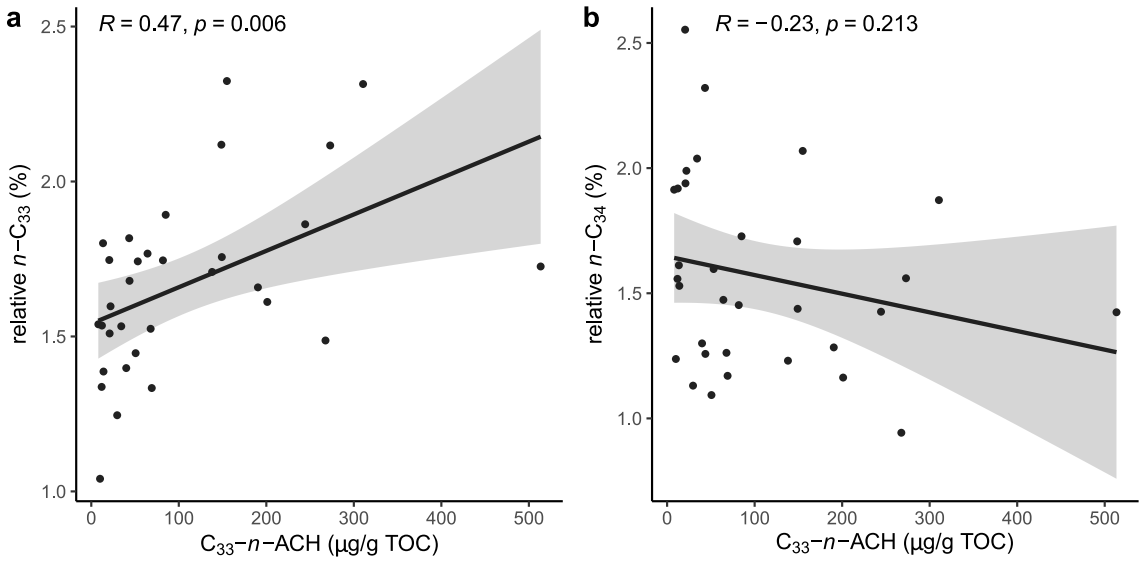

Figure S5. *Scatterplots of C_{33}-n-ACH and n-alkanes including (a) the abundance of n-C_{33} relative to all n-alkanes (100%), (b) the abundance of n-C_{34} relative to all n-alkanes (100%). Correlation coefficients (R) are indicated, and significance is assumed for p < 0.05.*

References

Altıner, D., & Zaninetti, L. (1980). Le Trias dans la région de Pinarbasi, Taurus oriental, Turquie: Unités lithologiques, micropaléontologie, milieux de dépôt. *Rivista Italiana di Paleontologia e Stratigrafia, 86*(4), 705–760.

Angiolini, L., Carabelli, L., Nicora, A., Crasquin-Soleau, S., Marcoux, J., & Rettori, R. (2007). Brachiopods and other fossils from the Permo–Triassic boundary beds of the Antalya Nappes (SW Taurus, Turkey). *Geobios, 40*(6), 715–729. https://doi.org/10.1016/j.geobios.2007.01.007

Baud, A., Richoz, S., & Marcoux, J. (2005). Calcimicrobial cap rocks from the basal Triassic units: Western Taurus occurrences (SW Turkey). *Comptes Rendus Palevol, 4*(6–7), 569–582. https://doi.org/10.1016/j.crpv.2005.03.001

Baud, A., Richoz, S., & Pruss, S. (2007). The Lower Triassic anachronistic carbonate facies in space and time. *Global and Planetary Change, 55*(1–3), 81–89. https://doi.org/10.1016/j.gloplacha.2006.06.008

Broglio Loriga, C., Góczán, F., Haas, J., Lenner, K., Neri, C., Oravecz Scheffer, A., et al. (1990). The Lower Triassic sequences of the Dolomites (Italy) and Transdanubian Mid-Mountains (Hungary) and their correlation. *Memorie Di Scienze Geologiche, 11*(2), 41–103.

Cassani, F., Gallango, O., Talukdar, S., Vallejos, C., & Ehrmann, U. (1988). Methylphenanthrene maturity index of marine source rock extracts and crude oils from the Maracaibo Basin. *Organic Geochemistry, 13*(3), 73–80. https://doi.org/10.1016/B978-0-08-037236-5.50013-0

Crasquin-Soleau, S., Marcoux, J., Angiolini, L., Richoz, S., Nicora, A., Baud, A., & Bertho, Y. (2004). A new ostracode fauna from the Permian-Triassic boundary in Turkey (Taurus, Antalya Nappes). *Micropaleontology, 50*(3), 281–295. https://doi.org/10.2113/50.3.281

Crasquin-Soleau, S., Richoz, S., Marcoux, J., Angiolini, L., Nicora, A., & Baud, A. (2002). Les événements de la limite Permien–Trias: Derniers survivants et/ou premiers re-colonisateurs parmi les ostracodes du Taurus (Sud-Ouest de la Turquie). *Comptes rendus. Géoscience, 334*(7), 489–495. https://doi.org/10.1016/S1631-0713(02)01782-0

Farabegoli, E., Perri, M. C., & Posenato, R. (2007). Environmental and biotic changes across the Permian-Triassic boundary in western Tethys: The Bulla parastratotype, Italy. *Global and Planetary Change, 55*(1–3), 109–135. https://doi.org/10.1016/j.gloplacha.2006.06.009

Foster, W. J., Asatryan, G., Rauzi, S., Botting, J. P., Buchwald, S. Z., Lazarus, D. B., et al. (2023). Response of siliceous marine organisms to the Permian-Triassic climate crisis based on new findings from central Spitsbergen, Svalbard. *Paleoceanography and Paleoclimatology*, *38*(12), e2023PA004766. https://doi.org/10.1029/2023PA004766

Foster, W. J., Lehrmann, D. J., Hirtz, J. A., White, M., Yu, M., Li, J., & Martindale, R. C. (2019). Early Triassic benthic invertebrates from the Great Bank of Guizhou, South China: Systematic palaeontology and palaeobiology. *Papers in Palaeontology, 5*(4), 613–656. https://doi.org/10.1002/spp2.1252

Foster, W. J., Lehrmann, D. J., Yu, M., Ji, L., & Martindale, R. C. (2018). Persistent environmental stress delayed the recovery of marine communities in the aftermath of the latest Permian mass extinction. *Paleoceanography and Paleoclimatology, 33*(4), 338–353. https://doi.org/10.1002/2018PA003328

Groves, J. R., Rettori, R., Payne, J. L., Boyce, M. D., Demi, D., & Altıner, D. (2007). End-Permian mass extinction of lagenide foraminifers in the Southern Alps (northern Italy). *Journal of Paleontology, 81*(3), 415–434. https://doi.org/10.1666/05123.1

Horacek, M., Povoden, E., Richoz, S., & Brandner, R. (2010). High-resolution carbon isotope changes, litho- and magnetostratigraphy across Permian-Triassic boundary sections in the Dolomites, N-Italy.

New constraints for global correlation. *Palaeogeography, Palaeoclimatology, Palaeoecology, 290*(1–4), 58–64. https://doi.org/10.1016/j.palaeo.2010.01.007

Lehrmann, D. J., Enos, P., Payne, J. L., Montgomery, P., Wei, J., Yu, Y., et al. (2005). Permian and Triassic depositional history of the Yangtze platform and Great Bank of Guizhou in the Nanpanjiang basin of Guizhou and Guangxi, south China. Albertiana, 33(1), 149–168.

Lehrmann, D. J., Jiayong, W., & Enos, P. (1998). Controls on facies architecture of a large Triassic carbonate platform; the Great Bank of Guizhou, Nanpanjiang Basin, South China. *Journal of Sedimentary Research, 68*(2), 311–326. https://doi.org/10.2110/jsr.68.311

Lehrmann, D. J., Payne, J. L., Felix, S. V., Dillett, P. M., Wang, H., Yu, Y., & Wei, J. (2003). Permian–Triassic boundary sections from shallow-marine carbonate platforms of the Nanpanjiang Basin, South China: Implications for oceanic conditions associated with the end-Permian extinction and its aftermath. *Palaios, 18*(2), 138–152. https://doi.org/10.1669/0883-1351(2003)18<138:PBSFSC>2.0.CO;2

Lehrmann, D. J., Payne, J. L., Pei, D., Enos, P., Druke, D., Steffen, K., et al. (2007). Record of the end-Permian extinction and Triassic biotic recovery in the Chongzuo-Pingguo platform, southern Nanpanjiang basin, Guangxi, south China. *Palaeogeography, Palaeoclimatology, Palaeoecology, 252*(1–2), 200–217. https://doi.org/10.1016/j.palaeo.2006.11.044

Lehrmann, D. J., Wan, Y., Wei, J., Yu, Y., & Xiao, J. (2001). Lower Triassic peritidal cyclic limestone: An example of anachronistic carbonate facies from the Great Bank of Guizhou, Nanpanjiang Basin, Guizhou province, South China. *Palaeogeography, Palaeoclimatology, Palaeoecology*, *173*(3-4), 103-123. https://doi.org/10.1016/S0031-0182(01)00302-9

Lys, M., Marcoux, J., 1978. Les niveaux du Permien supérieurdes Nappes d'Antalya (Taurides occidentales, Turquie). *Comptes Rendus de l'Académie des Sciences 286*, 1417–1420.

Marcoux, J., & Baud, A. (1988). The Permo-Triassic boundary in the Antalya Nappes (Western Taurides-Turkey). *Memoir Società Geologica Italiana, 34*, 243–252.

Massari, F., Neri, C., Pittau, P., Fontana, D., & Stefani, C. (1994). Sedimentology, palynostratigraphy and sequence stratigraphy of a continental to shallow-marine rift-related succession: Upper Permian of the eastern Southern Alps (Italy). *Memorie Di Scienze Geologiche, 46*, 119–243.

Nabbefeld, B., Grice, K., Twitchett, R. J., Summons, R. E., Hays, L., Böttcher, M. E., & Asif, M. (2010). An integrated biomarker, isotopic and palaeoenvironmental study through the late Permian event at

Lusitaniadalen, Spitsbergen. *Earth and Planetary Science Letters, 291*(1–4), 84–96. https://doi.org/10.1016/j.epsl.2009.12.053

Noé, S. (1987). Facies and paleogeography of the marine upper Permian and of the Permian-Triassic boundary in the Southern Alps (Bellerophon Formation, Tesero Horizon). *Facies, 16*, 89–142. https://doi.org/10.1007/BF02536749

Özgül, N. (1984). Stratigraphy and tectonic evolution of the Central Taurides. *Geology of the Taurus belt. International symposium*, 77–90.

Özgül, N. (1997). Bozkır-Hadım-Taşkent (orta toroslar'in kuzey kesimi) dolayinda yer alan tektono-stratigrafik birliklerin stratigrafisi. *Maden Tektik ve Arama Dergisi, 119*, 113–174.

Payne, J. L., Lehrmann, D. J., Wei, J., & Knoll, A. H. (2006). The pattern and timing of biotic recovery from the end-Permian extinction on the Great Bank of Guizhou, Guizhou Province, China. *Palaios, 21*(1), 63–85. https://doi.org/10.2110/palo.2005.p05-12p

Posenato, R. (2010). Marine biotic events in the lopingian succession and latest Permian extinction in the Southern Alps (Italy). *Geological Journal, 45(*2–3), 195–215. https://doi.org/10.1002/gj.1212

Prinoth, H., & Posenato, R. (2023). Bivalves from the Changhsingian (upper Permian) Bellerophon Formation of the Dolomites (Italy): Ancestors of Lower Triassic post-extinction benthic communities. *Papers in Palaeontology, 9*(2), e1486. https://doi.org/10.1002/spp2.1486

Richoz, S. (2006). Stratigraphie isotopique du Permien superieur et Trias inferieur de quelques localites de la Neotethys. *Memoire de Geologie (Lausanne), 46*, 283.

Şahin, N., & Altıner, D. (2019). Testing of Permian–Lower Triassic stratigraphic data in a half-graben/tilt-block system: evidence for the initial rifting phase in Antalya Nappes. *Canadian Journal of Earth Sciences, 56*(11), 1262–1283. https://doi.org/10.1139/cjes-2018-0169

Stampfli, G., Marcoux, J., & Baud, A. (1991). Tethyan margins in space and time. *Palaeogeography, Palaeoclimatology, Palaeoecology, 87*(1–4), 373–409. https://doi.org/10.1016/0031-0182(91)90142-E

Uchman, A., Hanken, N. M., Nielsen, J. K., Grundvåg, S.-A., & Piasecki, S. (2016). Depositional environment, ichnological features and oxygenation of Permian to earliest Triassic marine sediments in central Spitsbergen, Svalbard. *Polar Research, 35*(1), 24782. https://doi.org/10.3402/polar.v35.24782

Yin, H., Zhang, K., Tong, J., Yang, Z., & Wu, S. (2001). The Global Stratotype Section and Point (GSSP) of the Permian-Triassic boundary. *Episodes Journal of International Geoscience, 24*(2), 102–114.

Manuscript II

Buchwald SZ, Frank AB, Birgel D, Senger K, Mosociova T, Pei Y, Beaty B, Tarhan LG, Galasso F, Gómez Correa MA, Grasby SE, Struck U, Steinkrauss R, Gliwa J, Lahajnar N, Peckmannn J, Foster WJ. Reconstructing environmental and microbial ecosystem changes across the Permian–Triassic mass extinction at Lusitaniadalen, Svalbard. *Submitted to Paleoceanography and Paleoclimatology.* Preprint: https://doi.org/10.22541/essoar.175766816.64475408/v1

SZB, ABF and WJF conceptualized the study; SZB and AB performed the formal analysis; SZB curated the data; SZB and WJF acquired funding; SZB, KS, TM, YP, BB, LGT, FG, JG, and WJF were involved in planning and conducting fieldwork; KS, SEG, US, JP, DB and WJF provided institutional resources; SZB and RS conducted the lipid biomarker lab work; NL provided TOC data; SEG provided HAWK data; US provided stable carbon isotope data; SZB and ABF wrote and visualized the original draft; all co-authors were involved in reviewing and editing.

Reconstructing environmental and microbial ecosystem changes across the Permian–Triassic mass extinction at Lusitaniadalen, Svalbard

S. Z. Buchwald[1], A. B. Frank[1], D. Birgel[1], K. Senger[2], T. Mosociova[2,3], Y. Pei[4], B. Beaty[5], L. G. Tarhan[5], F. Galasso[1], M. A. Gómez Correa[1], S. E. Grasby[6], U. Struck[7], R. Steinkrauss[1], J. Gliwa[8], N. Lahajnar[1], J. Peckmann[1], and W. J. Foster[1]

[1]Department of Earth System Sciences, University of Hamburg, Hamburg, Germany

[2]Department of Arctic Geology, University Centre in Svalbard, Longyearbyen, Norway

[3]Department of Geosciences, University of Oslo, Oslo, Norway

[4]State Key Laboratory of Geomicrobiology and Environmental Changes, China University of Geosciences, Wuhan, China

[5]Department of Earth and Planetary Sciences, Yale University, New Haven, USA

[6]Geological Survey of Canada, Calgary, Canada

[7]Museum für Naturkunde, Leibniz Institute for Evolution and Biodiversity Science, Berlin, Germany

[8]Institut für Geologische Wissenschaften, Freie Universität Berlin, Berlin, Germany

Corresponding author: Stella Zora Buchwald (stella.buchwald@uni-hamburg.de)

Key Points:

- In the aftermath of the Permian–Triassic environmental crisis, increased input of terrigenous organic matter is preserved in Svalbard
- Shallow marine environments were mainly oxic but occasionally punctuated by suboxic to anoxic episodes
- Lipid biomarker assemblages change substantially in composition across the extinction event and do not return to the pre-extinction baseline

Abstract

The Permian–Triassic environmental crisis triggered fundamental changes in marine ecosystems, culminating in the most severe biodiversity crisis of the Phanerozoic. Yet, the environmental and geochemical conditions governing the crisis and ecosystem recovery remain debated. The sedimentary succession at Lusitaniadalen, Svalbard, deposited in the Permo–Triassic Boreal Realm, offers insights into mid-latitudinal, shallow marine ecosystem responses. In a multiproxy study combining lipid biomarker and geochemical data, we reconstruct environmental conditions and microbial ecosystem dynamics across the Permian–Triassic environmental crisis. Generally low enrichments of the redox-sensitive trace elements Re, V, U and Mo, predominantly negative Ce anomalies, and a pristane/phytane ratio > 1 suggest mainly oxic conditions in the investigated interval. However, while transient dysoxic to anoxic episodes recorded across the extinction horizon support that deoxygenation contributed to the severity of the mass extinction, the earlier occurrence of similar episodes of deoxygenation in the late Permian challenges the hypothesis of global anoxia as the sole extinction driver at this site. Lipid biomarkers reveal a post-extinction increase in abundance of long-chain *n*-alkanes derived from terrestrial plants due to increased terrigenous discharge into shallow marine settings across this interval. Pristane and phytane, lipid biomarkers mainly derived from chlorophyll, reveal a pronounced regional increase in primary productivity following the environmental crisis. The composition of the lipid biomarker inventory recorded in early Griesbachian strata remains distinct from the pre-crisis composition, and did not recover towards the pre-crisis state within the studied interval.

Plain Language Summary

The Permian–Triassic mass extinction (ca. 252 million years ago) was the most severe biodiversity crisis in Earth's history, wiping out most marine and terrestrial species. However, the environmental changes that led to this event, and shaped the recovery of life afterward, remain disputed. Rocks from Lusitaniadalen, Svalbard, provide a marine record of this time from northern hemisphere mid-paleolatitudes. In this study, we analyzed chemical elements and organic molecules (lipid biomarkers) preserved in these rocks to reconstruct environmental conditions before and after the extinction event. Chemical signatures indicate that the seawater was mostly

oxygenated. The extinction event coincided with a short episode of low oxygen availability, but similar low-oxygen episodes occurred prior to the extinction event and are not associated with evidence for major losses in diversity, which questions whether oxygen loss alone was the principal driver of this mass extinction. We find that, after the extinction event, more organic material from land was washed into the ocean. Biomarkers from chlorophyll suggest a regional marine primary productivity increase after the extinction. Finally, the post-extinction microbial community remained different from the pre-crisis community, with no sign of recovery to pre-extinction baselines in the ca. 136,000-year post-extinction interval covered by our study.

1 Introduction

The environmental crisis at the Permian/Triassic boundary, ca. 252 million years ago, led to the most severe mass extinction event in the Phanerozoic. It recorded unprecedented extinction rates and major changes in marine and terrestrial ecosystems (Rees, 2002; Stanley, 2016). The Permian–Triassic environmental crisis is thought to have been triggered by extensive flood basalt volcanism of the Siberian Traps, characterized by a massive release of greenhouse gases and other volatiles into the atmosphere from both lava flows and the associated feeding intrusive complex (Svensen et al., 2009). These gas releases are hypothesized to have had cascading effects on environmental conditions, like an increase in sea surface temperatures (e.g., Joachimski et al., 2012, 2020; Schobben et al., 2014; Gliwa et al., 2022) and the expansion of anoxic water masses (e.g., Cao et al., 2009; Nabbefeld et al., 2010a; Chen et al., 2011; Penn et al., 2018; Xiang et al., 2020; Zhang et al., 2020), which would have caused the extinction of many aquatic organisms. However, such paleoredox reconstructions show pronounced heterogeneities when comparing different proxy systems, as for example (I) redox-sensitive trace element concentrations, (II) redox-dependent isotope fractionation, or (III) lipid biomarker data. Such heterogeneities may point to different proxy thresholds to environmental redox conditions, different geochemical compositions of the mineral and organic phases of the host sediment, or integration over different spatial and temporal scales (e.g., Algeo & Liu, 2020; Elrick et al., 2017; Weyer et al., 2008). However, it also likely reflects spatial and temporal variability in the distribution of seawater oxygen, with disparities between different ocean basins and paleo-water

depths (Bond & Wignall, 2010; Schaal et al., 2015). Recent efforts to reassess regional patterns in paleoredox state (e.g., Frank et al., 2025) suggest that the role of anoxia in shaping Permian–Triassic extinction and post-extinction recovery dynamics merits further consideration.

Changes in redox conditions can significantly impact both benthic and pelagic ecological communities, as deoxygenation leads to hypoxia in aerobic organisms, acting as a direct killing mechanism. However, bottom-water anoxia can also support enhanced pelagic productivity by increasing the availability of nutrients for phytoplankton and other autotrophic microbes, for instance through phosphorus remobilization from anoxic seafloor sediments (e.g., Schobben et al., 2020). The microbial community directly interacts with the inorganic environment and provides nutrients and energy to other members of the ecosystem by mediating biogeochemical cycling, for instance of carbon, nitrogen and phosphorus (e.g., Arrigo, 2005; Karl, 2014; Pajares & Ramos, 2019) and thus provides important ecosystem services. A better understanding of how microbial communities responded to the severe environmental perturbations in the late Permian, and in the aftermath of the Permian–Triassic mass extinction event, would provide valuable insights into past ecosystem processes and functions.

While the effect of deteriorating environmental conditions during the Permian–Triassic crisis on metazoan communities can be studied through preserved micro- and macrofossil assemblages (e.g., Crasquin et al., 2010; Foster et al., 2019; Gliwa et al., 2021; Prinoth & Posenato, 2023), studying the microbial community of ancient ecosystems can be challenging. Molecular fossils, such as lipid biomarkers, provide an opportunity to investigate microbial communities. Like other organic macromolecules such as DNA, RNA, and proteins, lipids are microbially degraded in the water column during vertical transport to the seafloor, and further defunctionalized and degraded during diagenesis (Luo et al., 2019; Summons et al., 2022). In ancient systems like the Permian–Triassic transition, the lipid biomarker inventory of microbial communities is usually only preserved in the hydrocarbon fraction, representing the final stage of degradation products of former organic macromolecules (e.g., Brocks & Grice, 2011). Lipid biomarkers therefore preserve information about their precursor molecules with various degrees of specificity over geological timescales. They can be utilized to reconstruct past microbial communities including the community of both

primary producers and abundant heterotrophic microbes (e.g., Chen et al., 2011; Jia et al., 2012; Summons, 2014; Birgel et al., 2014; Heindel et al., 2018), and the depositional environment including redox state or degree of terrestrial organic matter input (Cao et al., 2009; Nabbefeld et al., 2010a; Xie et al., 2017), and provide metrics of thermal maturity (Sousa Júnior et al., 2013).

Most previous work on lipid biomarkers across the Permian–Triassic mass extinction has focused on samples from paleoequatorial to subtropical carbonate platforms of the Tethys Ocean (South China: Cao et al., 2009; Chen et al., 2011; Luo et al., 2013; northern Italy: Jia et al., 2012; Sephton et al., 2005, 2015; Iran and Turkey: Heindel et al., 2018), while mid- to higher-paleolatitude settings are less represented (Svalbard: Nabbefeld et al., 2010a; Greenland: Grice et al., 2005a; Hays et al., 2012; Canada: Hays et al., 2007; Australia: Grice et al., 2005b). However, sedimentary successions from the Boreal Realm are of special interest, because of the progressively increasing isolation of the Boreal Realm from the Tethys Ocean during the late Permian due to the closing of the Uralian seaway (Reid et al., 2007). The Svalbard Archipelago provides excellent archives from the Permian–Triassic transition due to well-exposed sedimentary successions. In this study, we investigate sedimentary geochemical proxies as well as the lipid biomarker inventory at Lusitaniadalen, Svalbard, across the Permian–Triassic environmental crisis and into the early Griesbachian. These complementary approaches enable a more comprehensive understanding of environmental changes, such as shifting redox conditions, that culminated in the mass extinction event, as well as of the response of the microbial community to these changes.

2 Materials and Methods

2.1 Geological setting

During the late Permian and the Early Triassic, the Svalbard Archipelago was located at the northern margin of Pangea on the Barents Shelf in the Boreal Realm (Fig. 2.1a). Today, Lusitaniadalen (N78° 17.845, E16° 44.000) is a valley located in the central part of the main island of the archipelago, Spitsbergen (Fig. 2.1b). The Kapp Starostin Formation records the late Permian and is characterized by a cyclic alternation between bioturbated silicified mud- and siltstones, and fine-grained bioturbated sandstones with high silica content expressed in cherty

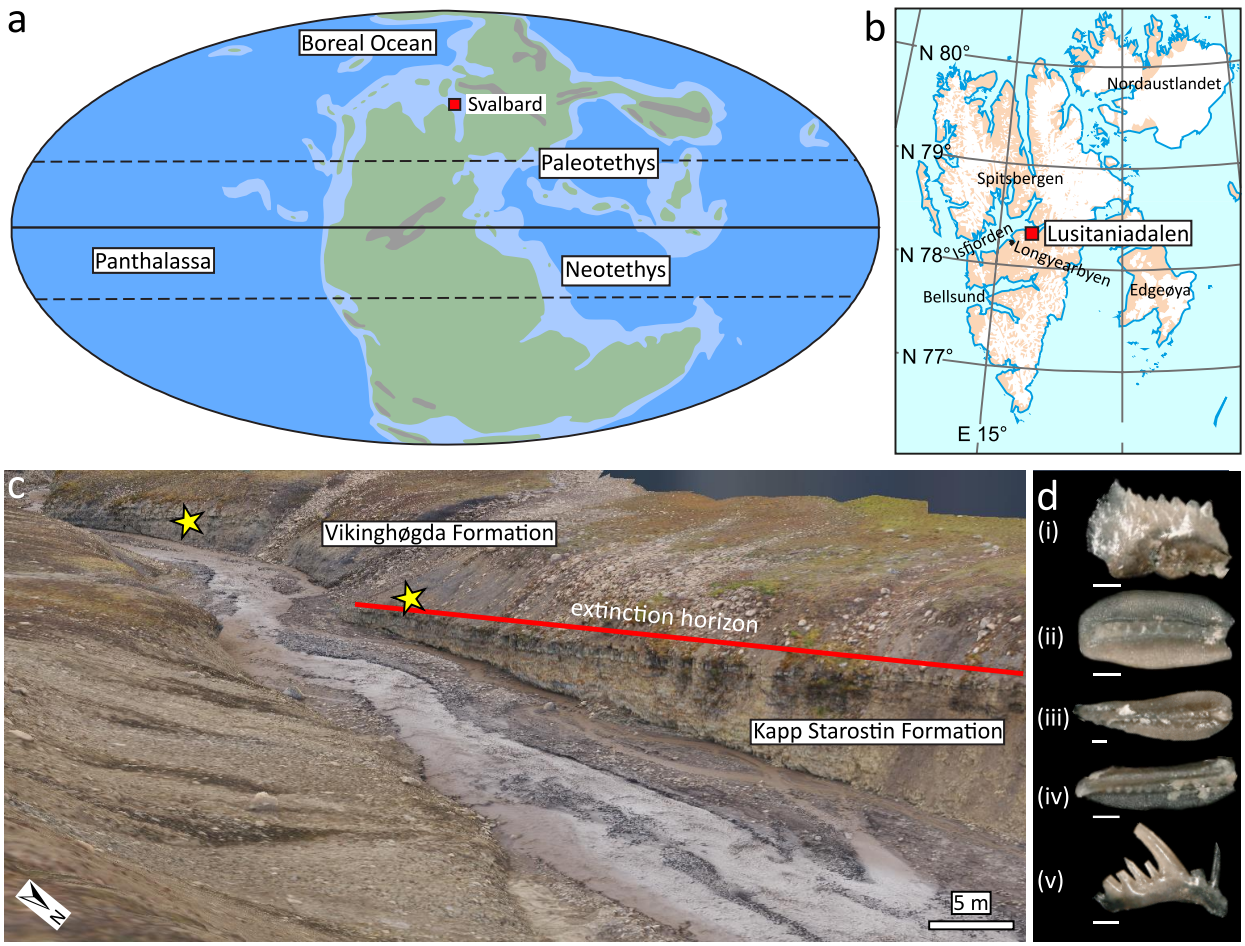

Figure 2.1: *(a) Paleogeographic location of Svalbard during the Permian–Triassic transition (base map: Blakey et al., 2012); (b) location of Lusitaniadalen on the main island of Svalbard, Spitsbergen (base map: Norwegian Polar Institute, projection: WGS 84/Arctic Polar Stereographic); (c) view towards the extinction horizon in the digital 3D outcrop model of Lusitaniadalen with concretionary horizons hosting conodonts marked with stars; (d) conodonts from concretionary horizons in the lower Deltadalen Member of the Vikinghøgda Formation exhibit a relatively pristine color according to the conodont color alteration index (Epstein et al., 1977): i: concretion 0.37 m above the formation boundary (right yellow star in c); ii–v: concretion 8.45 m above the formation boundary (left yellow star in c); scale bar = 100 µm.*

lenses or beds, which are overlain by bioturbated glauconitic sandstones in the uppermost 20 m of the formation (Figs. 2.1c, 2.2). Following the interpretation by Mørk et al. (1999), the base of the overlying Vikinghøgda Formation is located at an irregular, brownish or yellowish weathering

surface approximately 2 m below the top of the glauconitic sandstone beds. This surface, however, was not observed by others re-visiting the outcrop (Nabbefeld et al., 2010a), and we were also not able to identify this layer. Therefore, the interpretation of Nagy et al. (2025) is used, who suggested the top of the glauconitic sandstone beds represents the Kapp Starostin/Vikinghøgda formation boundary. The top of the glauconitic sandstones also coincides with the Permian–Triassic mass extinction horizon, which was previously defined as the loss of bioturbation (Nabbefeld et al., 2010a; Foster et al., 2017, 2023; Zuchuat et al., 2020), and is further supported by carbon isotopes (see below).

Based on the above definition, the glauconitic sandstones of the Kapp Starostin Formation are overlain by laminated siltstones and very fine-grained sandstones of the Vikinghøgda Formation. They host carbonate concretions containing a diverse and exceptionally well-preserved silicified fauna (Foster et al., 2017, 2023), as well as several tephra layers. At Deltadalen, a tephra layer just above the First Appearance Datum of the conodont *Hindeodus parvus*, the index fossil defining the base of the Triassic at the GSSP in Meishan (Yin et al., 2001), was dated to an age of 252.13 ± 0.62 Ma, placing the Permian/Triassic boundary ca. 2.40 m above the last glauconitic sandstone bed (Zuchuat et al., 2020). The tephra layers and concretionary horizons at Deltadalen (Zuchuat et al., 2020) and Lusitaniadalen can be used for correlating the two valleys, placing the Permian/Triassic boundary at Lusitaniadalen at ca. 3 m above the base of the Vikinghøgda Formation. Additionally, the *Neogondolella* conodont assemblage in association with ammonoids within the *Otoceras boreale* ammonoid zone at ca. 6 m above the base of the Vikinghøgda Formation confirms a Griesbachian age for the lower part of the Deltadalen Member (Nakrem et al., 2008).

A digital outcrop model (Fig. 2.1c) of the Lusitaniadalen section was generated from 1,437 photo-graphs acquired with an unmanned aerial vehicle (UAV; DJI Mavic 2 Pro,DJI Mavic 2 Pro camera with a 1'' CMOS sensor) following Senger et al. (2022). Structure from motion photogrammetry was performed with Agisoft Metashape (version 1.8.6) with sparse cloud data filtered for reconstruction uncertainty (level 10), projection accuracy (level 15) and projection error (level 0.3). After building a dense cloud resulting in 271,711,738 points, it was further filtered by removing all

points with a confidence below 5% and unconnected components. The model is available in an online repository (Buchwald et al., 2025a).

2.2 Fieldwork methods and sample processing

For lipid biomarker analysis, 32 samples were collected. Sixty additional samples were collected for geochemical analyses (92 samples in total). The lipid biomarker samples were immediately wrapped in aluminium foil to avoid contamination, whereas samples for geochemical analysis were stored in plastic bags to avoid metal contamination. To establish a late Permian pre-crisis baseline of the lipid biomarker inventory, the lowest samples were taken from −41.51 m to −30.58 m relative to the Kapp Starostin/Vikinghøgda formation boundary (eight samples). They represent the penultimate and last cycles of mudstones in the Kapp Starostin Formation, which are interpreted to reflect a similar depositional environment as the Deltadalen Member of the Vikinghøgda Formation (Blomeier et al., 2013; Zuchuat et al., 2020), enabling a comparison of the pre- and post-extinction lipid biomarker composition while reducing the effect of environmental variability on changes in the lipid biomarker inventory. Furthermore, the uppermost beds of the glauconitic sandstones at the top of the Kapp Starostin Formation (three samples) as well as the lowermost ca. 30 m of the Vikinghøgda Formation (21 samples) were analyzed for their lipid biomarker inventory. For geochemical analysis, samples were taken with higher resolution, also across the interval of glauconitic sandstones (28 samples from the Kapp Starostin Formation; 64 samples from the Vikinghøgda Formation).

For the bulk geochemistry, samples were powdered using an agate planetary ball mill. For stable organic carbon isotope analysis ($\delta^{13}C_{org}$ relative to the Vienna Pee-Dee Belemnite standard, VPDB), 2 g of the powdered samples were decalcified with 2M HCl. From the residue, 50–70 mg were used for measurements on a Thermo Fisher Delta V isotope ratio mass spectrometer coupled to a Thermo Flash EA 1112 elemental analyzer via a Thermo Fisher Conflo IV-interface. The standard deviation based on measurements of lab standard material (peptone) is ±0.15‰. To determine major, minor and trace elemental compositions, the samples were digested in a 2:2:1:1 solution of H_2O-HF-$HClO_4$-HNO_3 and analyzed with a PerkinElmer Elan 9000 mass spectrometer with a precision of ±2%. Additionally, HAWK pyrolysis (±5 %) was used to evaluate

rock maturity by measuring S_1 (free hydrocarbons), S_2 (kerogen-bound hydrocarbons) and S_3 (organic CO_2 from function groups). Additionally, T_{max} is recorded, which describes the temperature during the maximum rate of S_2 generation. The Production Index (PI) and the Hydrocarbon Index (HI) are calculated as $PI = S_1/(S_1+S_2)$ and $HI = (S_2/TOC)*100$ (Espitalie et al., 1977; Peters, 1986). Total organic carbon (TOC) from Buchwald et al. (2025b) was used for lipid biomarker quantification, determined by treating sample powders three times with 100 µL of 1M HCl for decarbonization, before analysis with a Euro EA 3000 (Euro Vector) elemental analyzer with a precision of ±0.05% and standard deviations <0.08. These TOC results were compared to TOC values received from HAWK pyrolysis. Both methods are comparable with a difference of 0.06 wt% to 0.30 wt% (average: 0.16 wt%), with HAWK pyrolysis providing consistently slightly higher values, which is expected as a small amount of organics is usually lost during the acid-washing procedure (Grasby et al., 2019).

For lipid biomarker analysis, 25–40 g per sample was ground into a homogenous powder with a ceramic mortar and pestle. Lipid biomarker extraction was done for 15 min in an ultrasound bath with a solvent mixture of dichloromethane:methanol (3+1). After extraction, samples were centrifuged for 5 min at 2,000 rpm to collect the lipid biomarkers from the organic supernatant. Each sample was extracted four times, and the supernatants were combined. The resulting total lipid extract (TLE) was evaporated and dried using a $NaSO_4$ filter. The TLE was separated into a maltene fraction (*n*-hexane soluble) and an asphaltene fraction (*n*-hexane insoluble). Maltenes were further separated by solid phase chromatography (fraction 1, F1: hydrocarbons, F2: ketones and aromatic compounds, F3: alcohols, F4: fatty acids) on a Chromabond NH_2 modified solid-phase extraction column (500 mg) following Birgel and Peckmann (2008). In the following, only saturated hydrocarbons are discussed, as functional groups are not preserved. Hydrocarbons were quantified using a gas chromatograph coupled to a flame ionization detector (GC-FID; Thermo Scientific Trace 1310 GC) with 5α(H)-cholestane (10 mg/L) co-injected as standard. Compounds were identified using coupled gas chromatography-mass spectrometry (GC-MS; Thermo Scientific Trace Ultra GC and Thermo Scientific DSQ II MS). Both instruments were equipped with a Thermo Scientific TG-5MS silica column (length = 30 m, diameter = 0.25 mm,

film thickness = 0.25 µm) and use H_2 (GC-FID) and He (GC-MS) as carrier gases with a flow rate of 2.0 mL/min. On both instruments, the temperature program was set to 50 °C (maintained for 3 min), followed by a temperature ramp to 325 °C (maintained for 25 min) at 6 °C/min. Because the *n*-alkanes showed highest intensities in the chromatograms and caused co-elutions with other compounds, for example acyclic and cyclic terpenoids, they were removed by treating an aliquot of the hydrocarbon fraction with a molecular sieve (pore size of 5 Å, dissolved in cyclohexane), as detailed by Sabino et al. (2021).

2.3 Data analysis

Redox-sensitive metal (RSM) enrichment factors (EF) are a useful tool to identify redox-driven metal transfer to the sediment (Algeo & Tribovillard, 2009) and are commonly calculated as:

$$\mathrm{RSM_{EF}} = \frac{\mathrm{RSM_{sample}}/\mathrm{Al_{sample}}}{\mathrm{RSM_{standard}}/\mathrm{Al_{standard}}}$$

However, this method has been shown to commonly record artificially elevated EF in low-aluminium lithologies (Krewer et al., 2024), which represents a challenge when comparing EF across a significant lithological change, such as recorded across the Permian–Triassic transition at Lusitaniadalen. To address this issue, an alternative method of calculating revised EF (EF*) was proposed by Krewer et al. (2024) using excess redox-sensitive metal concentrations (RSM_{excess}):

$$\mathrm{RSM_{excess}} = \mathrm{RSM_{sample}} - \left(\mathrm{Al_{sample}} * \frac{\mathrm{RSM_{standard}}}{\mathrm{Al_{standard}}}\right)$$

$$\mathrm{RSM^{*}_{EF}} = \frac{\mathrm{RSM_{excess}} + \mathrm{RSM_{standard}}}{\mathrm{RSM_{standard}}}$$

Both traditional EF and revised EF* were calculated for rhenium (Re), vanadium (V), uranium (U) and molybdenum (Mo) using the RSM and aluminium (Al) concentrations of the post-Archean Australian shale (PAAS) as a standard (Taylor & McLennan, 1985). These RSM were chosen due to their different redox potentials and thresholds for enrichment, with Re being most redox-sensitive and enrichment starts under dysoxic conditions, whereas V and U enrichment occurs

under both anoxic ferruginous and euxinic conditions, and Mo enrichment during euxinic conditions (e.g., Li et al., 2025).

To investigate the rare earth elements and yttrium (REY) patterns of the investigated samples, the REY concentrations were also normalized to PAAS. Further, cerium (Ce) anomalies were calculated according to Lawrence et al. (2006) with PAAS-normalized ("shale-normalized", SN) concentrations of Ce, praseodymium (Pr) and neodymium (Nd):

$$\mathrm{Ce/Ce^*} = \frac{\mathrm{Ce_{SN}}}{\mathrm{Pr_{SN}} * \frac{\mathrm{Pr_{SN}}}{\mathrm{Nd_{SN}}}}$$

Lipid biomarkers measured on the GC-MS were identified with Xcalibur (version 3.1.66.10; Thermo Fisher). Quantification of compounds was done on molecular sieve-treated samples using Chromeleon 7 (version 7.2.10; Thermo Fisher Dionex). Compound quantity was calculated against the 5α(H)-cholestane standard and normalized to the sample's TOC content. The contents of pristane, phytane and *n*-alkanes were obtained from Buchwald et al. (2025b), where *n*-alkanes are quantified from the hydrocarbon fraction prior to molecular sieve treatment.

The thermal maturity of the samples was also estimated by calculating the homohopane isomerization index (HHI) of the 17α(H),21β(H)-C_{31}-hopane from the integrated peak areas of the *m/z* = 191 of the respective 22*S*- and 22*R*-stereoisomers:

$$\text{homohopane isomerization index (HHI)} = \frac{22S}{22S + 22R}$$

The carbon preference index (CPI) was calculated from the quantified *n*-alkanes in the untreated hydrocarbon fraction:

$$\mathrm{CPI} = \left[\frac{nC_{25} + nC_{27} + nC_{29} + nC_{31} + nC_{33}}{nC_{24} + nC_{26} + nC_{28} + nC_{30} + nC_{32}} + \frac{nC_{25} + nC_{27} + nC_{29} + nC_{31} + nC_{33}}{nC_{26} + nC_{28} + nC_{30} + nC_{32} + nC_{34}}\right] \Big/ 2$$

The Terrigenous/Aquatic Ratio (TAR) was calculated as followed:

$$\mathrm{TAR} = \frac{nC_{27} + nC_{29} + nC_{31}}{nC_{15} + nC_{17} + nC_{19}}$$

3 Results

3.1 Sample Maturity

The overall low values of the production index (PI ≤ 0.30, except the samples at 0.51 m, 0.89 m and 1.93 m), a hydrogen index (HI) < 200 for all samples except at 4.23 m, and a T_{max} of 337–346 °C derived by pyrolysis place the samples in the oil generation window (Table 2.1). The thermal maturity calculations based on lipid biomarkers reveal an homohopane index (HHI) of 0.51–0.59. The color alteration index of conodonts (Epstein et al., 1977) found in carbonate concretions 0.37 m and 8.45 m above the extinction horizon record values between 1 and 1.5 (Fig. 2.1d), suggesting burial temperatures not exceeding 90°C, indicating a similar maturity as derived from the HHI and pyrolysis.

3.2 Geochemical proxies

The vertical distribution of geochemical proxies measured at Lusitaniadalen reveals a clear shift across the Permian–Triassic transition (Fig. 2.2). The Al concentration is characterized by an abrupt increase just below the extinction horizon. While the Kapp Starostin Formation generally records [Al] < 3 wt% (−41.45 m to −1.82 m), the uppermost 1.24 m record increased [Al] of up to 5 wt%. [Al] remains high in the Vikinghøgda Formation with a maximum of 8.9 wt% at 13.61 m.

The calculated RSM EF reveal similar results for the post-extinction siltstones and very fine-grained sandstones of the Vikinghøgda Formation, irrespective of whether they were calculated using bulk or excess metal concentrations, suggesting that either method may be appropriate for these strata (Fig. 2.2). However, in the Kapp Starostin Formation below the extinction horizon, the traditional EF record higher enrichments compared to the revised EF*. Whereas pre-extinction EF* are similar to post-extinction EF* and EF, the pre-extinction EF appear to be artificially elevated due to the low [Al] in the Kapp Starostin Formation, suggesting a lithological rather than a redox control on the RSM enrichments. Furthermore, unlike the traditional EF, EF* values are consistently within typical ranges of RSM enrichments recorded for modern marine sediments (Li et al., 2025). The revised EF*, therefore, seems to be less biased by the heterogeneous lithology across the Kapp Starostin/Vikinghøgda formation boundary. Hence, the following redox interpretations are based on the revised EF*.

Table 2.1: *Sample maturity parameters from HAWK pyrolysis. The stratigraphic log height for each sample is given relative to the Kapp Starostin/Vikinghøgda formation boundary at 0 m. PI — Production Index; HI — Hydrocarbon Index; TOC — Total Organic Carbon.*

Stratigraphic height (m)	T_{max} (°C)	S_1 (mg HC/ g rock)	S_2 (mg HC/ g rock)	S_3 (mg CO_2/ g rock)	PI	S_2/S_3	HI	TOC (wt%)
14.11	441	0.08	0.22	0.40	0.27	0.55	66	0.33
13.61	441	0.03	0.22	0.49	0.12	0.45	55	0.39
9.53	441	0.05	0.22	0.46	0.19	0.48	57	0.37
8.77	441	0.04	0.13	0.48	0.24	0.27	28	0.45
8.01	444	0.19	0.88	0.36	0.18	2.44	123	0.72
7.27	443	0.23	0.78	0.37	0.23	2.11	94	0.82
6.49	443	0.64	2.06	0.58	0.24	3.55	174	1.18
5.75	443	1.00	3.33	0.48	0.23	6.94	192	1.73
4.99	445	0.80	2.17	0.48	0.27	4.52	161	1.34
4.23	443	0.97	3.04	0.48	0.24	6.33	209	1.45
3.49	443	0.57	1.30	0.41	0.30	3.17	122	1.07
2.71	446	0.70	2.78	0.31	0.20	8.97	161	1.73
1.93	444	0.69	1.10	0.63	0.39	1.75	94	1.17
1.15	437	0.02	0.10	0.66	0.17	0.15	35	0.28
0.89	444	0.18	0.41	0.83	0.31	0.49	40	1.03
0.51	440	0.59	1.04	0.38	0.36	2.74	109	0.95
−33.76	445	0.11	0.43	0.42	0.20	1.02	67	0.64
−34.73	444	0.11	0.61	0.43	0.15	1.42	78	0.78
−36.87	444	0.05	0.27	0.80	0.16	0.34	40	0.67

The Kapp Starostin Formation generally records elevated EF* except for V_{EF}* (Fig. 2.2). The V_{EF}* is slightly enriched to values up to 1.21 between −41.51 m and −34.63 m and starting at approximately −14 m with values up to 1.45. The enhanced V_{EF}* in the uppermost 0.40 m of the Kapp Starostin Formation coincide with some of the highest enrichments of the other RSM (U_{EF}* = 3.47, Mo_{EF}* = 2.73, Re_{EF}* = 78.5). While the extinction horizon (0 m) is characterized by comparatively low EF*, the trend of increased RSM enrichments otherwise continues above the extinction horizon into the basal 3 m of the Vikinghøgda Formation. Between 3.14 m and 19.54 m, EF* of V, U and Mo are generally close to their respective PAAS baselines. Several samples are

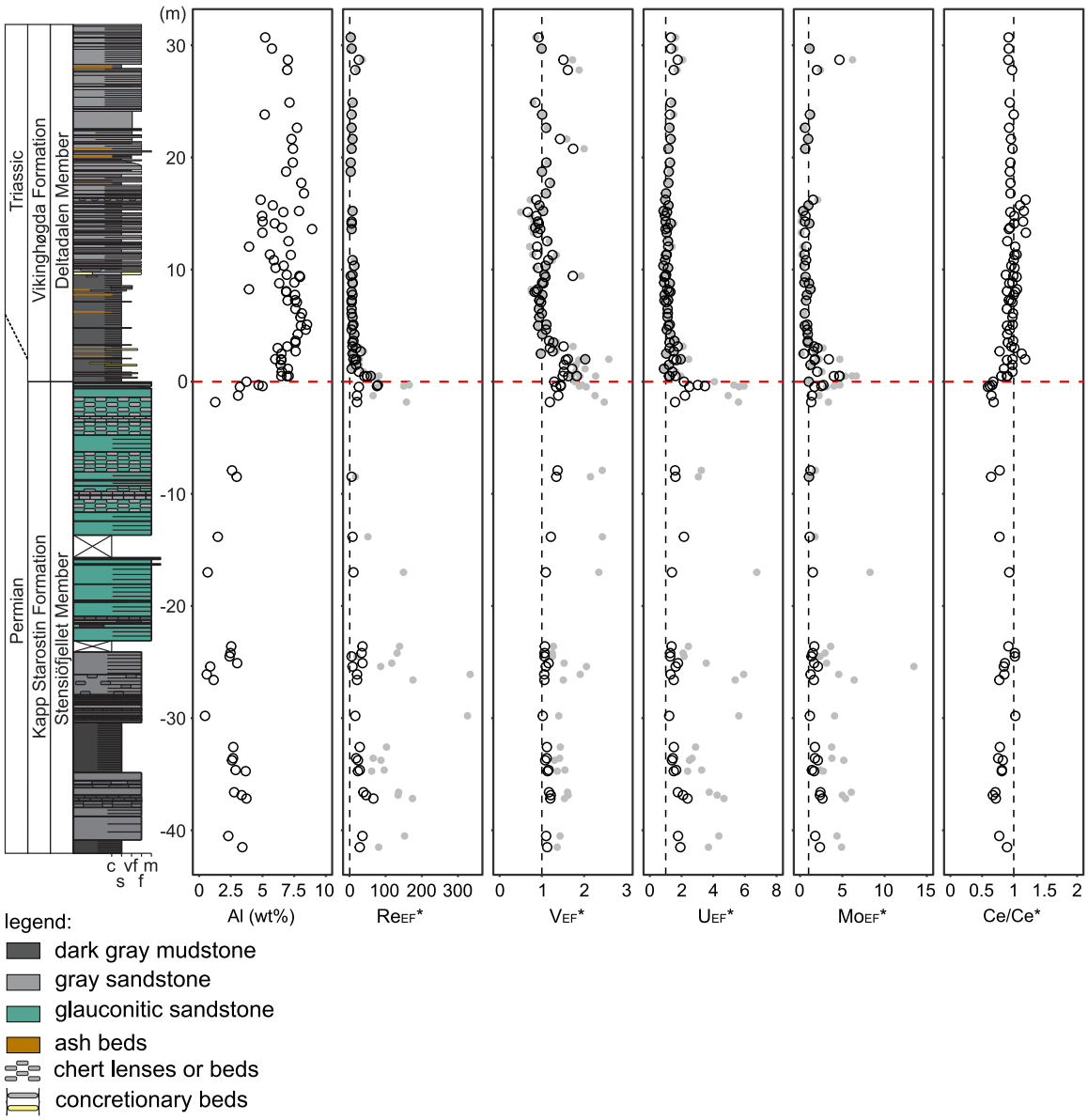

Figure 2.2: *Al concentrations, redox-sensitive metal (RSM) enrichment factors (EF) and Ce anomalies (Ce/Ce*) across the Permian–Triassic environmental crisis at Lusitaniadalen, Svalbard. The solid gray circles denote the traditional EF, the open circles represent revised EF* for Re, V, U and Mo. Heights are relative to the Kapp Starostin/Vikinghøgda formation boundary at 0 m, which also coincides with the extinction horizon (horizontal dashed line). The vertical dashed lines indicate the threshold for RSM enrichment compared to the PAAS standard. c — claystone; s — siltstone; vf — very fine-grained sandstone; f — fine-grained sandstone; m — medium-grained sandstone.*

found with Mo and Re concentrations below their respective detection limit. The uppermost 10 m of the investigated interval in the Vikinghøgda Formation reveal recurring RSM enrichments, in particular between 27.79 m and 28.70 m.

The standard-normalized REY patterns at Lusitaniadalen change throughout the investigated interval (Fig. 2.3). The interval below −35 m is characterized by a comparatively flat shale-like REY pattern, suggesting a predominantly detrital signal, and is very similar to the REY pattern in the Vikinghøgda Formation above the extinction horizon > 0 m. However, the former displays a negative Ce anomaly with Ce/Ce* between 0.67 and 0.89 (Fig. 2.2). The overlying 21 m up to −14 m covering the last cycle of silicified mudstones and cherty sandstones as well as the transition to glauconitic sandstones reveal a similar pattern; the majority of twelve samples still record negative Ce anomalies between 0.75 and 0.93, but three samples record Ce/Ce* > 1. Negative Ce anomalies become especially pronounced in the overlying interval up to the extinction horizon with Ce/Ce* values as low as 0.59, but unlike seawater-REY patterns, a decrease rather than an increase in heavy REY/light REY is recorded (Fig. 2.3). This suggests that these patterns may reflect diagenetic alteration or that the REY-hosting phases are porewater-derived authigenic precipitates, rather than recording seawater values.

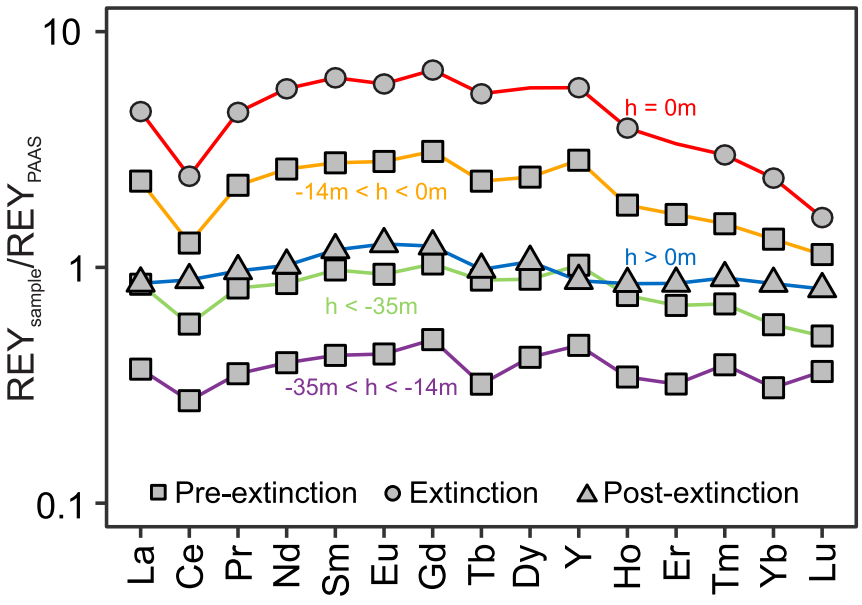

Figure 2.3: *PAAS-normalized rare earth elements and yttrium (REY) patterns averaged across different intervals at Lusitaniadalen.*

3.3 Lipid biomarker inventory

The homologous series of *n*-alkanes are the most abundant compounds in the saturated hydrocarbon fraction in all samples (Fig. 2.4). In the ten samples below −0.46 m, the *n*-alkanes comprise a unimodal distribution with a maximum at nC$_{16–20}$. The *n*-alkane distribution changes from −0.23 m up-section to a bimodal distribution with two maxima at nC$_{15–16}$ and nC$_{26–27}$. The CPI ranges between 1.0 and 1.1 across the entire section. The relative amount of terrigenous *n*-alkanes is highest at 0.51 m with a maximum TAR of 1.4 (Fig. 2.5). In the Vikinghøgda Formation, the TAR remains slightly elevated, compared to pre-extinction levels in the Kapp Starostin Formation (TAR between 0.3 to 0.6), until 24.89 m. A negative $\delta^{13}C_{org}$ excursion coincides with this shift in TAR, with $\delta^{13}C_{org}$ abruptly decreasing across the extinction horizon from −28.8‰ (−0.23 m) to −31.9‰ (0.49 m) and −33.9‰ (0.51 m) (Fig. 2.5).

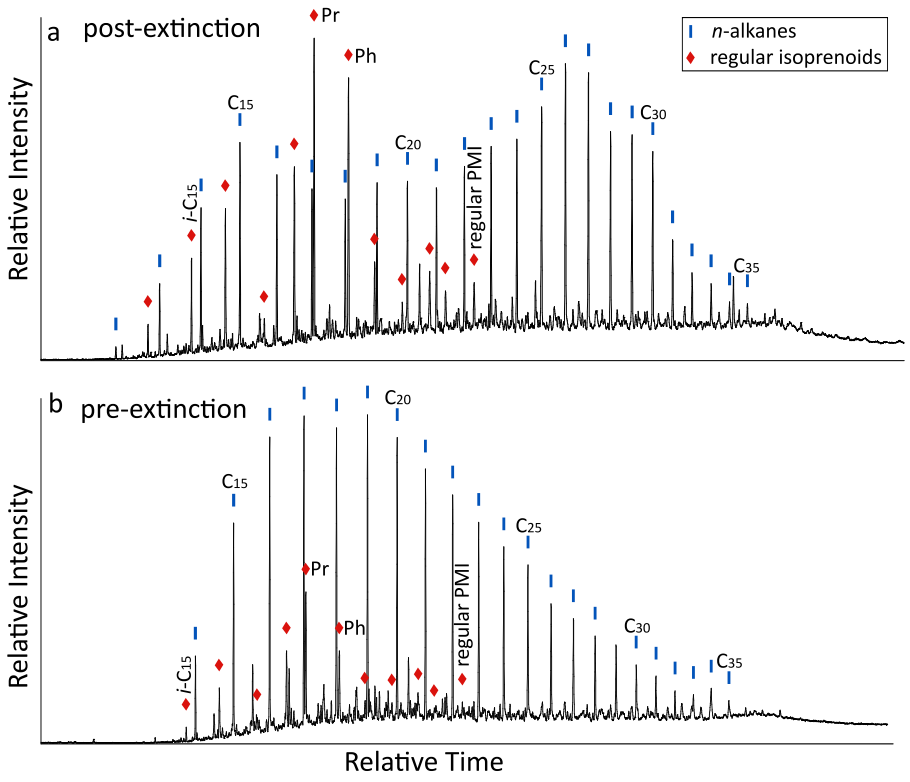

Figure 2.4: *Total ion chromatogram of a post-extinction sample taken at 0.51 m (a) and a pre-extinction sample taken at −36.87 m (b) before molecular sieve treatment. The series of n-alkanes and regular isoprenoids are marked. i-C_{15} — C_{15}-isoprenoid (farnesane); Pr — pristane; Ph — phytane; regular PMI —2,6,10,14,18-pentamethylicosane (C_{25}-isoprenoid).*

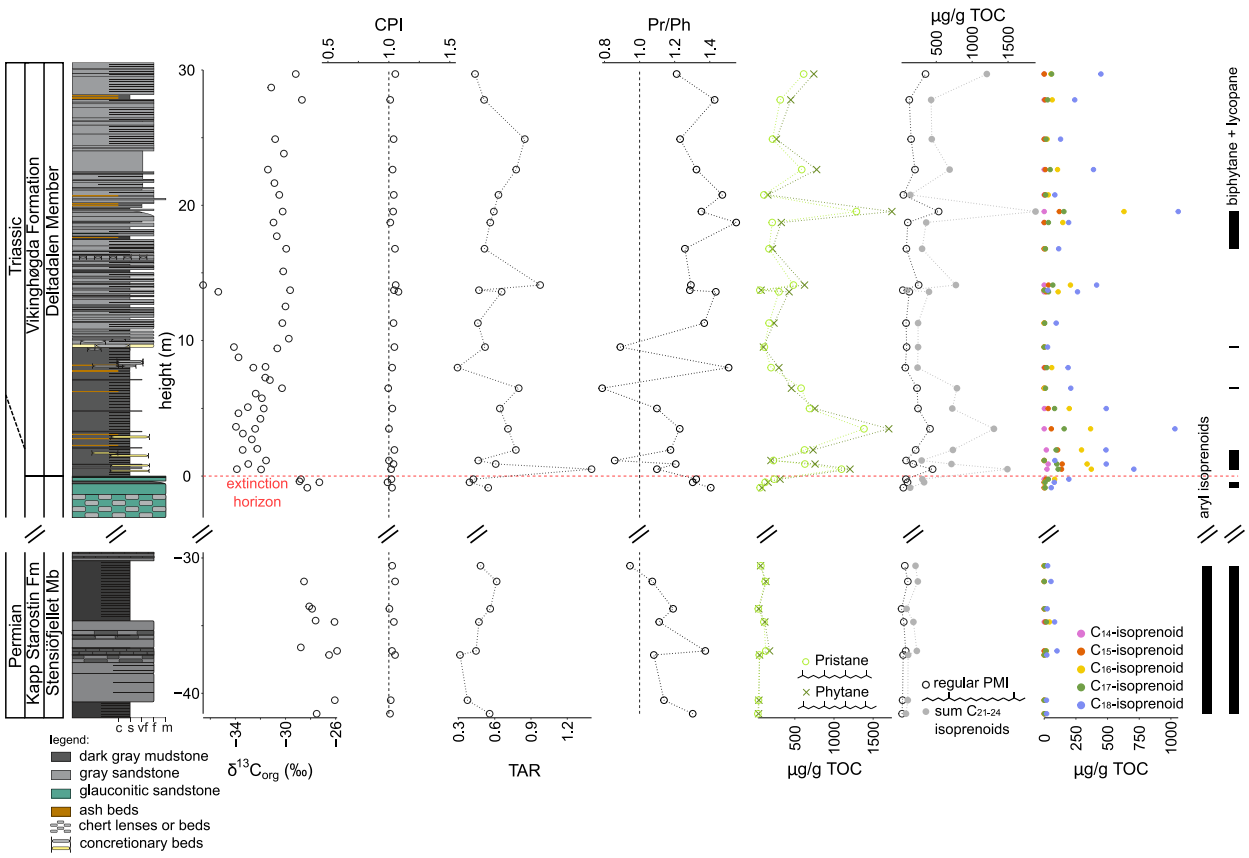

Figure 2.5: *Organic geochemical profiles recording $\delta^{13}C_{org}$ and lipid biomarkers across the Permian–Triassic transition at Lusitaniadalen. Aryl isoprenoids, biphytane and lycopane were present in trace amounts or co-eluted with other compounds and could not be quantified. Where present, they are marked with a black bar. Note the discontinuous scale of the y-axis as sampling efforts focused on strata recording similar depositional environments prior to and after the extinction event to reduce the effect of variability of the depositional environment on the lipid biomarker inventory. Heights are relative to the Kapp Starostin/Vikinghøgda formation boundary at 0 m, which also coincides with the extinction horizon (horizontal dashed red line). TOC – Total Organic Carbon; TAR — Terrigenous/Aquatic Ratio; CPI — Carbon Preference Index; Pr — Pristane, Ph — Phytane; regular PMI —2,6,10,14,18-pentamethylicosane.*

A pseudohomologous series of head-to-tail linked isoprenoids from C_{14} to C_{25} was detected in the molecular sieve-treated hydrocarbon fraction. Pristane and phytane (head-to-tail linked C_{19}- and

C_{20}-isoprenoids, respectively) are the most abundant isoprenoids (Fig. 2.4). In the Kapp Starostin Formation, pristane and phytane contents are low (28.8–178.4 µg/g TOC), but progressively increase at −0.23 m to 312.3 µg/g TOC and 236.1 µg/g TOC, respectively (Fig. 2.5). The lowermost post-extinction biomarker sample at 0.51 m is the first one with strongly elevated contents of pristane and phytane (1204.4 µg/g TOC and 1096.1 µg/g TOC, respectively). Except for an interval between 9.53 m and 13.73 m, pristane and phytane contents in the Vikinghøgda Formation are higher compared to the Kapp Starostin Formation and do not return to pre-extinction levels, with a second peak at 19.54 m (1739.0 µg/g TOC and 1285.9 µg/g TOC, respectively).

A further head-to-tail linked isoprenoid is 2,6,10,14,18-pentamethylicosane (regular PMI), accompanied by head-to-tail linked $C_{21–24}$ pseudohomologs (Fig. 2.5). The regular PMI content records a post-extinction increase from an average of 55.9 µg/g TOC in the Kapp Starostin Formation to 192.9 µg/g TOC in the Vikinghøgda Formation, with peak contents in the first post-extinction sample at 0.51 m (449.4 µg/g TOC) and at 19.54 m (533.6 µg/g TOC).

Furthermore, we detected the isoprenoids biphytane (head-to-head linked C_{40}-isoprenoid), lycopane (tail-to-tail linked C_{40}-isoprenoid) (Fig. 2.5), and their pseudohomologs until C_{38} (biphytane) and C_{37} (lycopane). However, these compounds were only present in trace amounts. As biphytane, lycopane and their pseudohomologs commonly co-elute with other compounds (e.g., hopanes), quantification was unfeasible. Still, it is noticeable that slightly higher intensities of these compounds were detected in gas chromatograms from samples below −0.46 m, whereas they have reduced intensities or are absent just below the extinction horizon and in post-extinction samples. Further, we detected traces of a pseudohomologous series of $C_{14–21}$ aryl isoprenoids in samples below −30.58 m (Fig. 2.5). Aryl isoprenoids are absent from both the uppermost Kapp Starostin Formation and the investigated interval of the Vikinghøgda Formation.

4 Discussion

4.1 Thermal maturity and preservation of organic matter at Lusitaniadalen

Lusitaniadalen was chosen to compare signals from geochemical proxies and lipid biomarkers across the Permian–Triassic transition due to minor tectonic reworking in central Svalbard, which

likely explains the moderate thermal maturity of organic material, especially when compared to successions from western Svalbard (Olaussen et al., 2025; Buchwald et al., 2025b), where intense tectonic deformation (Dallmann et al., 1993) may have compromised organic matter preservation (Knoll et al., 2012). The moderate thermal maturity at the Permian–Triassic transition at Lusitaniadalen is indicated by pyrolysis data and the HHI, both indicating burial temperatures between 80 and 100 °C (Mackenzie et al., 1984), and the conodont color alteration (Table 2.1, Fig. 2.1d) indicating maturity in the early oil generation window with a maximum temperature of < 90 °C (Epstein et al., 1977). This result is consistent with previous maturity estimates spanning the extinction horizon at Lusitaniadalen (Nabbefeld et al., 2010a), and from the adjacent Deltadalen (Zuchuat et al., 2020). The Lower to Middle Triassic succession at Stensiöfjellet, 24 km east of Lusitaniadalen, also yields conodonts with a conodont color alteration index of 1–1.5 (Leu et al., 2024), confirming relatively low maturity across central Svalbard.

Due to the scarcity of body fossils in the uppermost Kapp Starostin Formation, the stratigraphic position of the extinction event at Lusitaniadalen was formerly defined by the disappearance of bioturbation (Nabbefeld et al., 2010a; Foster et al., 2017, 2023; Uchman et al., 2016; Zuchuat et al., 2020). This aligns with a negative $\delta^{13}C_{org}$ excursion across the Kapp Starostin/Vikinghøgda formation boundary (Fig. 2.5). This change in $\delta^{13}C_{org}$ inferred to record the onset of the Permian–Triassic environmental crisis is observed globally (e.g., Cao et al., 2002, 2009; Sephton et al., 2005; Xie et al., 2007; Schobben et al., 2020; Grasby et al., 2024). Hence, $\delta^{13}C_{org}$ corroborates the position of the extinction horizon at Lusitaniadalen. Similar to sections at the northern margin of the paleogeographically adjacent Sverdrup Basin in the Canadian Arctic or at the GSSP in Meishan, the abrupt shift in $\delta^{13}C_{org}$ (Fig. 2.5) may indicate a hiatus around the extinction event (Grasby & Beauchamp, 2008). At Lusitaniadalen, the high-resolution $\delta^{13}C_{org}$ record by Nabbefeld et al. (2010), however, reveals a gradual decline in $\delta^{13}C_{org}$, that decreases from −28.3‰ in the penultimate glauconitic sandstone bed to −31.5‰ in the thin uppermost glauconitic bed, and further to −33.7‰ at 0.13 m above the top of the glauconitic sandstones. Similarly, Dustira et al. (2013) measured a gradual decline of $\delta^{13}C_{org}$ in the uppermost glauconitic sandstone bed at Kongressfjellet. Furthermore, *Reduviasporonites chalastus*, an enigmatic microfossil known to be

strongly increased in abundance during a short interval in the direct aftermath of the Permian–Triassic mass extinction (e.g., Rampino & Eshet, 2018) is reported from the lowermost Vikinghøgda Formation from several sections in central Svalbard (Vigran et al., 2014). Considering these data together with the gradual decline in $\delta^{13}C_{org}$, we assume that at Lusitaniadalen a relatively continuous succession is preserved without a major hiatus across the formation boundary.

4.2 Terrestrial input

In the Induan, sedimentation accumulation in central Svalbard was increased by 4 to 20 times compared to the late Permian sediment accumulation in the Kapp Starostin Formation (Zuchuat et al., 2020). A global increase in terrestrial sediment fluxes into shallow marine ecosystems has been observed, likely linked to enhanced physical and chemical continental erosion due to increased temperatures, acidity of precipitation, and soil destabilization (Algeo & Twitchett, 2010). Additionally, a large delta plain encompassing an area of >1.65 x 10^6 km^2 developed in the Early Triassic and propagated onto the Barents Shelf, covering the entire area of the modern Barents Sea shelf (Klausen et al., 2019). The catchment area of the rivers feeding into the delta covered large parts of northern Pangaea, including the Western Urals, West Siberia and the Central Asian Orogenic Belt with contributions also from Fennoscandia and the Siberian Traps Large Igneous Province (Gilmullina et al., 2022). At Lusitaniadalen, the low Al concentrations in the Kapp Starostin Formation compared to the overlying Vikinghøgda Formation (Fig. 2.2) could be biased by the high silica content in the Kapp Starostin Formation. However, the observed increase in terrigenous material was likely a major source of Al (e.g., Tribovillard et al., 2006), enhancing its concentrations in the Early Triassic. Similarly, the TAR as a proxy for the organic matter source records distinctly elevated values above the extinction horizon (Fig. 2.5), as long-chain *n*-alkanes ($nC_{27–31}$) are among the main constituents of epicuticular waxes of terrestrial plants (Buschhaus & Jetter, 2011; Eglington & Hamilton, 1967).

Additionally, the Permian–Triassic environmental crisis was marked by an intensification of wildfire activity affecting terrestrial ecosystems across paleolatitudes, reflected in the increased abundance of polyaromatic hydrocarbons derived from the high-temperature combustion of

organic matter (South China: Kaiho et al., 2021; Nabbefeld et al., 2010b; Saito et al., 2023; Shen W. et al., 2011; Northern Italy: Kaiho et al., 2021; eastern Greenland and western Canada: Nabbefeld et al., 2010b; Lusitaniadalen, Svalbard: Nabbefeld et al., 2010a). In contrast to marine biodiversity, no severe effect of the Permian–Triassic environmental crisis is recorded in the terrestrial floral diversity in the Boreal Realm (Schneebeli-Hermann et al., 2017). However, wildfires and the reduction of plant biomass could have still contributed to the destabilization of terrestrial ecosystems and facilitated soil erosion, further increasing terrestrial input into the marine realm.

4.3 Paleoredox conditions

The Permian–Triassic environmental crisis was marked by an expansion of oxygen minimum zones (e.g., Brennecka et al., 2011; Zhang et al., 2018, 2020). In Svalbard, paleoredox reconstructions argue for the development of dysoxic to anoxic conditions and even euxinia in the latest Permian (Wignall et al., 1998, 2016; Nabbefeld et al., 2010a; Dustira et al., 2013; Schobben et al., 2014, 2020; Grasby et al., 2015). The RSM EF* data from Lusitaniadalen reveal fluctuating metal enrichments consistent with extended periods of oxic conditions disrupted by intervals of reduced oxygen availability, which occurred prior, during and likely after the Permian–Triassic environmental crisis. Between −41.51 m and −34.63 m below the extinction horizon in the penultimate cycle of bioturbated mud- and siltstones and silica-rich fine-grained sandstones of the Kapp Starostin Formation, the RSM EF* are consistent with sediments deposited under dysoxic to anoxic conditions (Li et al., 2025). Hence, reducing conditions occurred prior to the Permian–Triassic environmental crisis (Fig. 2.2). However, the same interval is also strongly bioturbated (Beaty et al., 2025; Uchman et al., 2016), thus deoxygenation was not persistent. These findings are indicative of dynamic redox fluctuations marked by episodic deoxygenation. Similarly, negative Ce anomalies typical for oxic conditions are recorded persistently throughout the same interval and appear to contradict the anoxic or dysoxic conditions indicated by RSM enrichments, but REY patterns reveal a likely detrital origin of REY in this interval (Fig. 2.3) and thus may not represent the seawater signal.

The overlying ~20 m of the Kapp Starostin Formation comprising the last cycle of bioturbated mud- and siltstones, and silica-rich fine-grained sandstones record consistently comparatively low RSM EF*, suggesting a return to prevalently oxic conditions (Fig. 2.2). A decrease in oxygen availability is indicated by recurring RSM enrichments in the uppermost ~14 m of the Kapp Starostin Formation that eventually culminate in RSM EF* typical for anoxic, potentially even euxinic conditions (Li et al., 2025) at −0.39 m below the extinction horizon. A similar gradual development of anoxic conditions has been observed at Kongressfjellet by analyzing pyrite framboid size (Dustira et al., 2013). The onset of more reducing conditions in the uppermost Kapp Starostin Formation at Lusitaniadalen is further reflected by the lithological shift to glauconitic sandstones, as authigenic glauconite formation on the continental shelf requires weakly reducing or oscillating redox bottom-water or upper porewater conditions for iron to be present in both valences Fe^{2+} and Fe^{3+} (Tribovillard, 2024). At Lusitaniadalen, porewater redox conditions were reducing enough to foster the formation of glauconite during early diagenesis, but the oxygen supply to the sediment was, at least intermittently, sufficient to allow for seafloor inhabitation and burrowing by infauna, as reflected by large ichnofossils within the glauconitic sandstones (Beaty et al., 2025; Foster et al., 2017; Nabbefeld et al., 2010a; Rodriguez-Tovar et al., 2021; Uchman et al., 2016; Zuchuat et al., 2020).

At −0.39 m below the formation boundary, the data support the development of full anoxia that continues into the lowermost Vikinghøgda Formation (Fig. 2.2). An episode of severe deoxygenation right before the extinction has previously been identified as a potential kill mechanism in the eastern equatorial Paleotethys at the Nhi Tao section due to upwelling of sulfidic deep water (Algeo et al., 2007). While the V_{EF}* recorded between −0.39 m and −0.30 m are compatible with modern sediments deposited under euxinic conditions, the Mo_{EF}* appear rather low, in particular compared to U_{EF}* (Fig. 2.6). This suggests that local water masses were reducing but did not necessarily become euxinic (Algeo & Tribovillard, 2009; Li et al., 2025; Tribovillard et al., 2012). Furthermore, the extinction horizon itself (0 m) is characterized by low RSM EF* with only U revealing an enrichment, which supports a local development of dysoxic conditions rather than full anoxia. The only samples with an U_{EF}*-Mo_{EF}* pair plotting along the particle shuttle

trajectory are two Vikinghøgda Formation samples at ~0.50 m shortly above the extinction horizon (Fig. 2.6), suggesting that Mo might have been delivered to the sediment via upwelling of sulfidic deep water (Algeo and Tribovillard, 2009). This is in accordance with an increase of short-chain aryl isoprenoids reported by Nabbefeld et al. (2010a) up to 1.5 m above the extinction horizon.Short-chain aryl isoprenoids are degradation products of carotenoid derivatives, for example isorenieratane, chlorobacetane and okenane, and are commonly used as biomarkers

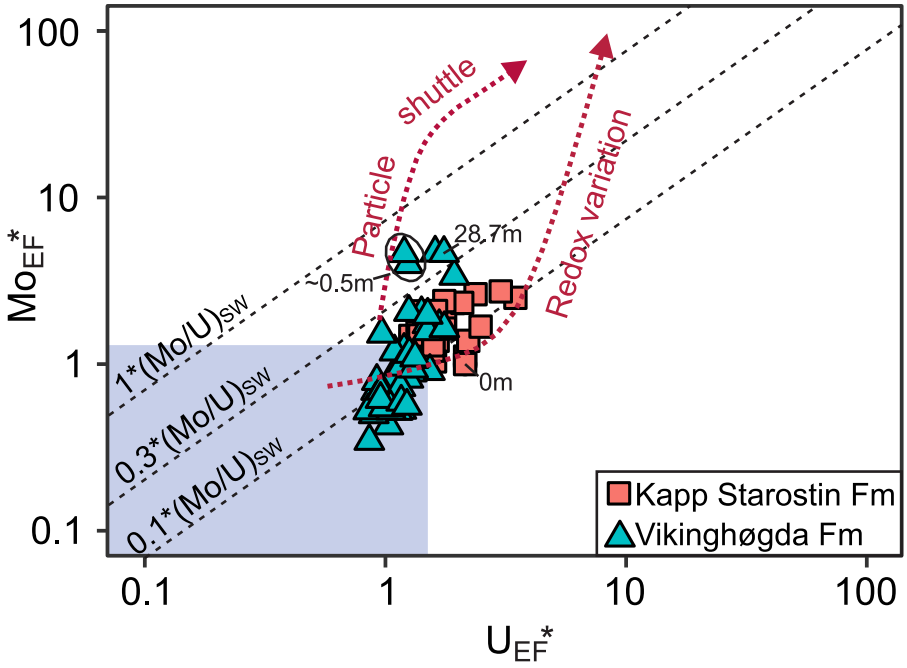

Figure 2.6: *Mo_{EF}* plotted against U_{EF}*. Different Mo accumulation pathways are indicated by the red arrows, with the redox variation trajectory illustrating benthic deoxygenation from oxic, through dysoxic and anoxic, to euxinic conditions, and the particle shuttle and uptake of Mo through redox cycling of oxyhydroxides (Tribovillard et al., 2012). The diagonal dotted lines represent proportions of modern seawater (SW) Mo/U molar ratio, and the blue box EFs expected for fully oxic conditions.*

for anoxygenic phototrophic bacteria, at least partially adapted to euxinic conditions (e.g., Sinninghe Damsté et al., 2001; Brocks and Schaeffer, 2008; Sousa Júnior et al., 2013; El-Shafeiy et al., 2014). However, Koopmans et al. (1996) have demonstrated that short-chain aryl

isoprenoids can also derive from the degradation of β-carotene, hence challenging interpretations of photic zone euxinia solely based on the presence of short-chain aryl isoprenoids. While we were not able to replicate the detection of short-chain aryl isoprenoids shortly above the extinction horizon, short-chain aryl isoprenoids occurred below −30.58 m, i.e., in the interval we identified to have experienced fluctuations in oxygenation prior to the Permian–Triassic environmental crisis (Figs. 2.2, 2.3, 2.5). However, at ~0.50 m above the extinction horizon, the Mo_{EF}* values are much lower than those recorded for modern euxinic sediments (Li et al., 2025) and the same samples still reveal slightly negative Ce anomalies, suggesting that if euxinic conditions occurred here, they were only episodic. The RSM EF* data also support a return to prevailing oxic conditions already ~3 m above the extinction horizon with only selected samples (e.g., at 28.70 m) indicating reoccurring anoxic conditions, suggesting that although anoxic conditions continued into the Early Triassic these were not persistent.

Complementary to redox-sensitive element enrichments, the ratio of pristane and phytane (Pr/Ph) is often used as a proxy for exploring paleoredox conditions in deep time, including across the Permian–Triassic environmental crisis (Cao et al., 2009; Chen et al., 2011; Jia et al., 2012; Nabbefeld et al., 2010a), as the degradation of the chlorophyll or bacteriochlorophyll phytol chain is redox-sensitive, producing pristane under oxic and phytane under anoxic conditions (Didyk et al., 1978; Rontani & Volkman, 2003). However, other sources of these biomarkers have to be considered before applying Pr/Ph as redox proxies. For example, the degradation of archaeal membrane tetraether lipids (GDGTs) can result in the preservation of biphytane and respective pseudohomologs (Rontani & Bonin, 2011; Rowland, 1990). In the samples from Lusitaniadalen, however, GDGTs, respectively biphytanes, are rather unlikely precursors of pristane and phytane, because the contents of both pristane and phytane strongly exceed the content of biphytane and pseudohomologs. Furthermore, archaeol and extended archaeol, both archaeal membrane diether lipids, must be considered as precursors of phytane and shorter pseudohomologs. Indeed, we detected regular PMI as a degradation product of extended archaeol (De Rosa et al., 1982; Fig. 2.5), which has regular PMI and phytane as isoprenoid chains. Hence, every molecule of extended archaeol that contributes regular PMI during degradation also adds phytane to the

biomarker pool. Additionally, extended archaeol is usually accompanied by archaeol, containing two phytanyl chains (Birgel et al., 2014; Natalicchio et al., 2017; Vandier et al., 2021), which would contribute two additional phytane molecules per archaeol molecule. An increase in the phytane content from a source other than chlorophyll would decrease the Pr/Ph independently of redox conditions. Anoxic conditions with Pr/Ph < 1 should therefore be interpreted with caution, and should be complemented by independent redox proxies like RSM enrichments. However, Pr/Ph > 1, and hence oxic conditions, require the pristane content to exceed the phytane content. In this case, an additional source of phytane would not change the interpretation of an oxic environment.

Similar to the redox proxies discussed above, Pr/Ph from the Kapp Starostin Formation indicates a mainly oxygenated water column prior to the environmental crisis, with Pr/Ph > 1 (Fig. 2.5). However, at −30.58 m, Pr/Ph < 1 might reveal a late Permian episode of water column deoxygenation prior to the extinction event, which is in accordance with RSM enrichments observed below the glauconitic sandstones (Fig. 2.2). In strata overlying the extinction horizon in the Vikinghøgda Formation, Pr/Ph might suggest several short dysoxic to anoxic episodes, with values < 1 that are in line with a previously reported decline in Pr/Ph in the lowermost Vikinghøgda Formation (Nabbefeld et al., 2010a). These data indicate a delay in the emergence of consistently oxic conditions in the Early Triassic, as recorded from around 10 m above the Kapp Starostin/Vikinghøgda formation boundary. In this light, our biomarker data suggest that the interval during which Early Triassic anoxic episodes occurred in the region may have been more protracted than indicated by the RSM enrichments, which could be explained by the additional sources of phytane discussed above, artificially decreasing Pr/Ph. However, like the RSM enrichments, the biomarker data also support a return to prevailing oxic conditions in the early Griesbachian at a similar stratigraphic height above the Kapp Starostin Formation, as observed at the more proximal Festningen section (Grasby et al., 2015).

The combined lipid biomarker and other geochemical redox proxies reveal a dynamic redox regime across the Permian–Triassic transition, with anoxia coinciding with the extinction event, but likely no persistent anoxia over longer time periods. In fact, the ecological community at Lusitaniadalen may have been exposed to fluctuating redox conditions throughout the late

Permian, prior to the mass extinction. Oxygen depletion was, therefore, likely not the sole driver of the extinction event in Svalbard. Grasby et al. (2015) argued for heavy metal toxicity as the primary extinction driver at Festningen, where the onset of anoxia post-dated the onset of the extinction, but the bioavailability of potentially toxic heavy metal species has to be carefully assessed before attributing the extinction event to increased heavy metal concentrations (Galasso et al., 2025). However, short-lived dysoxic and anoxic periods could have contributed to the severity of the extinction event. Deoxygenation of the water column coinciding with increasing sea surface temperatures would have exacerbated the effects of thermal stress on an organismal level, since oxygen solubility decreases and metabolic oxygen demand increases with increasing temperature (Pörtner et al., 2023). Thermal stress associated with the Permian–Triassic mass extinction (e.g., Sun et al., 2012; Joachimski et al., 2012, 2020; Schobben et al., 2014; Gliwa et al., 2022; Foster et al., 2024) is therefore most catastrophic when oxygen availability is reduced.

4.4 Biotic ecosystem response

The succession at Lusitaniadalen records a shift in the community of primary producers following the Permian–Triassic environmental crisis (Buchwald et al., 2025b). This compositional shift seems to be accompanied by an increase in primary productivity evident in the sharp increase in the chlorophyll- and/or bacteriochlorophyll-derived biomarkers pristane and phytane (Fig. 2.5), although additional archaeal sources should be considered (see section 4.3). The detected shorter $C_{14–18}$ isoprenoids could represent additional degradation products of pristane and phytane, but we cannot exclude contributions from other sources to the pool of shorter isoprenoids. For example, it has been shown that farnesane (C_{15}-isoprenoid) may also be derived directly from the side-chain of bacteriochlorophyll d from green sulfur bacteria (Grice et al., 1996). However, since post-extinction redox conditions were mostly oxic, green sulfur bacteria are unlikely the main source of farnesane. Furthermore, because peak contents of pristane and phytane do not coincide with peak input from terrestrial plant material as recorded in TAR (Fig. 2.5), chlorophyll of terrestrial plants is also not a major source of pristane and phytane, rendering marine photosynthetic organisms the main source (Grice et al., 2005b).

Regional primary productivity blooms or a restructuring of the community of primary producers following the Permian–Triassic mass extinction have been reported across different paleolatitudes and ocean basins (Grasby et al., 2024; Jia et al., 2012; Meyer et al., 2011; Saito et al., 2022), and have been assumed to be triggered by enhanced nutrient influx from land, or the remobilization of nutrients like phosphorus from the seafloor due to the expansion of bottom-water anoxia (e.g., Grasby et al., 2024). Primary productivity across the Permian–Triassic transition was likely highly variable, and other regions such as South China, which was located in the eastern Tethys Ocean, may record a productivity collapse in the aftermath of the extinction (e.g., Algeo et al., 2013; Shen J. et al., 2014). However, the quantification of primary productivity remains challenging as enhanced organic matter recycling in the water column could also produce a signal that may be interpreted as decrease in productivity (Shen J. et al., 2015). Nevertheless, in central Svalbard, there is evidence for both increased terrestrial input (this study; Klausen et al., 2019; Gilmullina et al., 2022) as well as an increase in the bioavailable phosphorus concentration in the Early Triassic, due to its release from anoxic bottom water (Schobben et al., 2020), coinciding with the Permian–Triassic environmental crisis. Enhanced nutrient loading from these sources after the extinction could have facilitated the local proliferation of photosynthetic organisms during the Griesbachian at Lusitaniadalen, causing the observed pulses in (bacterio)chlorophyll markers.

Alongside pristane and phytane, we detected regular PMI (Fig. 2.5). Although the more widely known tail-to-tail linked structural isomer 2,6,10,15,19-pentamethylicosane is diagnostic for methanogenic and methanotrophic archaea (Pancost et al., 2000; Risatti et al., 1984; Sakata et al., 2024), regular PMI is often used as indicator for hypersaline conditions (Grice et al., 1998). Regular PMI and shorter $C_{20–24}$ regular isoprenoids can derive from the degradation of the isoprenoid side chain of extended archaeol, characteristic for membrane lipids of Haloarchaea. Haloarchaea have recently been shown to also occur under only moderately elevated salinity (50 psu) (Vandier et al., 2021). The content of regular PMI and shorter head-to-tail linked isoprenoids at Lusitaniadalen increases above the extinction horizon during a period of marine transgression (Mørk et al., 1989; 1999). This suggests that the elevated salinity signal was not the result of restricted lagoonal conditions but rather linked to changes in water mass properties

like water column stratification or episodic upwelling of more saline water masses onto the Barents Shelf (Fig. 2.6).

Generally, the content of lipid biomarkers such as pristane, phytane, and regular PMI remains elevated in the post-extinction compared to the pre-extinction interval (Fig. 2.5). Although the silicified mudstones in the Kapp Starostin Formation and the mudstones of the Deltadalen Member of the Vikinghøgda Formation both record a similar distal outer ramp setting (Blomeier et al., 2013; Zuchuat et al., 2020), the difference in silica content may bias the comparison of the lipid biomarker composition between these facies. To account for the dilution of organic matter by the high silica content in the Kapp Starostin Formation, the lipid biomarker content was normalized to TOC (wt%). Hence, the extended sampling range into the Kapp Starostin Formation compared to previous studies (Grotheer et al., 2017; Nabbefeld et al., 2010a) enables us to attribute these changes in the lipid biomarker composition to the extinction event, while the lithological change across the extinction horizon was likely not the main factor.

The lack of a return to the pre-crisis lipid biomarker composition within the first 30 m above the extinction horizon suggests either that the sampled Lower Triassic interval records too short of an interval to capture the microbial ecological recovery, or that the post-crisis microbial community stabilized at a new equilibrium, corroborating observations from the fossil record (Jablonski & Edie, 2025). However, based on a calculated linear sediment accumulation rate of 220 m/Myr in the Induan from the adjacent site of Deltadalen (Zuchuat et al., 2020), the sampled 30 m above the extinction horizon represent only approximately 136 kyr. Depending on the criteria used to define ecosystem recovery, the earliest signs of biotic recovery from the Permian–Triassic mass extinction are observed in the first substage of the Triassic, the middle to late Griesbachian (Hofmann et al., 2011; Twitchett et al., 2004), while a complete reestablishment of biodiversity and ecosystem complexity in most regions appears to have not occurred until the Middle or even Late Triassic (Chen & Benton, 2012; Foster & Sebe, 2017; Song et al., 2018). Hence, even the youngest sample we collected from Lusitaniadalen is most likely still too old to record a stable post-crisis community.

5 Conclusions

This multiproxy analysis from Lusitaniadalen provides new insights into environmental and ecosystem responses to the Permian–Triassic environmental crisis at a temperate mid-latitude site in the Boreal Realm. Building upon previous studies of geochemical proxies and lipid biomarkers across the Permian–Triassic transition, we established a comprehensive baseline of the redox-sensitive metal and lipid biomarker inventory from the late Permian at Lusitaniadalen, Svalbard. To better understand ecosystem conditions prior to the environmental crisis, we extended our sampling range to over 40 m below the extinction horizon.

Calculation of revised enrichment factors of Re, V, U and Mo enabled us to account for changes in sedimentary Al concentrations associated with lithofacies changes across the Permian–Triassic transition, and provide a more robust reconstruction of marine redox conditions. Redox interpretations based on geochemical proxies were independently supported by the organic biomarker pristane/phytane ratio, which together reveal complex redox conditions across the Permian–Triassic transition. Short-lived episodes of deoxygenation also occurred prior to the Permian–Triassic mass extinction, whereas redox conditions immediately preceding and following the extinction event itself appear to have been characterized by more intense anoxic episodes, potentially caused by upwelling of sulfidic deep water. Eventually, prevalent oxic conditions were reestablished in the Early Triassic. Hence, in contrast to what has been hypothesized for some coeval equatorial settings, persistent water column anoxia or euxinia might not have been a dominant driver of the extinction event at this Boreal site, emphasizing spatial variability in ocean redox conditions during the Permian–Triassic transition. Nevertheless, transient dysoxic episodes, water column stratification and enhanced input of terrestrial organic matter in the early to middle Griesbachian likely affected local ecosystem structure and function, potentially providing beneficial conditions for some marine photosynthetic organisms to thrive and form regional phytoplankton blooms.

Finally, our extended biomarker record demonstrates that changes in the biomarker inventory across the extinction horizon do not simply reflect facies variability but likely record substantial changes in local planktonic microbial communities. However, we do not detect indications for

microbial ecosystem recovery such as a return towards a pre-crisis community composition within this interval.

Acknowledgments

We would like to thank Sysselmesteren på Svalbard for granting us the sampling permission (Permit No. 23/00910-2 and 24/00386-4). We further thank Sabine Beckmann (UHH) for the support in the lab, and Guillermo Molina and Adam Green (UHH) for their help picking conodonts. This research was funded by the Deutsche Forschungsgemeinschaft (Project No. FO1297/1). Fieldwork was co-funded by the Arctic Field Grant of the Research Council of Norway (Project No. 342069 and 250229).

Open Research

The dataset for the the digital 3D model of the Lusitaniadalen section (Buchwald et al., 2025a: https://doi.org/10.5281/zenodo.15981864) and data and R code used in this study (Buchwald et al., 2025c: https://doi.org/10.5281/zenodo.16983603) are available in the Zenodo repository.

References

Algeo, T. J., & Liu, J. (2020). A re-assessment of elemental proxies for paleoredox analysis. *Chemical Geology, 540*, 119549. https://doi.org/10.1016/j.chemgeo.2020.119549

Algeo, T. J., & Tribovillard, N. (2009). Environmental analysis of paleoceanographic systems based on molybdenum-uranium covariation. *Chemical Geology*, *268*(3–4), 211–225. https://doi.org/10.1016/j.chemgeo.2009.09.001

Algeo, T. J., & Twitchett, R. J. (2010). Anomalous Early Triassic sediment fluxes due to elevated weathering rates and their biological consequences. *Geology, 38*(11), 1023–1026. https://doi.org/10.1130/G31203.1

Algeo, T. J., Ellwood, B., Nguyen, T. K. T., Rowe, H., & Maynard, J. B. (2007). The Permian-Triassic boundary at Nhi Tao, Vietnam: Evidence for recurrent influx of sulfidic watermasses to a shallow-marine carbonate platform. *Palaeogeography, Palaeoclimatology, Palaeoecology*, *252*(1–2), 304–327. https://doi.org/10.1016/j.palaeo.2006.11.055

Algeo, T. J., Henderson, C. M., Tong, J., Feng, Q., Yin, H., & Tyson, R. V. (2013). Plankton and productivity during the Permian–Triassic boundary crisis: An analysis of organic carbon fluxes. *Global and Planetary Change, 105*, 52–67. https://doi.org/10.1016/j.gloplacha.2012.02.008

Arrigo, K. R. (2005). Marine microorganisms and global nutrient cycles. *Nature*, *437*(7057), 349–355. https://doi.org/10.1038/nature04159

Beaty, B., Foster, W. J., Zuchuat, V., Moller, S. R., Buchwald, S. Z., Brooks, H., et al. (2025). Bioturbation shapes marine biogeochemical cycling following the end-Permian mass extinction in northern Pangea. *Geobiology, 23*(5), e70032. https://doi.org/10.1111/gbi.70032

Birgel, D., & Peckmann, J. (2008). Aerobic methanotrophy at ancient marine methane seeps: A synthesis. *Organic Geochemistry, 39*(12), 1659–1667. https://doi.org/10.1016/j.orggeochem.2008.01.023

Birgel, D., Guido, A., Liu, X., Hinrichs, K.-U., Gier, S., & Peckmann, J. (2014). Hypersaline conditions during deposition of the Calcare di Base revealed from archaeal di- and tetraether inventories. *Organic Geochemistry*, *77*, 11–21. https://doi.org/10.1016/j.orggeochem.2014.09.002

Blakey, R. (2012). Global paleogeography. Retrieved from http://www2.nau.edu/rcb7/globaltext2.html [accessed July 2014]

Blomeier, D., Dustira, A. M., Forke, H., & Scheibner, C. (2013). Facies analysis and depositional environments of a storm-dominated, temperate to cold, mixed siliceous–carbonate ramp: The Permian Kapp Starostin Formation in NE Svalbard. *Norwegian Journal of Geology, 93*(2), 75–93.

Bond, D. P. G., & Wignall, P. B. (2010). Pyrite framboid study of marine Permian-Triassic boundary sections: A complex anoxic event and its relationship to contemporaneous mass extinction. *Bulletin of the Geological Society of America, 122*(7–8), 1265–1279. https://doi.org/10.1130/B30042.1

Brennecka, G. A., Herrmann, A. D., Algeo, T. J., & Anbar, A. D. (2011). Rapid expansion of oceanic anoxia immediately before the end-Permian mass extinction. *Proceedings of the National Academy of Sciences*, *43*(108), 17631–17634. https://doi.org/10.1073/pnas.1106039108

Brocks, J. J., & Grice, K. (2011). Biomarkers (molecular fossils). In J. Reitner & V. Thiel (Eds.), *Encyclopedia of Geobiology* (pp. 147–167). Springer.

Brocks, J. J., & Schaeffer, P. (2008). Okenane, a biomarker for purple sulfur bacteria (Chromatiaceae), and other new carotenoid derivatives from the 1640 Ma Barney Creek Formation. *Geochimica et Cosmochimica Acta*, *72*(5), 1396–1414. https://doi.org/10.1016/j.gca.2007.12.006

Buchwald, S. Z., Birgel, D., Senger, K., Mosociova, T., Pei, Y., Frank, A. B., et al. (2025b). Primary productivity blooms on the Barents Shelf, Svalbard, associated with the Permian-Triassic mass extinction. *Preprint at ESS Open Archive*. https://doi.org/10.22541/essoar.174558961.14311943/v1

Buchwald, S. Z., Frank A. B., Birgel D., Senger K., Mosociova T., Pei Y., et al. (2025c). Reconstructing environmental and microbial ecosystem changes across the Permian–Triassic mass extinction at Lusitaniadalen, Svalbard. StellaZBuchwald/Permian-Triassic_Lusitaniadalen, published Aug 28, 2025 [Dataset, Computational Notebook], Zenodo, https://doi.org/10.5281/zenodo.16983603

Buchwald, S. Z., Mosociova T., Gómez Correa M. A., Foster W. J., & Senger K. (2025a). Digital outcrop model Lusitaniadalen, published Sep 26, 2025 [Computational Notebook], Zenodo, https://doi.org/10.5281/zenodo.15981864

Buschhaus, C., & Jetter, R. (2011). Composition differences between epicuticular and intracuticular wax substructures: How do plants seal their epidermal surfaces? *Journal of Experimental Botany*, *62*(3), 841–853. https://doi.org/10.1093/jxb/erq366

Cao, C., Love, G. D., Hays, L. E., Wang, W., Shen, S., & Summons, R. E. (2009). Biogeochemical evidence for euxinic oceans and ecological disturbance presaging the end-Permian mass extinction event. *Earth and Planetary Science Letters*, *281*(3–4), 188–201. https://doi.org/10.1016/j.epsl.2009.02.012

Cao, C., Wang, W., & Yugan, J. (2002). Carbon isotope excursions across the Permian-Triassic boundary in the Meishan section, Zhejiang Province, China. *Chinese Science Bulletin*, *47*, 1125–1129. https://doi.org/10.1360/02tb9252

Chen, L., Wang, Y., Xie, S., Kershaw, S., Dong, M., Yang, H., et al. (2011). Molecular records of microbialites following the end-Permian mass extinction in Chongyang, Hubei Province, South China. *Palaeogeography, Palaeoclimatology, Palaeoecology*, *308*(1–2), 151–159. https://doi.org/10.1016/j.palaeo.2010.09.010

Chen, Z. Q., & Benton, M. J. (2012). The timing and pattern of biotic recovery following the end-Permian mass extinction. *Nature Geoscience*, *5*(6), 375–383. https://doi.org/10.1038/ngeo1475

Crasquin, S., Forel, M. B., Qinglai, F., Aihua, Y., Baudin, F., & Collin, P. Y. (2010). Ostracods (Crustacea) through the Permian-Triassic boundary in South China: The Meishan stratotype (Zhejiang Province). *Journal of Systematic Palaeontology*, *8*(3), 331–370. https://doi.org/10.1080/14772011003784992

Dallmann, W. K., Andersen, A., Bergh, S. G., Maher Jr., H. D., & Ohta, Y. (1993). *Tertiary fold-and-thrust belt of Spitsbergen, Svalbard: compilation map, summary and bibliography*. Norsk polarinstitutt.

Didyk, B. M., Simoneit, B. R. T., Brassell, S. C., & Eglinton, G. (1978). Organic geochemical indicators of palaeoenvironmental conditions of sedimentation. *Nature*, *272*(5650), 216–222. https://doi.org/10.1038/272216a0

Dustira, A. M., Wignall, P. B., Joachimski, M., Blomeier, D., Hartkopf-Fröder, C., & Bond, D. P. G. (2013). Gradual onset of anoxia across the Permian-Triassic boundary in Svalbard, Norway. *Palaeogeography, Palaeoclimatology, Palaeoecology*, *374*, 303–313. https://doi.org/10.1016/j.palaeo.2013.02.004

Eglington, G., & Hamilton, R. J. (1967). Leaf epicuticular waxes. *Science*, *3780*(156), 1322–1335. https://doi.org/10.1126/science.156.3780.1322

Elrick, M., Polyak, V., Algeo, T. J., Romaniello, S., Asmerom, Y., Herrmann, A. D., et al. (2017). Global-ocean redox variation during the middle-late Permian through Early Triassic based on uranium isotope and Th/U trends of marine carbonates. *Geology, 45*(2), 163–166. https://doi.org/10.1130/G38585.1

El-Shafeiy, M., Birgel, D., El-Kammar, A., El-Barkooky, A., Wagreich, M., Mohamed, O., & Peckmann, J. (2014). Palaeoecological and post-depositional changes recorded in Campanian-Maastrichtian black shales, Abu Tartur plateau, Egypt. *Cretaceous Research*, *50*, 38–51. https://doi.org/10.1016/j.cretres.2014.03.022

Epstein, A. G., Epstein, J. B., & Harris, L. D. (1977). Conodont color alteration: An index to organic metamorphism. *Geological Survey Professional Paper*, *995*.

Espitalié, J., Madec, M., Tissot, B., Menning, J. J., & Leplat, P. (1977). Source rock characerization method for petroleum exploration. In *Offshore technology conference* (p. OTC-2935).

Foster, W. J., & Sebe, K. (2017). Recovery and diversification of marine communities following the late Permian mass extinction event in the western Palaeotethys. *Global and Planetary Change*, *155*, 165–177. https://doi.org/10.1016/j.gloplacha.2017.07.009

Foster, W. J., Asatryan, G., Rauzi, S., Botting, J. P., Buchwald, S. Z., Lazarus, D. B., et al. (2023). Response of siliceous marine organisms to the Permian-Triassic climate crisis based on new findings from central Spitsbergen, Svalbard. *Paleoceanography and Paleoclimatology*, *38*(12), e2023PA004766. https://doi.org/10.1029/2023PA004766

Foster, W. J., Danise, S., & Twitchett, R. J. (2017). A silicified Early Triassic marine assemblage from Svalbard. *Journal of Systematic Palaeontology*, *15*(10), 851–877. https://doi.org/10.1080/14772019.2016.1245680

Foster, W. J., Frank, A. B., Li, Q., Danise, S., Wang, X., & Peckmann, J. (2024). Thermal and nutrient stress drove Permian–Triassic shallow marine extinctions. *Cambridge Prisms: Extinction*, *2*, e9. https://doi.org/10.1017/ext.2024.9

Foster, W. J., Lehrmann, D. J., Hirtz, J. A., White, M., Yu, M., Li, J., & Martindale, R. C. (2019). Early Triassic benthic invertebrates from the Great Bank of Guizhou, South China: Systematic palaeontology and palaeobiology. *Papers in Palaeontology*, *5*(4), 613–656. https://doi.org/10.1002/spp2.1252

Frank, A. B., Warncke-Rüting, E. L., Grasby, S. E., Kustatscher, E., Prinoth, H., Poulton, S. W., et al. (2025). Oxic conditions in shallow marine settings during the Permian-Triassic mass extinction. *Preprint at EarthArXiv*. https://doi.org/10.31223/X5K135

Galasso, F., Frank, A. B., & Foster, W. J. (2025). Heavy metal toxicity: A major driver of past biodiversity crises? *Preprint at EarthArXiv*. https://doi.org/10.31223/X5SX5R

Gilmullina, A., Klausen, T. G., Doré, A. G., Rossi, V. M., Suslova, A., & Eide, C. H. (2022). Linking sediment supply variations and tectonic evolution in deep time, source-to-sink systems—The Triassic Greater Barents Sea Basin. *Bulletin of the Geological Society of America*, *134*(7–8), 1760–1780. https://doi.org/10.1130/B36090.1

Gliwa, J., Forel, M. B., Crasquin, S., Ghaderi, A., & Korn, D. (2021). Ostracods from the end-Permian mass extinction in the Aras Valley section (north-west Iran). *Papers in Palaeontology*, *7*(2), 1003–1042. https://doi.org/10.1002/spp2.1330

Gliwa, J., Wiedenbeck, M., Schobben, M., Ullmann, C. V., Kiessling, W., Ghaderi, A., et al. (2022). Gradual warming prior to the end-Permian mass extinction. *Palaeontology*, *65*(5), e12621. https://doi.org/10.1111/pala.12621

Grasby, S. E., & Beauchamp, B. (2008). Intrabasin variability of the carbon-isotope record across the Permian–Triassic transition, Sverdrup Basin, Arctic Canada. *Chemical Geology*, *253*(3–4), 141–150. https://doi.org/10.1016/j.chemgeo.2008.05.005

Grasby, S. E., Beauchamp, B., Bond, D. P. G., Wignall, P., Talavera, C., Galloway, J. M., et al. (2015). Progressive environmental deterioration in northwestern Pangea leading to the latest Permian

extinction. *Bulletin of the Geological Society of America*, *127*(9–10), 1331–1347. https://doi.org/10.1130/B31197.1

Grasby, S. E., Them II, T. R., Chen, Z., Yin, R., & Ardakani, O. H. (2019). Mercury as a proxy for volcanic emissions in the geologic record. *Earth Science Reviews*, *196*, 102880. https://doi.org/10.1016/j.earscirev.2019.102880

Grasby, S. E., Ardakani, O. H., Liu, X., Bond, D. P. G., Wignall, P. B., & Strachan, L. J. (2024). Marine snowstorm during the Permian-Triassic mass extinction. *Geology*, *52*(2), 120–124. https://doi.org/10.1130/G51497.1

Grice, K., Cao, C., Love, G. D., Böttcher, M. E., Twitchett, R. J., Grosjean, E., et al. (2005b). Photic zone euxinia during the Permian-Triassic superanoxic event. *Science*, *307*(5710), 706–709. https://doi.org/10.1126/science.1104323

Grice, K., Schaeffert, P., Schwark, L., & Maxwell, J. R. (1996). Molecular indicators of palaeoenvironmental conditions in an immature Permian shale (Kupferschiefer, Lower Rhine Basin, north-west Germany) from free and S-bound lipids. *Organic Geochemistry*, *25*(314), 131–147. https://doi.org/10.1016/S0146-6380(96)00130-1

Grice, K., Schouten, S., Nissenbaum, A., Charrach, J., & Sinninghe Damsté, J. S. (1998). Isotopically heavy carbon in the C_{21} to C_{25} regular isoprenoids in halite-rich deposits from the Sdom Formation, Dead Sea Basin, Israel. *Organic Geochemistry*, *6*(28), 349–359. https://doi.org/10.1016/S0146-6380(98)00006-0

Grice, K., Twitchett, R. J., Alexander, R., Foster, C. B., & Looy, C. (2005a). A potential biomarker for the Permian-Triassic ecological crisis. *Earth and Planetary Science Letters*, *236*(1–2), 315–321. https://doi.org/10.1016/j.epsl.2005.05.008

Grotheer, H., Le Métayer, P., Piggott, M. J., Lindeboom, E. J., Holman, A. I., Twitchett, R. J., & Grice, K. (2017). Occurrence and significance of phytanyl arenes across the Permian-Triassic boundary interval. *Organic Geochemistry, 104*, 42–52. https://doi.org/10.1016/j.orggeochem.2016.12.002

Hays, L. E., Beatty, T., Henderson, C. M., Love, G. D., & Summons, R. E. (2007). Evidence for photic zone euxinia through the end-Permian mass extinction in the Panthalassic Ocean (Peace River Basin, Western Canada). *Palaeoworld*, *16*(1–3), 39–50. https://doi.org/10.1016/j.palwor.2007.05.008

Hays, L. E., Grice, K., Foster, C. B., & Summons, R. E. (2012). Biomarker and isotopic trends in a Permian-Triassic sedimentary section at Kap Stosch, Greenland. *Organic Geochemistry*, *43*, 67–82. https://doi.org/10.1016/j.orggeochem.2011.10.010

Heindel, K., Foster, W. J., Richoz, S., Birgel, D., Roden, V. J., Baud, A., et al. (2018). The formation of microbial-metazoan bioherms and biostromes following the latest Permian mass extinction. *Gondwana Research*, *61*, 187–202. https://doi.org/10.1016/j.gr.2018.05.007

Hofmann, R., Goudemand, N., Wasmer, M., Bucher, H., & Hautmann, M. (2011). New trace fossil evidence for an early recovery signal in the aftermath of the end-Permian mass extinction. *Palaeogeography, Palaeoclimatology, Palaeoecology*, *310*(3–4), 216–226. https://doi.org/10.1016/j.palaeo.2011.07.014

Jablonski, D., & Edie, S. M. (2025). Mass extinctions and their rebounds: A macroevolutionary framework. *Paleobiology*, *51*, 83–96. https://doi.org/10.1017/pab.2024.13

Jia, C., Huang, J., Kershaw, S., Luo, G., Farabegoli, E., Perri, M. C., et al. (2012). Microbial response to limited nutrients in shallow water immediately after the end-Permian mass extinction. *Geobiology*, *10*(1), 60–71. https://doi.org/10.1111/j.1472-4669.2011.00310.x

Joachimski, M. M., Alekseev, A. S., Grigoryan, A., & Gatovsky, Y. A. (2020). Siberian Trap volcanism, global warming and the Permian-Triassic mass extinction: New insights from Armenian Permian-Triassic sections. *Bulletin of the Geological Society of America*, *132*(1–2), 427–443. https://doi.org/10.1130/B35108.1

Joachimski, M. M., Lai, X., Shen, S., Jiang, H., Luo, G., Chen, B., et al. (2012). Climate warming in the latest Permian and the Permian-Triassic mass extinction. *Geology*, *40*(3), 195–198. https://doi.org/10.1130/G32707.1

Kaiho, K., Aftabuzzaman, M., Jones, D. S., & Tian, L. (2021). Pulsed volcanic combustion events coincident with the end-Permian terrestrial disturbance and the following global crisis. *Geology*, *49*(3), 289–293. https://doi.org/10.1130/G48022.1

Karl, D. M. (2014). Microbially mediated transformations of phosphorus in the sea: New views of an old cycle. *Annual Review of Marine Science*, *6*, 279–337. https://doi.org/10.1146/annurev-marine-010213-135046

Klausen, T. G., Nyberg, B., & Helland-Hansen, W. (2019). The largest delta plain in Earth's history. *Geology*, *47*(5), 470–474. https://doi.org/10.1130/G45507.1

Knoll, A. H., Canfield, D. E., & Konhauser, K. (2012). *Fundamentals of geobiology*. Wiely-Blackwell. https://doi.org/10.1002/9781118280874

Koopmans, M. P., Schouten, S., Kohnen, M. E. L., & Sinninghe Damsté, J. S. (1996). Restricted utility of aryl isoprenoids as indicators for photic zone anoxia. *Geochimica et Cosmochimica Acta*, *60*(23), 4873–4876. https://doi.org/10.1016/S0016-7037(96)00303-1

Krewer, C., Poulton, S. W., Newton, R. J., März, C., Mills, B. J. W., & Wagner, T. (2024). Controls on the termination of Cretaceous Oceanic Anoxic Event 2 in the Tarfaya Basin, Morocco. *American Journal of Science*, *324*, 11. https://doi.org/10.2475/001c.118797

Lawrence, M. G., Greig, A., Collerson, K. D., & Kamber, B. S. (2006). Rare earth element and yttrium variability in South East Queensland waterways. *Aquatic Geochemistry*, *12*(1), 39–72. https://doi.org/10.1007/s10498-005-4471-8

Leu, M., Schneebeli-Hermann, E., Hammer, Ø., Lindemann, F.-J., & Bucher, H. (2024). Spatiotemporal dynamics of nektonic biodiversity and vegetation shifts during the Smithian–Spathian transition: Conodont and palynomorph insights from Svalbard. *Lethaia*, *57*(2), 1–19. https://doi.org/10.18261/let.57.2.3

Li, S., Wignall, P. B., & Poulton, S. W. (2025). Co-application of rhenium, vanadium, uranium and molybdenum as paleo-redox proxies: Insight from modern and ancient environments. *Chemical Geology*, *674*, 122565. https://doi.org/10.1016/j.chemgeo.2024.122565

Luo, G., Wang, Y., Grice, K., Kershaw, S., Algeo, T. J., Ruan, X., et al. (2013). Microbial-algal community changes during the latest Permian ecological crisis: Evidence from lipid biomarkers at Cili, South China. *Global and Planetary Change*, *105*, 36–51. https://doi.org/10.1016/j.gloplacha.2012.11.015

Luo, G., Yang, H., Algeo, T. J., Hallmann, C., & Xie, S. (2019). Lipid biomarkers for the reconstruction of deep-time environmental conditions. *Earth-Science Reviews*, *189*, 99–124. https://doi.org/10.1016/j.earscirev.2018.03.005

Mackenzie, A. S., Beaumont, C., & McKenzie, D. P. (1984). Estimation of the kinetics of geochemical reactions with geophysical models of sedimentary basins and applications. *Organic Geochemistry*, *6*, 875–884. https://doi.org/10.1016/0146-6380(84)90110-4

Meyer, K. M., Yu, M., Jost, A. B., Kelley, B. M., & Payne, J. L. (2011). $\delta^{13}C$ evidence that high primary productivity delayed recovery from end-Permian mass extinction. *Earth and Planetary Science Letters*, *302*(3–4), 378–384. https://doi.org/10.1016/j.epsl.2010.12.033

Mørk, A., Elvebakk, G., Forsberg, A. W., Hounslow, M. W., Nakrem, H. A., Vigran, J. O., & Weitschat, W. (1999). The type section of the Vikinghøgda formation: A new Lower Triassic unit in central and eastern Svalbard. *Polar Research*, *18*(1), 51–82. https://doi.org/10.1111/j.1751-8369.1999.tb00277.x

Mørk, A., Embry, A. F., & Weitschat, W. (1989). Triassic transgressive-regressive cycles in the Sverdrup Basin, Svalbard and the Barents Shelf. In J. D. Collins (Ed.), *Correlation in Hydrocarbon Exploration* (pp. 113–130). Dordrecht: Springer Netherlands.

Mørk, A., Knarud, R., & Worsley, D. (1982). Depositional and diagenetic environments of the Triassic and Lower Jurassic succession of Svalbard. In A. F. Embry & H. R. Balkwill (Eds.), *Arctic Geology and Geophysics, Canadian Society of Petroleum Geologists* (pp. 371–398).

Nabbefeld, B., Grice, K., Summons, R. E., Hays, L. E., & Cao, C. (2010b). Significance of polycyclic aromatic hydrocarbons (PAHs) in Permian/Triassic boundary sections. *Applied Geochemistry*, *25*(9), 1374–1382. https://doi.org/10.1016/j.apgeochem.2010.06.008

Nabbefeld, B., Grice, K., Twitchett, R. J., Summons, R. E., Hays, L., Böttcher, M. E., & Asif, M. (2010a). An integrated biomarker, isotopic and palaeoenvironmental study through the late Permian event at Lusitaniadalen, Spitsbergen. *Earth and Planetary Science Letters*, *291*(1–4), 84–96. https://doi.org/10.1016/j.epsl.2009.12.053

Nagy, J., Svensen, H. H., & Planke, S. (2025). Severe oxygen and carbonate depletion during the end-Permian mass extinction and its aftermath in Boreal waters reflected by foraminifera from Spitsbergen. *Preprint at SSRN*, 4460346. https://ssrn.com/abstract=4460346

Nakrem, H. A., Orchard, M. J., Weitschat, W., Hounslow, M. W., Beatty, T. W., & Mørk, A. (2008). Triassic conodonts from Svalbard and their Boreal correlations. *Polar Research, 27*(3), 523–539. https://doi.org/10.1111/j.1751-8369.2008.00076.x

Natalicchio, M., Birgel, D., Peckmann, J., Lozar, F., Carnevale, G., Liu, X., et al. (2017). An archaeal biomarker record of paleoenvironmental change across the onset of the Messinian salinity crisis in the absence of evaporites (Piedmont Basin, Italy). *Organic Geochemistry*, *113*, 242–253. https://doi.org/10.1016/j.orggeochem.2017.08.014

Olaussen, S., Grundvåg, S.-A., Senger, K., Anell, I., Betlem, P., Birchall, T., et al. (2025). Svalbard composite tectono-sedimentary element, Barents Sea. *Geological Society, London, Memoirs*, *57*(1), M57-2021. https://doi.org/10.1144/M57-2021-36

Pajares, S., & Ramos, R. (2019). Processes and microorganisms involved in the marine nitrogen cycle: Knowledge and gaps. *Frontiers in Marine Science*, *6*, 739. https://doi.org/10.3389/fmars.2019.00739

Pancost, R. D., Sinninghe Damsté, J. S., De Lint, S., Van Der Maarel, M. J. E. C., Gottschal, J. C., Aloisi de Larderel, G., et al. (2000). Biomarker evidence for widespread anaerobic methane oxidation in Mediterranean sediments by a consortium of methanogenic Archaea and Bacteria. *Applied and Environmental Microbiology*, *66*(3), 1126–1132. https://doi.org/10.1128/AEM.66.3.1126-1132.2000

Penn, J. L., Deutsch, C., Payne, J. L., & Sperling, E. A. (2018). Temperature-dependent hypoxia explains biogeography and severity of end-Permian marine mass extinction. *Science*, *362*(6419), eaat1327. https://doi.org/10.1126/science.aat1327

Peters, K. E. (1986). Guidelines for evaluating petroleum source rock using programmed pyrolysis. *American Association of Petroleum Geologists Bulletin, 70*(3), 318–329. https://doi.org/10.1306/94885688-1704-11d7-8645000102c1865d

Pörtner, H. O., Scholes, R. J., Arneth, A., Barnes, D. K. A., Burrows, M. T., Diamond, S. E., et al. (2023). Overcoming the coupled climate and biodiversity crises and their societal impacts. *Science*, *380*(6642), eabl4881. https://doi.org/10.1126/science.abl4881

Prinoth, H., & Posenato, R. (2023). Bivalves from the Changhsingian (upper Permian) Bellerophon Formation of the Dolomites (Italy): Ancestors of Lower Triassic post-extinction benthic communities. *Papers in Palaeontology*, *9*(2), e1486. https://doi.org/10.1002/spp2.1486

Rees, P. M. (2002). Land-plant diversity and the end-Permian mass extinction. *Geology*, *30*(9), 827–830. https://doi.org/10.1130/0091-7613(2002)030<0827:LPDATE>2.0.CO;2

R Core Team (2023). R: A language and environment for statistical computing. R foundation for statistical computing, Vienna, Austria. URL: https://www.R-project.org/

Rampino, M. R., & Eshet, Y. (2018). The fungal and acritarch events as time markers for the latest Permian mass extinction: An update. *Geoscience Frontiers, 9*(1), 147–154. https://doi.org/10.1016/j.gsf.2017.06.005

Reid, C. M., James, N. P., Beauchamp, B., & Kyser, T. K. (2007). Faunal turnover and changing oceanography: Late Palaeozoic warm-to-cool water carbonates, Sverdrup Basin, Canadian Arctic Archipelago. *Palaeogeography, Palaeoclimatology, Palaeoecology*, *249*(1–2), 128–159. https://doi.org/10.1016/j.palaeo.2007.01.007

Risatti, J. B., Rowland, S. J., Yon, D. A., & Maxwell, J. R. (1984). Stereochemical studies of acyclic isoprenoids-XII. Lipids of methanogenic bacteria and possible contributions to sediments. *Organic Geochemistry*, *6*, 93–104. https://doi.org/10.1016/0146-6380(84)90030-5

Rodríguez-Tovar, F. J., Dorador, J., Zuchuat, V., Planke, S., & Hammer, Ø. (2021). Response of macrobenthic trace maker community to the end-Permian mass extinction in central Spitsbergen, Svalbard. *Palaeogeography, Palaeoclimatology, Palaeoecology, 581*, 110637. https://doi.org/10.1016/j.palaeo.2021.110637

Rontani, J. F., & Bonin, P. (2011). Production of pristane and phytane in the marine environment: Role of prokaryotes. *Research in Microbiology*, *162*(9), 923–933. https://doi.org/10.1016/j.resmic.2011.01.012

De Rosa, M., Gambacorta, A., Nicolaus, B., Ross, H. N., Grant, W. D., & Bu'Lock, J. D. (1982). An asymmetric archaebacterial diether lipid from alkaliphilic halophiles. *Journal of General Microbiology*, *128*(2), 343–348. https://doi.org/10.1099/00221287-128-2-343

Rowland, S. J. (1990). Production of acyclic isoprenoid hydrocarbons by laboratory maturation of methanogenic bacteria. *Organic Geochemistry*, *15*(15), 9–16. https://doi.org/10.1016/0146-6380(90)90181-X

Sabino, M., Dela Pierre, F., Natalicchio, M., Birgel, D., Gier, S., & Peckmann, J. (2021). The response of water column and sedimentary environments to the advent of the Messinian salinity crisis: Insights from an onshore deep-water section (Govone, NW Italy). *Geological Magazine*, *158*(5), 825–841. https://doi.org/10.1017/S0016756820000874

Saito, R., Tian, L., Kaiho, K., & Takahashi, S. (2022). Biomarker evidence for the prolongation of multiple phytoplankton blooms in the aftermath of the end-Permian mass extinction. *Palaeogeography, Palaeoclimatology, Palaeoecology*, *600*, 111077. https://doi.org/10.1016/j.palaeo.2022.111077

Saito, R., Wörmer, L., Taubner, H., Kaiho, K., Takahashi, S., Tian, L., et al. (2023). Centennial scale sequences of environmental deterioration preceded the end-Permian mass extinction. *Nature Communications*, *14*(1), 2113. https://doi.org/10.1038/s41467-023-37717-0

Sakata, S., Tsunogai, U., Oba, M., Ujiie, T., & Tanahashi, M. (2024). Archaeal lipid biomarkers in near-surface sediments at a giant colony of the bivalve *Calyptogena*: Molecular records of a massive methane release event associated with methane hydrate dissociation. *Organic Geochemistry*, *188*, 104739. https://doi.org/10.1016/j.orggeochem.2024.104739

Schaal, E. K., Meyer, K. M., Lau, K. V., Silva-Tamayo, J. C., & Payne, J. L. (2015). Oceanic anoxia during the Permian–Triassic transition and links to volcanism. In A. Schmidt, K. Fristad, & L. Elkins-Tanton (Eds.), *Volcanism and Global Environmental Change* (pp. 275–290). Cambridge University Press. https://doi.org/10.1017/cbo9781107415683.022

Schneebeli-Hermann, E., Hochuli, P. A., & Bucher, H. (2017). Palynofloral associations before and after the Permian–Triassic mass extinction, Kap Stosch, East Greenland. *Global and Planetary Change*, *155*, 178–195. https://doi.org/10.1016/j.gloplacha.2017.06.009

Schobben, M., Foster, W. J., Sleveland, A. R. N., Zuchuat, V., Svensen, H. H., Planke, S., et al. (2020). A nutrient control on marine anoxia during the end-Permian mass extinction. *Nature Geoscience*, *13*(9), 640–646. https://doi.org/10.1038/s41561-020-0622-1

Schobben, M., Joachimski, M. M., Korn, D., Leda, L., & Korte, C. (2014). Palaeotethys seawater temperature rise and an intensified hydrological cycle following the end-Permian mass extinction. *Gondwana Research*, *26*(2), 675–683. https://doi.org/10.1016/j.gr.2013.07.019

Senger, K., Betlem, P., Birchall, T., Gonzaga, L., Grundvåg, S. A., Horota, R. K., et al. (2022). Digitising Svalbard's geology: The Festningen digital outcrop model. *First Break, 40*(3), 47–55. https://doi.org/10.3997/1365-2397.fb2022021

Sephton, M. A., Jiao, D., Engel, M. H., Looy, C. V., & Visscher, H. (2015). Terrestrial acidification during the end-Permian biosphere crisis? *Geology*, *43*(2), 159–162. https://doi.org/10.1130/G36227.1

Sephton, M. A., Looy, C. V., Brinkhuis, H., Wignall, P. B., de Leeuw, J. W., & Visscher, H. (2005). Catastrophic soil erosion during the end-Permian biotic crisis. *Geology*, *33*(12), 941–944. https://doi.org/10.1130/G21784.1

Shen, J., Schoepfer, S. D., Feng, Q., Zhou, L., Yu, J., Song, H., et al. (2015). Marine productivity changes during the end-Permian crisis and Early Triassic recovery. *Earth-Science Reviews, 149*, 136–162. https://doi.org/10.1016/j.earscirev.2014.11.002

Shen, J., Zhou, L., Feng, Q., Zhang, M., Lei, Y. Zhang N., et al. (2014). Paleo-productivity evolution across the Permian-Triassic boundary and quantitative calculation of primary productivity of black rock series from the Dalong Formation, South China. *Science China Earth Sciences, 57*(7), 1583–1594. https://doi.org/10.1007/s11430-013-4780-5

Shen, W., Sun, Y., Lin, Y., Liu, D., & Chai, P. (2011). Evidence for wildfire in the Meishan section and implications for Permian-Triassic events. *Geochimica et Cosmochimica Acta*, *75*(7), 1992–2006. https://doi.org/10.1016/j.gca.2011.01.027

Sinninghe Damsté, J. S., Schouten, S., & Van Duin, A. C. T. (2001). Isorenieratene derivatives in sediments: Possible controls on their distribution. *Geochimica et Cosmochimica Acta*, *65*(10), 1557–1571. https://doi.org/10.1016/S0016-7037(01)00549-X

Song, H., Wignall, P. B., & Dunhill, A. M. (2018). Decoupled taxonomic and ecological recoveries from the Permo-Triassic extinction. *Science Advances*, *4*(10), eaat5091. https://doi.org/10.1126/sciadv.aat5091

Sousa Júnior, G. R., Santos, A. Ô. L. S., De Lima, S. G., Lopes, J. A. D., Reis, F. A. M., Santos Neto, E. V., & Chang, H. K. (2013). Evidence for euphotic zone anoxia during the deposition of Aptian source rocks based on aryl isoprenoids in petroleum, Sergipe-Alagoas Basin, northeastern Brazil. *Organic Geochemistry*, *63*, 94–104. https://doi.org/10.1016/j.orggeochem.2013.07.009

Stanley, S. M. (2016). Estimates of the magnitudes of major marine mass extinctions in earth history. *Proceedings of the National Academy of Sciences*, *113*(42), E6325–E6334. https://doi.org/10.1073/pnas.1613094113

Summons, R. E. (2014). The exceptional preservation of interesting and informative biomolecules. *The Paleontological Society Papers*, *20*, 217–236. https://doi.org/10.1017/s1089332600002862

Summons, R. E., Welander, P. V., & Gold, D. A. (2022). Lipid biomarkers: Molecular tools for illuminating the history of microbial life. *Nature Reviews Microbiology*, *20*(3), 174–185. https://doi.org/10.1038/s41579-021-00636-2

Sun, Y., Joachimski, M. M., Wignall, P., Yan, C., Chen, Y., Jiang, H., et al. (2012). Lethally hot temperatures during the Early Triassic greenhouse. *Science, 338*(6105), 363–366. https://doi.org/10.1126/science.1224126

Svensen, H., Planke, S., Polozov, A. G., Schmidbauer, N., Corfu, F., Podladchikov, Y. Y., & Jamtveit, B. (2009). Siberian gas venting and the end-Permian environmental crisis. *Earth and Planetary Science Letters*, *277*(3–4), 490–500. https://doi.org/10.1016/j.epsl.2008.11.015

Taylor, S. R., & McLennan, S. M. (1985). *The Continental Crust: Its Composition and Evolution*. In A. Hallam (Ed.), Blackwell Scientific Publications (Oxford).

Tribovillard, N. (2024). Revisiting shallow glauconite factories: Intertwined fates of glauconite and iron. *Comptes Rendus. Géoscience e — Sciences de La Planète*, *356*(G1), 139–155. https://doi.org/10.5802/crgeos.274

Tribovillard, N., Algeo, T. J., Baudin, F., & Riboulleau, A. (2012). Analysis of marine environmental conditions based on molybdenum-uranium covariation-Applications to Mesozoic paleoceanography. *Chemical Geology*, *324*, 46–58. https://doi.org/10.1016/j.chemgeo.2011.09.009

Tribovillard, N., Algeo, T. J., Lyons, T., & Riboulleau, A. (2006). Trace metals as paleoredox and paleoproductivity proxies: An update. *Chemical geology*, *232*(1–2), 12–32. https://doi.org/10.1016/j.chemgeo.2006.02.012

Twitchett, R. J., Krystyn, L., Baud, A., Wheeley, J. R., & Richoz, S. (2004). Rapid marine recovery after the end-Permian mass-extinction event in the absence of marine anoxia. *Geology*, *32*(9), 805–808. https://doi.org/10.1130/G20585.1

Uchman, A., Hanken, N. M., Nielsen, J. K., Grundvåg, S. A., & Piasecki, S. (2016). Depositional environment, ichnological features and oxygenation of Permian to earliest Triassic marine sediments in central Spitsbergen, Svalbard. *Polar Research, 35*(1), 24782. https://doi.org/10.3402/polar.v35.24782

Vandier, F., Tourte, M., Doumbe-Kingue, C., Plancq, J., Schaeffer, P., Oger, P., & Grossi, V. (2021). Reappraisal of archaeal C_{20}-C_{25} diether lipid (extended archaeol) origin and use as a biomarker of hypersalinity. *Organic Geochemistry*, *159*, 104276. https://doi.org/10.1016/j.orggeochem.2021.104276

Vigran, J. O. (2014). *Palynology and geology of the Triassic succession of Svalbard and the Barents Sea.* In T. Slagstad (Ed.), 14th edition, Geological Survey of Norway.

Weyer, S., Anbar, A. D., Gerdes, A., Gordon, G. W., Algeo, T. J., & Boyle, E. A. (2008). Natural fractionation of $^{238}U/^{235}U$. *Geochimica et Cosmochimica Acta, 72*(2), 345–359. https://doi.org/10.1016/j.gca.2007.11.012

Wignall, P. B., Morante, R., & Newton, R. (1998). The Permo-Triassic transition in Spitsbergen: $\delta^{13}C_{org}$ chemostratigraphy, Fe and S geochemistry, facies, fauna and trace fossils. *Geological Magazine*, *135*(1), 47–62. https://doi.org/10.1017/S0016756897008121

Xiang, L., Zhang, H., Schoepfer, S. D., Cao, C., Zheng, Q., Yuan, D., et al. (2020). Oceanic redox evolution around the end-Permian mass extinction at Meishan, South China. *Palaeogeography, Palaeoclimatology, Palaeoecology*, *544*, 109626. https://doi.org/10.1016/j.palaeo.2020.109626

Xie, S., Algeo, T. J., Zhou, W., Ruan, X., Luo, G., Huang, J., & Yan, J. (2017). Contrasting microbial community changes during mass extinctions at the middle/late Permian and Permian/Triassic boundaries. *Earth and Planetary Science Letters*, *460*, 180–191. https://doi.org/10.1016/j.epsl.2016.12.015

Xie, S., Pancost, R. D., Huang, J., Wignall, P. B., Yu, J., Tang, X., et al. (2007). Changes in the global carbon cycle occurred as two episodes during the Permian-Triassic crisis. *Geology*, *35*(12), 1083–1086. https://doi.org/10.1130/G24224A.1

Yin, H., Zhang, K., Tong, J., Yang, Z., & Wu, S. (2001). The Global Stratotype Section and Point (GSSP) of the Permian-Triassic boundary. *Episodes Journal of International Geoscience*, *24*(2), 102–114.

Zhang, F., Algeo, T. J., Romaniello, S. J., Cui, Y., Zhao, L., Chen, Z. Q., & Anbar, A. D. (2018). Congruent Permian-Triassic $\delta^{238}U$ records at Panthalassic and Tethyan sites: Confirmation of global-oceanic anoxia and validation of the U-isotope paleoredox proxy. *Geology*, *46*(4), 327–330. https://doi.org/10.1130/G39695.1

Zhang, F., Shen, S., Cui, Y., Lenton, T. M., Dahl, T. W., Zhang, H., et al. (2020). Two distinct episodes of marine anoxia during the Permian-Triassic crisis evidenced by uranium isotopes in marine dolostones. *Geochimica et Cosmochimica Acta*, *287*, 165–179. https://doi.org/10.1016/j.gca.2020.01.032

Zuchuat, V., Sleveland, A. R. N., Twitchett, R. J., Svensen, H. H., Turner, H., Augland, L. E., et al. (2020). A new high-resolution stratigraphic and palaeoenvironmental record spanning the end-Permian mass extinction and its aftermath in central Spitsbergen, Svalbard. *Palaeogeography, Palaeoclimatology, Palaeoecology*, *554*, 109732. https://doi.org/10.1016/j.palaeo.2020.109732

Manuscript III

Buchwald SZ, Birgel D, Kustatscher E, Prinoth H, Galasso F, Karapunar B, Frank AB, Gómez Correa MA, Lahajnar N, Peckmann J, Foster WJ. Molecular fossils record marine and terrestrial ecosystem changes prior to and across the Permian–Triassic mass extinction in the Dolomites (Italy). *Submitted to Biogeosciences.*

SZB and WJF conceptualized the study; SZB curated the data and performed the formal analysis; WJF acquired funding; SZB, EK, HP, FG, BK, ABF, MAGC and WJF were involved in planning and conducting fieldwork; JP, DB and WJF provided institutional resources; SZB conducted the lipid biomarker lab work; NL provided TOC data; SZB wrote and visualized the original draft; all co-authors were involved in reviewing and editing.

Molecular fossils record shallow marine ecosystem changes prior to and across the Permian–Triassic mass extinction in the Dolomites (Italy)

S. Z. Buchwald[1], D. Birgel[1], E. Kustatscher[2], H. Prinoth[3], F. Galasso[1], B. Karapunar[4], A. B. Frank[1], M. A. Gómez Correa[1], N. Lahajnar[1], J. Peckmann[1], and W. J. Foster[1]

[1] Department of Earth System Sciences, University of Hamburg, Hamburg, Germany

[2] Department of Natural History, Tirolean State Museums, Hall in Tirol, Austria

[3] Museum Ladin Ciastel de Tor, San Martino in Badia, Italy

[4] School of Earth and Environment, University of Leeds, Leeds, United Kingdom

Corresponding author: Stella Zora Buchwald (stella.buchwald@uni-hamburg.de)

Abstract

The Permian–Triassic mass extinction, the most severe biotic crisis of the Phanerozoic, has been linked to environmental perturbations triggered by the eruptions of the Siberian Traps Large Igneous Province. However, multiple of these perturbations have previously been demonstrated to have started already several hundred thousand of years prior to the main extinction phase. To explore this timing and its ecological implications, we analyzed molecular fossils across the Permian–Triassic transition from two shallow marine carbonate ramp sections in the tropical Tethys Ocean from the Dolomites (northern Italy). Both the shallower (Siusi/Seis) and the deeper (Seres) setting record a sudden increase in polycyclic aromatic hydrocarbons (PAHs) such as pyrene and coronene just above the extinction, probably deriving from the combustion of organic-rich sedimentary rocks during Siberian Traps sill emplacement, and the subsequent distribution of these compounds. Redox-sensitive and source-indicative molecular fossil indices such as pristane/phytane (Pr/Ph), the terrigenous-aquatic ratio (TAR), and (Pr + Ph)/(*n*-C_{17} + *n*-C_{18}) reveal that redox conditions, the amount of terrestrially derived organic matter, and relative abundance of photoautotrophs were more variable in the shallower compared to the deeper setting. This variability suggests that ecosystems in shallow restricted environments experienced greater

stress than those in deeper settings. The shallower setting thereby records the effect of ubiquitous sea level fluctuation rather than an early onset of the environmental crises preceding the extinction event, highlighting spatial heterogeneity in ecosystem responses and underscoring the importance of regional environmental context when interpreting extinction dynamics.

1 Introduction

The Permian–Triassic mass extinction, which occurred approximately 252 million years ago, was the most severe biotic crisis of the Phanerozoic resulting in substantial loss of both marine and terrestrial biodiversity (e.g., Benton & Newell, 2014; Stanley, 2016). In marine ecosystems, the main environmental stressors hypothesized to have driven this crisis include thermal stress (e.g., Joachimski et al., 2012, 2020; Schobben et al., 2014; Sun et al., 2012), expansion of ocean anoxia (e.g., Brennecka et al., 2011; Cao et al., 2009; Grasby et al., 2013; Zhang et al., 2020), and ocean acidification (e.g., Clarkson et al., 2015; Hinojosa et al., 2012; Jurikova et al., 2020; Payne et al., 2010). The combined effects of these stressors are thought to have led to extreme environmental perturbations causing the global collapse of ecosystems (Payne & Clapham, 2012).

A close temporal relationship exists between the Permian–Triassic mass extinction and the emplacement of the Siberian Traps Large Igneous Province, which released massive amounts of greenhouse gases and other volatiles into the atmosphere, and especially the initial emplacement of sill intrusions likely triggered the extinction event (Burgess et al., 2017). However, while the main extinction pulse occurred over a geologically brief interval of 61 ka ± 48 ka, at least in the well-dated Meishan section (Burgess et al., 2014), the onset of Siberian Traps volcanism began several hundred thousand years earlier as evident from zircon dates (Burgess & Bowring, 2015) as well as the detection of fly ash and the long-term trend of decreasing $\delta^{13}C$ values in the late Permian (Grasby et al., 2011). Consequently, environmental changes typically linked to the mass extinction were initiated already well before the event, as demonstrated by increasing ocean warming and intensified chemical weathering likely caused by enhanced atmospheric pCO_2, that started already approximately 300 ka prior to the main extinction (Gliwa et al., 2022; Sun et al., 2018).

These gradual changes, eventually culminating in the Permian–Triassic mass extinction, are not only recorded in the geochemical record, but there is also evidence for a biotic response preceding the main extinction event. For instance, the decline of ammonoid diversity and pedomorphism coincided with a loss in their morphological complexity several hundred thousand years prior to the main extinction pulse (Kiessling et al., 2018; Korn et al., 2016), and a collapse of equatorial terrestrial ecosystems predating the marine extinction by ca. 270 ka (Guo et al., 2022; Zhang et al., 2023), and even ca. 370 ka in southern high latitudes (Fielding et al., 2019). Taken together, abiotic and biotic records challenge a simple and direct causal link between individual environmental stressors and the mass extinction, rather pointing toward a progressive deterioration of environmental conditions, and eventually the crossing of a tipping point that triggered global ecosystem collapse (Gliwa et al., 2022). Understanding the causes and consequences of the Permian–Triassic mass extinction thus requires investigating not only the extinction interval itself, but also its extended prelude.

Molecular fossils, the degradation products of biologically synthesized molecules, are a powerful tool to study the environmental conditions during the time of deposition as well as the phylogenetic affiliation of their source organisms (Luo et al., 2019). During biodegradation of organic matter, diagenesis, and maturation of the host rock, molecular fossils experience chemical transformations commonly resulting in the preservation of only the carbon skeleton of the parental molecule over geological timescales (Summons et al., 2022). Depending on their structural specificity, molecular fossils can be diagnostic for particular groups of organisms. For instance, phototrophic organisms such as cyanobacteria can be identified based on the molecular fossil inventory (Coates et al., 2014; Heindel et al., 2018), thereby offering the opportunity to complement the micro- and macrofossil record by capturing changes also in microbial ecosystems. Furthermore, molecular fossils can be specific for some environmental conditions, like certain polycyclic aromatic hydrocarbons (PAHs) that are indicative of high-temperature combustion of organic matter (Kaiho et al., 2021a, b; Saito et al., 2023; Shen et al., 2011), and the pristane/phytane (Pr/Ph) ratio (Didyk et al., 1978), which is used to assess redox conditions at the time of deposition (e.g., Cao et al., 2009; Chen et al., 2011; Jia et al., 2012).

The lithostratigraphy and fossil assemblages of the Permian–Triassic successions in the Dolomites (northern Italy) are well-studied (e.g., Brandner et al., 2009; Broglio Loriga et al., 1988, 1990; Farabegoli et al., 2007; Kustatscher et al., 2017; Posenato, 2010; Prinoth & Posenato, 2023). However, only a few studies exist on molecular fossils with limited number of samples (e.g., focusing on the biomarker inventory of a single sample), and a strong focus on the main extinction interval, hence existing pre-extinction data is limited to only a few centimeters up to 1–2 meters below the extinction, covering not enough strata to observe environmental and microbial community changes preceding the extinction event (Jia et al., 2012; Sephton et al., 1999, 2005, 2015; Watson et al., 2005). Here, we introduce a new molecular fossil dataset from two sections representing different water depths on a late Permian mixed carbonate-siliciclastic ramp setting in the Dolomites. Our study aims to reconstruct environmental changes and microbial ecosystem dynamics during the critical interval in the late Permian culminating in the Permian–Triassic mass extinction.

2 Material and Methods

2.1 Geological Setting

During the Permian–Triassic transition, the Dolomites in northern Italy were located on the continental shelf in the tropical western Tethys Ocean (Fig. 3.1a). Despite the opening of the Neotethys Ocean since the middle Permian (Robertson et al., 2012), northern Italy was situated on the same broad continental shelf of central Pangaea (Dercourt et al., 2000) as other well-studied Permian–Triassic sites such as in Turkey (e.g., Altıner et al., 2000) and Hungary (e.g., Haas et al., 2007; Hips, 1998). A similar depositional environment between these sites can also be inferred by the similar lithostratigraphy of sections that were hundreds of kilometers apart from each other (Karapunar et al., 2025).

During the Permian–Triassic transition, the sediments of northern Italy were deposited on a mixed siliciclastic-carbonate homoclinal ramp with increasing water depths from southwest to northeast

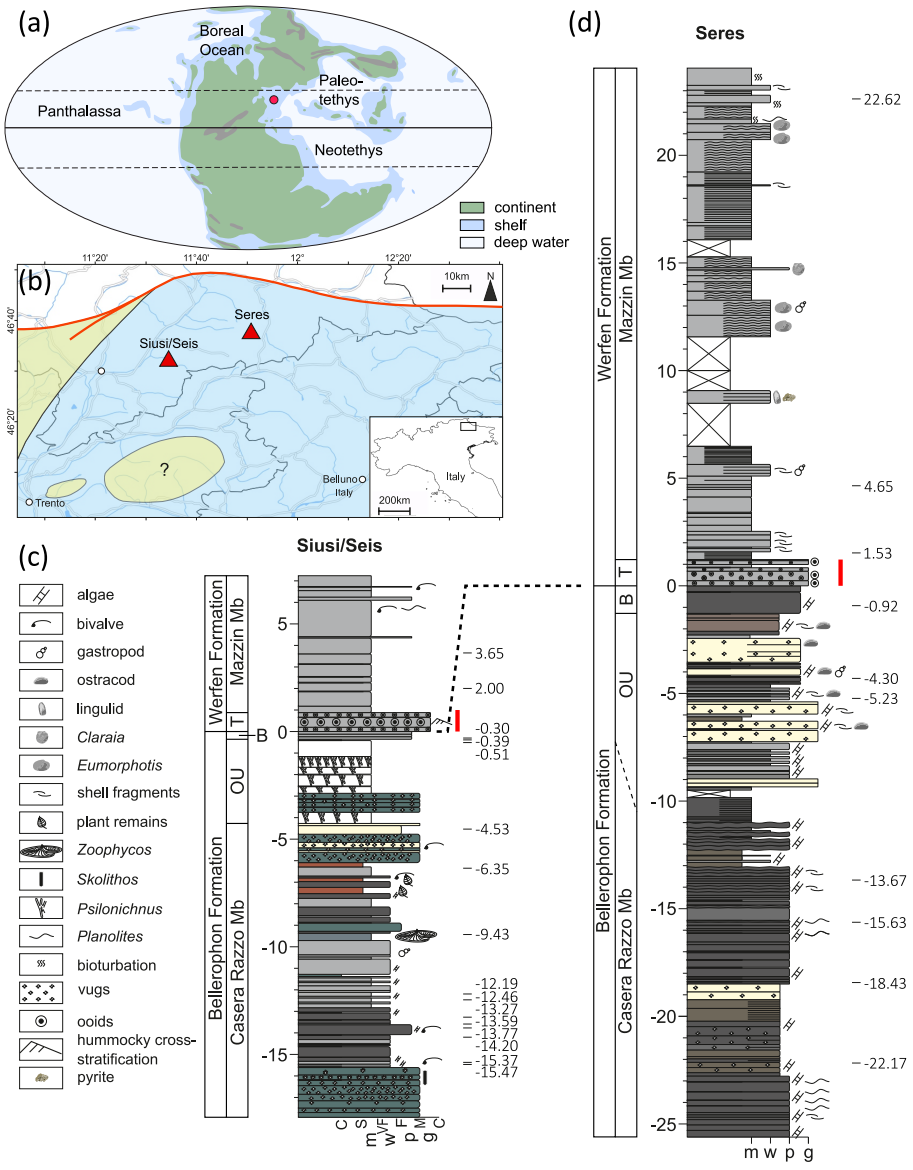

Figure 3.1: *a — Paleogeographic map at the Permian/Triassic boundary 252 Ma (after Blakey et al., 2012) with the location of northern Italy in the western Paleotethys; b — Current location of Siusi/Seis and Seres in northern Italy; paleo-shoreline indicated with yellow shade; c, d — Stratigraphic columns of the Permian–Triassic transition at Siusi/Seis and Seres with 0 m corresponding to the Bellerophon/Werfen Formation boundary. The position of the extinction event is marked with the red bar. OU = Ostracod Unit; B = Bulla Member; T = Tesero Member; C = claystone; S = siltstone; VF = very fine-grained sandstone; F = fine-grained sandstone; M = medium-grained sandstone; m = mudstone; w = wackestone; p = packstone; g = grainstone; the beds sampled for biomarker analysis are indicated with their corresponding height.*

(Noé, 1987). The two sites Siusi/Seis (46°32.024'N; 11°33.685'E; also referred to as Seiser Kamm) and Seres (46°38.395'N; 11°50.465'E; also referred to as Misci-Seres or Val Badia) thereby represent a more proximal and shallower environment, and a more distal and deeper environment, respectively (Fig. 3.1b). Interactive, digital 3D outcrop models of the Siusi/Seis (https://outcrop3d.deep-time.org/?model=e66bae4b-5b8b-ea6f-bf99-be110b6559d7) and Seres section (https://outcrop3d.deep-time.org/?model=837b9860-57ba-1bf5-0997-2a30e00d9efe) are openly accessible (Wang et al., 2024). The Permian Bellerophon Formation records carbonate-dominated deposits characterized by packstones interbedded with marly mud- and siltstones (e.g., Massari et al., 1994; Posenato, 2010; Prinoth & Posenato, 2023; Fig. 3.1c, d). Dolomitization is more frequently observed at the shallower Siusi/Seis section, and generally increases toward the top of the Bellerophon Formation, especially within the Ostracod Unit. While the Bellerophon Formation records an overall marine transgressive phase, several third-order transgressive-regressive cycles are recognized. These cycles led to variations in sea level from restricted and extremely shallow marine conditions with potentially subaerial exposure at locations on the inner shelf to a shallow open shelf environment (e.g., Massari et al., 1994; Prinoth & Posenato, 2023).

The mixed carbonate-siliciclastic Werfen Formation (e.g., Broglio Loriga et al., 1990) overlies the Bellerophon Formation and records the main phase of the Permian–Triassic mass extinction event at its base in the Tesero Member (Farabegoli et al., 2007; Groves et al., 2007; Posenato, 2010). The conodont *Hindeodus parvus* was found 1.45 m above the base of the Werfen Formation at Siusi/Seis (Horacek et al., 2010), and 1.30 m above the base of the Werfen Formation at the nearby Bulla section (Farabegoli et al., 2007; Perri & Farabegoli, 2003), placing the Permian/Triassic boundary slightly above the extinction. The Werfen Formation records the entire Early Triassic; however, herein we focus on the late Permian and the Permian–Triassic transition from the upper Bellerophon Formation (Casera Razzo Member, Ostracod Unit, Bulla Member) to the lower Griesbachian layers of the Werfen Formation (Tesero Member, Mazzin Member).

2.2 Sample acquisition and laboratory processing

In total, 15 samples were taken across the Permian–Triassic transition at Siusi/Seis and ten samples at Seres. For carbonate samples, large blocks with a weight of 2–4 kg were collected to ensure sufficient material after cutting off the weathered surfaces to avoid contamination. Samples were manually cleaned with acetone, and subsequently dissolved by slowly pouring 10% HCl on approximately 1 cm^3-sized pieces. Marly mud- and siltstone samples were manually crushed into powder using an agate mortar. As an internal standard, 10-methylnonadecane was added to the residue of the dissolved carbonate samples and the powdered samples, respectively.

Molecular fossil extraction was achieved by repeated sonication with dichloromethane:methanol (3:1, v:v) and centrifugation at 2,000 rpm for 5 min. The supernatants of each extraction step were combined. The organic solvent was reduced by rotation evaporation, and the remaining solvent was air-dried overnight to receive the total lipid extract (TLE). The TLE was split into an *n*-hexane insoluble fraction (asphaltenes) and an *n*-hexane soluble fraction (maltenes). Activated copper was added to the maltene fraction overnight to remove free sulfur. Maltenes were then further polarity-separated by column chromatography on a Chromabond NH_2 column after Birgel & Peckmann (2008). The fractions F1 (hydrocarbons) and F2 (aromatic compounds) were measured on a gas chromatograph-mass spectrometer (GC-MS; Thermo Scientific Trace Ultra GC and Thermo Scientific DSQ II MS) for identification, and a gas chromatograph coupled to a flame ionization detector (GC-FID; Thermo Scientific Trace 1310 GC) for quantification. The GC-MS and GC-FID were both equipped with a Thermo Scientific TG-5MS silica column (length = 30 m, diameter = 0.25 mm, film thickness = 0.25 µm). Carrier gases with a flow rate of 2 mL/min were He (GC-MS) and H_2 (GC-FID). The temperature program was set to 3 min at 50°C, followed by an increase of 6°C/min to 325°C, held for 25 min. Total organic carbon (TOC) was determined by acidifying powdered samples three times with 1 M HCl, before analyzing them on a Euro EA 3000 (Euro Vector) elemental analyzer (precision ± 0.05%).

2.3 Data analysis

Compound identification was achieved by analyzing their mass spectra with Xcalibur (version 3.1.66.10; Thermo Fisher). The integration of *n*-alkanes and the head-to-tail linked C_{19}- and C_{20}-isoprenoids pristane and phytane was performed based on the GC-FID chromatograms using Chromeleon 7 (version 7.2.10; Thermo Fisher Dionex). However, several compounds, mainly hopanes (F1) and aromatic compounds (F2), were co-eluting with other compounds, and therefore could only be identified when extracting their respective specific masses (*m/z*) from the total ion current of the GC-MS chromatogram (Fig. 3.2). For these compounds, peak integration was done on the respective base peak ion chromatogram in Xcalibur.

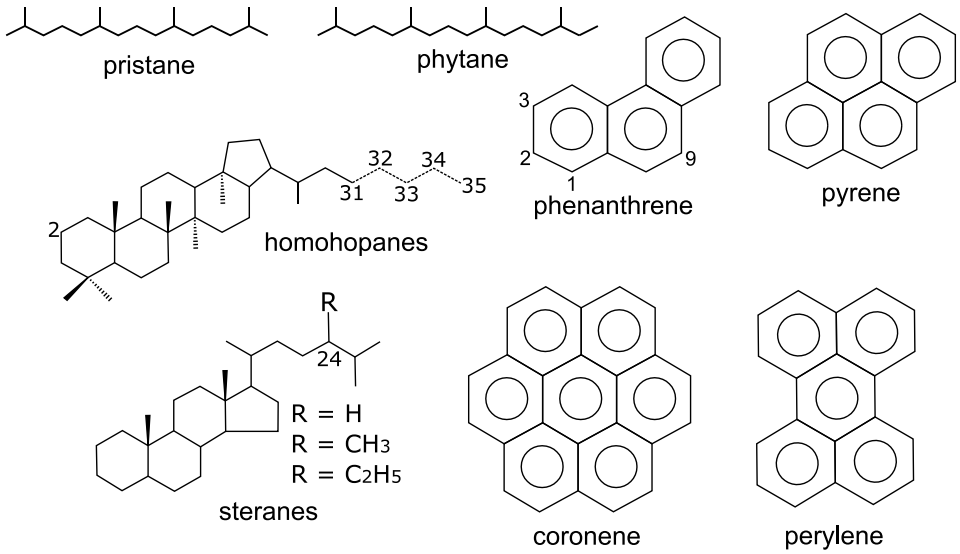

Figure 3.2: *Structures of investigated molecular fossils. Compounds were identified based on their respective base peaks, molecular weight and relative retention times. Homohopanes: m/z = 191; M+ = 426 (C_{31}), 440 (C_{32}), 454 (C_{33}), 468 (C_{34}), 482 (C_{35}), the methylation at C_2 for 2α-methylhopanes (m/z = 205) is indicated; steranes: m/z = 217; M+ = 372 (regular C_{27}-steranes); M+ = 386 (regular C_{28}-steranes); M+ = 400 (regular C_{29}-steranes); phenanthrene: m/z = 178; M+ = 178, with carbon numbers marked for 1-, 2-, 3- and 9-methylphenanthrene: m/z = 192; M+ = 192; pyrene: m/z = 202; M+ = 202; coronene: m/z = 300; M+ = 300; perylene: m/z = 252; M+ = 252.*

For an estimation of the thermal maturity of the material, the methylphenanthrene index (MPI) was calculated after Cassani et al. (1988) as MPI = 1.89(2-MP + 3-MP)/[P + 1.26(1-MP + 9-MP)] by using the peak areas from *m/z* = 178 for phenanthrene (P) and *m/z* = 192 for 1-, 2-, 3-, and 9-methylphenanthrene (MP). The carbon preference index (CPI) as modified by Marzi et al. (1993) was calculated from the peak areas of *n*-alkanes as CPI = [(*n*C_{21} + *n*C_{23} + *n*C_{25} + *n*C_{27} + *n*C_{29} + *n*C_{31} + *n*C_{33}) + (*n*C_{23} + *n*C_{25} + *n*C_{27} + *n*C_{29} + *n*C_{31} + *n*C_{33}+ *n*C_{35})]/[2*(*n*C_{22}+ *n*C_{24} + *n*C_{26}+ *n*C_{28} + *n*C_{30}+ *n*C_{32} + *n*C_{34})]. The homohopane isomerization index (HHI) was calculated from the peak areas of the *S*- and *R*-stereoisomers of the 17α,21β-C_{31}-hopane and 17α,21β-C_{32}-hopane in the *m/z* = 191 ion chromatogram as HHI = 22*S*/(22*S* + 22*R*). The 2α-methylhopane index (2-MHI) was calculated from the peak areas in *m/z* = 191 of 2α-methyl-17α(H),21β(H)-hopane and its unmethylated homolog 17α(H),21β(H)-hopane (C_{30}-hopane) as [2α-methylhopane/(C_{30}-hopane + 2α-methylhopane)]*100. The relative abundances of 5α(H),14α(H),17α(H)-22*R*-cholestane, 5α(H),14α(H),17α(H)-22*R*-24-methylcholestane and 5α(H),14α(H),17α(H)-22*R*-24-ethylcholestane (regular $C_{27–29}$-steranes) were calculated from the *m/z* = 217 ion chromatogram.

Results

For estimating organic matter maturity, several indices were calculated (Fig. 3.3). The mean MPI is lower in the Siusi/Seis than in the Seres section with a value of 0.42 and 0.65, respectively. For Seres, homohopanes were only detected in post-extinction samples, but the HHI is in the same range in both locations and within the homohopane series with HHI_{C31} = 0.54–0.59 and HHI_{C32} = 0.50–0.59. The CPI for Seres ranges from 0.97–1.03, while it is > 1 with values up to 1.62 in the Siusi/Seis section. The ratios Pr/*n*-C_{17} and Ph/*n*-C_{18} are consistently higher for Siusi/Seis than for Seres (Fig. 3.4), and their variability is highest in the Casera Razzo Member of the Bellerophon Formation, whereas Pr/*n*-C_{17} and Ph/*n*-C_{18} are in a relatively narrow range across the section in Seres (0.27–0.87 and 0.23–0.41, respectively).

The TOC content is generally low for both sites, and especially in the Seres section, it is in a narrow range from 0.15 wt% to 0.61 wt% (Fig. 3.5). In the Siusi/Seis section, there are intervals of increased TOC > 1.5 wt% at −15.47 m, −12.46 m and −0.39 m, whereas all other samples exhibit a TOC between 0.06 wt% and 0.65 wt%. For Siusi/Seis, several samples record TAR > 1

with highest values up to 1.85 prior to the extinction event in the Casera Razzo Member and most of the Ostracod Unit (Fig. 3.5). In the uppermost Ostracod Unit, the Bulla Member and the lowermost Mazzin Member, a low TAR (0.46–0.85) is recorded. For Seres, TAR reaches values as low as 0.38 at the base of the section (−22.17 m) and has a maximum value of only 0.72 (−4.30 m). Generally, the content of pristane exceeds that of phytane with Pr/Ph > 1 in both sections, except for two intervals in the Siusi/Seis section, between −13.77 m and −12.19 m, and just below the Bellerophon/Werfen formation boundary. The Pr/Ph ratio correlates with TOC neither in Siusi/Seis (r = −0.21, p = 0.43) nor in Seres (r = −0.30, p = 0.40).

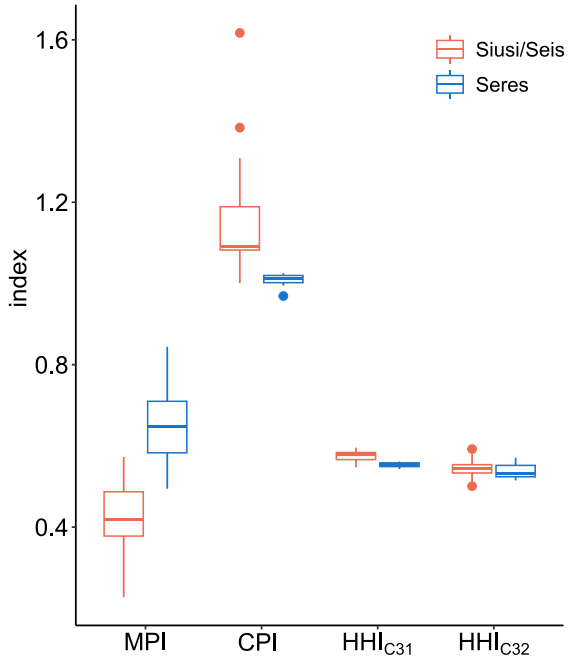

Figure 3.3: *Maturity indices methylphenanthrene index (MPI), carbon preference index (CPI), and homohopane isomerization index (HHI) for the C_{31}- and C_{32}-homohopanes in the Siusi/Seis and Seres section.*

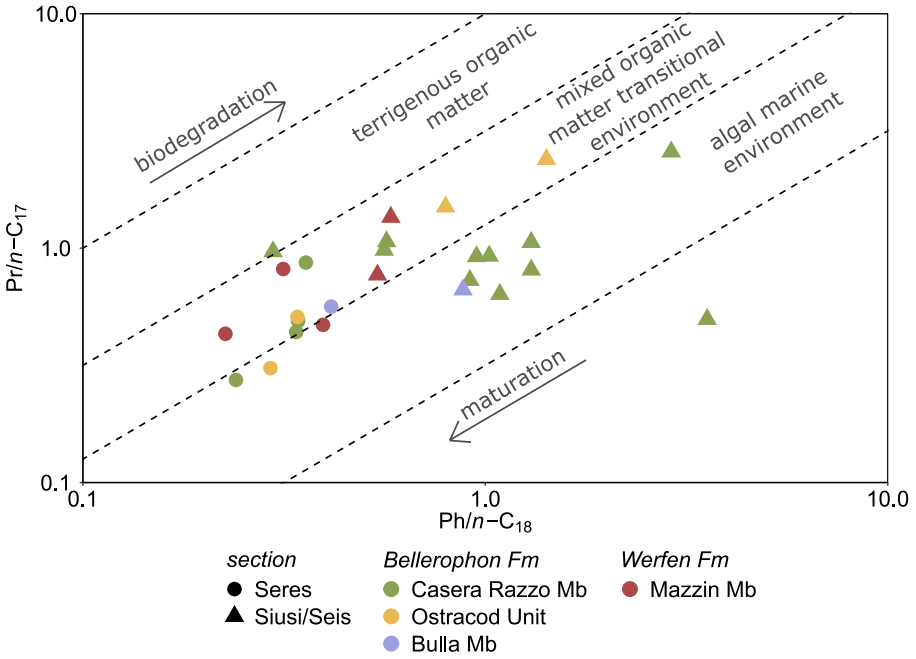

Figure 3.4: *Pristane (Pr)/n-C_{17} vs. phytane (Ph)/n-C_{18} crossplot after (Shanmugam, 1985). Sections are characterized by symbol shape, members of the Bellerophon (pre-extinction) and Werfen Formation (post-extinction) are color coded.*

For Siusi/Seis, (Pr + Ph)/(*n*-C_{17} + *n*-C_{18}) is generally higher compared to Seres (Fig. 3.5), with two episodes between −13.59 m and −12.19 m in the Casera Razzo Member and −0.51 m and −0.39 m in the uppermost Ostracod Unit recording peak values of 2.65 and 1.81, respectively. A moderate positive correlation exists between (Pr + Ph)/(*n*-C_{17} + *n*-C_{18}) and TOC for Siusi/Seis ($r = 0.59$, $p = 0.02$). The 2α-methylhopane index (2-MHI) increases in a similar interval with up to 15.1%, and again shortly below the extinction in the Bulla Member with 14.0% (Fig. 3.5). Regular ααα-*R*-steranes are strongly dominated by the C_{29}-sterane (Fig. 3.5), with intervals where only C_{29}-sterane was detected (between −15.47 m and −14.20 m, and between −0.51 m and −0.39 m). Above the extinction interval, steranes are not detected. In the Seres section, (Pr + Ph)/(*n*-C_{17} + *n*-C_{18}) is less variable between 0.26 and 0.62 across the section, whereas no 2α-methylhopanes or steranes are detected. Also, (Pr + Ph)/(*n*-C_{17} + *n*-C_{18}) and TOC do not correlate in Seres ($r = -0.28$, $p = 0.43$).

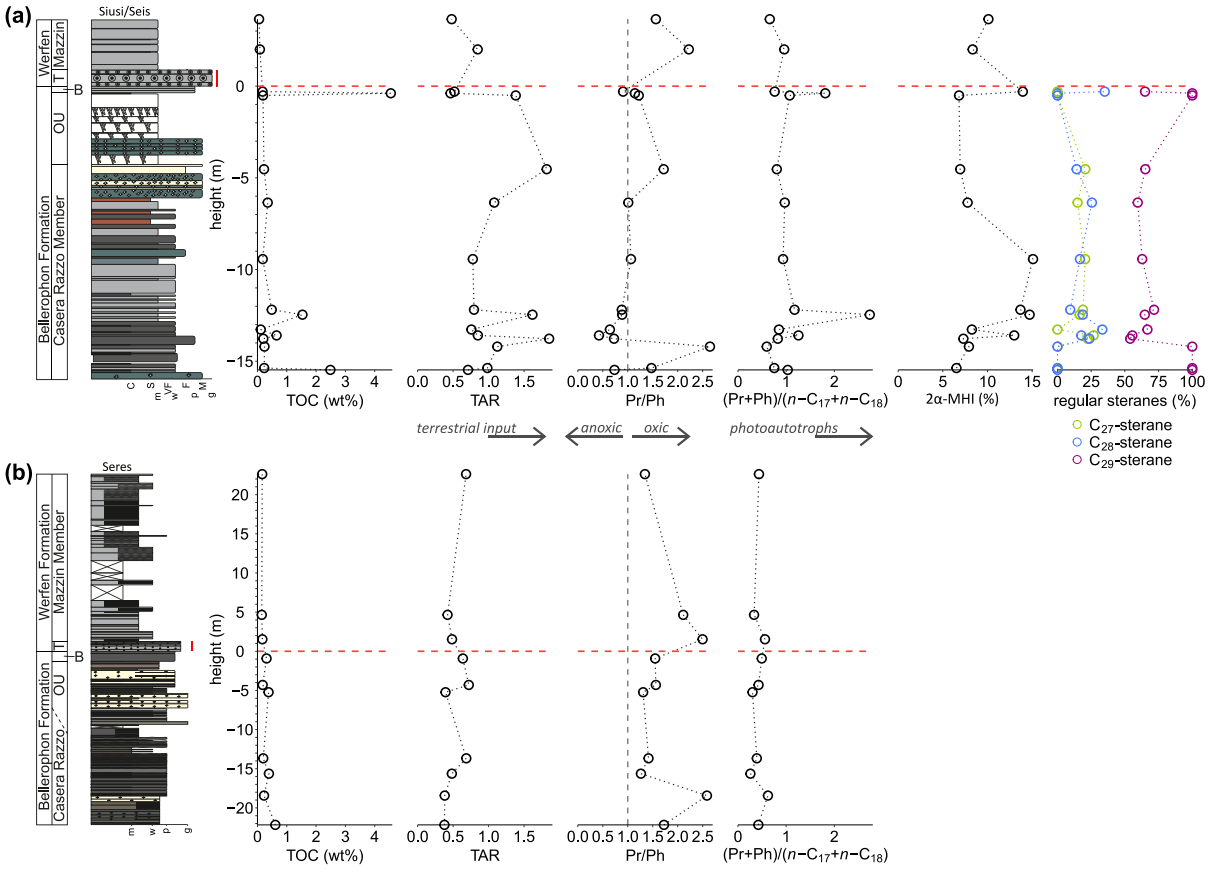

Figure 3.5: *Total organic carbon (TOC) and hydrocarbon molecular fossils from the shallower Siusi/Seis section (a) and the deeper Seres section (b) prior to and across the Permian–Triassic mass extinction event. The extinction interval is marked with a red line next to the stratigraphic column. OU = Ostracod Unit; B = Bulla Member; T = Tesero Member; C = claystone; S = siltstone; VF = very fine-grained sandstone; F = fine-grained sandstone; M = medium-grained sandstone; m = mudstone; w = wackestone; p = packstone; g = grainstone; TAR = terrigenous-aquatic ratio; Pr = pristane; Ph = phytane; (Pr + Ph)/(n-C_{17} + n-C_{18}) as a proxy for photoautotrophs; 2α-MHI: 2α-methylhopane index; C_{27}-sterane = 5α(H),14α(H),17α(H)-22R-cholestane; C_{28}-sterane = 5α(H),14α(H),17α(H)-22R-24-methylcholestane (ergosterane); C_{29}-sterane = 5α(H),14α(H),17α(H)-22R-24-ethylcholestane (stigmastane).*

In addition to saturated hydrocarbons, polycyclic aromatic hydrocarbons (PAHs) are present (Fig. 3.6). The two PAHs coronene and pyrene reveal a similar trend across the Permian–Triassic transition depending on the location. For Siusi/Seis, relative abundances of coronene and pyrene increase across the extinction. For Seres, the relative abundance of these compounds is low below the extinction level, increases abruptly in the first post-extinction sample, and subsequently returns to pre-extinction levels. Furthermore, we detect trace amounts of perylene in the Siusi/Seis section (Fig. 3.6), whereas perylene remains below detection limit in Seres.

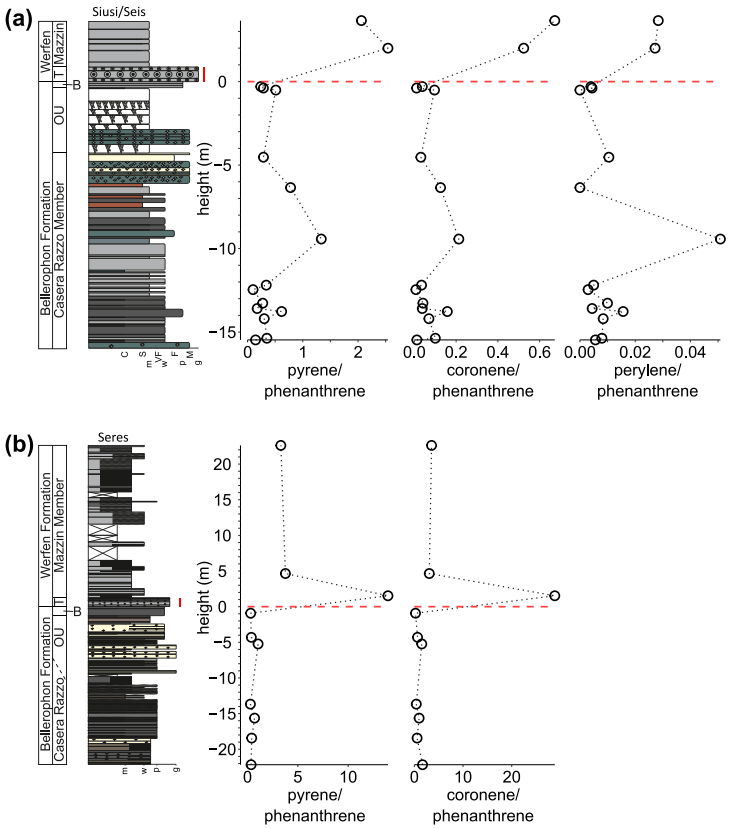

Figure 3.6: *Polycyclic aromatic hydrocarbons (PAHs) at the shallower Siusi/Seis section (a) and the deeper Seres section (b) prior to and across the Permian–Triassic mass extinction event. The extinction interval is marked with a red line next to the stratigraphic column. OU = Ostracod Unit; B = Bulla Member; T = Tesero Member; C = claystone; S = siltstone; VF = very fine-grained sandstone; F = fine-grained sandstone; M = medium-grained sandstone; m = mudstone; w = wackestone; p = packstone; g = grainstone.*

The biomarker composition of the Siusi/Seis and Seres samples is well represented in two dimensions in a NMDS plot, indicated by a good stress value of 0.08 (Fig. 3.7). Samples from Siusi/Seis and Seres are separated by the diagonal, with samples from Siusi/Seis being associated with enhanced input from photoautotrophs and higher TAR, whereas samples from Seres are associated with enhanced Pr/Ph and MPI. Pre-extinction samples in the Bellerophon Formation are separated from post-extinction samples in the Werfen Formation by the first MDS axis, and are mainly associated with high coronene and pyrene contents.

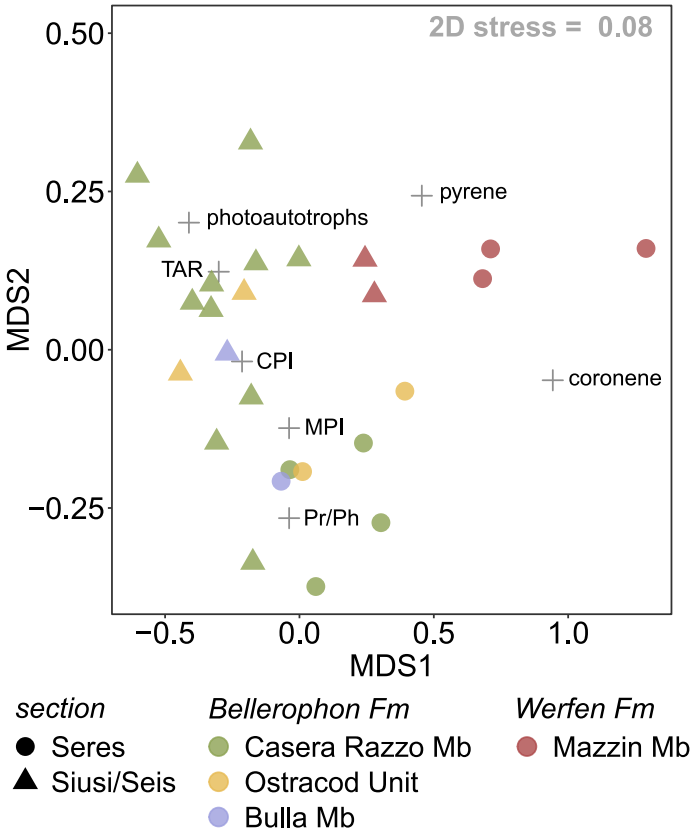

Figure 3.7: *Non-metric multidimensional scaling (NMDS). Molecular fossils and resulting indices found across the Permian–Triassic transition at the locations Siusi/Seis and Seres were used as input variables marked with crosses in the NMDS plot. Pr/Ph = pristane/phytane; TAR = terrigenous-aquatic ratio; CPI = carbon preference index; MPI = methylphenanthrene index; photoautotrophs = (Pr +Ph)/(n-C_{17} + n-C_{18}); coronene = coronene/phenanthrene; pyrene = pyrene/phenanthrene. Samples are color coded based on the member of the Bellerophon (pre-extinction) and Werfen Formation (post-extinction); symbol shape refers to the section.*

4 Discussion

4.1 Maturity parameters

The preservation of molecular fossils strongly depends on the maturity of the rocks from which organic matter is extracted. In both locations, Siusi/Seis and Seres, the extracted organic matter is thermally mature (Fig. 3.3). However, while the HHI records a high rate of isomerization from the biological 22*R* epimer to the 22*S* configuration within the homohopane series (Peters et al., 1996), it does not show an overmature signature, which would be reflected in HHI = 0.6 at which 22*S*- and 22*R*- stereoisomers are at equilibrium (Mackenzie et al., 1984). Also, organic matter from Siusi/Seis seems to be generally slightly less mature with lower mean MPI, and a CPI indicating a preference of long-chain odd over even carbon-numbered *n*-alkanes, which can only be preserved in lower-maturity rocks and when organic matter input by terrestrial plant was high (Eglington & Hamilton, 1967). In contrast, the CPI records values close to 1 in the Seres section, which is indicative of either a predominance of marine organic matter input or relatively high thermal maturity. Combined with the MPI and the HHI, the latter is suggested. Furthermore, hopanes and steranes constitute common molecular fossils in hydrocarbon extracts (e.g., Cao et al., 2009; Hays et al., 2007; Zumberge et al., 2018). Because these compounds are usually more resistant to biodegradation than *n*-alkanes and isoprenoids (Wenger et al., 2002), their absence in Seres is possibly caused by the increased thermal maturity, which agrees with the Pr/*n*-C_{17}-Ph/*n*-C_{18} crossplot (Fig. 3.4). These maturity estimates are consistent with Rock Eval and vitrinite reflectance data from the Permian Val Gardena Sandstone to the Middle Triassic Wengen Formation in the Dolomites, that indicate burial temperatures in the early to peak oil generation window (Grobe et al., 2015).

4.2 Source of molecular fossils

The molecular fossil content of the studies sections has been affected by alteration caused by the locally relatively high maturity, for instance through defunctionalization and isomerization. However, hydrocarbons, that represent the carbon skeleton of their precursor molecules (Luo et al., 2019; Summons et al., 2022), persisted. These hydrocarbons yield information about the

source of the organic matter. The Bellerophon Formation has been shown to record late Permian sea level fluctuations, previously recognized based on sedimentological data (Massari et al., 1994), and changes in the fossil assemblages (Prinoth & Posenato, 2023). The variability of the source of molecular fossils ranging from predominantly marine algal to terrigenous organic matter (Fig. 3.4) reflects these late Permian transgressive-regressive cycles. The organic matter source variability is especially high in Siusi/Seis in the shallower part of the carbonate platform compared to Seres (Fig. 3.1; Noé, 1987). The proximity to the shore is also reflected in the higher amplitude and episodically higher TAR in the Casera Razzo Member and the Ostracod Unit in Siusi/Seis, which records enhanced input of long-chain *n*-alkanes from terrestrial land plants. In contrast, the TAR is more stable and rather low, indicative of a primarily marine origin of *n*-alkanes (Bush & McInerney, 2013) in the deeper Seres section (Fig. 3.5). These observations are in accordance with reconstructions of episodically very restricted marine condition in both the Casera Razzo Member, with also terrestrial plant remains preserved during regressive phases (Fig. 3.1; Mette & Roozbahani, 2012), and the Ostracod Unit from Siusi/Seis and the nearby Bulla section, where the ostracod and foraminifera assemblage records a community adapted to a potentially brackish environment (Crasquin et al., 2008; Mette & Roozbahani, 2012). In contrast, the overlying Bulla Member deposited during a transgressive phase and more open marine conditions favored a more diverse heterotrophic fauna (Crasquin et al., 2008; Farabegoli et al., 2007).

4.3 The photosynthetic community

In the marine realm, global environmental stress during the late Permian is generally assumed to have caused a major restructuring of the phototrophic community from the predominance of eukaryotic algae to the proliferation prokaryotes such as green sulfur bacteria adapted to photic zone euxinia (e.g., Cao et al., 2009; Grice et al., 2005; Hays et al., 2007, 2012). However, whether this restructuring has led to an increase in primary productivity (e.g., Meyer et al., 2011; Schobben et al., 2020; Woods et al., 2023) or whether primary productivity collapsed (e.g., Grasby et al., 2016; Müller et al., 2022) is still debated and was likely heterogenous across paleolatitudes and oceans. Global meta-analyses suggest an overall increase in primary productivity across paleolatitudes, with the exception of South China, where a rapid post-extinction decline in

productivity is inferred (Algeo et al., 2013; Shen et al., 2015). These studies reveal geographic variability in primary productivity across the Permian–Triassic transition, but they especially focus on post-extinction successions: For example, in Algeo et al. (2013), northern Italy is represented by the shallow marine Bulla section with at maximum 6 m covered below the Bellerophon/Werfen Formation boundary, and the l'Uomo section, from which unpublished data without stratigraphic information was presented. Hence, an extended record of changes in the photoautotrophic community is necessary for evaluating regional patterns in the development of the inferred increase in post-extinction productivity in the western Tethys.

Molecular fossils that derive from the degradation of photopigments are among the most prominent biomarkers of phototrophic organisms (e.g., Brooks et al., 1969; Knoll et al., 2007). Pristane and phytane can derive from the degradation of the phytol side chain of chlorophyll (Didyk et al., 1978). Since no other major sources of pristane and phytane were recognized in the Siusi/Seis and Seres sections, such as degradation products of archaeal tetraether lipids (GDGTs) or archaeols (De Rosa et al., 1982), their abundance relative to the amount of their neighboring *n*-alkanes *n*-C_{17} and *n*-C_{18} indicates variations in the relative contribution from photoautotrophs to the molecular fossil inventory (Chen et al., 2011; Xiaoyan et al., 2008). Input from photoautotrophic organisms is generally enhanced in the Siusi/Seis section compared to Seres with two episodes of potentially increased productivity between −13.59 m and −12.19 m, and just below the onset of the extinction (Fig. 3.5). Also, TOC does not correlate with the redox proxy Pr/Ph, therefore enhanced preservation of organic matter is apparently not related to dysoxic or anoxic episodes, and rather point towards increased productivity, or at least increased export production, reflected also in the moderate correlation between TOC and (Pr + Ph)/(*n*-C_{17} + *n*-C_{18}). For the Seres section, where both variables stay rather low and constant across the investigated interval, no significant relationship between TOC and (Pr + Ph)/(*n*-C_{17} + *n*-C_{18}) is detected (Fig. 3.5).

Compositionally, C_{29}-steranes dominate over C_{27}- and C_{28}-steranes (Fig. 3.5). C_{29}-steranes can be produced by a variety of organisms, with terrestrial plants (Akinsanpe et al., 2024; Volkman, 1986) and marine green algae (Kodner et al., 2008; Volkman, 2003; Volkman et al., 1994) as

main sources. TAR and the relative contribution of C_{29}-steranes to the total pool of regular steranes do not correlate ($r = -0.26$, $p = 0.36$) in Siusi/Seis. We therefore assume green algae, which are common primary producers in Paleozoic marine ecosystems (Knoll et al., 2007), as the main contributors of C_{29}-steranes and the dominant photoautotrophic group throughout the investigated interval in the Bellerophon Formation. However, the loss of steranes in the strata above the extinction event in the Werfen Formation may constitute a preservation bias or a decline in eukaryotic biomass following the mass extinction as suggested by the biomarker inventory of the Meishan section in South China (Cao et al., 2009), and the widespread proliferation of microbial mats forming thick successions of microbialites across the Tethys in the Early Triassic (Foster et al., 2020; Kershaw et al., 2012).

4.4 The 2α-methylhopane index as an indicator for environmental stress

To further investigate the response of the microbial community, we analyzed the 2-MHI, with 2α-methylhopanes (Fig. 3.2) only identified in Siusi/Seis, where it is increased in several intervals including the uppermost Bellerophon Formation just prior to the extinction event, as well as further below in the section in the Casera Razzo Member (Fig. 3.5). First culture experiments have shown that high proportions of 2α-methylbacteriohopanepolyols can be extracted from cyanobacteria, and their defunctionalized derivatives, 2α-methylhopanes, were assumed to be indicative of cyanobacterial activity (Summons et al., 1999). Therefore, the 2-MHI has commonly been applied as a proxy for the relative contribution of cyanobacteria to the photoautotrophic community with elevated 2-MHI being associated with moderate $\delta^{15}N$ depletion (Cao et al., 2009; Kuypers et al., 2004), which, for example, can result from atmospheric N_2 fixation by cyanobacteria (e.g., Bauersachs et al., 2009; Minagawa & Wada, 1984). However, there is no consensus which values of the 2-MHI are considered as high, hence indicating a cyanobacterial bloom. For example, the 2-MHI has been used as a proxy for cyanobacterial blooms associated with the Permian–Triassic mass extinction at Meishan in South China with a 2-MHI up to 6.6% in beds 26 and 29 (Xie et al., 2005) and up to 32.54% in the Early Triassic (Cao et al., 2009), and at Bulla in northern Italy where it increases from 1.4% to 5.1% (Jia et al., 2012). In contrast, 2-MHI values between 1–11%

are also reported from the Permian–Triassic boundary in Kap Stosch, Greenland, where they are interpreted to be not especially high for Phanerozoic sedimentary rocks (Hays et al., 2012).

However, the concept of cyanobacteria as the sole source of 2α-methylbacteriohopanepolyols in the marine realm has been challenged by Talbot et al. (2008), because also alphaproteobacteria have been found to produce 2α-methylbacteriohopanepolyols (e.g., Eickhoff et al., 2013; Welander et al., 2010). Additionally, the gene regulating the expression of the methylase catalyzing the C_2 methylation of bacteriohopanepolyols has been identified in both cyanobacteria and alphaproteobacteria (Kulkarni et al., 2013; Ricci et al., 2015), as well as in one actionbacterium (Naafs et al., 2022; Sinninghe Damsté et al., 2017). Consequently, the widespread production of 2α-methylbacteriohopanepolyols challenges the applicability of the 2-MHI as a biomarker of cyanobacteria (Welander et al., 2010). Nonetheless, due to the scarcity of marine strains of cultured alphaproteobacteria, also the known number of marine alphaproteobacteria producing 2α-methylbacteriohopanepolyols is limited (Naafs et al., 2022).

Regardless of the producer of 2α-methylbacteriohopanepolyols, many studies suggest that an increase in C_2 methylated bacteriohopanepolyols is indicative of a stress response of bacteria exposed to changing environmental conditions (Saito et al., 2016), including high temperature, osmotic and pH stress (Garby et al., 2017; Kulkarni et al., 2013), low oxygen and nitrogen availability (Ricci et al., 2014), anoxic ferrous conditions (Eickhoff et al., 2013), or N cycle perturbations (Naafs et al., 2022). Several mechanisms have been suggested to improve stress resistance, such as increased 2α-methylbacteriohopanepolyol production in resting cells (Doughty et al., 2009) or to enhance cell membrane rigidity (Wu et al., 2015). Following this argument, our new record of high 2-MHI from the late Permian equatorial Tethys suggests that the microbial community did respond to environmental stress preceding the actual mass extinction. Possible stressors include enhanced global temperature (Gliwa et al., 2022; Sun et al., 2018), increased terrestrial influx as reflected in episodically enhanced TAR (Fig. 3.5) due to sea level fluctuations (Massari et al., 1994), that might also have led to salinity fluctuations (Mette & Roozbahani, 2012), and variable oxygen availability as shown by Pr/Ph fluctuations already in the Casera Razzo Member (Fig. 3.5). Yet, which stressor or which combination of stressors in particular was

responsible for the enhanced production of the precursor molecule of 2α-methylhopanes remains undetermined.

4.5 Polycyclic aromatic hydrocarbons

Polycyclic aromatic hydrocarbons (PAHs) and their methylated derivatives are very common free aromatic compounds in modern and ancient environments (e.g., Arinobu et al., 1999; Baumard et al., 1998; Boitsov et al., 2009; Cheng et al., 2018). Several PAHs have been associated with incomplete combustion of organic matter, such as pyrene and coronene (Fig. 3.2), which show increased contents following the extinction event at both the Siusi/Seis and Seres section (Fig. 3.6). Previous studies have suggested a link between increased PAH abundance and the combustion of terrestrial plant material during wildfires (e.g., Jiao et al., 2024; Luo et al., 2019; Nabbefeld et al., 2010; Song et al., 2022), hence inferring an increased wildfire activity associated with the Permian–Triassic mass extinction, which may have contributed to soil destabilization and terrestrial ecosystem collapse (Algeo & Twitchett, 2010; Benton & Newell, 2014; Lu et al., 2022; Saito et al., 2023). Others have argued that the combustion temperature during wildfires is usually not high enough to produce large PAHs such as coronene (Kaiho et al., 2021a, b; Norinaga et al., 2009). It was therefore suggested that high abundances of coronene derive from the combustion of organic-rich sedimentary rocks during phases of intense Siberian Traps volcanism (Kaiho, 2025; Kaiho et al., 2021a, b). Coronene and other PAHs were subsequently distributed in the form of fly ashes (Grasby et al., 2011), with modelling of volcanic ash cloud formation suggesting that ashes can disperse over thousands of kilometers or even globally during large-scale eruptions (Baines et al., 2008). Hence, the increase of these combustion-derived biomarkers in northern Italy reflects deteriorating environmental conditions due to intense volcanism, which directly caused environmental perturbations by the ejection of massive amounts of carbon dioxide and other greenhouse gases into the atmosphere (Svensen et al., 2009), and the introduction of potentially toxic heavy metals to marine and terrestrial ecosystems (Galasso et al., 2025; Grasby et al., 2017). In contrast to the evidence deriving from the molecular fossils discussed above, the increase in PAHs is independent from the late Permian sea level fluctuations and reflects environmental stress associated with the mass extinction event itself. Furthermore, the high

abundances of pyrene and coronene are also the key variables causing the separation of the pre- and post-extinction cluster in the MNDS analysis (Fig. 3.7), emphasizing the significance of these compounds in the overall inventory of the post-extinction molecular fossils.

Another PAH irregularly noted increasing in abundance across the Permian–Triassic mass extinction is perylene (Fig. 3.2). This compound has been found to increase in the Bulla Member at the Bulla section (Jia et al., 2012) as well as at the onset of the extinction event at Meishan, South China (Nabbefeld et al., 2010). In contrast, perylene is absent in higher-latitude settings such as Kap Stosch, Greenland (Nabbefeld et al., 2010), or Western Australia (Grice et al., 2007). We only detected trace amounts of perylene in Siusi/Seis (Fig. 3.6); however, also the relative abundance reported by Jia et al. (2012) from the nearby Bulla section is very low. Perylene has been attributed to wood-degrading fungi, hypothesized to have flourished in a stressed and vulnerable terrestrial ecosystem (Grice et al., 2009; Marynowski et al., 2013). We, therefore, do not find supporting evidence for such a “fungi event” in the sedimentary record across the carbonate ramp of northern Italy, suggesting enhanced perylene deposition was rather a local phenomenon in more proximal settings.

Conclusion

We present a molecular fossil dataset from the Permian–Triassic transition in the western equatorial Tethys Ocean across a shallow marine carbonate ramp in northern Italy. The analysis yields new insights into spatial heterogeneity of environmental stress and the response of the microbial community. Both study sites, Siusi/Seis and Seres, record an increase in molecular fossils derived from the high-temperature combustion of organic material above the main level of extinction, probably derived from the combustion of organic-rich sedimentary rocks, related to Siberian Traps sill emplacement. However, several molecular signatures differ between the studied sections, reflecting different environmental conditions, microbial community responses, and organic matter preservation histories along the carbonate ramp.

Some of the differences in the molecular fossil inventory are attributed to different thermal maturities, with a less diverse molecular fossil inventory in the more thermally mature Seres

section, where compounds such as steranes and methylhopanes were not detected. However, several molecular fossils were detected at both sites and across the sections, revealing an episodically stressed ecosystem in the shallower Siusi/Seis section, with greater variability in redox conditions, terrestrial organic matter input, and the microbial community structure in the late Permian. In contrast, the deeper Seres section is characterized by more stable conditions. Hence, it is suggested that environmental stress was primarily linked to sea level fluctuations in the late Permian, which had a stronger effect on the inner shelf that became episodically restricted or even subaerially exposed. We therefore find no evidence for a stress response to globally deteriorating environmental conditions preceding the mass extinction at these sites, but a response to the local conditions. These findings emphasize the importance of a careful evaluation of regional environmental variables for accurately interpreting biological responses to global events.

Data availability

All data and code used in this study are available at in the Zenodo repository (Buchwald et al., 2025: https://doi.org/10.5281/zenodo.17139994).

Author's contributions

SZB and WJF conceptualized the study; SZB curated the data and performed the formal analysis; WJF acquired funding; SZB, EK, HP, FG, BK, ABF, MAGC and WJF were involved in planning and conducting fieldwork; JP, DB and WJF provided resources; NL provided TOC data; SZB wrote and visualized the original draft; all co-authors were involved in reviewing and editing.

Competing Interests

The authors declare that they have no conflict of interest.

Acknowledgments

We thank Sabine Beckmann for her support in the lab and the Outcrop3D team from Deep-time Digital Earth for the digitalization of the sections. This project was funded by the Deutsche Forschungsgemeinschaft (project no.: FO1297/1).

References

Akinsanpe, T. O., Bowden, S. A., & Parnell, J. (2024). Molecular and mineral biomarker record of terrestrialization in the Rhynie Chert. *Palaeogeography, Palaeoclimatology, Palaeoecology*, *640*, 112101. https://doi.org/10.1016/j.palaeo.2024.112101

Algeo, T. J., & Twitchett, R. J. (2010). Anomalous Early Triassic sediment fluxes due to elevated weathering rates and their biological consequences. *Geology*, *38*(11), 1023–1026. https://doi.org/10.1130/G31203.1

Algeo, T. J., Henderson, C. M., Tong, J., Feng, Q., Yin, H., & Tyson, R. V. (2013). Plankton and productivity during the Permian-Triassic boundary crisis: An analysis of organic carbon fluxes. *Global and Planetary Change*, *105*, 52–67. https://doi.org/10.1016/j.gloplacha.2012.02.008

Altıner, D., Özkan-Altiner, S., & Koçyiğit, A. (2000). Late Permian foraminiferal biofacies belts in Turkey: Palaeogeographic and tectonic implications. *Geological Society Special Publication*, *173*, 83–96. https://doi.org/10.1144/GSL.SP.2000.173.01.04

Arinobu, T., Ishiwatari, R., Kaiho, K., & Lamolda, M. A. (1999). Spike of pyrosynthetic polycyclic aromatic hydrocarbons associated with an abrupt decrease in $\delta^{13}C$ of a terrestrial biomarker at the Cretaceous-Tertiary boundary at Caravaca, Spain. *Geology*, *27*(8), 723–726. https://doi.org/10.1130/0091-7613(1999)027<0723:SOPPAH>2.3.CO;2

Baines, P. G., Jones, M. T., & Sparks, R. S. J. (2008). The variation of large-magnitude volcanic ash cloud formation with source latitude. *Journal of Geophysical Research: Atmospheres, 113*, D21204. https://doi.org/10.1029/2007JD009568

Bauersachs, T., Schouten, S., Compaore, J., Wollenzien, U., Stal, L. J., & Sinninghe Damsté, J. S. (2009). Nitrogen isotopic fractionation associated with growth on dinitrogen gas and nitrate by cyanobacteria. *Limnology and Oceanography*, *54*(4), 1403–1411. https://doi.org/10.4319/lo.2009.54.4.1403

Baumard, P., Budzinski, H., Michon, Q., Garrigues, P., Burgeot, T., & Bellocq, J. (1998). Origin and bioavailability of PAHs in the Mediterranean Sea from mussel and sediment records. *Estuarine, Coastal and Shelf Science*, *47*(1), 77–90. https://doi.org/10.1006/ecss.1998.0337

Benton, M. J., & Newell, A. J. (2014). Impacts of global warming on Permo-Triassic terrestrial ecosystems. *Gondwana Research*, *25*(4), 1308–1337. https://doi.org/10.1016/j.gr.2012.12.010

Birgel, D., & Peckmann, J. (2008). Aerobic methanotrophy at ancient marine methane seeps: A synthesis. *Organic Geochemistry*, *39*(12), 1659–1667. https://doi.org/10.1016/j.orggeochem.2008.01.023

Blakey, R. (2012). Global paleogeography. Retrieved from http://www2.nau.edu/rcb7/globaltext2.html [accessed July 2014]

Boitsov, S., Jensen, H. K. B., & Klungsøyr, J. (2009). Natural background and anthropogenic inputs of polycyclic aromatic hydrocarbons (PAH) in sediments of South-Western Barents Sea. *Marine Environmental Research*, *68*(5), 236–245. https://doi.org/10.1016/j.marenvres.2009.06.013

Brandner, R., Horacek, M., Keim, L., & Scholger, R. (2009). The Pufels/Bulla road section: Deciphering environmental changes across the Permian-Triassic boundary to the Olenekian by integrated litho-, magneto-and isotope stratigraphy. A field trip guide. *Geo.Alp*, *6*, 116–132.

Brennecka, G. A., Herrmann, A. D., Algeo, T. J., & Anbar, A. D. (2011). Rapid expansion of oceanic anoxia immediately before the end-Permian mass extinction. *Proceedings of the National Academy of Sciences*, *43*(108), 17631–17634. https://doi.org/10.1073/pnas.1106039108

Broglio Loriga, C., Neri, C., Pasini, M., & Posenato, R. (1988). Marine fossil assemblages from upper Permian to lowermost Triassic in the western Dolomites (Italy). *Memoire Della Societa Geologica Italiana*, *34*, 5–44.

Broglio Loriga, C., Góczán, F., Haas, J., Lenner, K., Neri, C., Oravecz Scheffer, A., et al. (1990). The Lower Triassic sequences of the Dolomites (Italy) and Transdanubian Mid-Mountains (Hungary) and their correlation. *Memorie Di Scienze Geologiche*, *11*(2), 41–103.

Brooks, J. D., Gould, K., & Smith, J. W. (1969). Isoprenoid hydrocarbons in coal and petroleum. *Nature*, *222*(5190), 257–259. https://doi.org/10.1038/222257a0

Buchwald, S. Z., Birgel, D., Kustatscher, E., Prinoth, H., Galasso, F., Karapunar, B., et al. (2025). Molecular fossils record shallow marine ecosystem changes prior to and across the Permian–Triassic mass extinction in the Dolomites (Italy). StellaZBuchwald/Permian-Triassic_Dolomites_Biomarker: version1.0.0, published Sep 17, 2025 [Dataset, Computational Notebook], Zenodo, https://doi.org/10.5281/zenodo.17139994

Burgess, S. D., Bowring, S., & Shen, S. Z. (2014). High-precision timeline for Earth's most severe extinction. *Proceedings of the National Academy of Sciences*, *111*(9), 3316–3321. https://doi.org/10.1073/pnas.1317692111

Burgess, S. D., & Bowring, S. A. (2015). High-precision geochronology confirms voluminous magmatism before, during, and after Earth's most severe extinction. *Science Advances*, *1*(7), e1500470. https://doi.org/10.1126/sciadv.1500470

Burgess, S. D., Muirhead, J. D., & Bowring, S. A. (2017). Initial pulse of Siberian Traps sills as the trigger of the end-Permian mass extinction. *Nature Communications*, *8*(1), 164. https://doi.org/10.1038/s41467-017-00083-9

Bush, R. T., & McInerney, F. A. (2013). Leaf wax *n*-alkane distributions in and across modern plants: Implications for paleoecology and chemotaxonomy. *Geochimica et Cosmochimica Acta*, *117*, 161–179. https://doi.org/10.1016/j.gca.2013.04.016

Cao, C., Love, G. D., Hays, L. E., Wang, W., Shen, S., & Summons, R. E. (2009). Biogeochemical evidence for euxinic oceans and ecological disturbance presaging the end-Permian mass extinction event. *Earth and Planetary Science Letters*, *281*(3–4), 188–201. https://doi.org/10.1016/j.epsl.2009.02.012

Cassani, F., Gallango, O., Talukdar, S., Vallejos, C., & Ehrmann, U. (1988). Methylphenanthrene maturity index of marine source rock extracts and crude oils from the Maracaibo Basin. *Organic Geochemistry*, *13*(3), 73–80. https://doi.org/10.1016/B978-0-08-037236-5.50013-0

Chen, L., Wang, Y., Xie, S., Kershaw, S., Dong, M., Yang, H., et al. (2011). Molecular records of microbialites following the end-Permian mass extinction in Chongyang, Hubei Province, South China. *Palaeogeography, Palaeoclimatology, Palaeoecology*, *308*(1–2), 151–159. https://doi.org/10.1016/j.palaeo.2010.09.010

Cheng, B., Chen, Z., Chen, T., Yang, C., & Wang, T. G. (2018). Biomarker signatures of the Ediacaran–early Cambrian origin petroleum from the central Sichuan Basin, South China: Implications for source rock characteristics. *Marine and Petroleum Geology*, *96*, 577–590. https://doi.org/10.1016/j.marpetgeo.2018.05.012

Clarkson, M. O., Kasemann, S. A., Wood, R. A., Lenton, T. M., Daines, S. J., Richoz, S., et al. (2015). Ocean acidification and the Permo-Triassic mass extinction. *Science*, *348*(6231), 229–232. https://doi.org/10.1126/science.aaa0193

Coates, R. C., Podell, S., Korobeynikov, A., Lapidus, A., Pevzner, P., Sherman, D. H., et al. (2014). Characterization of cyanobacterial hydrocarbon composition and distribution of biosynthetic pathways. *PLoS ONE*, *9*(1), e85140. https://doi.org/10.1371/journal.pone.0085140

Crasquin, S., Perri, M. C., Nicora, A., & De Wever, P. (2008). Ostracods across the Permian-Triassic boundary in Western Tethys: The Bulla parastratotype (Southern Alps, Italy). *Rivista Italiana Di Paleontologia e Stratigrafia*, *114*(2), 233–262.

Dercourt, J., Gaetani, M., & Vrielynck, B. (Eds.). (2000). *Atlas Peri-Tethys palaeogeographical maps.* CCGM.

De Rosa, M., Gambacorta, A., Nicolaus, B., Ross, H. N., Grant, W. D., & Bu'Lock, J. D. (1982). An asymmetric archaebacterial diether lipid from alkaliphilic halophiles. *Journal of General Microbiology*, *128*(2), 343–348. https://doi.org/10.1099/00221287-128-2-343

Didyk, B. M., Simoneit, B. R. T., Brassell, S. C., & Eglinton, G. (1978). Organic geochemical indicators of palaeoenvironmental conditions of sedimentation. *Nature*, *272*(5650), 216–222. https://doi.org/10.1038/272216a0

Doughty, D. M., Hunter, R. C., Summons, R. E., & Newman, D. K. (2009). 2-Methylhopanoids are maximally produced in akinetes of *Nostoc punctiforme*: Geobiological implications. *Geobiology*, *7*(5), 524–532. https://doi.org/10.1111/j.1472-4669.2009.00217.x

Eglington, G., & Hamilton, R. J. (1967). Leaf epicuticular waxes. *Science*, *3780*(156), 1322–1335. https://doi.org/10.1126/science.156.3780.1322

Eickhoff, M., Birgel, D., Talbot, H. M., Peckmann, J., & Kappler, A. (2013). Oxidation of Fe(II) leads to increased C-2 methylation of pentacyclic triterpenoids in the anoxygenic phototrophic bacterium *Rhodopseudomonas palustris* strain TIE-1. *Geobiology*, *11*(3), 268–278. https://doi.org/10.1111/gbi.12033

Farabegoli, E., Perri, M. C., & Posenato, R. (2007). Environmental and biotic changes across the Permian-Triassic boundary in western Tethys: The Bulla parastratotype, Italy. *Global and Planetary Change*, *55*(1–3), 109–135. https://doi.org/10.1016/j.gloplacha.2006.06.009

Fielding, C. R., Frank, T. D., McLoughlin, S., Vajda, V., Mays, C., Tevyaw, A. P., et al. (2019). Age and pattern of the southern high-latitude continental end-Permian extinction constrained by multiproxy analysis. *Nature Communications*, *10*(1), 385. https://doi.org/10.1038/s41467-018-07934-z

Foster, W. J., Heindel, K., Richoz, S., Gliwa, J., Lehrmann, D. J., Baud, A., et al. (2020). Suppressed competitive exclusion enabled the proliferation of Permian/Triassic boundary microbialites. *Depositional Record*, *6*(1), 62–74. https://doi.org/10.1002/dep2.97

Galasso, F., Frank, A. B., & Foster, W. J. (2025). Heavy metal toxicity: A major driver of past biodiversity crises? *Preprint at EarthArXiv*. https://doi.org/10.31223/X5SX5R

Garby, T. J., Matys, E. D., Ongley, S. E., & Salih, A. (2017). Lack of methylated hopanoids renders the cyanobacterium *Nostoc punctiforme* sensitive to osmotic and pH stress. *Applied and Environmental Microbiology*, *83*(13), e00777-17. https://doi.org/10.1128/AEM.00777-17

Gliwa, J., Wiedenbeck, M., Schobben, M., Ullmann, C. V., Kiessling, W., Ghaderi, A., et al. (2022). Gradual warming prior to the end-Permian mass extinction. *Palaeontology*, *65*(5), e12621. https://doi.org/10.1111/pala.12621

Grasby, S. E., Sanei, H., & Beauchamp, B. (2011). Catastrophic dispersion of coal fly ash into oceans during the latest Permian extinction. *Nature Geoscience*, *4*(2), 104–107. https://doi.org/10.1038/ngeo1069

Grasby, S. E., Beauchamp, B., & Knies, J. (2016). Early Triassic productivity crises delayed recovery from world's worst mass extinction. *Geology*, *44*(9), 779–782. https://doi.org/10.1130/G38141.1

Grasby, S. E., Shen, W., Yin, R., Gleason, J. D., Blum, J. D., Lepak, R. F., et al. (2017). Isotopic signatures of mercury contamination in latest Permian oceans. *Geology*, *45*(1), 55–58. https://doi.org/10.1130/G38487.1

Grice, K., Cao, C., Love, G. D., Böttcher, M. E., Twitchett, R. J., Grosjean, E., et al. (2005). Photic zone euxinia during the Permian-Triassic superanoxic event. *Science*, *307*(5710), 706–709. https://doi.org/10.1126/science.1104323

Grice, K., Nabbefeld, B., & Maslen, E. (2007). Source and significance of selected polycyclic aromatic hydrocarbons in sediments (Hovea-3 well, Perth Basin, Western Australia) spanning the Permian-Triassic boundary. *Organic Geochemistry*, *38*(11), 1795–1803. https://doi.org/10.1016/j.orggeochem.2007.07.001

Grice, K., Lu, H., Atahan, P., Asif, M., Hallmann, C., Greenwood, P., Maslen, E., et al. (2009). New insights into the origin of perylene in geological samples. *Geochimica et Cosmochimica Acta*, *73*(21), 6531–6543. https://doi.org/10.1016/j.gca.2009.07.029

Grobe, A., Littke, R., Sachse, V., & Leythaeuser, D. (2015). Burial history and thermal maturity of Mesozoic rocks of the Dolomites, northern Italy. *Swiss Journal of Geosciences, 108*(2), 253–271. https://doi.org/10.1007/s00015-015-0191-2

Groves, J. R., Rettori, R., Payne, J. L., Boyce, M. D., & Altıner, D. (2007). End-Permian mass extinction of lagenide foraminifers in the Southern Alps (northern Italy). *Journal of Paleontology*, *81*(3), 415–434. https://doi.org/10.1666/05123.1

Guo, W., Tong, J., He, Q., Hounslow, M. W., Song, H., Dal Corso, J., et al. (2022). Late Permian–Middle Triassic magnetostratigraphy in North China and its implications for terrestrial-marine correlations. *Earth and Planetary Science Letters*, *585*, 117519. https://doi.org/10.1016/j.epsl.2022.117519

Haas, J., Demény, A., Hips, K., Zajzon, N., Weiszburg, T. G., Sudar, M., & Pálfy, J. (2007). Biotic and environmental changes in the Permian-Triassic boundary interval recorded on a western Tethyan ramp in the Bükk Mountains, Hungary. *Global and Planetary Change*, *55*(1–3), 136–154. https://doi.org/10.1016/j.gloplacha.2006.06.010

Hays, L. E., Beatty, T., Henderson, C. M., Love, G. D., & Summons, R. E. (2007). Evidence for photic zone euxinia through the end-Permian mass extinction in the Panthalassic Ocean (Peace River Basin, Western Canada). *Palaeoworld*, *16*(1–3), 39–50. https://doi.org/10.1016/j.palwor.2007.05.008

Hays, L. E., Grice, K., Foster, C. B., & Summons, R. E. (2012). Biomarker and isotopic trends in a Permian-Triassic sedimentary section at Kap Stosch, Greenland. *Organic Geochemistry*, *43*, 67–82. https://doi.org/10.1016/j.orggeochem.2011.10.010

Heindel, K., Foster, W. J., Richoz, S., Birgel, D., Roden, V. J., Baud, A., et al. (2018). The formation of microbial-metazoan bioherms and biostromes following the latest Permian mass extinction. *Gondwana Research*, *61*, 187–202. https://doi.org/10.1016/j.gr.2018.05.007

Hinojosa, J. L., Brown, S. T., Chen, J., DePaolo, D. J., Paytan, A., Shen, S. Z., & Payne, J. L. (2012). Evidence for end-Permian ocean acidification from calcium isotopes in biogenic apatite. *Geology*, *40*(8), 743–746. https://doi.org/10.1130/G33048.1

Hips, K. (1998). Lower Triassic storm-dominated ramp sequence in northern Hungary: An example of evolution from homoclinal through distally steepened ramp to Middle Triassic flat-topped platform. *Geological Society Special Publication*, *149*(2), 315–338. https://doi.org/10.1144/GSL.SP.1999.149.01.15

Horacek, M., Povoden, E., Richoz, S., & Brandner, R. (2010). High-resolution carbon isotope changes, litho- and magnetostratigraphy across Permian-Triassic boundary sections in the Dolomites, N-Italy. New constraints for global correlation. *Palaeogeography, Palaeoclimatology, Palaeoecology*, *290*(1–4), 58–64. https://doi.org/10.1016/j.palaeo.2010.01.007

Jia, C., Huang, J., Kershaw, S., Luo, G., Farabegoli, E., Perri, M. C., et al. (2012). Microbial response to limited nutrients in shallow water immediately after the end-Permian mass extinction. *Geobiology*, *10*(1), 60–71. https://doi.org/10.1111/j.1472-4669.2011.00310.x

Jiao, S., Zhang, H., Cai, Y., Jin, C., & Shen, S. (2024). Polycyclic aromatic hydrocarbons (PAHs) evidence for frequent combustion events on land during the Permian–Triassic transition in northwest China. *Palaeogeography, Palaeoclimatology, Palaeoecology*, *642*, 112152. https://doi.org/10.1016/j.palaeo.2024.112152

Joachimski, M. M., Lai, X., Shen, S., Jiang, H., Luo, G., Chen, B., et al. (2012). Climate warming in the latest Permian and the Permian-Triassic mass extinction. *Geology*, *40*(3), 195–198. https://doi.org/10.1130/G32707.1

Joachimski, M. M., Alekseev, A. S., Grigoryan, A., & Gatovsky, Y. A. (2020). Siberian Trap volcanism, global warming and the Permian-Triassic mass extinction: New insights from Armenian Permian-Triassic sections. *Bulletin of the Geological Society of America*, *132*(1–2), 427–443. https://doi.org/10.1130/B35108.1

Jurikova, H., Gutjahr, M., Wallmann, K., Flögel, S., Liebetrau, V., Posenato, R., et al. (2020). Permian–Triassic mass extinction pulses driven by major marine carbon cycle perturbations. *Nature Geoscience*, *13*(11), 745–750. https://doi.org/10.1038/s41561-020-00646-4

Kaiho, K., Aftabuzzaman, M., Jones, D. S., & Tian, L. (2021a). Pulsed volcanic combustion events coincident with the end-Permian terrestrial disturbance and the following global crisis. *Geology*, *49*(3), 289–293. https://doi.org/10.1130/G48022.1

Kaiho, K., Miura, M., Tezuka, M., Hayashi, N., Jones, D. S., Oikawa, K., et al. (2021b). Coronene, mercury, and biomarker data support a link between extinction magnitude and volcanic intensity in the Late Devonian. *Global and Planetary Change*, *199*, 103452. https://doi.org/10.1016/j.gloplacha.2021.103452

Kaiho, K. (2025). Mechanisms of global climate change during the five major mass extinctions. *Scientific Reports*, *15*(1), 16498. https://doi.org/10.1038/s41598-025-01203-y

Karapunar, B., Wang, X., Frank, A. B., Gürsoy, M., Buchwald, S. Z., Gómez Correa, M. A., et al. (2025). Environmental and ecological changes across the Permian–Triassic transition in Türkiye: Integrating virtual outcrop models and new fieldwork data. *Preprint at EarthArXiv*. https://doi.org/10.31223/X5KQ9B

Kershaw, S., Crasquin, S., Li, Y., Collin, P. Y., Forel, M. B., Mu, X., et al. (2012). Microbialites and global environmental change across the Permian-Triassic boundary: A synthesis. *Geobiology*, *10*(1), 25–47. https://doi.org/10.1111/j.1472-4669.2011.00302.x

Kiessling, W., Schobben, M., Ghaderi, A., Hairapetian, V., Leda, L., & Korn, D. (2018). Pre-mass extinction decline of latest Permian ammonoids. *Geology*, *46*(3), 283–286. https://doi.org/10.1130/G39866.1

Knoll, A. H., Summons, R. E., Waldbauer, J. R., & Zumberge, J. E. (2007). The geological succession of primary producers in the oceans. In P. G. Falkowsk & A. H. Knoll (Eds.), *Evolution of Primary Producers in the Sea* (pp. 133–163). Elsevier, Burlington, MA. https://doi.org/10.1016/B978-012370518-1/50009-6

Kodner, R. B., Pearson, A., Summons, R. E., & Knoll, A. H. (2008). Sterols in red and green algae: Quantification, phylogeny, and relevance for the interpretation of geologic steranes. *Geobiology*, *6*(4), 411–420. https://doi.org/10.1111/j.1472-4669.2008.00167.x

Korn, D., Ghaderi, A., Leda, L., Schobben, M., & Ashouri, A. R. (2016). The ammonoids from the late Permian *Paratirolites* Limestone of Julfa (East Azerbaijan, Iran). *Journal of Systematic Palaeontology*, *14*(10), 841–890. https://doi.org/10.1080/14772019.2015.1119211

Kulkarni, G., Wu, C. H., & Newmana, D. K. (2013). The general stress response factor EcfG regulates expression of the C-2 hopanoid methylase HpnP in *Rhodopseudomonas palustris* TIE-1. *Journal of Bacteriology*, *195*(11), 2490–2498. https://doi.org/10.1128/JB.00186-13

Kustatscher, E., van Konijnenburg-van Cittert, J. H. A., Looy, C. V., Labandeira, C. C., Butzmann, R., Fischer, T. C., et al. (2017). The Lopingian (late Permian) flora from the Bletterbach Gorge in the Dolomites, northern Italy: A review. *Geo.Alp*, *14*, 39–61.

Kuypers, M. M. M., van Breugel, Y., Schouten, S., Erba, E., & Sinninghe Damsté, J. S. (2004). N_2-fixing cyanobacteria supplied nutrient N for Cretaceous oceanic anoxic events. *Geology*, *32*(10), 853–856. https://doi.org/10.1130/G20458.1

Lu, J., Wang, Y., Yang, M., Zhang, P., Bond, D. P. G., Shao, L., & Hilton, J. (2022). Diachronous end-Permian terrestrial ecosystem collapse with its origin in wildfires. *Palaeogeography, Palaeoclimatology, Palaeoecology*, *594*, 110960. https://doi.org/10.1016/j.palaeo.2022.110960

Luo, G., Yang, H., Algeo, T. J., Hallmann, C., & Xie, S. (2019). Lipid biomarkers for the reconstruction of deep-time environmental conditions. *Earth-Science Reviews*, *189*, 99–124. https://doi.org/10.1016/j.earscirev.2018.03.005

Mackenzie, A. S., Beaumont, C., & McKenzie, D. P. (1984). Estimation of the kinetics of geochemical reactions with geophysical models of sedimentary basins and applications. *Organic Geochemistry*, *6*, 875–884. https://doi.org/10.1016/0146-6380(84)90110-4

Marynowski, L., Smolarek, J., Bechtel, A., Philippe, M., Kurkiewicz, S., & Simoneit, B. R. T. (2013). Perylene as an indicator of conifer fossil wood degradation by wood-degrading fungi. *Organic Geochemistry*, *59*, 143–151. https://doi.org/10.1016/j.orggeochem.2013.04.006

Marzi, R., Torkelson, B. E., & Olson, R. K. (1993). A revised carbon preference index. *Organic Geochemistry*, *20*(8), 1303–1306. https://doi.org/10.1016/0146-6380(93)90016-5

Massari, F., Neri, C., Pittau, P., Fontana, D., & Stefani, C. (1994). Sedimentology, palynostratigraphy and sequence stratigraphy of a continental to shallow-marine rift-related succession: Upper Permian of the eastern Southern Alps (Italy). *Memorie Di Scienze Geologiche*, *46*, 119–243.

Mette, W., & Roozbahani, P. (2012). Late Permian (Changsingian) ostracods of the Bellerophon Formation at Seis (Siusi) (Dolomites, Italy). *Journal of Micropalaeontology*, *31*(1), 73–87. https://doi.org/10.1144/0262-821x11-010

Meyer, K. M., Yu, M., Jost, A. B., Kelley, B. M., & Payne, J. L. (2011). $\delta^{13}C$ evidence that high primary productivity delayed recovery from end-Permian mass extinction. *Earth and Planetary Science Letters*, *302*(3–4), 378–384. https://doi.org/10.1016/j.epsl.2010.12.033

Minagawa, M., & Wada, E. (1984). Stepwise enrichment of ^{15}N along food chains: Further evidence and the relation between $\delta^{15}N$ and animal age. *Geochimica et Cosmochimica Acta*, *48*(5), 1135–1140. https://doi.org/10.1016/0016-7037(84)90204-7

Müller, J., Sun, Y., Yang, F., Fantasia, A., & Joachimski, M. (2022). Phosphorus cycle and primary productivity changes in the Tethys Ocean during the Permian-Triassic transition: Starving marine ecosystems. *Frontiers in Earth Science*, *10*, 832308. https://doi.org/10.3389/feart.2022.832308

Naafs, B. D. A., Bianchini, G., Monteiro, F. M., & Sánchez-Baracaldo, P. (2022). The occurrence of 2-methylhopanoids in modern bacteria and the geological record. *Geobiology*, *20*(1), 41–59. https://doi.org/10.1111/gbi.12465

Nabbefeld, B., Grice, K., Summons, R. E., Hays, L. E., & Cao, C. (2010). Significance of polycyclic aromatic hydrocarbons (PAHs) in Permian/Triassic boundary sections. *Applied Geochemistry*, *25*(9), 1374–1382. https://doi.org/10.1016/j.apgeochem.2010.06.008

Noé, S. (1987). Facies and paleogeography of the marine upper Permian and of the Permian-Triassic boundary in the Southern Alps (Bellerophon Formation, Tesero Horizon). *Facies*, *16*, 89–142. https://doi.org/10.1007/BF02536749

Norinaga, K., Deutschmann, O., Saegusa, N., & Hayashi, J. (2009). Analysis of pyrolysis products from light hydrocarbons and kinetic modeling for growth of polycyclic aromatic hydrocarbons with detailed chemistry. *Journal of Analytical and Applied Pyrolysis*, *86*(1), 148–160. https://doi.org/10.1016/j.jaap.2009.05.001

Payne, J. L., Turchyn, A. V, Paytan, A., Depaolo, D. J., Lehrmann, D. J., Yu, M., & Wei, J. (2010). Calcium isotope constraints on the end-Permian mass extinction. *Proceedings of the National Academy of Sciences*, *107*(19), 8543–8548. https://doi.org/10.1073/pnas.0914065107

Payne, J. L., & Clapham, M. E. (2012). End-Permian mass extinction in the oceans: An ancient analog for the twenty-first century? *Annual Review of Earth and Planetary Sciences*, *40*, 89–111. https://doi.org/10.1146/annurev-earth-042711-105329

Perri, C. M., & Farabegoli, E. (2003). Conodonts across the Permian-Triassic boundary in the Southern Alps. *Courier Forschungsinstitut Senckenberg*, *245*, 281–313.

Peters, K. E., Moldowan, M. J., Mccaffreyt, M. A., & Fago, F. J. (1996). Selective biodegradation of extended hopanes to 25-norhopanes in petroleum reservoirs. Insights from molecular mechanics. *Organic Geochemistry*, *24*(8–9), 765–783. https://doi.org/10.1016/S0146-6380(96)00086-1

Posenato, R. (2010). Marine biotic events in the Lopingian succession and latest Permian extinction in the Southern Alps (Italy). *Geological Journal*, *45*(2–3), 195–215. https://doi.org/10.1002/gj.1212

Prinoth, H., & Posenato, R. (2023). Bivalves from the Changhsingian (upper Permian) Bellerophon Formation of the Dolomites (Italy): Ancestors of Lower Triassic post-extinction benthic communities. *Papers in Palaeontology*, *9*(2), e1486. https://doi.org/10.1002/spp2.1486

Ricci, J. N., Coleman, M. L., Welander, P. V., Sessions, A. L., Summons, R. E., Spear, J. R., & Newman, D. K. (2014). Diverse capacity for 2-methylhopanoid production correlates with a specific ecological niche. *ISME Journal*, *8*(3), 675–684. https://doi.org/10.1038/ismej.2013.191

Ricci, J. N., Michel, A. J., & Newman, D. K. (2015). Phylogenetic analysis of HpnP reveals the origin of 2-methylhopanoid production in Alphaproteobacteria. *Geobiology*, *13*(3), 267–277. https://doi.org/10.1111/gbi.12129

Robertson, A. H. F., Parlak, O., & Ustaömer, T. (2012). Overview of the Palaeozoic-Neogene evolution of Neotethys in the Eastern Mediterranean region (Southern Turkey, Cyprus, Syria). *Petroleum Geoscience*, *18*(4), 381–404. https://doi.org/10.1144/petgeo2011-091

Saito, R., Kaiho, K., Oba, M., Tong, J., Chen, Z. Q., Takahashi, S., et al. (2016). Secular changes in environmental stresses and eukaryotes during the Early Triassic to the early Middle Triassic. *Palaeogeography, Palaeoclimatology, Palaeoecology*, *451*, 35–45. https://doi.org/10.1016/j.palaeo.2016.03.006

Saito, R., Wörmer, L., Taubner, H., Kaiho, K., Takahashi, S., Tian, L., et al. (2023). Centennial scale sequences of environmental deterioration preceded the end-Permian mass extinction. *Nature Communications*, *14*(1), 2113. https://doi.org/10.1038/s41467-023-37717-0

Schobben, M., Joachimski, M. M., Korn, D., Leda, L., & Korte, C. (2014). Palaeotethys seawater temperature rise and an intensified hydrological cycle following the end-Permian mass extinction. *Gondwana Research*, *26*(2), 675–683. https://doi.org/10.1016/j.gr.2013.07.019

Schobben, M., Foster, W. J., Sleveland, A. R. N., Zuchuat, V., Svensen, H. H., Planke, S., et al. (2020). A nutrient control on marine anoxia during the end-Permian mass extinction. *Nature Geoscience*, *13*(9), 640–646. https://doi.org/10.1038/s41561-020-0622-1

Sephton, M. A., Looy, C. V, Veefkind, R. J., Visscher, H., Brinkhuis, H., & De Leeuw, J. W. (1999). Cyclic diaryl ethers in a late Permian sediment. *Organic Geochemistry, 30*(4), 267–273. https://doi.org/10.1016/S0146-6380(99)00002-9

Sephton, M. A., Looy, C. V., Brinkhuis, H., Wignall, P. B., de Leeuw, J. W., & Visscher, H. (2005). Catastrophic soil erosion during the end-Permian biotic crisis. *Geology*, *33*(12), 941–944. https://doi.org/10.1130/G21784.1

Sephton, M. A., Jiao, D., Engel, M. H., Looy, C. V., & Visscher, H. (2015). Terrestrial acidification during the end-Permian biosphere crisis? *Geology*, *43*(2), 159–162. https://doi.org/10.1130/G36227.1

Shanmugam, G. (1985). Significance of coniferous rain forests and related organic matter in generating commercial quantities of oil, Gippsland Basin, Australia. *American Association of Petroleum*

Geologists Bulletin, *69*(8), 1241–1254. https://doi.org/10.1306/ad462bc3-16f7-11d7-8645000102c1865d

Shen, J., Schoepfer, S. D., Feng, Q., Zhou, L., Yu, J., Song, H., et al. (2015). Marine productivity changes during the end-Permian crisis and Early Triassic recovery. *Earth-Science Reviews*, *149*, 136–162. https://doi.org/10.1016/j.earscirev.2014.11.002

Shen, W., Sun, Y., Lin, Y., Liu, D., & Chai, P. (2011). Evidence for wildfire in the Meishan section and implications for Permian-Triassic events. *Geochimica et Cosmochimica Acta*, *75*(7), 1992–2006. https://doi.org/10.1016/j.gca.2011.01.027

Sinninghe Damsté, J. S., Rijpstra, W. I. C., Dedysh, S. N., Foesel, B. U., & Villanueva, L. (2017). Pheno- and genotyping of hopanoid production in Acidobacteria. *Frontiers in Microbiology*, *8*, 968. https://doi.org/10.3389/fmicb.2017.00968

Song, Y., Tian, Y., Yu, J., Algeo, T. J., Luo, G., Chu, D., & Xie, S. (2022). Wildfire response to rapid climate change during the Permian-Triassic biotic crisis. *Global and Planetary Change*, *215*, 103872. https://doi.org/10.1016/j.gloplacha.2022.103872

Stanley, S. M. (2016). Estimates of the magnitudes of major marine mass extinctions in earth history. *Proceedings of the National Academy of Sciences*, *113*(42), E6325–E6334. https://doi.org/10.1073/pnas.1613094113

Summons, R. E., Jahnke, L. L., Hope, J. M., & Logan, G. A. (1999). 2-Methylhopanoids as biomarkers for cyanobacterial oxygenic photosynthesis. *Nature*, *400*(5), 554–557. https://doi.org/10.1038/23005

Summons, R. E., Welander, P. V., & Gold, D. A. (2022). Lipid biomarkers: Molecular tools for illuminating the history of microbial life. *Nature Reviews Microbiology*, *20*(3), 174–185. https://doi.org/10.1038/s41579-021-00636-2

Sun, H., Xiao, Y., Gao, Y., Zhang, G., Casey, J. F., & Shen, Y. (2018). Rapid enhancement of chemical weathering recorded by extremely light seawater lithium isotopes at the Permian-Triassic boundary. *Proceedings of the National Academy of Sciences, 115*(15), 3782–3787. https://doi.org/10.1073/pnas.1711862115

Sun, Y., Joachimski, M. M., Wignall, P., Yan, C., Chen, Y., Jiang, H., et al. (2012). Lethally hot temperatures during the Early Triassic greenhouse. *Science*, *338*(6105), 363–366. https://doi.org/10.1126/science.1224126

Svensen, H., Planke, S., Polozov, A. G., Schmidbauer, N., Corfu, F., Podladchikov, Y. Y., & Jamtveit, B. (2009). Siberian gas venting and the end-Permian environmental crisis. *Earth and Planetary Science Letters*, *277*(3–4), 490–500. https://doi.org/10.1016/j.epsl.2008.11.015

Talbot, H. M., Summons, R. E., Jahnke, L. L., Cockell, C. S., Rohmer, M., & Farrimond, P. (2008). Cyanobacterial bacteriohopanepolyol signatures from cultures and natural environmental settings. *Organic Geochemistry*, *39*(2), 232–263. https://doi.org/10.1016/j.orggeochem.2007.08.006

Volkman, J. K. (1986). A review of sterol markers for marine and terrigenous organic matter. *Organic Geochemistry*, *9*(2), 83–99. https://doi.org/10.1016/0146-6380(86)90089-6

Volkman, J. K. (2003). Sterols in microorganisms. *Applied Microbiology and Biotechnology*, *60*(5), 495–506. https://doi.org/10.1007/s00253-002-1172-8

Volkman, J. K., Barrett, S. M., Dunstan, G. A., & Jeffrey, S. W. (1994). Sterol biomarkers for microalgae from the green algal class Prasinophyceae. *Organic Geochemistry*, *21*(12), 1211–1218. https://doi.org/10.1016/0146-6380(94)90164-3

Wang, X., Zhong, H., Chen, J., Lin, Z., Wang, B., Hou, M., et al. (2024) DDEOutcrop3D: A new pathway to the Deep-time Earth*, EGU General Assembly 2024*, Vienna, Austria, 14–19 Apr 2024, EGU24-16328, https://doi.org/10.5194/egusphere-egu24-16328.

Watson, J. S., Sephton, M. A., Looy, C. V., & Gilmour, I. (2005). Oxygen-containing aromatic compounds in a late Permian sediment. *Organic Geochemistry*, *36*(3), 371–384. https://doi.org/10.1016/j.orggeochem.2004.10.006

Welander, P. V., Coleman, M. L., Sessions, A. L., Summons, R. E., & Newman, D. K. (2010). Identification of a methylase required for 2-methylhopanoid production and implications for the interpretation of sedimentary hopanes. *Proceedings of the National Academy of Sciences*, *107*(19), 8537–8542. https://doi.org/10.1073/pnas.0912949107

Wenger, L. M., Davis, C. L., & Isaksen, G. H. (2002). Multiple controls on petroleum biodegradation and impact on oil quality. *SPE Reservoir Evaluation & Engineering*, *5*(5), 375–383. https://doi.org/10.2523/71450-ms

Woods, A. D., Zonneveld, J. P., & Wakefield, R. (2023). Hyperthermal-driven anoxia and reduced productivity in the aftermath of the Permian-Triassic mass extinction: A case study from Western Canada. *Frontiers in Earth Science*, *11*, 1323413. https://doi.org/10.3389/feart.2023.1323413

Wu, C. H., Bialecka-Fornal, M., & Newman, D. K. (2015). Methylation at the C-2 position of hopanoids increases rigidity in native bacterial membranes. *ELife*, *4*, e05663. https://doi.org/10.7554/eLife.05663

Xiaoyan, R., Genming, L., Shouzhi, H., Feng, C., Si, S., Wenjun, W., et al. (2008). Molecular records of primary producers and sedimentary environmental conditions of late Permian rocks in northeast Sichuan, China. *Journal of China University of Geosciences*, *19*(5), 471–480. https://doi.org/10.1016/S1002-0705(08)60052-7

Xie, S., Pancost, R. D., Yin, H., Wang, H., & Evershed, R. P. (2005). Two episodes of microbial change coupled with Permo/Triassic faunal mass extinction. *Nature*, *434*(7032), 494–497. https://doi.org/10.1029/2002jd003120

Zhang, F., Shen, S., Cui, Y., Lenton, T. M., Dahl, T. W., Zhang, H., et al. (2020). Two distinct episodes of marine anoxia during the Permian-Triassic crisis evidenced by uranium isotopes in marine dolostones. *Geochimica et Cosmochimica Acta*, *287*, 165–179. https://doi.org/10.1016/j.gca.2020.01.032

Zhang, P., Yang, M., Lu, J., Bond, D. P. G., Zhou, K., Xu, X., et al. (2023). End-Permian terrestrial ecosystem collapse in North China: Evidence from palynology and geochemistry. *Global and Planetary Change*, *222*, 104070. https://doi.org/10.1016/j.gloplacha.2023.104070

Zumberge, J. A., Love, G. D., Cárdenas, P., Sperling, E. A., Gunasekera, S., Rohrssen, M., et al. (2018). Demosponge steroid biomarker 26-methylstigmastane provides evidence for Neoproterozoic animals. *Nature Ecology and Evolution*, *2*(11), 1709–1714. https://doi.org/10.1038/s41559-018-0676-2

4. Conclusions and outlook

This thesis focused on different aspects of the effects of the Permian–Triassic environmental crisis on shallow marine ecosystems with varying temporal and spatial scales: Manuscript III is covering the extinction prelude, whereas Manuscript I and II cover late Permian to Griesbachian strata. Manuscript II is focusing on local processes, whereas Manuscript III and Manuscript I are covering regional and global scales, respectively. In three studies, the following questions were approached:

1. **Do lipid biomarker signatures associated with the Permian–Triassic environmental crisis vary with paleolatitude, and what do these patterns reveal about the variability in the phytoplankton community composition and primary productivity?**

Both C_{33}-*n*-alkylcyclohexane (C_{33}-*n*-ACH) and phytanyl toluene are biomarkers associated to the Permian–Triassic environmental crisis. However, only C_{33}-*n*-ACH provides an unambiguous biomarker of the onset of the Permian–Triassic environmental crisis in mid- to higher-latitude ecosystems, as peak contents of C_{33}-*n*-ACH were found exclusively in latest Permian post-extinction and Early Triassic strata thus far (e.g., Grice et al., 2005b; Grotheer et al., 2017; Hays et al., 2012; Nabbefeld et al., 2010b; Saito et al., 2022; Xie et al., 2017). In contrast, phytanyl toluene seems to have a wider stratigraphic distribution (Grotheer et al., 2017; Moura et al., 2019; Plet et al., 2020; Sinninghe Damsté et al., 1993), and is restricted to higher paleolatitude ecosystems across the Permian–Triassic transition, whereas traces of C_{33}-*n*-ACH or its pseudohomologs can be detected at least in some paleotropical settings. Both biomarkers were assigned to oxygenic photoautotrophic source organisms occupying similar ecological niches, that were thriving in the Early Triassic Boreal Realm.

The investigation of the photoautotrophic community in a paleotropical setting in the western Paleotethys (Dolomites, norther Italy) revealed a pre-extinction community dominated by eukaryotic algae. However, only traces of C_{33}-*n*-ACH and its pseudohomologs could be detected, if any,

and phytanyl toluene was absent. These algae were, therefore, phylogenetically distinct from the source organisms of C_{33}-*n*-ACH and phytanyl toluene. Furthermore, lowermost post-extinction strata do not record an increase in the relative abundance of photoautotrophs at the paleotropical site. Hence, the response of the photoautotrophic community was highly variable across paleolatitudes, with regional phytoplankton blooms in the aftermath of the extinction event in higher paleolatitude settings such as the Boreal Realm, while neither a collapse of the photoautotrophic community nor similar phytoplankton blooms were detected in lower paleolatitude settings.

2. What are the baseline redox conditions prior to the Permian–Triassic environmental crisis, and is anoxia the main extinction driver across paleolatitudes?

The pre-extinction environmental conditions were investigated at both a higher paleolatitude site (Svalbard) and a paleotropical site (Dolomites, northern Italy) to establish late Permian baseline conditions. In the Lusitaniadalen section in central Svalbard, the lipid biomarker record was complemented by independent geochemical proxies, such as redox sensitive trace metal enrichments, to evaluate lithology-independent redox patterns. Both proxy systems indicate redox variations in the late Permian with intervals of water column deoxygenation, that were temporally not associated with the mass extinction event. Consequently, the pre-extinction biota was likely adapted to fluctuating oxygen availability prior to the environmental crisis. While anoxia became more intense immediately below the extinction horizon, redox-sensitive trace metal enrichment and lipid biomarkers indicate a return to oxic conditions shortly above the extinction horizon.

In the Dolomites, the analysis of the late Permian lipid biomarker inventory from two sites along a water depth gradient on the shallow marine carbonate ramp has revealed that the biomarker composition at the more proximal sites mainly responded to sea level fluctuations, with regressive episodes leading to naturally stressed ecosystem with variabile redox conditions. In contrast, the more distal site was less affected by transgresssive/regressive cycles, and regressive episodes did not record restricted marine conditions. Hence, lipid biomarker inventory was more stable over time with oxic conditions throughout the invetigated pre-extinction interval.

Taken together, these findings point towards the need for regional or even local assessments of extinction drivers across various paleolatitudes. The ecosystem of both the higher paleolatitude site and the shallower of the paleotropical sites was exposed to fluctuating redox conditions due to local or regional environmental effects such as regional sea level changes, which were not associated with a global environmental deterioration in the late Permian preceding the mass extinction event. An ecological community regularly exposed to redox fluctuations is, therefore, better adapted to these conditions, and responds differently to deoxygenation, than a community previously exposed to more stable conditions. Consequently, although anoxia is often hypothesized as the main driver of the Permian–Triassic mass extinction globally, the isolated effect of anoxia in shallow marine ecosystems that were exposed to intervals of deoxygenation throughout the late Permian was likely less severe. However, combined with other stressors, for example thermal stress, anoxia remains a critical extinction driver.

3. **Did the microbial community respond to late Permian environmental stress culminating in the mass extinction event, and is a recovery of the microbial ecosystem recorded by molecular fossils?**

The analysis of the lipid biomarker inventory in the late Permian paleotropical Tethys Ocean (Dolomites, northern Italy) revealed variability in the organic matter origin, redox conditions, and composition of the photoautotrophic community especially at the more proximal of the investigated sites. However, this variablilty appears to be mainly related to sea level changes rather than representing a response to progressively deteriorating conditons culminating into the mass extinction event. In Lusitaniadalen (Svalbard), the lipid biomarker composition also changes relatively abruptly across the extinction horizon, whereas the composition is more stable below the extinction horizon, indicating that changes in the microbial ecosystem were rapid rather than gradual. This emphasizes the need for carefully evaluating the local and regional environmental context before assigning a change in the community composition and a stress response in an ecological community to globally deteriorating environmental conditions.

Finally, pre- and post-extinction lipid biomarker inventories differ distinctly both locations Lusitaniadalen and the Dolomites. In the latter, the difference in the lipid biomarker composition is mainly due to the sudden increase in the combustion-derived PAHs coronene and pyrene associated with Siberian Traps emplacement. At Lusitaniadalen, an increase in chlorophyll-derived biomarkers is accompanied by increased abundance other isoprenoid biomarkers following the extinction event. However, the post-extinction signals do not return towards the pre-crisis baseline values, hence no recovery is recorded within the investigated interval.

These results contribute to a better understanding of the extinction dynamics and microbial ecosystem changes during a major environmental crisis. They emphasize the importance of assessing ecosystem baseline conditions before inferring extinction drivers, and provide a new perspective on the response of the photoautotrophic community to the Permian–Triassic environmental crisis. Additionally, the application of revised enrichment factors of redox-sensitive metals to the siliciclastic lithology at Lusitaniadalen highlights the possibility of a broader application of this method, that was so far only applied to carbonate-rich facies (Krewer et al., 2024).

Based on the three studies presented in this thesis, also new questions arise. For example, whether the paleogeographical pattern of the two biomarkers C_{33}-*n*-ACH and phytanyl toluene associated with the extinction event is caused by (a) unsuitable conditions for the source organisms to proliferate in equatorial settings (e.g., thermal exclusion), or (b) a lithological bias with differential preservation of these biomarkers in the studied paleotropical carbonate and higher-latitude siliciclastic lithologies, needs further investigation. Low paleolatitude siliciclastic Permian–Triassic successions should, therefore, be analyzed for their lipid biomarker inventory and the presence of C_{33}-*n*-ACH and phytanyl toluene, such as the late Permian pre-extinction strata at the Mingtang section (South China), the post-extinction Yinkeng Formation in Meishan (South China), the post-extinction mixed carbonate-siliciclastic Werfen Formation in northern Italy or the Bódvaszilas Sandstone Formation in Hungary, for broadening the understanding of the phytoplankton community structure and responses, and primary productivity dynamics during major environmental crises.

Furthermore, to better understand changes in the microbial community, the recovery dynamics, and the temporal extent of regional phytoplankton blooms, as well as the consequences of subsequent environmental events in the Early Triassic, such as the Smithian/Spathian event, a longer record is required. Lusitaniadalen, Svalbard, provides excellent outcrop conditions for such studies, as the stratigraphy is continuously exposed up to the Middle Triassic Botneheia Formation. Also, the nearby Ledalen section could be targeted to study the Early Triassic and the Smithian/Spathian boundary, as well as the Middle to Upper Triassic, which are exposed in the Vikinghøgda, Botneheia and Tschermakfjellet formations there. However, several sill intrusions from the emplacement of the High Arctic Large Igneous Province in the Cretaceous (Senger et al., 2014) in the area west of Vindodden may compromise preservation of organic matter and affect the lipid biomarker preservation by a high thermal maturity at Ledalen.

Moreover, the stratigraphy at Lusitaniadalen is thus far not well constrained, and the position of the Permian/Triassic boundary is not yet defined. The change in the lipid biomarker composition starting shortly below the extinction horizon presented here represents evidence for a continuous succession despite the sudden change in lithology at the extinction horizon. However, further analysis of the conodont assemblage, which has been shown to be possible to be extracted at Lusitaniadalen (Manuscript II), could implement a biostratigraphic framework, and if *H*. *parvus* is found, also determine the Permian/Triassic boundary. Additionally, dating of the ash beds in the lower Vikinghødga Formation could refine calculations of sediment accumulation rates and provide absolute dates for a chronostratigraphic framework for future studies.

Finally, the example of the 2α-methylhopane index has shown how the interpretation of lipid biomarker signals depends highly on studies on modern microbial communities, with technological advances in metabolomic and metagenomic studies providing new findings that challenge previously established phylogenetic assignments of lipid biomarkers to specific source organisms. To fully explore ancient microbial ecosystems and the environmental conditions during major global crises in Earth's history, an interdisciplinary approach combining geological (e.g., sedimentological, paleontological), chemical (both organic and inorganic) and biological (e.g., genomic, metagenomic, metabolomic) evidences is, therefore, necessary.

5. References

Armbrecht, L. H. (2020). The potential of sedimentary ancient DNA to reconstruct past ocean ecosystems. *Oceanography, 33*(2), 116–123. https://doi.org/10.5670/oceanog.2020.211

Arrigo, K. R. (2005). Marine microorganisms and global nutrient cycles. *Nature, 437*(7057), 349–355. https://doi.org/10.1038/nature04159

Augland, L. E., Ryabov, V. V., Vernikovsky, V. A., Planke, S., Polozov, A. G., Callegaro, S., Jerram, D. A., & Svensen, H. H. (2019). The main pulse of the Siberian Traps expanded in size and composition. *Scientific Reports, 9*(1), 18723. https://doi.org/10.1038/s41598-019-54023-2

Belt, S. T., Massé, G., Rowland, S. J., Poulin, M., Michel, C., & LeBlanc, B. (2007). A novel chemical fossil of palaeo sea ice: IP_{25}. *Organic Geochemistry, 38*, 16–27. https://doi.org/10.1016/j.orggeochem.2006.09.013

Benca, J. P., Duijnstee, I. A. P., & Looy, C. V. (2018). UV-B–induced forest sterility: Implications of ozone shield failure in earth's largest extinction. *Science Advances, 4*(2), e1700618. https://doi.org/10.1126/sciadv.1700618

Bentley, J. N., Ventura, G. T., Dalzell, C. J., Walters, C. C., Peters, C. A., Mennito, A. S., et al. (2022). Archaeal lipid diversity, alteration, and preservation at the Cathedral Hill deep sea hydrothermal vent, Guaymas Basin, Gulf of California, and its implications regarding the deep time preservation paradox. *Organic Geochemistry, 163*, 104302. https://doi.org/10.1016/j.orggeochem.2021.104302

Benton, M. J., & Newell, A. J. (2014). Impacts of global warming on Permo-Triassic terrestrial ecosystems. *Gondwana Research, 25*(4), 1308–1337. https://doi.org/10.1016/j.gr.2012.12.010

Benton, M. J., & Twitchett, R. J. (2003). How to kill (almost) all life: The end-Permian extinction event. *Trends in Ecology & Evolution, 18*(7), 358–365. https://doi.org/doi:10.1016/S0169-5347(03)00093-4

Bond, D. P. G., & Grasby, S. E. (2017). On the causes of mass extinctions. *Palaeogeography, Palaeoclimatology, Palaeoecology, 478*, 3–29. https://doi.org/10.1016/j.palaeo.2016.11.005

Brennecka, G. A., Herrmann, A. D., Algeo, T. J., & Anbar, A. D. (2011). Rapid expansion of oceanic anoxia immediately before the end-Permian mass extinction. *Proceedings of the National Academy of Sciences, 43*(108), 17631–17634. https://doi.org/10.1073/pnas.1106039108

Brocks, J. J., & Grice, K. (2011). Biomarkers (molecular fossils). In J. Reitner & V. Thiel (Eds.), *Encyclopedia of Geobiology* (pp. 147–167). Springer. https://doi.org/10.1007/978-1-4020-9212-1

Brocks, J. J., Love, G. D., Summons, R. E., Knoll, A. H., Logan, G. A., & Bowden, S. A. (2005). Biomarker evidence for green and purple sulphur bacteria in a stratified Palaeoproterozoic sea. *Nature, 437*(7060), 866–870. https://doi.org/10.1038/nature04068

Burgess, S. D., & Bowring, S. A. (2015). High-precision geochronology confirms voluminous magmatism before, during, and after Earth's most severe extinction. *Science Advances, 1*(7), e1500470. https://doi.org/10.1126/sciadv.1500470

Burgess, S. D., Bowring, S., & Shen, S. Z. (2014). High-precision timeline for Earth's most severe extinction. *Proceedings of the National Academy of Sciences, 111*(9), 3316–3321. https://doi.org/10.1073/pnas.1317692111

Burgess, S. D., Muirhead, J. D., & Bowring, S. A. (2017). Initial pulse of Siberian Traps sills as the trigger of the end-Permian mass extinction. *Nature Communications, 8*(1), 164. https://doi.org/10.1038/s41467-017-00083-9

Canfield, D. E. (1994). Factors influencing organic carbon preservation in marine sediments. *Chemical Geology, 114*(3–4), 315–329. https://doi.org/10.1016/0009-2541(94)90061-2

Cao, C., Love, G. D., Hays, L. E., Wang, W., Shen, S., & Summons, R. E. (2009). Biogeochemical evidence for euxinic oceans and ecological disturbance presaging the end-Permian mass extinction event. *Earth and Planetary Science Letters, 281*(3–4), 188–201. https://doi.org/10.1016/j.epsl.2009.02.012

Capo, E., Monchamp, M. E., Coolen, M. J. L., Domaizon, I., Armbrecht, L., & Bertilsson, S. (2022). Environmental paleomicrobiology: Using DNA preserved in aquatic sediments to its full potential. *Environmental Microbiology, 24*(5), 2201–2209. https://doi.org/10.1111/1462-2920.15913

Cassani, F., Gallango, O., Talukdar, S., Vallejos, C., & Ehrmann, U. (1988). Methylphenanthrene maturity index of marine source rock extracts and crude oils from the Maracaibo Basin. *Organic Geochemistry, 13*(3), 73–80. https://doi.org/10.1016/B978-0-08-037236-5.50013-0

Chen, J., Shen, S. Z., Li, X. H., Xu, Y. G., Joachimski, M. M., Bowring, et al. (2016). High-resolution SIMS oxygen isotope analysis on conodont apatite from South China and implications for the end-Permian mass extinction. *Palaeogeography, Palaeoclimatology, Palaeoecology, 448*, 26–38. https://doi.org/10.1016/j.palaeo.2015.11.025

Chen, Z. Q., & Benton, M. J. (2012). The timing and pattern of biotic recovery following the end-Permian mass extinction. *Nature Geoscience, 5*(6), 375–383. https://doi.org/10.1038/ngeo1475

Clapham, M. E., & Payne, J. L. (2011). Acidification, anoxia, and extinction: A multiple logistic regression analysis of extinction selectivity during the middle and late Permian. *Geology, 39*(11), 1059–1062. https://doi.org/10.1130/G32230.1

Clarkson, M. O., Kasemann, S. A., Wood, R. A., Lenton, T. M., Daines, S. J., Richoz, S., et al. (2015). Ocean acidification and the Permo-Triassic mass extinction. *Science, 348*(6231), 229–232. https://doi.org/10.1126/science.aaa0193

Coates, R. C., Podell, S., Korobeynikov, A., Lapidus, A., Pevzner, P., Sherman, D. H., et al. (2014). Characterization of cyanobacterial hydrocarbon composition and distribution of biosynthetic pathways. *PLoS ONE, 9*(1), e85140. https://doi.org/10.1371/journal.pone.0085140

Cui, Y., Li, M., Van Soelen, E. E., Peterse, F., & Kürschner, W. M. (2021). Massive and rapid predominantly volcanic CO_2 emission during the end-Permian mass extinction. *Proceedings of the National Academy of Sciences, 118*(37), e2014701118. https://doi.org/10.1073/pnas.2014701118

Demarchi, B., Mackie, M., Li, Z., Deng, T., Collins, M. J., & Clarke, J. (2022). Survival of mineral-bound peptides into the Miocene. *ELife, 11*, e82849. https://doi.org/10.7554/ELIFE.82849

Didyk, B. M., Simoneit, B. R. T., Brassell, S. C., & Eglinton, G. (1978). Organic geochemical indicators of palaeoenvironmental conditions of sedimentation. *Nature, 272*(5650), 216–222. https://doi.org/10.1038/272216a0

Dufourc, E. J. (2008). Sterols and membrane dynamics. *Journal of Chemical Biology, 1*(1–4), 63–77. https://doi.org/10.1007/s12154-008-0010-6

Fedorenko, V. A., Lightfoot, P. C., Naldrett, A. J., Czamanske, G. K., Hawkesworth, C. J., Wooden, J. L., & Ebel, D. S. (1996). Petrogenesis of the flood-basalt sequence at Noril'sk, North Central Siberia. *International Geology Review, 38*(2), 99–135. https://doi.org/10.1080/00206819709465327

Forel, M. B., Crasquin, S., Kershaw, S., & Collin, P. Y. (2013). In the aftermath of the end-Permian extinction: The microbialite refuge? *Terra Nova, 25*(2), 137–143. https://doi.org/10.1111/ter.12017

Foster, W. J., Allen, B. J., Kitzmann, N. H., Münchmeyer, J., Rettelbach, T., Witts, J. D., et al. (2023). How predictable are mass extinction events? *Royal Society Open Science, 10*(3), 221507. https://doi.org/10.1098/rsos.221507

Foster, W. J., Frank, A. B., Li, Q., Danise, S., Wang, X., & Peckmann, J. (2024). Thermal and nutrient stress drove Permian–Triassic shallow marine extinctions. *Cambridge Prisms: Extinction, 2*, e9. https://doi.org/10.1017/ext.2024.9

Foster, W. J., Heindel, K., Richoz, S., Gliwa, J., Lehrmann, D. J., Baud, A., et al. (2020). Suppressed competitive exclusion enabled the proliferation of Permian/Triassic boundary microbialites. *Depositional Record, 6*(1), 62–74. https://doi.org/10.1002/dep2.97

Foster, W. J., & Sebe, K. (2017). Recovery and diversification of marine communities following the late Permian mass extinction event in the western Palaeotethys. *Global and Planetary Change, 155*, 165–177. https://doi.org/10.1016/j.gloplacha.2017.07.009

Galasso, F., Frank, A. B., & Foster, W. J. (2025). Heavy metal toxicity: A major driver of past biodiversity crises? *Preprint at EarthArXiv.* https://doi.org/10.31223/X5SX5R

Gelpi, E., Schneider, H., Mann, J., & Oró, J. (1970). Hydrocarbons of geochemical significance in microscopic algae. *Phytochemistry, 9*(3), 603–612. https://doi.org/10.1016/S0031-9422(00)85700-3

Gliwa, J., Forel, M. B., Crasquin, S., Ghaderi, A., & Korn, D. (2021). Ostracods from the end-Permian mass extinction in the Aras Valley section (north-west Iran). *Papers in Palaeontology, 7*(2), 1003–1042. https://doi.org/10.1002/spp2.1330

Gliwa, J., Wiedenbeck, M., Schobben, M., Ullmann, C. V., Kiessling, W., Ghaderi, A., et al. (2022). Gradual warming prior to the end-Permian mass extinction. *Palaeontology, 65*(5), e12621. https://doi.org/10.1111/pala.12621

Grasby, S. E., & Bond, D. P. G. (2023). How large igneous provinces have killed most life on Earth—numerous times. *Elements, 19*(5), 276–281. https://doi.org/10.2138/gselements.19.5.276

Grasby, S. E., Sanei, H., & Beauchamp, B. (2011). Catastrophic dispersion of coal fly ash into oceans during the latest Permian extinction. *Nature Geoscience, 4*(2), 104–107. https://doi.org/10.1038/ngeo1069

Grasby, S. E., Sanei, H., Beauchamp, B., & Chen, Z. (2013). Mercury deposition through the Permo-Triassic biotic crisis. *Chemical Geology, 351*, 209–216. https://doi.org/10.1016/j.chemgeo.2013.05.022

Grasby, S. E., Shen, W., Yin, R., Gleason, J. D., Blum, J. D., Lepak, R. F., et al. (2017). Isotopic signatures of mercury contamination in latest Permian oceans. *Geology, 45*(1), 55–58. https://doi.org/10.1130/G38487.1

Grice, K., Cao, C., Love, G. D., Böttcher, M. E., Twitchett, R. J., Grosjean, E., et al. (2005a). Photic zone euxinia during the Permian-Triassic superanoxic event. *Science, 307*(5710), 706–709. https://doi.org/10.1126/science.1104323

Grice, K., Twitchett, R. J., Alexander, R., Foster, C. B., & Looy, C. (2005b). A potential biomarker for the Permian-Triassic ecological crisis. *Earth and Planetary Science Letters, 236*(1–2), 315–321. https://doi.org/10.1016/j.epsl.2005.05.008

Grotheer, H., Le Métayer, P., Piggott, M. J., Lindeboom, E. J., Holman, A. I., Twitchett, R. J., & Grice, K. (2017). Occurrence and significance of phytanyl arenes across the Permian-Triassic boundary interval. *Organic Geochemistry, 104*, 42–52. https://doi.org/10.1016/j.orggeochem.2016.12.002

Hays, L. E., Grice, K., Foster, C. B., & Summons, R. E. (2012). Biomarker and isotopic trends in a Permian-Triassic sedimentary section at Kap Stosch, Greenland. *Organic Geochemistry, 43*, 67–82. https://doi.org/10.1016/j.orggeochem.2011.10.010

Heindel, K., Foster, W. J., Richoz, S., Birgel, D., Roden, V. J., Baud, A., et al. (2018). The formation of microbial-metazoan bioherms and biostromes following the latest Permian mass extinction. *Gondwana Research, 61*, 187–202. https://doi.org/10.1016/j.gr.2018.05.007

Hermann, E., Hochuli, P. A., Bucher, H., Brühwiler, T., Hautmann, M., Ware, D., & Roohi, G. (2011). Terrestrial ecosystems on North Gondwana following the end-Permian mass extinction. *Gondwana Research, 20*(2–3), 630–637. https://doi.org/10.1016/j.gr.2011.01.008

Hinojosa, J. L., Brown, S. T., Chen, J., DePaolo, D. J., Paytan, A., Shen, S. Z., & Payne, J. L. (2012). Evidence for end-Permian ocean acidification from calcium isotopes in biogenic apatite. *Geology, 40*(8), 743–746. https://doi.org/10.1130/G33048.1

Ho, S. Y. W., & Duchêne, S. (2014). Molecular-clock methods for estimating evolutionary rates and timescales. *Molecular Ecology, 23*(24), 5947–5965. https://doi.org/10.1111/mec.12953

Hochuli, P. A., Hermann, E., Vigran, J. O., Bucher, H., & Weissert, H. (2010). Rapid demise and recovery of plant ecosystems across the end-Permian extinction event. *Global and Planetary Change, 74*(3–4), 144–155. https://doi.org/10.1016/j.gloplacha.2010.10.004

Hopmans, E. C., Weijers, J. W. H., Schefuß, E., Herfort, L., Sinninghe Damsté, J. S., & Schouten, S. (2004). A novel proxy for terrestrial organic matter in sediments based on branched and isoprenoid tetraether lipids. *Earth and Planetary Science Letters, 224*(1–2), 107–116. https://doi.org/10.1016/j.epsl.2004.05.012

Imhoff, J. F. (2014). Biology of green sulfur bacteria. *Encyclopedia of Life Sciences*. https://doi.org/10.1002/9780470015902.a0000458.pub2

Jablonski, D., & Edie, S. M. (2025). Mass extinctions and their rebounds: A macroevolutionary framework. *Paleobiology, 51*, 83–96. https://doi.org/10.1017/pab.2024.13

Jia, C., Huang, J., Kershaw, S., Luo, G., Farabegoli, E., Perri, M. C., et al. (2012). Microbial response to limited nutrients in shallow water immediately after the end-Permian mass extinction. *Geobiology, 10*(1), 60–71. https://doi.org/10.1111/j.1472-4669.2011.00310.x

Jiao, S., Zhang, H., Cai, Y., Jin, C., & Shen, S. (2024). Polycyclic aromatic hydrocarbons (PAHs) evidence for frequent combustion events on land during the Permian–Triassic transition in

Northwest China. *Palaeogeography, Palaeoclimatology, Palaeoecology, 642*, 112152. https://doi.org/10.1016/j.palaeo.2024.112152

Joachimski, M. M., Lai, X., Shen, S., Jiang, H., Luo, G., Chen, B., et al. (2012). Climate warming in the latest Permian and the Permian-Triassic mass extinction. *Geology, 40*(3), 195–198. https://doi.org/10.1130/G32707.1

Joachimski, M. M., Müller, J., Gallagher, T. M., Mathes, G., Chu, D. L., Mouraviev, F., et al. (2022). Five million years of high atmospheric CO_2 in the aftermath of the Permian-Triassic mass extinction. *Geology, 50*(6), 650–654. https://doi.org/10.1130/G49714.1

Kamble, A., Sawant, S., & Singh, H. (2020). 16S Ribosomal RNA gene-based metagenomics: A Review. *Biomedical Research Journal, 7*(1), 5–11. https://doi.org/10.4103/BMRJ.BMRJ

Karl, D. M. (2014). Microbially mediated transformations of phosphorus in the sea: New views of an old cycle. *Annual Review of Marine Science, 6*, 279–337. https://doi.org/10.1146/annurev-marine-010213-135046

Kershaw, S., Crasquin, S., Li, Y., Collin, P. Y., Forel, M. B., Mu, X., et al. (2012). Microbialites and global environmental change across the Permian-Triassic boundary: A synthesis. *Geobiology, 10*(1), 25–47. https://doi.org/10.1111/j.1472-4669.2011.00302.x

Kershaw, S., Zhang, T., & Lan, G. (1999). A? microbialite carbonate crust at the Permian–Triassic boundary in South China, and its palaeoenvironmental significance. *Palaeogeography, Palaeoclimatology, Palaeoecology, 146*(1–4), 1–18. https://doi.org/10.1016/S0031-0182(98)00139-4

Knoll, A. H., Bambach, R. K., Payne, J. L., Pruss, S., & Fischer, W. W. (2007a). Paleophysiology and end-Permian mass extinction. *Earth and Planetary Science Letters, 256*(3–4), 295–313. https://doi.org/10.1016/j.epsl.2007.02.018

Knoll, A. H., Canfield, D. E., & Konhauser, K. (2012). *Fundamentals of geobiology.* Wiely-Blackwell. https://doi.org/10.1002/9781118280874

Knoll, A. H., Summons, R. E., Waldbauer, J. R., & Zumberge, J. E. (2007b). The geological succession of primary producers in the oceans. In P. G. Falkowsk & A. H. Knoll (Eds.), *Evolution of Primary*

Producers in the Sea (pp. 133–163). Elsevier, Burlington, MA. https://doi.org/10.1016/B978-012370518-1/50009-6

Koopmans, M. P., Schouten, S., Kohnen, M. E. L., & Sinninghe Damsté, J. S. (1996). Restricted utility of aryl isoprenoids as indicators for photic zone anoxia. *Geochimica et Cosmochimica Acta, 60*(23), 4873–4876. https://doi.org/10.1016/S0016-7037(96)00303-1

Krewer, C., Poulton, S. W., Newton, R. J., März, C., Mills, B. J. W., & Wagner, T. (2024). Controls on the termination of Cretaceous Oceanic Anoxic Event 2 in the Tarfaya Basin, Morocco. *American Journal of Science, 324*, 11. https://doi.org/10.2475/001c.118797

Lau, K. V., Maher, K., Altıner, D., Kelley, B. M., Kump, L. R., Lehrmann, D. J., et al. (2016). Marine anoxia and delayed Earth system recovery after the end-Permian extinction. *Proceedings of the National Academy of Sciences, 113*(9), 2360–2365. https://doi.org/10.1073/pnas.1515080113

Lloyd, K. G., Steen, A. D., Ladau, J., Yin, J., & Crosby, L. (2018). Phylogenetically novel uncultured microbial cells dominate Earth microbiomes. *MSystems, 3*(5), e00055-18. https://doi.org/10.1128/msystems.00055-18

Luo, G., Yang, H., Algeo, T. J., Hallmann, C., & Xie, S. (2019). Lipid biomarkers for the reconstruction of deep-time environmental conditions. *Earth-Science Reviews, 189*, 99–124. https://doi.org/10.1016/j.earscirev.2018.03.005

Mackenzie, A. S., Beaumont, C., & Mckenzie, D. P. (1984). Estimation of the kinetics of geochemical reactions with geophysical models of sedimentary basins and applications. *Organic Geochemistry, 6*, 875–884. https://doi.org/10.1016/0146-6380(84)90110-4

Moura, A. K. S., Ribeiro, D. O., Do Carmo, I. S., Araújo, B. Q., Pereira, V. B., Azevedo, D. A., & Citó, A. M. G. L. (2019). An assay on alkyl aromatic hydrocarbons: Unexpected group-type separation of diaromatic hydrocarbons in Cretaceous crude oils from Brazilian marginal basin. *Energy and Fuels, 33*(2), 691–699. https://doi.org/10.1021/acs.energyfuels.8b03268

Müller, J., Sun, Y., Yang, F., Fantasia, A., & Joachimski, M. (2022). Phosphorus cycle and primary productivity changes in the Tethys Ocean during the Permian-Triassic transition: Starving marine ecosystems. *Frontiers in Earth Science, 10*, 832308. https://doi.org/10.3389/feart.2022.832308

Nabbefeld, B., Grice, K., Summons, R. E., Hays, L. E., & Cao, C. (2010a). Significance of polycyclic aromatic hydrocarbons (PAHs) in Permian/Triassic boundary sections. *Applied Geochemistry, 25*(9), 1374–1382. https://doi.org/10.1016/j.apgeochem.2010.06.008

Nabbefeld, B., Grice, K., Twitchett, R. J., Summons, R. E., Hays, L., Böttcher, M. E., & Asif, M. (2010b). An integrated biomarker, isotopic and palaeoenvironmental study through the late Permian event at Lusitaniadalen, Spitsbergen. *Earth and Planetary Science Letters, 291*(1–4), 84–96. https://doi.org/10.1016/j.epsl.2009.12.053

Nowak, H., Schneebeli-Hermann, E., & Kustatscher, E. (2019). No mass extinction for land plants at the Permian–Triassic transition. *Nature Communications, 10*(1), 384. https://doi.org/10.1038/s41467-018-07945-w

Pajares, S., & Ramos, R. (2019). Processes and microorganisms involved in the marine nitrogen cycle: Knowledge and gaps. *Frontiers in Marine Science, 6*, 739. https://doi.org/10.3389/fmars.2019.00739

Paterson, R. S., Mackie, M., Capobianco, A., Heckeberg, N. S., Fraser, D., Demarchi, B., et al. (2025). Phylogenetically informative proteins from an Early Miocene rhinocerotid. *Nature, 643*(8072), 719–724. https://doi.org/10.1038/s41586-025-09231-4

Payne, J. L., Turchyn, A. V, Paytan, A., Depaolo, D. J., Lehrmann, D. J., Yu, M., & Wei, J. (2010). Calcium isotope constraints on the end-Permian mass extinction. *Proceedings of the National Academy of Sciences, 107*(19), 8543–8548. https://doi.org/10.1073/pnas.0914065107

Pearson, A., Flood Page, S. R., Jorgenson, T. L., Fischer, W. W., & Higgins, M. B. (2007). Novel hopanoid cyclases from the environment. *Environmental Microbiology, 9*(9), 2175–2188. https://doi.org/10.1111/j.1462-2920.2007.01331.x

Peters, K. E., Walters, C. C., & Moldowan, J. M. (2005). *The Biomarker Guide: Volume 2, Biomarkers and Isotopes in Petroleum Exploration and Earth History*, 2nd ed., Vol. 1. Cambridge University Press.

Peters, K. E., Moldowan, J. M., Mccaffreyt, M. A., & Fago, F. J. (1996). Selective biodegradation of extended hopanes to 25-norhopanes in petroleum reservoirs. Insights from molecular mechanics. *Organic Geochemistry, 24*(8–9), 765–783. https://doi.org/10.1016/S0146-6380(96)00086-1

Peterse, F., van der Meer, J., Schouten, S., Weijers, J. W. H., Fierer, N., Jackson, R. B., et al. (2012). Revised calibration of the MBT-CBT paleotemperature proxy based on branched tetraether membrane lipids in surface soils. *Geochimica et Cosmochimica Acta, 96*, 215–229. https://doi.org/10.1016/j.gca.2012.08.011

Plet, C., Grice, K., Scarlett, A. G., Ruebsam, W., Holman, A. I., & Schwark, L. (2020). Aromatic hydrocarbons provide new insight into carbonate concretion formation and the impact of eogenesis on organic matter. *Organic Geochemistry, 143*, 103961. https://doi.org/10.1016/j.orggeochem.2019.103961

Prinoth, H., & Posenato, R. (2023). Bivalves from the Changhsingian (upper Permian) Bellerophon Formation of the Dolomites (Italy): Ancestors of Lower Triassic post-extinction benthic communities. *Papers in Palaeontology, 9*(2), e1486. https://doi.org/10.1002/spp2.1486

Radke, M., Welte, D. H., & Willsch, H. (1982). Geochemical study on a well in the Western Canada Basin: Relation of the aromatic distribution pattern to maturity of organic matter. *Geochimica et Cosmochimica Acta, 46*(1), 1–10. https://doi.org/10.1016/0016-7037(82)90285-X

Reichow, M. K., Pringle, M. S., Al'Mukhamedov, A. I., Allen, M. B., Andreichev, V. L., Buslov, M. M., et al. (2009). The timing and extent of the eruption of the Siberian Traps large igneous province: Implications for the end-Permian environmental crisis. *Earth and Planetary Science Letters, 277*(1–2), 9–20. https://doi.org/10.1016/j.epsl.2008.09.030

Robinson, S. A., Ruhl, M., Astley, D. L., Naafs, B. D. A., Farnsworth, A. J., Bown, P. R., et al. (2017). Early Jurassic North Atlantic sea-surface temperatures from TEX_{86} palaeothermometry. *Sedimentology, 64*, 215–230. https://doi.org/10.1111/sed.12321

Rontani, J. F., & Bonin, P. (2011). Production of pristane and phytane in the marine environment: Role of prokaryotes. *Research in Microbiology, 162*(9), 923–933. https://doi.org/10.1016/j.resmic.2011.01.012

Rowland, S. J. (1990). Production of acyclic isoprenoid hydrocarbons by laboratory maturation of methanogenic bacteria. *Organic Geochemistry, 15*(15), 9–16. https://doi.org/10.1016/0146-6380(90)90181-X

Sabino, M., Birgel, D., Natalicchio, M., Dela Pierre, F., & Peckmann, J. (2021). Carbon isotope excursions during the late Miocene recorded by lipids of marine Thaumarchaeota, Piedmont Basin, Mediterranean Sea. *Geology, 50*(1), 32–36. https://doi.org/10.1130/G49360.1

Saito, R., Tian, L., Kaiho, K., & Takahashi, S. (2022). Biomarker evidence for the prolongation of multiple phytoplankton blooms in the aftermath of the end-Permian mass extinction. *Palaeogeography, Palaeoclimatology, Palaeoecology, 600*, 111077. https://doi.org/10.1016/j.palaeo.2022.111077

Schobben, M., Foster, W. J., Sleveland, A. R. N., Zuchuat, V., Svensen, H. H., Planke, S., et al. (2020). A nutrient control on marine anoxia during the end-Permian mass extinction. *Nature Geoscience, 13*(9), 640–646. https://doi.org/10.1038/s41561-020-0622-1

Schouten, S., Hopmans, E. C., Schefuß, E., & Sinninghe Damsté, J. S. (2002). Distributional variations in marine crenarchaeotal membrane lipids: A new tool for reconstructing ancient sea water temperatures? *Earth and Planetary Science Letters, 204*(1–2), 265–274. https://doi.org/10.1016/S0012-821X(02)00979-2

Segers, K., Declerck, S., Mangelings, D., Vander Heyden, Y., & Van Eeckhaut, A. (2019). Analytical techniques for metabolomic studies: A review. *Bioanalysis, 11*(24), 2297–2318. https://doi.org/10.4155/bio-2019-0014

Senger, K., Tveranger, J., Ogata, K., Braathen, A., & Planke, S. (2014). Late Mesozoic magmatism in Svalbard: A review. *Earth-Science Reviews, 139*, 123–144. https://doi.org/10.1016/j.earscirev.2014.09.002

Sephton, M. A., Jiao, D., Engel, M. H., Looy, C. V., & Visscher, H. (2015). Terrestrial acidification during the end-Permian biosphere crisis? *Geology, 43*(2), 159–162. https://doi.org/10.1130/G36227.1

Sephton, M. A., Looy, C. V., Brinkhuis, H., Wignall, P. B., de Leeuw, J. W., & Visscher, H. (2005). Catastrophic soil erosion during the end-Permian biotic crisis. *Geology, 33*(12), 941–944. https://doi.org/10.1130/G21784.1

Sephton, M. A., Looy, C. V, Veefkind, R. J., Visscher, H., Brinkhuis, H., & De Leeuw, J. W. (1999). Cyclic diaryl ethers in a late Permian sediment. *Organic Geochemistry, 30*(4), 267–273. https://doi.org/10.1016/S0146-6380(99)00002-9

Sepkoski, J. J. (1981). A factor analytic description of the Phanerozoic marine fossil record. *Paleobiology, 7*(1), 36–53. https://doi.org/10.1017/s0094837300003778

Shen, J., Chen, J., Yu, J., Algeo, T. J., Smith, R. M. H., Botha, J., et al. (2023). Mercury evidence from southern Pangea terrestrial sections for end-Permian global volcanic effects. *Nature Communications, 14*(1), 6–14. https://doi.org/10.1038/s41467-022-35272-8

Sinninghe Damsté, J. S., Keely, B. J., Betts, S. E., Baas, M., Maxwell, J. R., & de Leeuw, J. W. (1993). Variations in abundances and distributions of isoprenoid chromans and long-chain alkylbenzenes in sediments of the Mulhouse Basin: A molecular sedimentary record of palaeosalinity. *Organic Geochemistry, 20*(8), 1201–1215. https://doi.org/10.1016/0146-6380(93)90009-Z

Sinninghe Damsté, J. S., Rijpstra, W. I. C., Coolen, M. J., Schouten, S., & Volkman, J. K. (2007). Rapid sulfurisation of highly branched isoprenoid (HBI) alkenes in sulfidic Holocene sediments from Ellis Fjord, Antarctica. *Organic Geochemistry, 38*(1), 128–139. https://doi.org/10.1016/j.orggeochem.2006.08.003

Sinninghe Damsté, J. S., Rijpstra, W. I. C., Dedysh, S. N., Foesel, B. U., & Villanueva, L. (2017). Pheno- and genotyping of hopanoid production in Acidobacteria. *Frontiers in Microbiology, 8*, 968. https://doi.org/10.3389/fmicb.2017.00968

Sinninghe Damsté, J. S., Schouten, S., De Leeuw, J. W., Van Duin, A. C., & Geenevasen, J. A. (1999). Identification of novel sulfur-containing steroids in sediments and petroleum: Probable incorporation of sulfur into $\delta^{5,7}$-sterols during early diagenesis. *Geochimica et Cosmochimica Acta*, 63(1), 31–38. https://doi.org/10.1016/S0016-7037(98)00295-6

Soman, V., Suresh, A., Krishnankutty Remani, A., Kalladathvalappil Venugopalan, V., & Keedakkadan, H. R. (2024). A holistic review on diverse lipid biomarkers as environmental indicators: Extraction and analysis from sediments to microbial communities. *Geomicrobiology Journal, 41*(9), 891–909. https://doi.org/10.1080/01490451.2024.2397685

Song, H., Kemp, D. B., Tian, L., Chu, D., Song, H., & Dai, X. (2021). Thresholds of temperature change for mass extinctions. *Nature Communications, 12*, 4694. https://doi.org/10.1038/s41467-021-25019-2

Song, H., Wignall, P. B., & Dunhill, A. M. (2018). Decoupled taxonomic and ecological recoveries from the Permo-Triassic extinction. *Science Advances, 4*(10), eaat5091. https://doi.org/10.1126/sciadv.aat5091

Song, Y., Tian, Y., Yu, J., Algeo, T. J., Luo, G., Chu, D., & Xie, S. (2022). Wildfire response to rapid climate change during the Permian-Triassic biotic crisis. *Global and Planetary Change, 215*, 103872. https://doi.org/10.1016/j.gloplacha.2022.103872

Sousa Júnior, G. R., Santos, A. L. S., De Lima, S. G., Lopes, J. A. D., Reis, F. A. M., Santos Neto, E. V., & Chang, H. K. (2013). Evidence for euphotic zone anoxia during the deposition of Aptian source rocks based on aryl isoprenoids in petroleum, Sergipe-Alagoas Basin, northeastern Brazil. *Organic Geochemistry, 63*, 94–104. https://doi.org/10.1016/j.orggeochem.2013.07.009

Staley, J., & Konopka, A. (1985). Measurement of *in situ* activities of nonphotosynthetic microorganisms in aquatic and terrestrial habitats. *Annual Review of Microbiology, 39*(1), 321–346. https://doi.org/10.1146/annurev.micro.39.1.321

Stanley, S. M. (2016). Estimates of the magnitudes of major marine mass extinctions in earth history. *Proceedings of the National Academy of Sciences, 113*(42), E6325–E6334. https://doi.org/10.1073/pnas.1613094113

Stein, R., & Fahl, K. (2013). Biomarker proxy shows potential for studying the entire Quaternary Arctic sea ice history. *Organic Geochemistry, 55*, 98–102. https://doi.org/10.1016/j.orggeochem.2012.11.005

Stolarski, J., Drake, J., Coronado, I., Vieira, A. R., Radwańska, U., Heath-Heckman, E. A. C., et al. (2023). First paleoproteome study of fossil fish otoliths and the pristine preservation of the biomineral crystal host. *Scientific Reports, 13*(1), 3822. https://doi.org/10.1038/s41598-023-30537-8

Summons, R. E., & Powell, T. G. (1987). Identification of aryl isoprenoids in source rocks and crude oils: Biological markers for the green sulphur bacteria. *Geochimica et Cosmochimica Acta, 51*(3), 557–566. https://doi.org/10.1016/0016-7037(87)90069-X

Summons, Roger E., Welander, P. V., & Gold, D. A. (2022). Lipid biomarkers: Molecular tools for illuminating the history of microbial life. *Nature Reviews Microbiology, 20*(3), 174–185. https://doi.org/10.1038/s41579-021-00636-2

Sun, H., Xiao, Y., Gao, Y., Zhang, G., Casey, J. F., & Shen, Y. (2018). Rapid enhancement of chemical weathering recorded by extremely light seawater lithium isotopes at the Permian-Triassic boundary. *Proceedings of the National Academy of Sciences, 115*(15), 3782–3787. https://doi.org/10.1073/pnas.1711862115

Sun, Y., Joachimski, M. M., Wignall, P., Yan, C., Chen, Y., Jiang, H., et al. (2012). Lethally hot temperatures during the Early Triassic greenhouse. *Science, 338*(6105), 363–366. https://doi.org/10.1126/science.1224126

Svensen, H., Planke, S., Polozov, A. G., Schmidbauer, N., Corfu, F., Podladchikov, Y. Y., & Jamtveit, B. (2009). Siberian gas venting and the end-Permian environmental crisis. *Earth and Planetary Science Letters, 277*(3–4), 490–500. https://doi.org/10.1016/j.epsl.2008.11.015

Takahashi, S., Hori, R. S., Yamakita, S., Aita, Y., Takemura, A., Ikehara, M., et al. (2021). Progressive development of ocean anoxia in the end-Permian pelagic Panthalassa. *Global and Planetary Change, 207*, 103650. https://doi.org/10.1016/j.gloplacha.2021.103650

Vandier, F., Tourte, M., Doumbe-Kingue, C., Plancq, J., Schaeffer, P., Oger, P., & Grossi, V. (2021). Reappraisal of archaeal C_{20}-C_{25} diether lipid (extended archaeol) origin and use as a biomarker of hypersalinity. *Organic Geochemistry, 159*, 104276. https://doi.org/10.1016/j.orggeochem.2021.104276

Volkman, J. K. (2003). Sterols in microorganisms. *Applied Microbiology and Biotechnology, 60*(5), 495–506. https://doi.org/10.1007/s00253-002-1172-8

Wan, J., Foster, W. J., Tian, L., Stubbs, T. L., Benton, M. J., Qiu, X., & Yuan, A. (2021). Decoupling of morphological disparity and taxonomic diversity during the end-Permian mass extinction. *Paleobiology, 47*(3), 402–417. https://doi.org/10.1017/pab.2020.57

Wang, S., Birgel, D., Krake, N., Shen, C., Haig, D. W., & Peckmann, J. (2024). Lessons from lipid biomarkers preserved in methane-seep carbonates from the early Permian of Western Australia. *Chemical Geology, 668*, 122343. https://doi.org/10.1016/j.chemgeo.2024.122343

Wang, Y., Sadler, P. M., Shen, S., Erwin, D. H., Zhang, Y., Wang, X., et al. (2014). Quantifying the process and abruptness of the end-Permian mass extinction. *Paleobiology, 40*(1), 113–129. https://doi.org/10.1666/13022

Watson, J. S., Sephton, M. A., Looy, C. V., & Gilmour, I. (2005). Oxygen-containing aromatic compounds in a late Permian sediment. *Organic Geochemistry, 36*(3), 371–384. https://doi.org/10.1016/j.orggeochem.2004.10.006

Welander, P. V., Coleman, M. L., Sessions, A. L., Summons, R. E., & Newman, D. K. (2010). Identification of a methylase required for 2-methylhopanoid production and implications for the interpretation of sedimentary hopanes. *Proceedings of the National Academy of Sciences, 107*(19), 8537–8542. https://doi.org/10.1073/pnas.0912949107

Wenger, L. M., Davis, C. L., & Isaksen, G. H. (2002). Multiple controls on petroleum biodegradation and impact on oil quality. *SPE Reservoir Evaluation & Engineering, 5*(5), 375–383. https://doi.org/10.2523/71450-ms

Wu, Y., Chu, D., Tong, J., Song, H., Dal Corso, J., Wignall, P. B., et al. (2021). Six-fold increase of atmospheric pCO_2 during the Permian–Triassic mass extinction. *Nature Communications, 12*(1), 2137. https://doi.org/10.1038/s41467-021-22298-7

Xie, S., Algeo, T. J., Zhou, W., Ruan, X., Luo, G., Huang, J., & Yan, J. (2017). Contrasting microbial community changes during mass extinctions at the middle/late Permian and Permian/Triassic boundaries. *Earth and Planetary Science Letters, 460*, 180–191. https://doi.org/10.1016/j.epsl.2016.12.015

6. Appendix

A1.1 The Boreal Realm: Svalbard

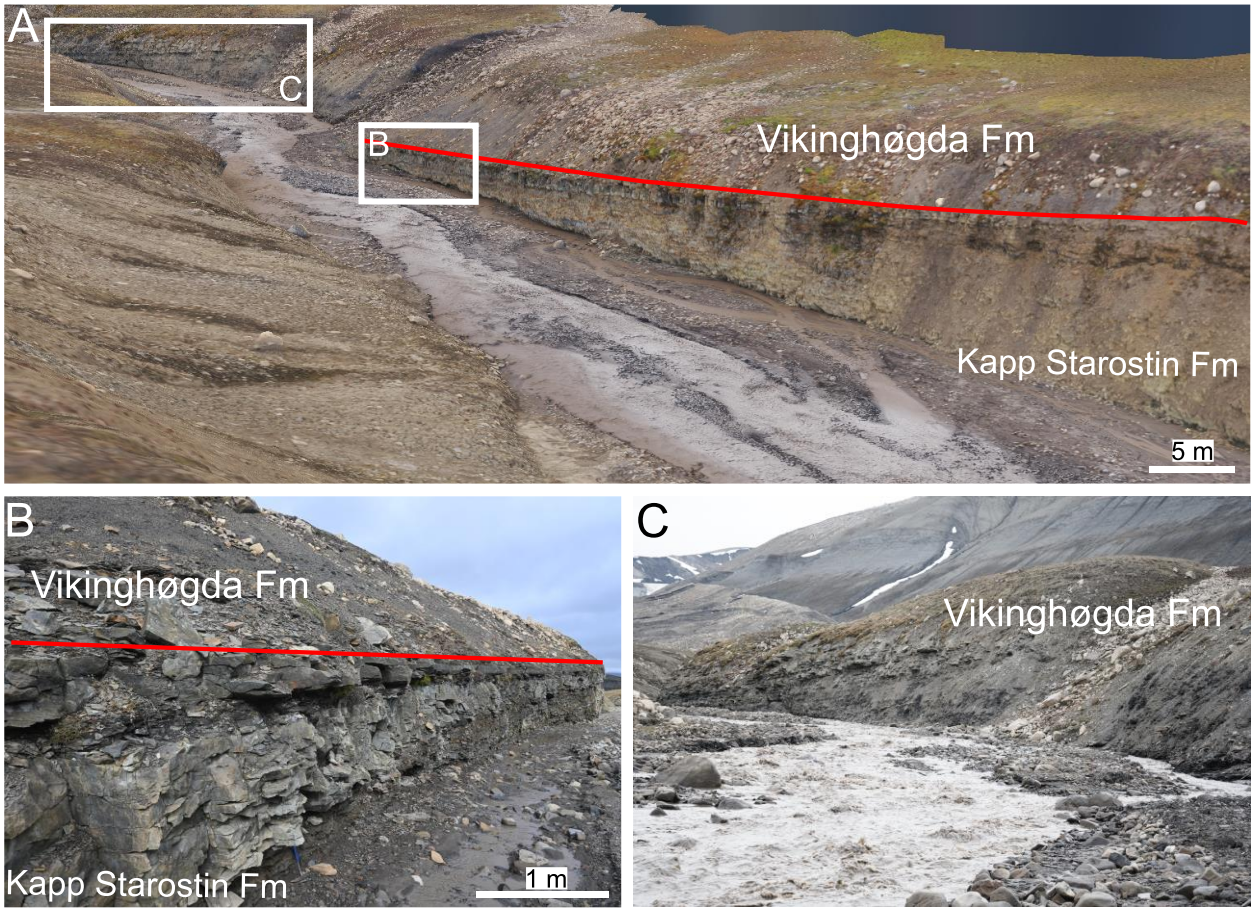

Figure A1: *Lusitaniadalen (78.29742°N; 16.73333°E) in central Svalbard. A – Virtual 3D outcrop model composed out of 1,437 photographs acquired with a DJI Mavic 2 Pro and computed with Agisoft Metashape Professional, the extinction horizon is marked with the red line; B – View towards the extinction horizon (red line) at Lusitaniadalen, hammer is approximately 30 cm; C – View towards the Early Triassic concretionary horizons in the Vikinghøgda Formation at Lusitaniadalen.*

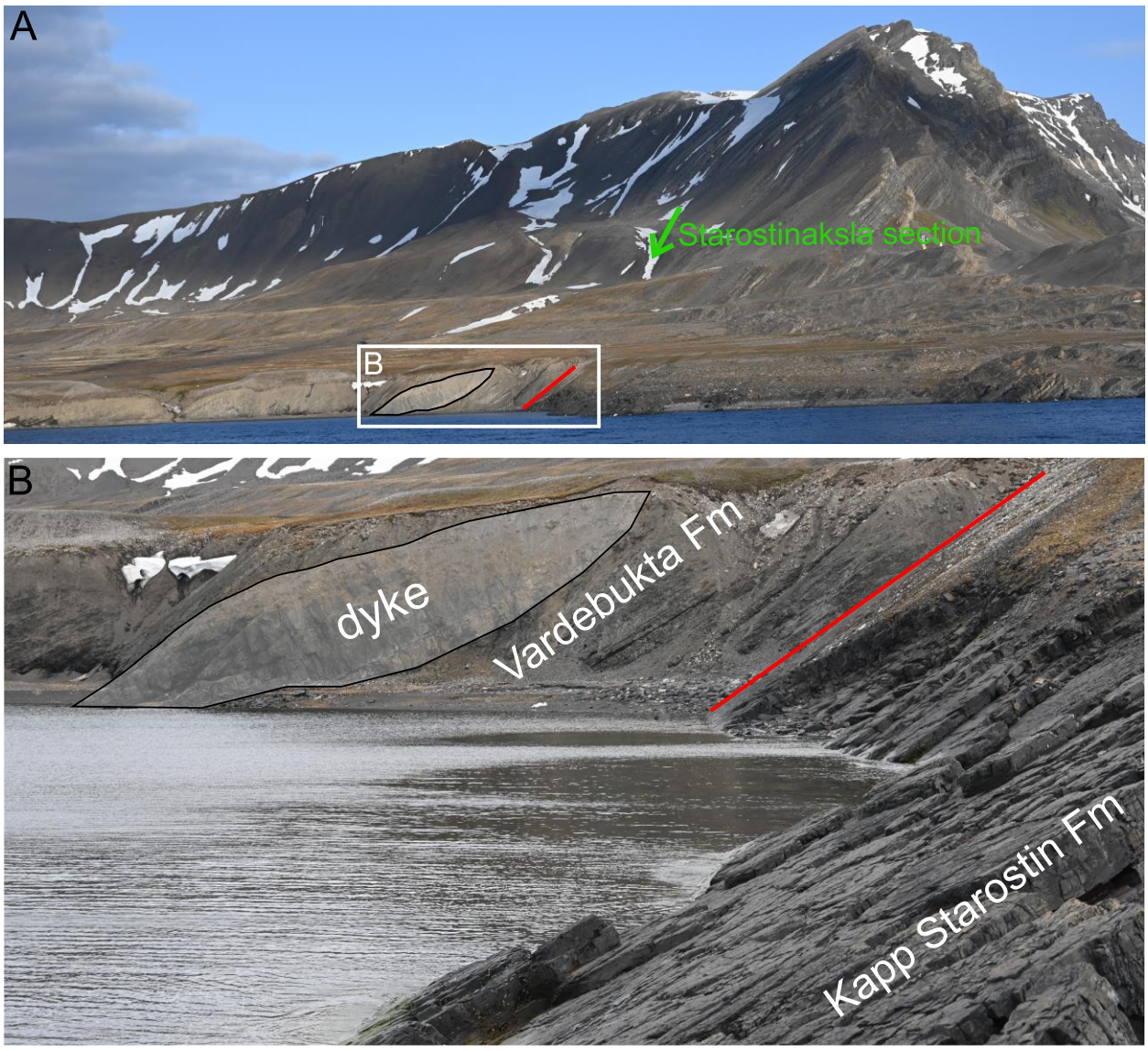

Figure A2: *Festningen (Vardebukta) (78.09377°N; 13.83455°E) and Starostinaksla (78.08648°N; 13.85088°E) in western Svalbard. A – The bay Vardebukta with the red line marking the extinction horizon on top of the heavily silicified Kapp Starostin Formation; the Starostinaksla section is exposed in a river bed further away from the dyke, and is marked with the green arrow; B – View towards the Kapp Starostin/Vardebukta formation boundary and the extinction horizon (red line) at the Festningen (Vardebukta) section, where the dyke (shaded grey) affects the preservation of organic matter in its proximity.*

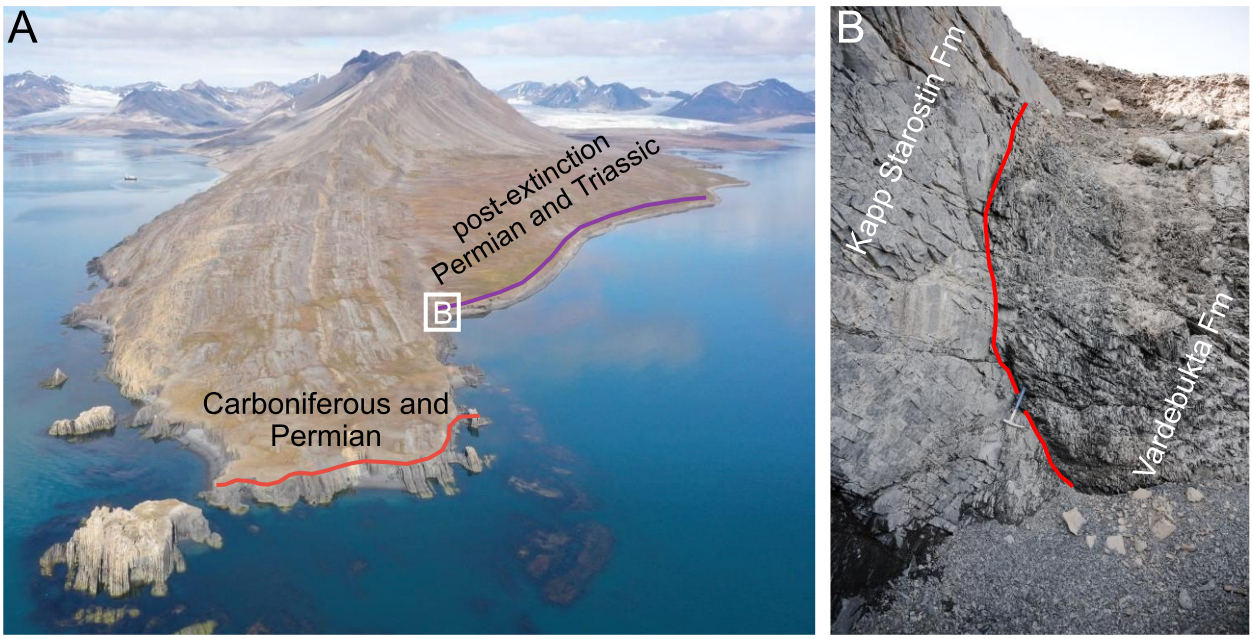

Figure A3: *Selmaneset (78.22882°N; 13.91818°E) in western Svalbard. A – Aerial picture of the Selmaneset headland with the topography reflecting the change from the heavily silicified Carboniferous and Permian strata forming the mountain, and the soft post-extinction strata exposed along the beach towards the glacier (picture taken by Tereza Mosočiová); B – View towards the extinction horizon at the Selmaneset section (red line); hammer is approximately 30 cm.*

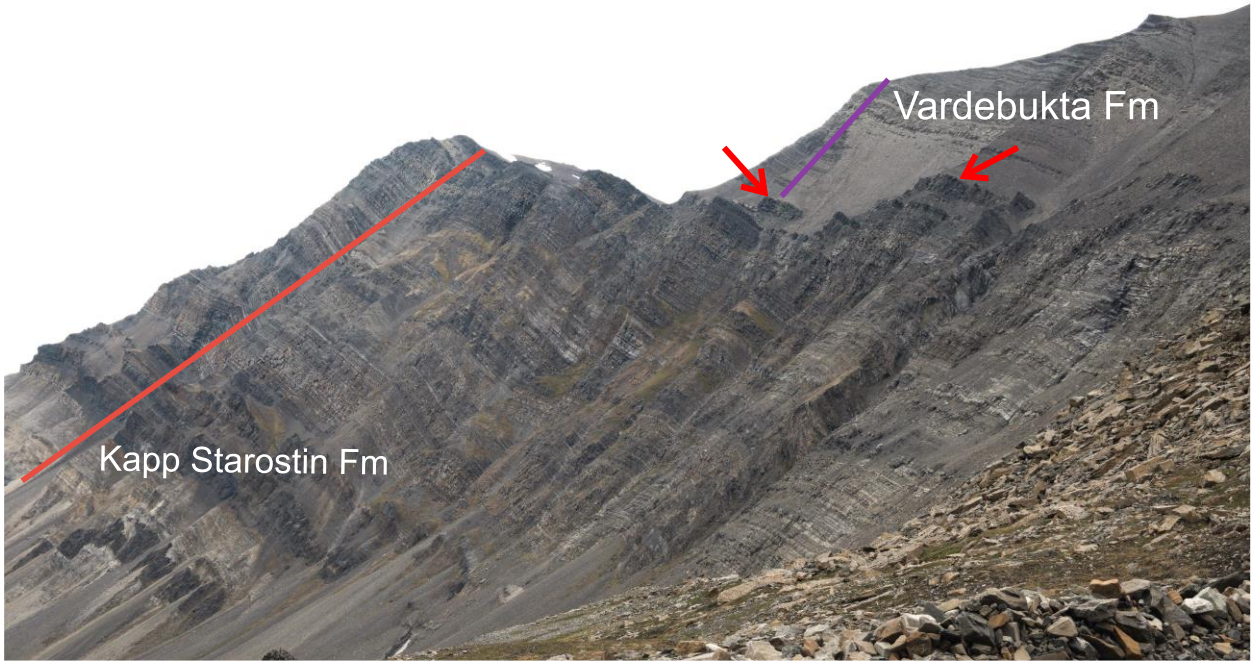

Figure A4: *Bravaisberget (77.62205°N; 14.95542°E) in western Svalbard. The heavily silicified Kapp Starostin Formation forms a cliff; the red arrows mark where the extinction horizon is exposed at the Kapp Starostin/Vardebukta formation boundary.*

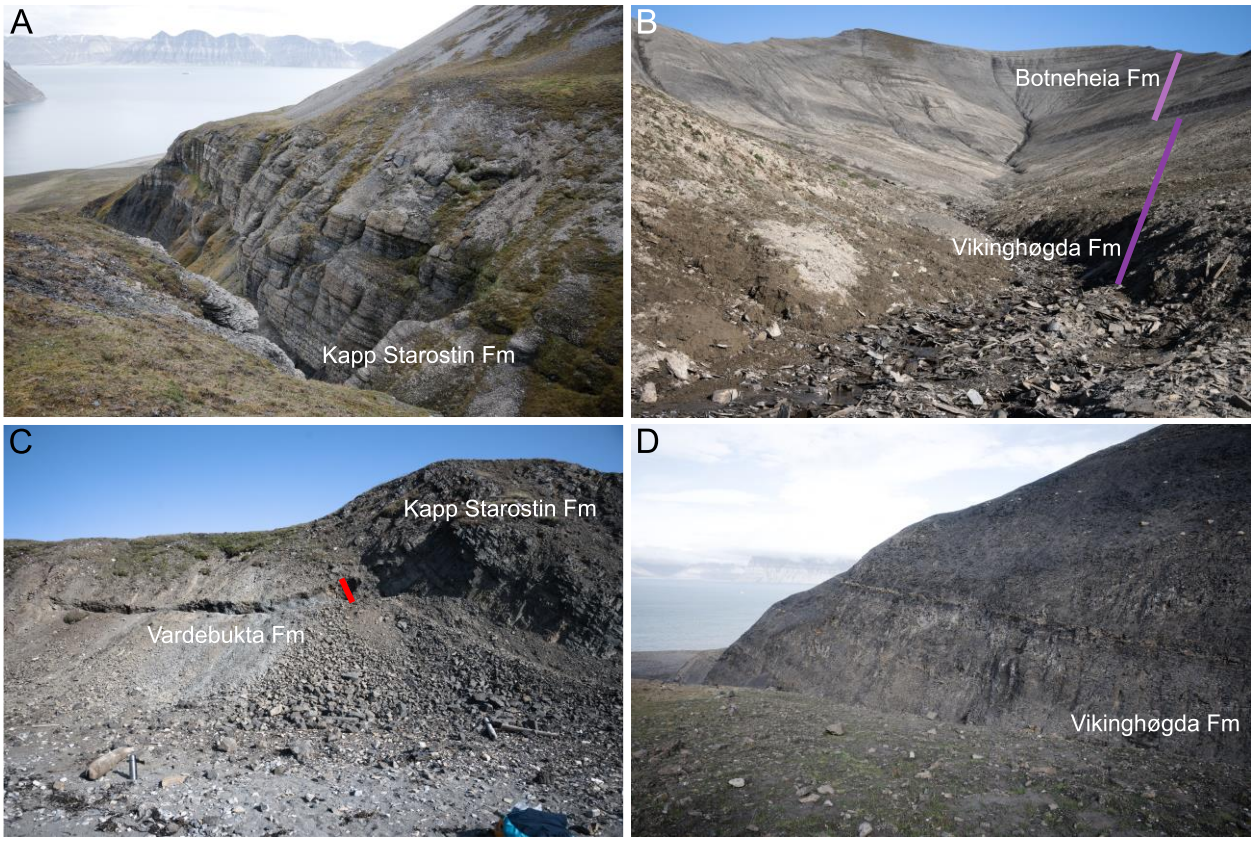

Figure A5: *A – Høgskulefjellet (78.52250°N; 15.94325°E) in central Svalbard; B – Kongressfjellet (78.54898°N; 15.24788°E) in central Svalbard; C – Reinodden (77.54353°N; 14.76448°E) in western Svalbard, with the extinction horizon marked with the red line; D – Ledalen (78.33028°N; 16.48657°E) in central Svalbard; the extinction horizon is not exposed; the yellow-weathering concretions are marking the base of the Vendomdalen Member of the Vikinghøgda Formation.*

A1.2: The western Paleotethys: Dolomites, Italy

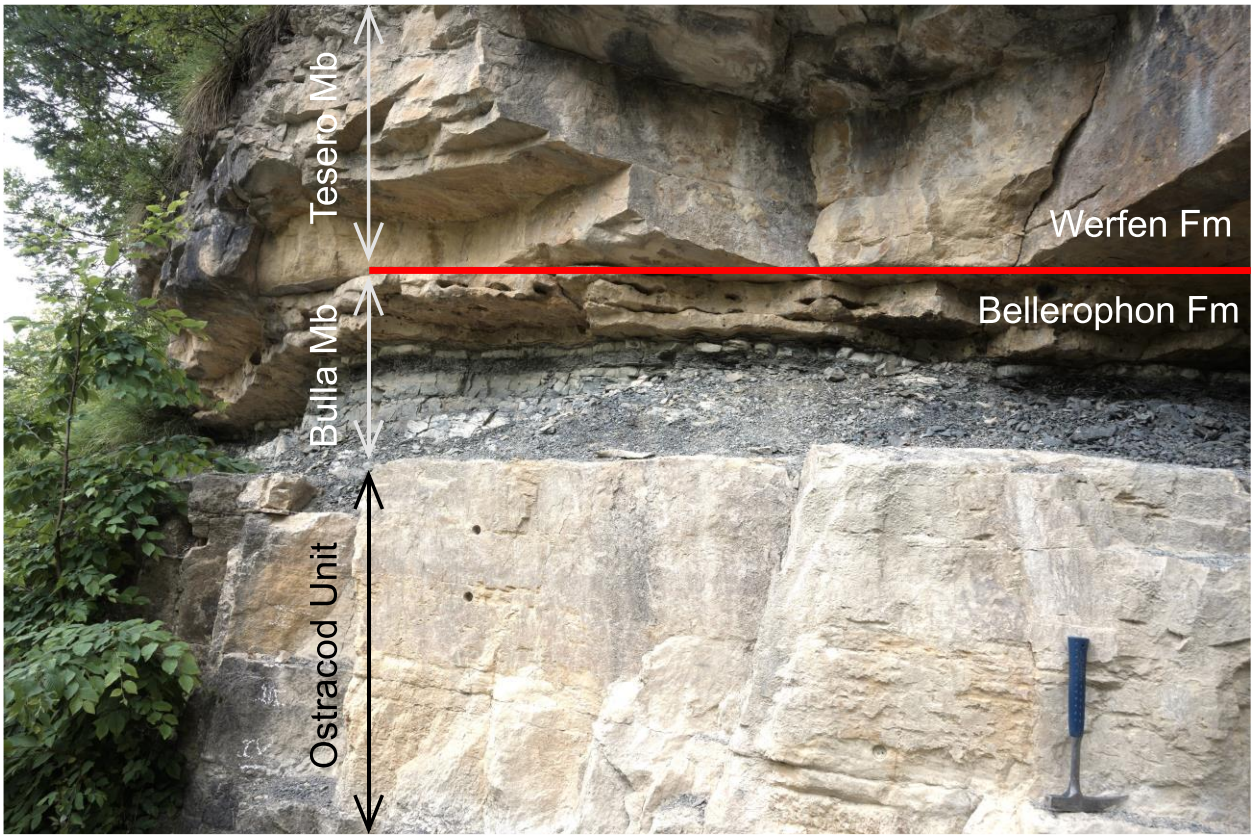

Figure A6: *Tramin (46.34307°N; 11.23453°E). Very shallow carbonate ramp setting with the pre-extinction Ostracod Unit and Bulla Member of the uppermost Bellerophon Formation, and the Tesero Member at the base of the Werfen Formation; the Permian–Triassic mass extinction is recorded in the lowermost Werfen Formation; the formation boundary is marked (red line); hammer is approximately 30 cm.*

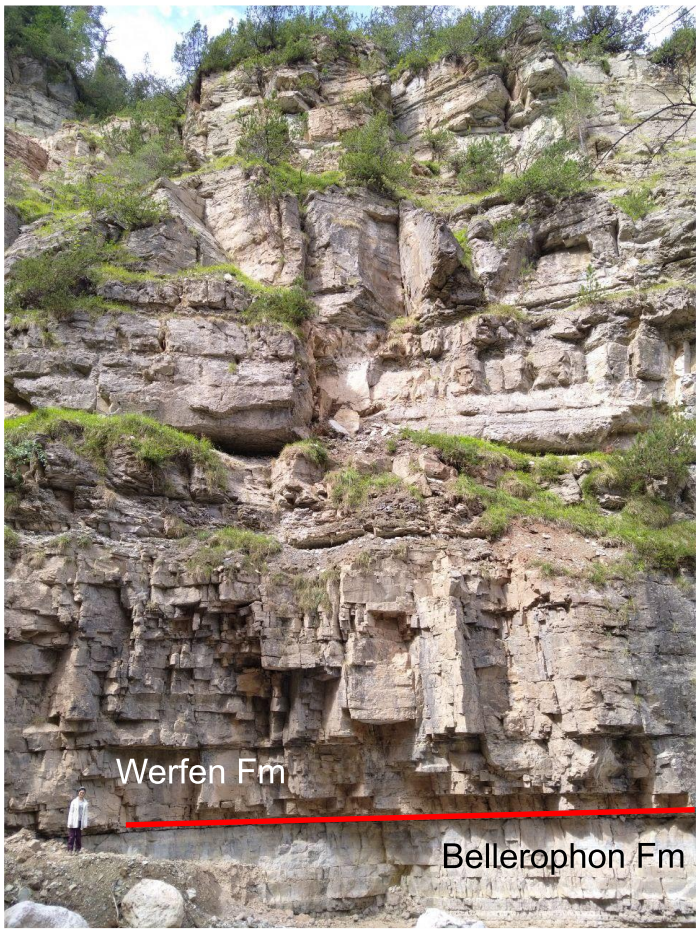

Figure A7: *Siusi (46.53280°N; 11.56213°E). The Bellerophon/Werfen formation boundary (red line) with the Permian–Triassic mass extinction at the base of the Werfen Formation cropping out in a river bed; person is approximately 1.60 m.*

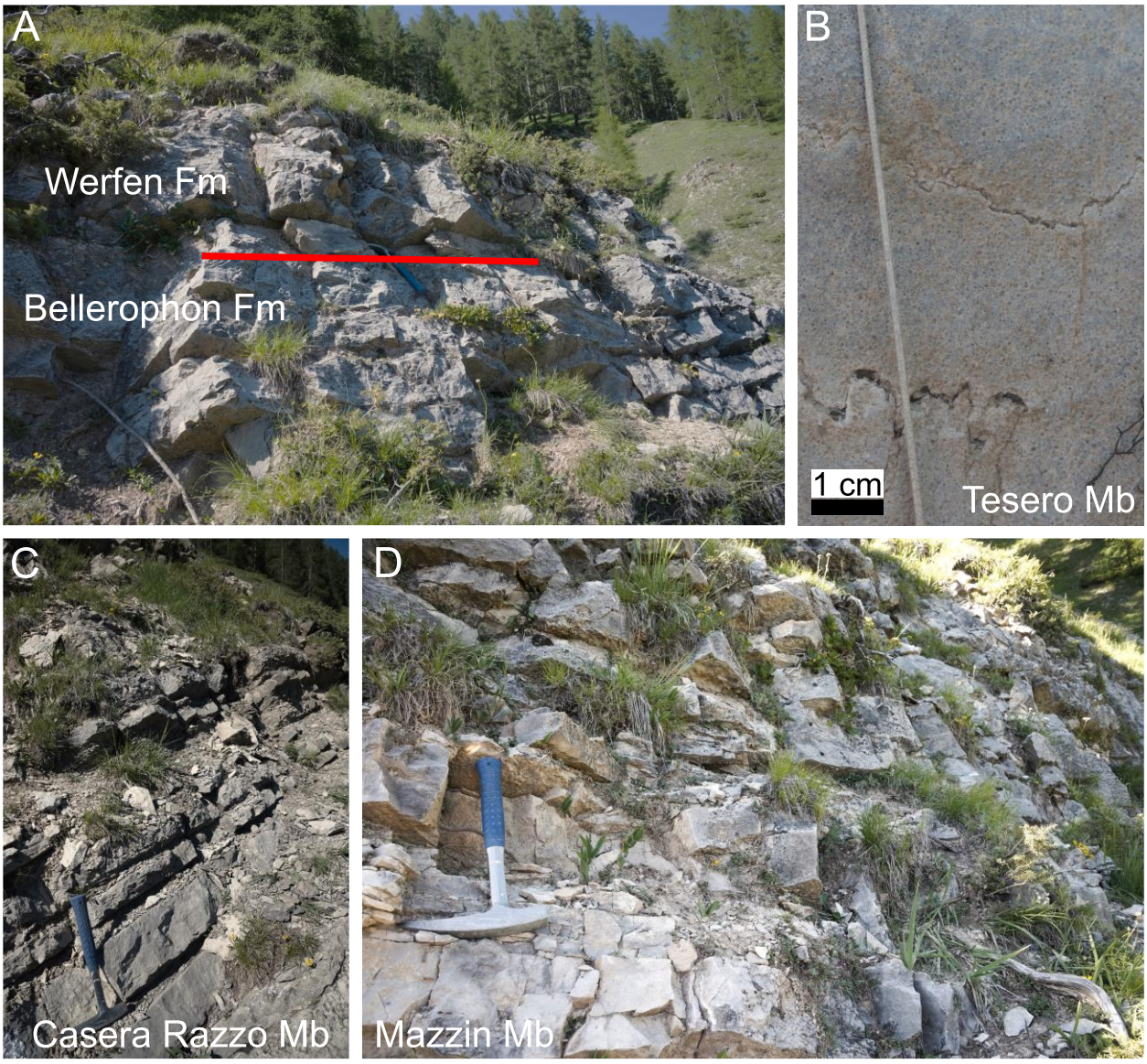

Figure A8: *Seres (46.63990°N; 11.67433°E). A – Bellerophon/Werfen formation boundary marked with the red line; B – Tesero Member at the base of the Werfen Formation with ooids and stylolitic contacts; the extinction event occurs within the oolitic bed; C – Late Permian packstones of the Casera Razzo Member of the Bellerophon Formation; D – Dolomitized mudstones of the lower Mazzin Member of the Werfen Formation; hammer in A, C, and D is approximately 30 cm.*

A1.3: The western Neotethys: Taurus Mountains, Turkey

Figure A9: *Çürük Dağ (36.70100°N; 30.45118°E). Pre-extinction Permian packstones of the Pamucak Formation and post-extinction microbialites of the Kokarkuyu Formation forming the cliff at Çürük Dağ mountain; the formation boundary is marked with the red line; the succession can be sampled at the base of the mountain in the valley (left side of the picture; mainly pre-extinction due to a fault within the first post-extinction microbialites), on the crest (extinction interval and post-extinction), and when climbing down the cliff (pre- and post-extinction).*

A1.4: The eastern Paleotethys: South China

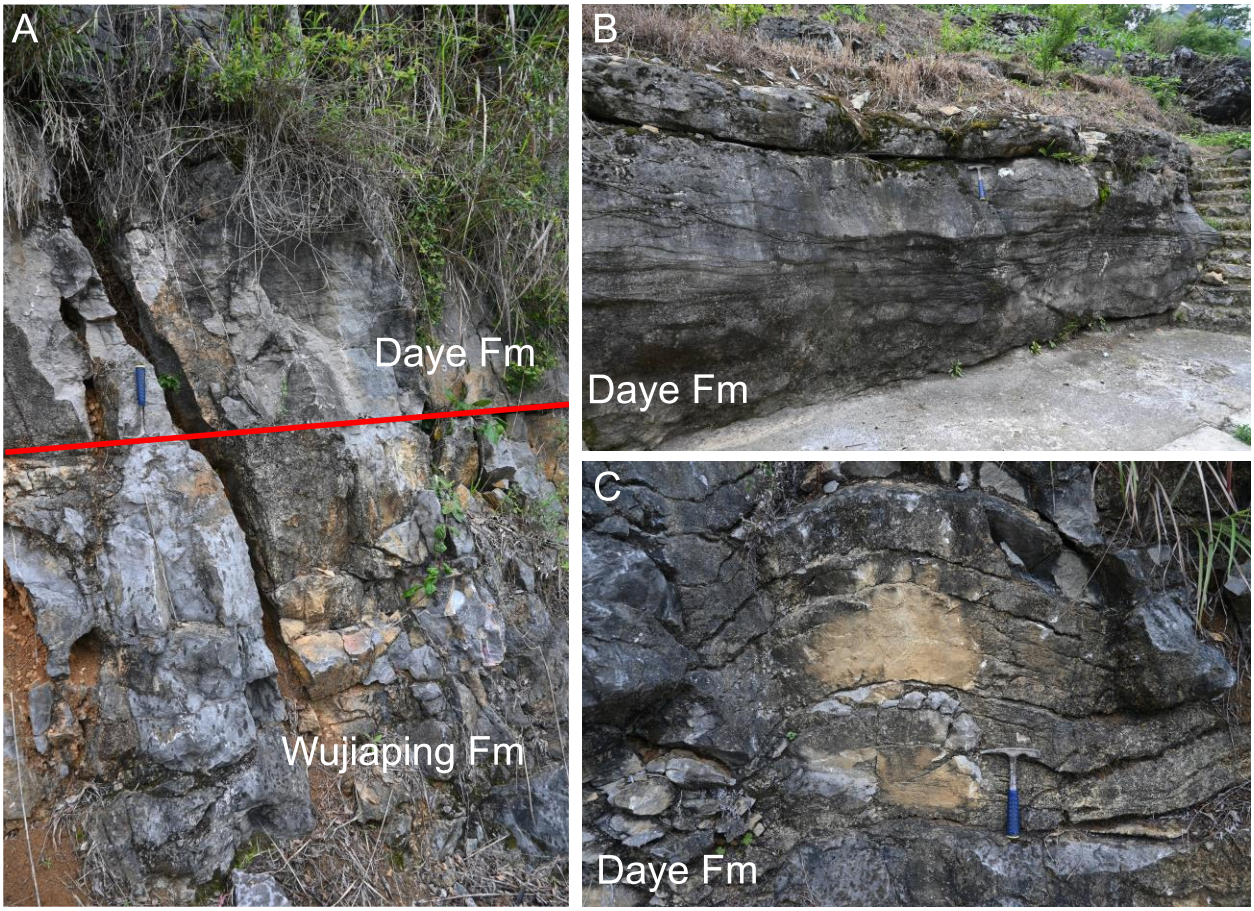

Figure A10: *Xinbaihou (25.58265°N; 106.74832°E). A – Formation boundary (red line) at the contact of pre-extinction packstones of the Wujiaping Formation and post-extinction microbialites of the Daye Formation; B – Thick microbialitic deposits following the Permian–Triassic mass extinction; C – Domal microbial structures at the base of the Daye Formation; hammer in all pictures is approximately 30 cm.*

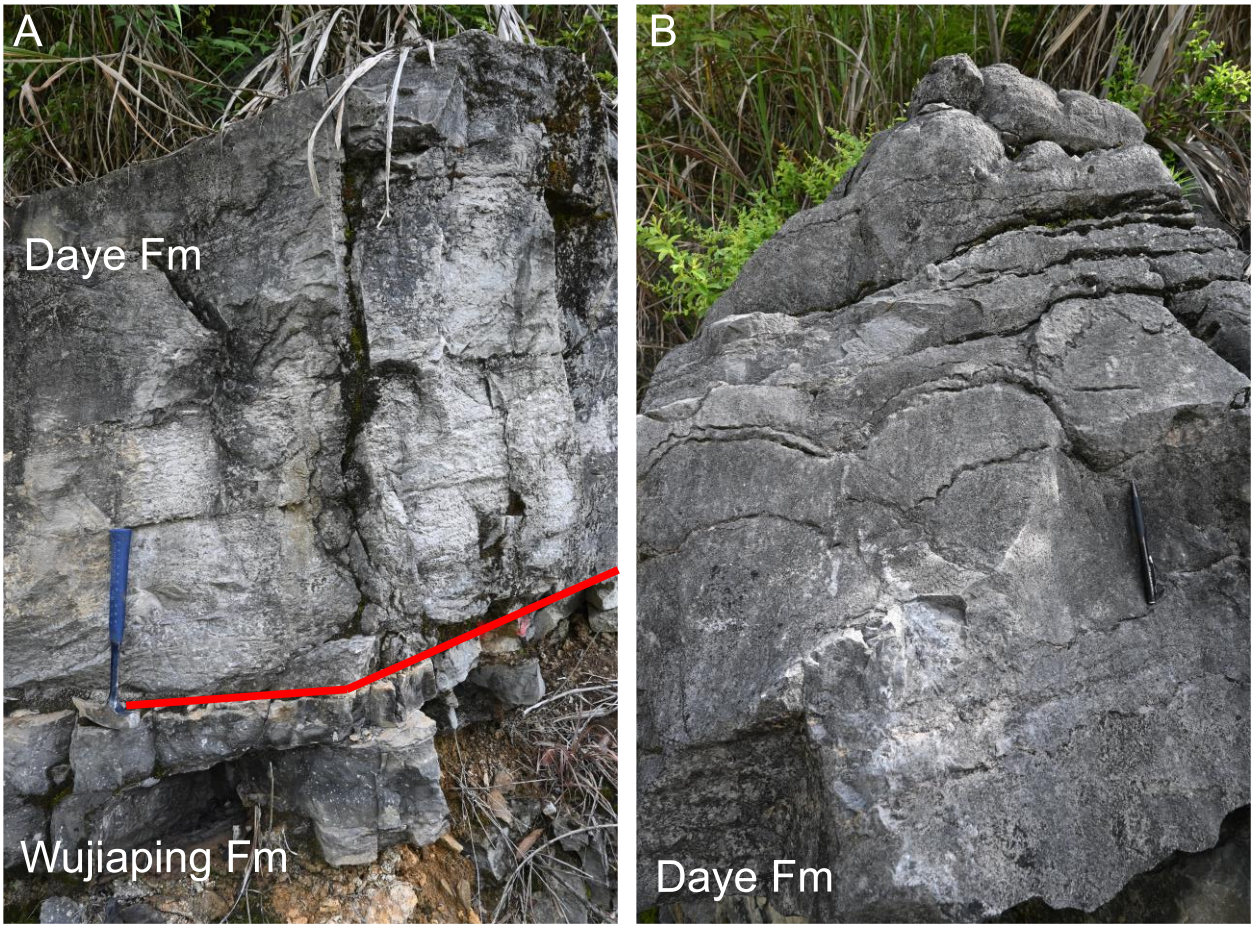

Figure A11: *Youzjianzhai (25.74803°N; 106.97622°E). A – Formation contact (red line) of the pre-extinction packstones of the Wujiaping Formation and post-extinction microbialites of the Daye Formation; hammer is approximately 30 cm; B – Domal microbial structures at the base of the Daye Formation; pencil is approximately 15 cm.*